Efficient Novel Approaches for the Calculation of Molecular Response Properties:

Second-Order Many-Body Perturbation and Double-Hybrid Density Functional Theory

---

Dissertation

zur

Erlangung der akademischen Doktorwürde

(Dr. rer. nat.)

der

Mathematisch–Naturwissenschaftlichen Fakultät

der

Rheinischen Friedrich-Wilhelms-Universität Bonn

vorgelegt von

Simone Koßmann

aus Andernach

Bonn, 1. Juni 2011

Dissertation in Chemie angefertigt mit Genehmingung der Mathematisch–Naturwissenschaftlichen Fakultät der Rheinischen Friedrich-Wilhelms-Universität Bonn.

1. Gutachter:	Prof. Dr. F. Neese
2. Gutachter:	Prof. Dr. T. Bredow
Tag der mündlichen Prüfung:	21. Dezember 2011
Erscheinungsjahr der Dissertation:	2012

Ihrer wahren Wesensbestimmung nach

ist die Wissenschaft das Studium der Schönheit der Welt.

Simone Weil (1909–1943), frz. Philosophin

meiner Familie

Abstract

This thesis reports on an efficient implementation of first- and second-order derivatives for non-variational wave functions used for the calculation of molecular properties in a linear response framework. Since, the accurate quantum chemical description of second-order molecular properties is strongly limited by the size of the system, a reliable method, which can be routinely applied from medium-sized to large molecular compounds is desirable.
Inspired by the excellent performance of the recently developed double-hybrid density functionals for energetics, thermodynamics and electron spin resonance hyperfine coupling tensors, this work focused on the efficient implementation of second derivatives for these 'fifth rung' functionals. The phrase 'fifth rung' functional is used in the context of 'Jacob's ladder', which categorizes the development of density functionals into five different stages, referred to as rungs. Density functionals of the 'fifth rung' include non-local correlation by involving virtual Kohn-Sham molecular orbitals.

In double-hybrid functionals part of the semi-local correlation introduced by a gradient corrected exchange correlation functional is replaced by nonlocal, orbital-dependent dynamic correlation by second-order Møller-Plesset (MP2) perturbation theory.

$$E = V_{NN} + \sum_{\mu\nu} P_{\mu\nu} h_{\mu\nu} + \frac{1}{2} \int\int \frac{\rho(\mathbf{r}_1)\rho(\mathbf{r}_2)}{|\mathbf{r}_1 - \mathbf{r}_2|} - \frac{1}{2} a_x \sum_{\mu\nu\kappa\tau\sigma} P^{\sigma}_{\mu\kappa} P^{\sigma}_{\nu\tau} (\mu\nu|\kappa\tau) + c_{DF} E^{XC}[\rho_\alpha, \rho_\beta] + c_{MP2} E_{MP2}$$

Therefore, the theory of second derivatives with respect to imaginary (magnetic) and real (electric) perturbations for non-variational wave functions has been rederived and extended to the use of the popular 'Resolution of the Identity' approximation. The first derivation of second double-hybrid functional derivatives within the 'density fitting' approach is presented.
Besides numerical results for static polarizabilities, chemical shifts and electronic g-tensors, a benchmark study on a fairly large system with an extended basis set ($\sim$1400 basis functions) employing the recently developed RIJCOSX approximation is presented in this thesis. Such a calculation is performed within a few days of computer time. We are not aware of any other method beyond self-consistent field theory (Hartree-Fock, density functional theory) that can routinely applied to molecules of dimension.

MP2 is well known as the simplest *ab initio* method, that accounts for dynamic correlation effects. Besides its plenty advantages MP2 often fails for complicated electronic structures. The reason could be attributed to the poor reference wave function, which is usually of Hartree-Fock quality. A new Ansatz has been derived based on the well-known Hylleraas functional, which minimizes the total energy with respect to the molecular orbital coefficients and the double excitation amplitudes.

$$\mathcal{E}_2[\mathbf{t}, \mathbf{R}] = \mathcal{E}_0^{(0)}[\mathbf{R}] + 2\Re\mathfrak{e}\langle\Psi_0^{(1)}|\mathcal{H}|\Psi_0^{(0)}\rangle + \langle\Psi_0^{(1)}|\mathcal{H}_0 - \mathcal{E}_0^{(0)}|\Psi_0^{(1)}\rangle$$

Consequently, the molecular orbitals can relax in the presence of the dynamic correlation field.
This orbital-optimized MP2 method has shown to provide drastically improved energetics compared to the canonical MP2 method. Furthermore, the calculated electron spin resonance hyperfine coupling tensors

have almost been of the same quality as what can be achieved with the more rigorous Coupled-Cluster Singles Doubles (CCSD) method, but with substantially less computational effort. The orbital-optimized MP2 method is characterized as an iterative $\mathcal{O}(N^5)$ procedure, whereas CCSD scales with $\mathcal{O}(N^6)$ per iteration.
The formalism of the orbital-optimized MP2 method has, also for the first time, been extended for the calculation of first- and second-order properties.

In the last part of this thesis, two complex molecular compounds, 2,3,5,6-Tetrafluorophenylnitren-4-yl and 3,4,5,6-Tetrafluorophenylnitren-2-yl, could be characterized as σ, σ, π-triradicals through analysis of the singly occupied spin-unrestricted natural orbitals in a localized representation. Multireference *ab initio* calculations predict well isolated $^4A_2$ and $^4A''$ ground states for the radical compounds. The calculation of the zero-field splitting tensor provides a detailed insight into the orientation and the individual contributions of the D-tensor. This application nicely demonstrates the interplay of high-resolution spectroscopy and high-level quantum-chemical methods.

Publications

Publications emanated from this thesis:

Sander, W.; Grote, D.; Koßmann, S.; Neese, F. *J. Am. Chem. Soc.* **2008,** *130,* 4396
2,3,5,6-Tetrafluorophenylnitren-4-yl: Electron paramagnetic resonance spectroscopic characterization of a quartet-ground-state nitreno radical

All electronic structure calculations for the characterization of the 2,3,5,6-tetrafluorophenyinitren-4-yl radical performed with the ORCA program package and the molecular property calculations have been carried out by S. Koßmann.

Koßmann, S.; Neese, F. *Chem. Phys. Lett.* **2009,** *481,* 240
Comparison of two efficient approximate Hartree-Fock approaches

All benchmark calculations have been performed by S. Koßmann.

Neese, F.; Schwabe, T.; Koßmann, S.; Schirmer, B.; Grimme, S. *J. Chem. Theory Comput.* **2009,** *5,* 3060
Assessment of Orbital-Optimized Spin-Component Scaled Second-Order Many-Body Perturbation Theory for Thermochemistry and Kinetics

The theory for the orbital-optimized spin-component scaled MP2 method has been reported by S. Koßmann.

Grote, D.; Finke, C.; Koßmann, S.; Neese, F.; Sander, W. *Chem. Eur. J.* **2010,** *16,* 4496
3,4,5,6-Tetrafluorophenylnitren-2-yl: A Ground-State Quartet Triradical

All electronic structure calculations performed with the ORCA program have been done by S. Koßmann.

Koßmann, S.; Neese, F. *J. Chem. Theory Comput.* **2010,** *6,* 2325
Efficient Structure Optimization with Second-Order Many-Body Perturbation Theory: The RIJCOSX-MP2 Method

S. Koßmann implemented the RIJCOSX approximation for the use in MP2 gradient calculations into the ORCA package. All benchmark calculations have been performed by S. Koßmann.

Koßmann, S.; Neese, F. *J. Phys. Chem. A* **2010,** *114,* 11768
Correlated ab Initio Spin Densities for Larger Molecules: Orbital-Optimized Spin-Component-Scaled MP2 Method

All hyperfine coupling tensor calculations have been carried out by S. Koßmann.

Further Publications:

Pham, D.-T.; Gentz, K.; Zörlein, C.; Hai, N. T. M.; Tsay, S.-L.; Kirchner, B.; Koßmann, S.; Wandelt, K.; Broekmann, P. *New J. Chem.* **2006,** *30,* 1439
Surface redox chemistry of adsorbed viologens on Cu(100)

Koßmann, S.; Thar, J.; Kirchner, B. *J. Chem. Phys.* **2006,** *124,* 174506
Cooperativity in ionic liquids

Nockemann, P.; Thijs, B.; Driesen, K.; Janssen, C. R.; Van Hecke, K.; Van Meervelt, L.; Koßmann, S.; Kirchner, B.; Binnemans, K. *J. Phys. Chem. B* **2007,** *111,* 5254
Choline saccharinate and choline acesulfamate: Ionic liquids with low toxicities

Pham, D.-T.; Tsay, S.-L.; Gentz, K.; Zörlein, C.; Koßmann, S.; Tsay, J.-S.; Kirchner, B.; Wandelt, K.; Broekmann, P. *J. Phys. Chem. C* **2007,** *111,* 16428
Quasi-reversible chloride adsorption/desorption through a polycationic organic film on Cu(100)

Koßmann, S.; Kirchner, B.; Neese, F. *Mol. Phys.* **2007,** *105,* 2049
Performance of modern density functional theory for the prediction of hyperfine structure: meta-GGA and double-hybrid functionals

Petrenko, T.; Koßmann, S.; Neese, F. *J. Chem. Phys.* **2011,** *134,* 054116
Efficient time-dependent density functional theory approximations for hybrid density functionals: Analytical gradients and parallelization

Contents

List of Tables

List of Figures

Nomenclature

$\mu, \nu, \kappa, \tau, ...$	Atomic basis functions
$i, j, k, l, ...$	Internal orbitals in the reference determinant
$a, b, c, d, ...$	Virtual orbitals in the reference determinant
$p, q, r, s, ...$	General orbitals in the reference determinant, either internal or virtual
$K, L, M, N, ...$	Auxiliary basis function for Coulomb fitting
$P, Q, R, S, ...$	Auxiliary basis function for correlation fitting
λ	Total derivative w.r.t. perturbation λ
(λ)	Basis function derivative w.r.t. perturbation λ
$[\lambda]$	Operator derivative w.r.t. perturbation λ
$\{\lambda\}$	Basis function and operator derivative w.r.t. perturbation λ
$\langle\lambda\rangle$	MO coefficient derivative w.r.t. perturbation λ
$\mathbf{r}$	Spatial coordinates x, y, z
$\mathbf{x}$	Spatial coordinates and spin coordinate x, y, z, σ
$\Re$	Index referencing real perturbations
$\Im$	Index referencing imaginary perturbations
$\star$	Index referencing the complex conjugate
a_q^p	Replacement operator in second quantization
B_{ai}^{λ}	Right-hand side of the coupled-perturbed Hartree-Fock equations
B_{pq}^{P}	Half-transformed 3-index RI-integral
$c_{\mu p}$	Hartree-Fock MO coefficient
D	Relaxed MP2 difference density matrix
D'	Unrelaxed MP2 difference density matrix
ε_p	pth eigenvalue of the Fock operator
$\mathcal{E}_n$	Exact Energy to wave function Ψ_n
$E_n^{(m)}$	mth order Energy to wave function $\Psi_n^{(m)}$
E^{XC}	Exchange-correlation energy
$\mathcal{F}(\mathbf{x})$	Fock operator
Γ_{pqrs}	Element of second-order reduced density matrix in MO basis
γ_{pq}	Element of first-order reduced density matrix in MO basis
Γ'^{P}_{pq}	3-index 2-particle density matrix
$\hat{h}(\mathbf{x})$	One-electron operator
$\mathcal{H}_0$	Zero-order Hamiltonian
$\mathcal{H}$	Exact Hamiltonian
$\mathcal{J}(\mathbf{x})$	Coulomb operator
$\mathcal{K}(\mathbf{x})$	Exchange operator

$\psi_p(\mathbf{x})$	Spin orbital
P_{pq}	Element of Hartree-Fock density matrix in MO basis
Ψ_n	Wave function
$\Psi_n^{(m)}$	mth order wave function
$\hat{r}_{ij}^{-1}$	Exact two-electron operator
$\rho(\mathbf{r})$	Electron density
$\overline{R}(\mathbf{D}')_{pq}$	Response operator for real perturbations
$\overline{\overline{R}}(\mathbf{D}')_{pq}$	Response operator for imaginary perturbations
$S_{pq}^{(\lambda)}$	Derivative of the overlap matrix
$t_a^{i(m)}, t_{ab}^{ij(m)}, \ldots$	mth order single, double, ... excitation amplitudes
U_{pq}^{λ}	Coupled-perturbed Hartree-Fock coefficient
$\mathcal{V}$	Perturbation
V^{XC}	Exchange-correlation potential
W_{pq}	Element of Hartree-Fock energy weighted density matrix in MO basis
X_{ai}	Lagrangian for real perturbations
x_{pq}^{λ}	Real part of coupled-perturbed Hartree-Fock coefficient
Y_{ai}	Lagrangian for imaginary perturbations
$\mathbf{i}y_{pq}^{\lambda}$	Imaginary part of coupled-perturbed Hartree-Fock coefficient
$\overline{z}_{ai}$	z-vector for real perturbations
$\overline{\overline{z}}_{ai}$	z-vector for imaginary perturbations

1. Motivation

Quantum chemical methods play an important role in nowadays chemical applications, since they provide a profound insight into the electronic structure of the molecular system. Therefore, the development of accurate electronic structure methods and their efficient implementation in quantum chemical program packages is of great interest for academical as well as industrial research.

The theory most quantum chemical calculations are based on, is Hartree-Fock (HF) theory, which yields a reasonable description of the electronic structure of the system in question. However, due to the exaggeration of the electron repulsion caused by the mean-field approach, electron correlation has to be accounted for in a suitable way. The concept of full configuration interaction allows the exact description of electron correlation effects in a given basis, but the number of determinants grows rapidly, and truncated configuration interaction methods are not size consistent. Size consistency and size extensitivity represent fundamental requirements for *ab initio* theories.

The development of density functional theory in the Kohn-Sham framework permits the incorporation of electron correlation effects at the cost of Hartree-Fock calculations. But since the exact density functional is not known, the way and to which extend different density functionals incorporate electron correlation is most often questionable. Furthermore, many density functionals violate fundamental constraints, e.g. predicting correlation energies for one-electron systems. Nevertheless, density functional theory, especially the hybrid variant, which contains a fraction of Hartree-Fock exchange, often yields reliable results for energetics and thermodynamic properties. [1]

The simplest *ab initio* method which accounts for dynamic electron correlation effects is second-order many body perturbation theory with the Møller-Plesset partitioning of the Hamiltonian. [2] The idea to take the Hartree-Fock wave function and the corresponding energy as zero-order approximation to the exact solution of the Schrödinger equation and to treat the difference between the exact Hamiltonian and the HF Hamiltonian as small perturbation, was developed by Møller and Plesset already in the early 1930s. [2] The big breakthrough of Møller-Plesset perturbation theory (MPPT) came with the development of many-body perturbation theory from second- to fourth-order for general use in electronic structure calculations in the 1970s. [3] The rivaling pioneers of MPPT John A. Pople and Roger J. Bartlett developed perturbation theory up to fourth-order by employing the algebraic and the diagrammatic approach to many-body perturbation theory, respectively. [3–10] In the following years the routine application of MPPT in electronic structure calculations was encouraged by the development of analytic derivatives and corresponding efficient algorithms. Pople *et al.* reported first derivatives for second-order MPPT (MP2) already in 1979. [11] Bartlett and co-workers were the first who established the concept of relaxed densities [12, 13] in the framework of second and higher order MPPT. Furthermore, the removal of the perturbation dependence from the coupled-perturbed Hartree-Fock equations was adopted for MPPT and Coupled-Cluster gradients. [13–15] In 1986 the first analytical evaluation of second MP2 derivatives for the calculation of analytic harmonic frequencies has been published. [16] The generalization of the second MP2 derivatives for the calculation of magnetic properties with purely imaginary perturbations has been reported by Gauss. [17]

The popularity of MPPT is due to its formal simplicity as well as to the availability in most quantum chemical program packages. [3] MPPT is size extensive to all orders, as could be demonstrated by Goldstone [18] via the 'linked cluster' theorem. Second-order MPPT already recovers 80–90% of the basis set correlation energy with a formal scaling of $\mathcal{O}(N^5)$. The shortcomings of MP2 theory are also well known, i.e. MP2 is not variational or even stationary with respect to wave function parameters, and it does not incorporate any orbital relaxation when based on a HF reference determinant. Orbital relaxation is partially taken into account, if Brillouins' theorem [19] no longer applies, and single excitations contribute to the first-order wave function. The non-variational character of MP2 is of minor consequence for the calculation of electron correlation effects, but complicates and increases the computational effort for the evaluation of MP2 derivatives.

Therefore, it is desirable to develop efficient and robust approximations to MPPT. The most popular approximation used in combination with the MP2 method is the 'Resolution of the Identity' (RI) approximation, in which products of orbitals are expanded in an auxiliary basis set. [20] The RI-MP2 method was first reported by Feyereisen *et al.* [21] and was based on the results of Vahtras, Feyereisen and Almlöf who showed that the RI technique performs best in the Coulomb metric. [22] But the use of the 'density fitting' technique has never been extendend to MP2 second derivatives, which is one goal of the present thesis. Furthermore, the evaluation of second derivatives for the new class of double-hybrid density functionals, which incorporate a fraction of MP2 dynamic correlation, has recently been reported for analytical frequencies, [23] but has not been extended to magnetic properties yet. Thus, analytic second derivatives for the double-hybrid functionals for purely real and purely imaginary perturbations have also been derived within this thesis.

Besides the outstanding performance of the RI approximation in conjunction with MP2, which yields speedups of one to two orders of magnitude in energy calculations, it is worthwhile to develop further approximations, which efficiently accelerate the self-consistent field calculation, that represents the bottleneck in large-scale RI-MP2 calculations. Therefore, the RIJCOSX approximation to MP2 first- and second-order property calculations is presented.

On the other hand, the calculation of accurate first principles spin densities requires the incorporation of a substantial amount of dynamic correlation. But MP2 is known to be insufficient and often provides somewhat erratic results when applied to open-shell systems. So, an orbital-optimized MP2 method has been developed, which optimizes the orbitals alongside with the double excitation amplitudes based on the well-known Hylleraas functional [24]. The orbital-optimized MP2 (OO-MP2) method has been successfully applied to the calculation of hyperfine coupling constants. Furthermore the OO-MP2 gradient as well as OO-MP2 second derivatives have been derived.

The derived equations have been efficiently implemented into a development version of the ORCA program package [25] and will be available soon.

Finally, the application of high-level *ab initio* methods for electronic structure calculations on chemically complex systems is demonstrated on the example of 2,3,5,6-Tetrafluorophenylnitren-4-yl and 3,4,5,6-Tetrafluorophenylnitren-2-yl, two quartet ground-state nitreno radicals.

2. Theory

2.1. Introduction to Møller-Plesset Perturbation Theory

2.1.1. Hartree-Fock Theory

Hartree-Fock (HF) theory represents the most popular approximate method for solving the electronic time-independent Schrödinger equation. It is often referred to as a mean-field theory, since the motion of each electron is described in the averaged field generated by all other electrons. Thus, the motion of the reference electron is independent of the motion of the remaining electrons (independent particle model). The wave function for the independent particle model is a single Slater determinant built up of one spin orbital per electron.

The minimization of the expectation value of the Born-Oppenheimer Hamiltonian via the variational principle ensures that the energy obtained represents an upper bound to the exact solution. The canonical HF equations are obtained by minimizing a functional of the spin orbitals $\{\Psi\}$ through a constraint optimization via Lagrange multipliers, and setting the variation to zero,

$$\left\{\hat{h}(\mathbf{x}) + \sum_j \mathcal{J}_j(\mathbf{x}) - \mathcal{K}_j(\mathbf{x})\right\}\psi_i(\mathbf{x}) = \varepsilon_i\psi_i(\mathbf{x}) \tag{2.1}$$

$$\mathcal{F}(\mathbf{x})\psi_i(\mathbf{x}) = \varepsilon_i\psi_i(\mathbf{x}). \tag{2.2}$$

The operator $\hat{h}$ contains the one-electron kinetic and potential energy operator. The HF Hamiltonian is an effective one-electron operator since it depends only on the coordinates $\mathbf{x}$ of the considered electron. The HF equations are a set of coupled one-electron eigenvalue equations, in which the Fock operator $\mathcal{F}$ depends on all spin orbitals through the Coulomb $\mathcal{J}$ and exchange $\mathcal{K}$ operators,

$$\mathcal{J}_j(\mathbf{x}_1)\psi_i(\mathbf{x}_1) = \left[\int d\mathbf{x}_2\psi_j^\star(\mathbf{x}_2)r_{12}^{-1}\psi_j(\mathbf{x}_2)\right]\psi_i(\mathbf{x}_1) \tag{2.3}$$

$$\mathcal{K}_j(\mathbf{x}_1)\psi_i(\mathbf{x}_1) = \left[\int d\mathbf{x}_2\psi_j^\star(\mathbf{x}_2)r_{12}^{-1}\psi_i(\mathbf{x}_2)\right]\psi_j(\mathbf{x}_1). \tag{2.4}$$

where the superscript * denotes the complex conjugate of the spin orbital. Therefore, these equations are solved iteratively. The diagonalized matrix of the Lagrange multipliers ε can be interpreted as orbital energies. The solution of the HF equations can obtained either by numerical methods, or by expanding the spin orbitals in a finite basis set and searching for the lowest energy solution (Hartree-Fock-Roothaan equations). The iterative procedure for solving the Hartree-Fock-Roothaan equations is called self-consistent field (SCF) method.

The drawback of HF theory is its lack of instantaneous electron-electron interactions, the so-called electron correlation. The correlation energy is defined as the difference between the exact non relativistic energy

and the HF energy,

$$\Delta E_{corr} = E_{exact} - E_{HF}. \tag{2.5}$$

Post-HF methods improve on the HF method by (partial) inclusion of different electron correlation effects. Dynamic correlation arises from the instantaneous correlation in electron motions due to their mutual repulsion. By contrast, static correlation originates from the qualitative error of the single-configuration model. In this thesis special emphasis is paid to dynamic correlation effects.

2.1.2. Rayleigh-Schrödinger Perturbation Theory

In this subsection the formal expressions of Rayleigh-Schrödinger perturbation theory in the quantum mechanical framework are derived. Starting from the Schrödinger equation, the Hamiltonian $\mathcal{H}$ is separated into a zero-order part $\mathcal{H}_0$ and a perturbation $\lambda\mathcal{V}$, with $|\Psi_n\rangle$ denoting the exact solutions.

$$\mathcal{H}|\Psi_n\rangle = (\mathcal{H}_0 + \lambda\mathcal{V})|\Psi_n\rangle = \mathcal{E}_n|\Psi_n\rangle. \tag{2.6}$$

The eigenfunctions $|\Phi_n\rangle$ and the eigenvalues $E_n^{(0)}$ of the unperturbed Hamiltonian $\mathcal{H}_0$ are assumed to be known,

$$\mathcal{H}_0|\Phi_n\rangle = E_n^{(0)}|\Phi_n\rangle \qquad \text{with } \langle\Phi_n|\Phi_m\rangle = \delta_{nm}. \tag{2.7}$$

If the perturbation $\mathcal{V}$ is small compared to the unperturbed Hamiltonian $\mathcal{H}_0$, we can expect $|\Psi_n\rangle$ and $\mathcal{E}_n$ to be reasonably close to $|\Phi_n\rangle$ and $E_n^{(0)}$, respectively. In order to systematically improve the eigenfunctions and eigenvalues of $\mathcal{H}_0$ so that they converge to the eigenvalues and eigenfunctions of the total Hamiltonian $\mathcal{H}$, the exact eigenfunctions and eigenvalues are expanded in a Taylor series in the ordering parameter λ.

$$\mathcal{E}_n = E_n^{(0)} + \lambda E_n^{(1)} + \lambda^2 E_n^{(2)} + ... \tag{2.8}$$

$$|\Psi_n\rangle = |\Psi_n^{(0)}\rangle + \lambda|\Psi_n^{(1)}\rangle + \lambda^2|\Psi_n^{(2)}\rangle + ... \qquad (|\Psi_n^{(0)}\rangle = |\Phi_n\rangle) \tag{2.9}$$

For convenience, intermediate normalization is chosen,

$$\langle\Phi_n|\Psi_n\rangle = \langle\Phi_n|\Psi_n^{(0)}\rangle + \lambda\langle\Phi_n|\Psi_n^{(1)}\rangle + \lambda^2\langle\Phi_n|\Psi_n^{(2)}\rangle + ... = \langle\Phi_n|\Psi_n^{(0)}\rangle = 1. \tag{2.10}$$

Insertion of the Taylor expansions of eqs. 2.8 and 2.9 into the Schrödinger equation (eq. 2.6) yields,

$$\begin{aligned}(\mathcal{H}_0 + \mathcal{V})(|\Psi_n^{(0)}\rangle + \lambda|\Psi_n^{(1)}\rangle + \lambda^2|\Psi_n^{(2)}\rangle + ...) \\ = (E_n^{(0)} + \lambda E_n^{(1)} + \lambda^2 E_n^{(2)} + ...)(|\Psi_n^{(0)}\rangle + \lambda|\Psi_n^{(1)}\rangle + \lambda^2|\Psi_n^{(2)}\rangle + ...).\end{aligned} \tag{2.11}$$

Equating coefficients of powers of λ,

$$\mathcal{H}_0|\Psi_n^{(0)}\rangle = E_n^{(0)}|\Psi_n^{(0)}\rangle \tag{2.12}$$
$$\mathcal{H}_0|\Psi_n^{(1)}\rangle + \mathcal{V}|\Psi_n^{(0)}\rangle = E_n^{(0)}|\Psi_n^{(1)}\rangle + E_n^{(1)}|\Psi_n^{(0)}\rangle \tag{2.13}$$
$$\mathcal{H}_0|\Psi_n^{(2)}\rangle + \mathcal{V}|\Psi_n^{(1)}\rangle = E_n^{(0)}|\Psi_n^{(2)}\rangle + E_n^{(1)}|\Psi_n^{(1)}\rangle + E_n^{(2)}|\Psi_n^{(0)}\rangle \tag{2.14}$$
$$\mathcal{H}_0|\Psi_n^{(3)}\rangle + \mathcal{V}|\Psi_n^{(2)}\rangle = E_n^{(0)}|\Psi_n^{(3)}\rangle + E_n^{(1)}|\Psi_n^{(2)}\rangle + E_n^{(2)}|\Psi_n^{(1)}\rangle + E_n^{(3)}|\Psi_n^{(0)}\rangle \tag{2.15}$$
$$(E_n^{(0)} - \mathcal{H}_0)|\Psi_n^{(m)}\rangle = \mathcal{V}|\Psi_n^{(m-1)}\rangle - \sum_{l=0}^{m-1} E_n^{(m-l)}|\Psi_n^{(l)}\rangle. \tag{2.16}$$

In eq. 2.16 the general expression for the mth-order perturbation equation is given. Multiplying the above equations with $\langle\Phi_n|$ and using the normalization condition, eq. 2.10, yields the following expressions for the mth-order energies,

$$E_n^{(0)} = \langle\Phi_n|\mathcal{H}_0|\Psi_n^{(0)}\rangle \tag{2.17}$$
$$E_n^{(1)} = \langle\Phi_n|\mathcal{V}|\Psi_n^{(0)}\rangle \tag{2.18}$$
$$E_n^{(2)} = \langle\Phi_n|\mathcal{V}|\Psi_n^{(1)}\rangle \tag{2.19}$$
$$E_n^{(3)} = \langle\Phi_n|\mathcal{V}|\Psi_n^{(2)}\rangle \tag{2.20}$$
$$E_n^{(m)} = \langle\Phi_n|\mathcal{V}|\Psi_n^{(m-1)}\rangle. \tag{2.21}$$

Expansion of the perturbed wave functions $|\Psi_n^{(m)}\rangle$ in the complete set of eigenfunctions of the zero-order Hamiltonian $|\Phi_n\rangle$,

$$|\Psi_n^{(m)}\rangle = \sum_k a_{kn}^{(m)}|\Phi_k\rangle = \sum_k |\Phi_k\rangle\langle\Phi_k|\Psi_n^{(m)}\rangle \tag{2.22}$$

leads to the conditional equation for the expansion coefficients $a_{kn}^{(m)}$, by multiplying the mth-order equation (eq. 2.16) with $\langle\Phi_k|$,

$$\underbrace{\langle\Phi_k|(E_n^{(0)} - \mathcal{H}_0)|}_{=(E_n^{(0)}-E_k^{(0)})\langle\Phi_k|}\Psi_n^{(m)}\rangle = \underbrace{\langle\Phi_k|\mathcal{V}|\Psi_n^{(m-1)}\rangle}_{\sum_j\langle\Phi_k|\mathcal{V}|\Phi_j\rangle\langle\Phi_j|\Psi_n^{(m-1)}\rangle} - \sum_{l=0}^{m-1} E_n^{(m-l)}\underbrace{\langle\Phi_k|\Psi_n^{(l)}\rangle}_{=a_{kn}^{(l)}}$$
$$(E_n^{(0)} - E_k^{(0)})a_{kn}^{(m)} = \sum_j \langle\Phi_k|\mathcal{V}|\Phi_j\rangle a_{jn}^{(m-1)} - \sum_{l=0}^{m-1} E_n^{(m-l)} a_{kn}^{(l)}. \tag{2.23}$$

Since, there exists no equation, that determines $a_{nn}^{(m)}$, intermediate normalization can be chosen once more,

$$\langle\Phi_n|\Psi_n^{(m)}\rangle = 0 \qquad (m > 0)$$
$$a_{nn}^{(m)} = \delta_{m0}. \tag{2.24}$$

The explicit form of the first-order equations become,

$$\begin{aligned}(E_n^{(0)} - E_k^{(0)})a_{kn}^{(1)} &= \langle\Phi_k|\mathcal{V}|\Phi_n\rangle - E_n^{(1)}\underbrace{a_{kn}^{(0)}}_{=\delta_{kn}} \\ &= \langle\Phi_k|\mathcal{V}|\Phi_n\rangle \qquad (n \neq k) \\ \Leftrightarrow a_{kn}^{(1)} &= \frac{\langle\Phi_k|\mathcal{V}|\Phi_n\rangle}{E_n^{(0)} - E_k^{(0)}} \qquad (n \neq k) \end{aligned} \tag{2.25}$$

where $|\Phi_k\rangle$ represents any state but the ground state. Finally, the well-known expression for the second-order energy is obtained,

$$\begin{aligned}E_n^{(2)} &= \langle\Phi_n|\mathcal{V}|\Psi_n^{(1)}\rangle = \sum_k a_{kn}^{(1)}\langle\Phi_n|\mathcal{V}|\Phi_k\rangle \\ &= \sum_{k(k\neq n)} \frac{|\langle\Phi_n|\mathcal{V}|\Phi_k\rangle|^2}{E_n^{(0)} - E_k^{(0)}}.\end{aligned} \tag{2.26}$$

Analogue considerations yield the expressions for $E_n^{(3)}, E_n^{(4)}, \ldots$ but for our purposes the expressions up to second-order are sufficient. The famous Wigner's (2n+1) rule states that knowledge of the mth-order correction to the wave function $\Psi_n^{(m)}$ allows the direct determination of all energy expressions up to $(2m+1)$th-order. In the case of the third-order energy correction the knowledge of the second-order correction to the wave function is formally required. This can be circumvented by resolving eq. 2.14 for the second-order wave function correction,

$$|\Psi_n^{(2)}\rangle = \left(\mathcal{H}_0 - E_n^{(0)}\right)^{-1}\left[\left(E_n^{(1)} - \mathcal{V}\right)|\Psi_n^{(1)}\rangle + E_n^{(2)}|\Psi_n^{(0)}\rangle\right] \tag{2.27}$$

projecting from the left on $|\Phi_k\rangle$ for $k \neq n$ yields,

$$\langle\Phi_k|\Psi_n^{(2)}\rangle = \left(E_k^{(0)} - E_n^{(0)}\right)^{-1}\left[\langle\Phi_k|\left(E_n^{(1)} - \mathcal{V}\right)|\Psi_n^{(1)}\rangle\right]. \tag{2.28}$$

Insertion of eq. 2.28 into eq. 2.20 leads finally to the third-order energy expression.

$$\begin{aligned}E_n^{(3)} &= \langle\Phi_n|\mathcal{V}|\Psi_n^{(2)}\rangle \\ &= \sum_{n\neq k}\langle\Phi_n|\mathcal{V}|\Phi_k\rangle\langle\Phi_k|\Psi_n^{(2)}\rangle \\ &= \sum_{n\neq k}\frac{\langle\Phi_n|\mathcal{V}|\Phi_k\rangle\langle\Phi_k|\mathcal{V}|\Psi_n^{(1)}\rangle}{E_n^{(0)} - E_k^{(0)}} - E_n^{(1)}\frac{\langle\Phi_n|\mathcal{V}|\Phi_k\rangle\langle\Phi_k|\Psi_n^{(1)}\rangle}{E_n^{(0)} - E_k^{(0)}}\end{aligned} \tag{2.29}$$

2.1.3. Møller-Plesset Perturbation Theory

The suggestion of using the HF wave function and the corresponding HF energy as 0th-order approximation to the exact wave function and energy, respectively, was first proposed by Møller and Plesset in 1934. [2] The Fock operator $\mathcal{F}$ is assigned to the appropriate Hamiltonian $\mathcal{H}_0$ of the unperturbed problem,

$$\mathcal{H}_0 = \mathcal{F} = \sum_i \hat{h}(i) + \mathcal{V}^{HF}(i) = \sum_i \hat{h}(i) + \sum_i \sum_j \Big[\mathcal{J}_j(i) - \mathcal{K}_j(i)\Big] \tag{2.30}$$

$$F_{pq} = h_{pq} + \sum_j \underbrace{\Big[\langle p|\mathcal{J}_j|q\rangle - \langle p|\mathcal{K}_j|q\rangle\Big]}_{\langle pj|qj\rangle - \langle pj|jq\rangle = \langle pj||qj\rangle}. \tag{2.31}$$

The Fock operator $\mathcal{F}$ is an effective one-electron operator, which describes the motion of each electron in the averaged field of all other (N-1) electrons (mean-field theory). The perturbation $\mathcal{V}$ is then defined as the difference between the exact Hamiltonian $\mathcal{H}$ and the zero-order Hamiltonian $\mathcal{H}_0$,

$$\mathcal{H} = \sum_i \hat{h}(i) + \sum_i \sum_{j<i} \hat{r}_{ij}^{-1} \tag{2.32}$$

$$\mathcal{V} = \sum_i \sum_{j<i} \hat{r}_{ij}^{-1} - \sum_i \sum_j \Big[\mathcal{J}_j(i) - \mathcal{K}_j(i)\Big]. \tag{2.33}$$

This perturbation is often referred to as fluctuation potential, as it describes the difference between the instantaneous electron-electron interaction and the mean field treatment. The expansion of the perturbed ground state wave functions becomes,

$$|\Psi_0^{(0)}\rangle = |\Phi_0^{HF}\rangle \tag{2.34}$$

$$|\Psi_0^{(m>0)}\rangle = \sum_{k(k\neq 0)} a_{k0}^{(m)} |\Phi_k\rangle = \sum_{ia} t_a^{i(m)} |\Phi_i^a\rangle + \frac{1}{4} \sum_{ijab} t_{ab}^{ij(m)} |\Phi_{ij}^{ab}\rangle + ... \tag{2.35}$$

where the mth-order expansion coefficients $a_{k0}^{(m)}$ have been replaced by the corresponding single, double, ... excitation amplitudes $t_a^{i(m)}, t_{ab}^{ij(m)}, ...$ The zero-order wave functions $|\Phi_k\rangle$, which are the eigenfunctions to the higher order eigenvalues, correspond to single, double, ... excited determinants. Insertion of the Møller-Plesset (MP) partitioning of the Hamiltonian into the energy expressions, eqs. 2.17, 2.18 and 2.19, yields the corresponding MPm energy terms for the ground state,

$$E_0^{(0)} = \langle \Phi_0 | \mathcal{H}_0 | \Psi_0^{(0)} \rangle = \sum_i \varepsilon_i \tag{2.36}$$

$$E_0^{(1)} = \langle \Phi_0 | \mathcal{V} | \Psi_0^{(0)} \rangle = -\frac{1}{2} \sum_{ij} \langle ij||ij\rangle \tag{2.37}$$

$$E_0^{(2)} = \langle \Phi_0 | \mathcal{V} | \Psi_0^{(1)} \rangle = \frac{1}{4} \sum_{ijab} t_{ab}^{ij(1)} \langle \Phi_0 | \mathcal{V} | \Phi_{ij}^{ab} \rangle = \frac{1}{4} \sum_{ijab} t_{ab}^{ij(1)} \langle ij||ab\rangle. \tag{2.38}$$

The sum of the zero-order and first-order energies yield the Hartree-Fock energy. Thus, the correlation energy first appears in second-order MP (MP2) perturbation theory. The singly excited determinants do not contribute to the second-order energy correction, since they have no nonzero matrix elements with the HF determinant due to Brillouins' theorem.

The first-order double excitation amplitudes are defined by eq. 2.25,

$$t_{ab}^{ij(1)} = -\frac{\langle \Phi_{ij}^{ab}|\mathcal{V}|\Phi_0\rangle}{E_0^{(0)} - E_2^{(0)}} = -\frac{\langle ab||ij\rangle}{\varepsilon_a + \varepsilon_b - \varepsilon_i - \varepsilon_j}. \tag{2.39}$$

Finally, the well-known MP2 energy correction is derived,

$$E_0^{(2)} = -\frac{1}{4}\sum_{ijab}\frac{\left|\langle ij||ab\rangle\right|^2}{\varepsilon_a + \varepsilon_b - \varepsilon_i - \varepsilon_j}. \tag{2.40}$$

Higher order MP2 energy expressions can be obtained similarly, e.g. the third-order energy correction is given as [3],

$$E_0^{(3)} = -\frac{1}{4}\sum_{ijab}\langle ij||ab\rangle b_{ab}^{ij} \tag{2.41}$$

with

$$b_{ab}^{ij} = (\varepsilon_a + \varepsilon_b - \varepsilon_i - \varepsilon_j)^{-1}\left[\frac{1}{2}\left(\sum_{cd}\langle ab||cd\rangle t_{cd}^{ij(1)} + \sum_{kl}\langle kl||ij\rangle t_{ab}^{kl(1)}\right) - \sum_{kc}P(ij)P(ab)\langle kb||jc\rangle t_{ac}^{ik(1)}\right] \tag{2.42}$$

where P permutes the indices i, j and a, b by simultaneously accounting for the sign.

2.2. The Hylleraas functional

The idea of the Hylleraas variation principle is to obtain the even-order energy corrections and the corresponding perturbed wave functions by minimizing a functional of the wave function in question. The Hylleraas functional for the second-order MP2 energy is obtained by multiplying the first-order equation (2.13) by $\langle\Psi_n^{(1)}|$,

$$\langle\Psi_n^{(1)}|\mathcal{H}_0 - E_n^{(0)}|\Psi_n^{(1)}\rangle = \langle\Psi_n^{(1)}|E_n^{(1)} - \mathcal{V}|\Phi_n\rangle \tag{2.43}$$

and adding the equation for the second-order energy (2.19),

$$E_n^{(2)} = \langle\Phi_n|\mathcal{V} - E_n^{(1)}|\Psi_n^{(1)}\rangle + \langle\Psi_n^{(1)}|\mathcal{V} - E_n^{(1)}|\Phi_n\rangle + \langle\Psi_n^{(1)}|\mathcal{H}_0 - E_n^{(0)}|\Psi_n^{(1)}\rangle. \tag{2.44}$$

The Hylleraas functional is then defined as,

$$\mathcal{J}_2[\Psi] = 2\Re\mathfrak{e}\langle\Psi|\mathcal{V} - E_n^{(1)}|\Phi_n\rangle + \langle\Psi|\mathcal{H}_0 - E_n^{(0)}|\Psi\rangle \tag{2.45}$$

and it is obvious, that the insertion of $\Psi_n^{(1)}$ yields the second-order energy $E_n^{(2)}$. By varying the Hylleraas functional and requiring that $\delta\mathcal{J}_2[\Psi] = 0$ for any $\delta\Psi$, the first-order equation is obtained,

$$\mathcal{V} - E_n^{(1)}|\Phi_n\rangle + \mathcal{H}_0 - E_n^{(0)}|\Psi\rangle = 0 \tag{2.46}$$

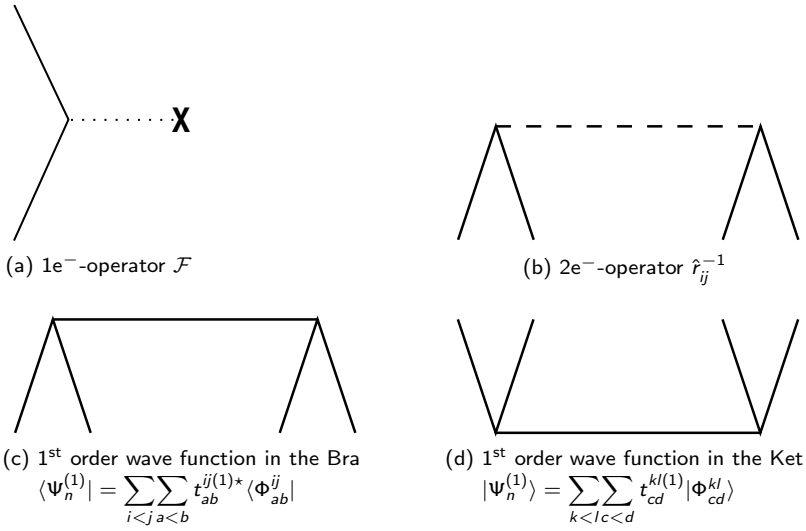

Figure 2.1.: Required diagram elements to derive the exact form of the Hylleraas functional for MP2, employing the diagrammatic method.

for which $\Psi = \Psi_n^{(1)}$ represents a solution. By enforcing intermediate normalization, the Hylleraas functional simplifies to,

$$\mathcal{J}_2[\Psi] = 2\Re\mathfrak{e}\langle\Psi|\mathcal{V}|\Phi_n\rangle + \langle\Psi|\mathcal{H}_0 - E_n^{(0)}|\Psi\rangle. \tag{2.47}$$

Finally, it can be shown, that if $E_n^{(0)}$ is the lowest eigenvalue of $\mathcal{H}_0$ then $\mathcal{J}_2[\Psi]$ is an upper bound to $E_n^{(2)}$. Therefore, $\Psi = \Psi_n^{(1)} + \chi$ is inserted in eq. 2.47,

$$\mathcal{J}_2[\Psi] = E_n^{(2)} + \langle\chi|\mathcal{H}_0 - E_n^{(0)}|\chi\rangle. \tag{2.48}$$

If $E_n^{(0)}$ is the lowest eigenvalue of $\mathcal{H}_0$ then the integral $\langle\chi|\mathcal{H}_0 - E_n^{(0)}|\chi\rangle$ is nonnegative and is only zero if χ is the corresponding eigenfunction. Thus, it holds that $\mathcal{J}_2[\Psi] \geq E_n^{(2)}$ if Φ_0 is an exact eigenfunction of $\mathcal{H}_0$, and therefore the first-order wave function and the second-order energy can be obtained by minimizing the Hylleraas functional of an arbitrary trial function Ψ.

Explicit formulation of Hylleraas MP2

In this subsection the explicit formulae for the Hylleraas MP2 Ansatz are derived via diagrammatic techniques. The first reformulation of MP2 theory in terms of the Hylleraas functional was presented by Pulay and Saebø and leads to an orbital-invariant MP2 theory. [26] Starting from the general expression of the Hylleraas functional (eq. 2.47) and inserting the first-order wave function, yields,

$$\mathcal{J}_2[\Psi_n^{(1)}] = 2\Re\mathfrak{e}\langle\Psi_n^{(1)}|\mathcal{V}|\Phi_n\rangle + \langle\Psi_n^{(1)}|\mathcal{H}_0 - E_n^{(0)}|\Psi_n^{(1)}\rangle. \tag{2.49}$$

In Fig. 2.1 the required diagrammatic representations of the operators and the wave functions are illustrated. Combining the corresponding diagram elements and labeling yields the three diagrams displayed in Fig. 2.2. The lines labeled with the indices $i, j, k, ...$ correspond to hole lines, since they annihilate an electron in an orbital occupied in the HF reference determinant. In contrast, the indices $a, b, c, ...$ indicate particle lines, in that they create an electron in a virtual orbital, which is unoccupied in the HF reference

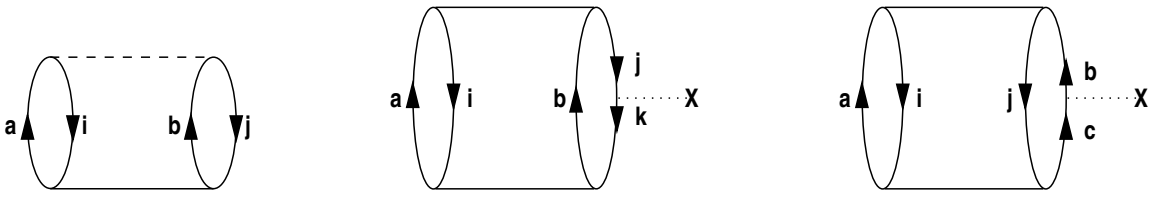

(a) $\frac{1}{4}\sum_{ijab} t_{ab}^{ij(1)}\langle ij||ab\rangle$ (b) $-\frac{1}{2}\sum_{ijkab} t_{ab}^{ij(1)\star} t_{ab}^{ik(1)} F_{kj}$ (c) $\frac{1}{2}\sum_{ijabc} t_{ab}^{ij(1)\star} t_{ac}^{ij(1)} F_{bc}$

Figure 2.2.: Constructed diagrams corresponding to eq. 2.49.

determinant. Thus, the following explicit expression for the MP2 Hylleraas functional is obtained,

$$\mathcal{E}_2[\mathbf{t}] = \left\{ \frac{1}{2}\sum_{ijab}\langle ij||ab\rangle t_{ab}^{ij(1)} - \frac{1}{2}\sum_{ijkab} F_{kj} t_{ab}^{ij(1)} t_{ab}^{ik(1)} + \frac{1}{2}\sum_{ijabc} F_{cb} t_{ab}^{ij(1)} t_{ac}^{ij(1)} \right\}. \tag{2.50}$$

The MP2 Hylleraas functional now becomes a functional of the MP2 double excitation amplitudes, since the expansion of the perturbed wave function in the basis of the zero-order wave function has been inserted (eq. 2.35). The MP2 residual R_{ij}^{ab} is in general defined as,

$$\langle \Phi_{ij}^{ab}|\mathcal{H}|\Phi_0\rangle + \langle \Phi_{ab}^{ij}|\mathcal{H}_0 - \mathcal{E}_0|\Psi_n^{(1)}\rangle = 0 \tag{2.51}$$

$$R_{ab}^{ij} = \langle ij||ab\rangle - \sum_k \left(t_{ab}^{kj(1)} F_{ki} + t_{ab}^{ik(1)} F_{kj} \right) + \sum_c \left(t_{ac}^{ij(1)} F_{bc} + t_{cb}^{ij(1)} F_{ac} \right) = 0 \tag{2.52}$$

and the derivative of the MP2 Hylleraas energy functional with respect to the MP2 double excitation amplitudes is,

$$\frac{\partial \mathcal{E}_2}{\partial t_{ab}^{ij(1)}} = 2R_{ab}^{ij} = 0. \tag{2.53}$$

If eq. 2.53 is fulfilled, the conditional equation for the MP2 amplitudes assuming canonical HF orbitals, corresponds exactly to the first-order amplitude equation derived from conventional MP2 theory (eq. 2.39).

$$t_{ab}^{ij(1)} = -\frac{\langle ab||ij\rangle}{\varepsilon_a + \varepsilon_b - \varepsilon_i - \varepsilon_j}. \tag{2.54}$$

Rewriting the MP2 Hylleraas functional shows, that the conventional MP2 energy expression is obtained, if the Hylleraas functional is stationary with respect to small changes in the first-order amplitudes.

$$\mathcal{E}_2[\mathbf{t}] = \frac{1}{4}\sum_{ijab}\left(\langle ij||ab\rangle + R_{ab}^{ij} \right) t_{ab}^{ij(1)} \tag{2.55}$$

Hence, the MP2 double excitation amplitudes can be regarded as having been optimized by minimizing the Hylleraas functional.

2.3. Derivative Theory

2.3.1. Density Matrices

The construction of a density matrix [27] from an approximate wave function represents a convenient way to treat one- and two-electron properties. The first-order reduced density matrix is defined as,

$$\gamma(\mathbf{x}_1|\mathbf{x}_1') = N \int \Psi(\mathbf{x}_1, \cdots, \mathbf{x}_N)\Psi^\star(\mathbf{x}_1', \cdots, \mathbf{x}_N) d\mathbf{x}_2 \cdots d\mathbf{x}_N = \sum_{pq} \gamma_{pq}\psi_p(\mathbf{x}_1)\psi_q^\star(\mathbf{x}_1'). \tag{2.56}$$

with the diagonal elements representing the probability of finding an electron in $d\mathbf{x}_1$ at $\mathbf{x}_1$, independent of the location of all other $(N-1)$ electrons,

$$\gamma(\mathbf{x}_1|\mathbf{x}_1) = \rho(\mathbf{x}_1). \tag{2.57}$$

The expectation value of an arbitrary one-electron operator $\mathcal{O}(\mathbf{x})$ can then be expressed by,

$$\left\langle \Psi \middle| \mathcal{O}(\mathbf{x}) \middle| \Psi \right\rangle = \sum_{pq} \gamma_{pq} \langle \psi_p | \mathcal{O} | \psi_q \rangle_{x=x'} = \sum_{pq} \gamma_{pq} O_{pq}. \tag{2.58}$$

The second-order reduced density matrix is analogously defined as,

$$\begin{aligned} \Gamma(\mathbf{x}_1, \mathbf{x}_2|\mathbf{x}_1', \mathbf{x}_2') &= N(N-1) \int \Psi(\mathbf{x}_1, \mathbf{x}_2, \cdots, \mathbf{x}_N)\Psi^\star(\mathbf{x}_1', \mathbf{x}_2', \cdots, \mathbf{x}_N) d\mathbf{x}_3 \cdots d\mathbf{x}_N \\ &= \sum_{pqrs} \Gamma_{pqrs}\psi_p(\mathbf{x}_1)\psi_q^\star(\mathbf{x}_1')\psi_r(\mathbf{x}_2)\psi_s^\star(\mathbf{x}_2'). \end{aligned} \tag{2.59}$$

Thus, the expectation value of the Born-Oppenheimer Hamiltonian $\mathcal{H}_{BO}$ over the HF determinant can be rewritten as,

$$\langle \Psi | \mathcal{H}_{BO} | \Psi \rangle = \sum_{pq} h_{pq}\gamma_{pq} + \frac{1}{2} \sum_{pqrs} g_{pqrs}\Gamma_{pqrs} \tag{2.60}$$

where h_{pq} and g_{pqrs} represent the matrix elements of the one- and two-electron operators, respectively. Furthermore, molecular properties represented as first derivatives of the energy with respect to an external perturbation, can always be written in the form,

$$\frac{dE}{d\lambda} = \sum_{pq} \gamma_{pq} h_{pq}^{\{\lambda\}} + \sum_{pq} W_{pq} S_{pq}^{(\lambda)} + \sum_{pqrs} \Gamma_{pqrs} g_{pqrs}^{(\lambda)}. \tag{2.61}$$

In eq. 2.61, W_{pq} is the energy-weighted density matrix and $S_{pq}^{(\lambda)}$ represents the derivative of the overlap matrix element with respect to the external perturbation. The index (λ) indicates the explicit derivative of the basis functions with respect to the perturbation parameter λ. $\{\lambda\}$ refers to the explicit derivative of basis functions and operators. If the basis functions are independent of the perturbation, e.g. in the case of an external electric field, the derivative simplifies to,

$$\frac{dE}{d\lambda} = \sum_{pq} \gamma_{pq} h_{pq}^{[\lambda]} \tag{2.62}$$

with $[\lambda]$ denoting the derivative of the operator. A convenient formula for the calculation of reduced density matrices in second quantization is,

$$\gamma_{pq} = \langle \Psi | a_q^p | \Psi \rangle \tag{2.63}$$

$$\Gamma_{pqrs} = \langle \Psi | a_r^p a_s^q - \delta_r^q a_s^p | \Psi \rangle \tag{2.64}$$

where a_q^p represents a replacement operator, which annihilates one electron in spin orbital ψ_q and creates an electron in ψ_p. In eq. 2.64 it was made use of the fact, that for a single determinant wave function the second-order density matrix is fully determined from the reduced one-particle density matrix.

2.3.2. Linear Response Theory

The calculation of molecular properties, which are specific for a given electronic state, can be interpreted as the 'response' of the system to an external perturbation. The energy can then be expanded as a Taylor series around the energy in the unperturbed case E_0,

$$E(\lambda) = E_0 + \left.\frac{dE}{d\lambda}\right|_{\lambda=0} \lambda + \frac{1}{2}\left.\frac{d^2E}{d\lambda^2}\right|_{\lambda=0} \lambda^2 + \dots . \tag{2.65}$$

Whereas first-order properties involve the first derivative (gradient) of the energy with respect to λ, second-order properties require the calculation of the corresponding second derivative, etc. These derivatives can be easily calculated via finite-differentiation techniques, but besides its formal simplicity these approaches recover some disadvantages, i.e. the limited accuracy and the tremendous computational effort. Therefore, analytic derivatives are preferred for the calculation of molecular properties.

Introduction to General Derivative Theory

The energy as well as the wave function incorporate a specific dependence on the perturbation. The explicit dependence on the perturbation is given through the Hamiltonian and through the basis functions, respectively, whereas the implicit dependence occurs through the wave function parameters, e.g. the molecular orbital (MO) coefficients. The energy then becomes a functional of the perturbation λ, and the perturbation dependent wave function parameters $c(\lambda)$,

$$E = E[\lambda, \mathbf{c}(\lambda)]. \tag{2.66}$$

Differentiation of the energy with respect to the corresponding perturbation leads to the following gradient expression,

$$\frac{dE}{d\lambda} = \left(\frac{\partial E}{\partial \lambda}\right) + \left(\frac{\partial E}{\partial c}\right)\left(\frac{\partial c}{\partial \lambda}\right). \tag{2.67}$$

In the case of variationally determined wave function parameters, the energy is stationary with respect to changes in c and the partial derivative $\left(\frac{\partial E}{\partial c}\right)$ vanishes. Thus, the general derivative expression simplifies to,

$$\frac{dE}{d\lambda} = \left(\frac{\partial E}{\partial \lambda}\right) \tag{2.68}$$

and there is no need to determine the perturbed wave function parameters. The expression for the second energy derivative takes the form,

$$\frac{d^2E}{d\lambda d\kappa} = \left(\frac{\partial^2 E}{\partial\lambda\partial\kappa}\right) + \left(\frac{\partial^2 E}{\partial\lambda\partial c}\right)\left(\frac{\partial c}{\partial\kappa}\right) + \left(\frac{\partial^2 E}{\partial\kappa\partial c}\right)\left(\frac{\partial c}{\partial\lambda}\right) + \left(\frac{\partial^2 E}{\partial c^2}\right)\left(\frac{\partial c}{\partial\lambda}\frac{\partial c}{\partial\kappa}\right) + \left(\frac{\partial E}{\partial c}\right)\left(\frac{\partial^2 c}{\partial\lambda\partial\kappa}\right) \quad (2.69)$$

whereas the last term of eq. 2.69 vanishes for variational wave functions.

Derivatives of the Hartree-Fock Energy

The Hartree-Fock energy is defined as,

$$E_{HF} = \sum_i h_{ii} + \frac{1}{2}\sum_{ij}\langle ij||ij\rangle = \sum_{\mu\nu} P_{\mu\nu}h_{\mu\nu} + \frac{1}{2}\sum_{\mu\nu\kappa\tau} P_{\mu\nu}P_{\kappa\tau}\langle\mu\kappa||\nu\tau\rangle \quad (2.70)$$

with $P_{\mu\nu}$ denoting the SCF density matrix,

$$P_{\mu\nu} = \sum_i c^\star_{\mu i}c_{\nu i}. \quad (2.71)$$

The derivative of the HF energy under the additional constraint enforcing the orthonormality of the MO coefficients can be derived in the AO basis as,

$$\frac{dE_{HF}}{d\lambda} = \sum_{\mu\nu} P_{\mu\nu}h^{\{\lambda\}}_{\mu\nu} + \frac{1}{2}\sum_{\mu\nu\kappa\tau} P_{\mu\nu}P_{\kappa\tau}\langle\mu\kappa||\nu\tau\rangle^{(\lambda)} - \sum_{\mu\nu} W_{\mu\nu}S^{(\lambda)}_{\mu\nu}. \quad (2.72)$$

In eq. 2.72 $\{\lambda\}$ indicates the derivative of the operator and of the basis functions with respect to λ, whereas (λ) denotes only the basis function derivative itself. The energy-weighted density matrix $W_{\mu\nu}$ arises from the orthonormality constraint and is defined as,

$$W_{\mu\nu} = \sum_i c^\star_{\mu i}\varepsilon_i c_{\nu i}. \quad (2.73)$$

The first-order derivative of the SCF energy with respect to the perturbation λ can be rewritten in terms of the 1- and 2-particle density matrices as,

$$\frac{dE_{HF}}{d\lambda} = \sum_{\mu\nu}\gamma_{\mu\nu}h^{\{\lambda\}}_{\mu\nu} + \sum_{\mu\nu\kappa\tau}\Gamma_{\mu\nu\kappa\tau}\langle\mu\nu|\kappa\tau\rangle^{(\lambda)} - \sum_{\mu\nu} W_{\mu\nu}S^{(\lambda)}_{\mu\nu}. \quad (2.74)$$

with the density matrices given by,

$$\gamma_{\mu\nu} = P_{\mu\nu} \quad (2.75)$$

$$\Gamma_{\mu\nu\kappa\tau} = \frac{1}{2}P_{\mu\kappa}P_{\nu\tau} - \frac{1}{2}P_{\mu\tau}P_{\nu\kappa}. \quad (2.76)$$

The derivative of the SCF density matrix is not required for the calculation of the HF gradient, since the MO coefficients are the variational wave function parameters in HF theory. The first HF energy derivative simplifies in the case of perturbation independent basis functions to,

$$\frac{dE_{HF}}{d\lambda} = \sum_{\mu\nu} P_{\mu\nu}h^{[\lambda]}_{\mu\nu} \quad (2.77)$$

where $[\lambda]$ refers to the derivative of the one-electron operator.

The second derivative of the HF energy yields the following expression,

$$\frac{d^2E_{HF}}{d\lambda d\kappa} = \sum_{\mu\nu} P_{\mu\nu} h^{\{\lambda,\kappa\}}_{\mu\nu} + \frac{1}{2}\sum_{\mu\nu\kappa\tau} P_{\mu\nu}P_{\kappa\tau}\langle\mu\kappa||\nu\tau\rangle^{(\lambda,\kappa)} - \sum_{\mu\nu} W_{\mu\nu}S^{(\lambda,\kappa)}_{\mu\nu} + \sum_{\mu\nu} P^{\langle\kappa\rangle}_{\mu\nu}\left(h^{\{\lambda\}}_{\mu\nu} + \sum_{\kappa\tau} P_{\kappa\tau}\langle\mu\kappa||\nu\tau\rangle^{(\lambda)}\right) - \sum_{\mu\nu} W^{\langle\kappa\rangle}_{\mu\nu}S^{(\lambda)}_{\mu\nu}, \tag{2.78}$$

with $\langle\kappa\rangle$ denoting the MO coefficient derivatives and

$$P^{\langle\kappa\rangle}_{\mu\nu} = \sum_i \left\{\frac{\partial c^\star_{\mu i}}{\partial\kappa}c_{\nu i} + c^\star_{\mu i}\frac{\partial c_{\nu i}}{\partial\kappa}\right\} \tag{2.79}$$

$$W^{\langle\kappa\rangle}_{\mu\nu} = \sum_i \left\{\frac{\partial c^\star_{\mu i}}{\partial\kappa}\varepsilon_i c_{\nu i} + c^\star_{\mu i}\varepsilon_i\frac{\partial c_{\nu i}}{\partial\kappa}\right\} + \sum_i c^\star_{\mu i}\frac{\partial\varepsilon_i}{\partial\kappa}c_{\nu i}. \tag{2.80}$$

The perturbed MO coefficients are expanded in terms of the zero-order coefficients by means of the orbital rotation or coupled-perturbed HF (CPHF) coefficients U^λ_{pi},

$$c^\lambda_{\mu i} = \sum_p U^\lambda_{pi}c_{\mu p} = \sum_p (x^\lambda_{pi} + \mathbf{i}y^\lambda_{pi})c_{\mu p}. \tag{2.81}$$

The virtual-occupied block of the CPHF coefficients are determined from differentiating the Brillouin condition,

$$\sum_{\mu\nu} c^\star_{\mu a}F_{\mu\nu}c_{\nu i} = F_{ai} = 0 \tag{2.82}$$

with

$$F_{\mu\nu} = h_{\mu\nu} + \sum_{\kappa\tau} P_{\kappa\tau}\langle\mu\kappa||\nu\tau\rangle. \tag{2.83}$$

The resulting CPHF equations take the following form,

$$(\varepsilon_a - \varepsilon_i)U^\lambda_{ai} + \sum_{jb} U^{\lambda\star}_{bj}\langle ab||ij\rangle + U^\lambda_{bj}\langle aj||ib\rangle = B^\lambda_{ai} \tag{2.84}$$

with the right-hand side given as,

$$B^\lambda_{ai} = -h^{\{\lambda\}}_{ai} - \sum_j \langle aj||ij\rangle^{(\lambda)} + \frac{1}{2}\sum_{jk} S^{(\lambda)}_{kj}\left[\langle ak||ij\rangle + \langle aj||ik\rangle\right] + \varepsilon_i S^{(\lambda)}_{ai} \tag{2.85}$$

and the derivative of the overlap matrix,

$$S^{(\lambda)}_{pq} = \sum_{\mu\nu} c^\star_{\mu p}\frac{\partial S_{\mu\nu}}{\partial\lambda}c_{\nu q}. \tag{2.86}$$

The occupied-occupied and virtual-virtual block of the U-coefficient matrix can be chosen arbitrarily as

long as the differentiated orthonormality condition is fulfilled,

$$\frac{\partial}{\partial\lambda}\left(S_{pq}=\delta_{pq}\right)$$
$$\sum_r\left(U^{\lambda\star}_{rp}S_{rq}+U^{\lambda}_{rq}S_{pr}\right)+S^{(\lambda)}_{pq}=0. \tag{2.87}$$

The most convenient choice is,

$$U^{\lambda}_{ij}=-\frac{1}{2}S^{(\lambda)}_{ij} \tag{2.88}$$
$$U^{\lambda}_{ab}=-\frac{1}{2}S^{(\lambda)}_{ab}. \tag{2.89}$$

If the basis functions are independent on the perturbation the right-hand side simplifies to,

$$B^{\lambda}_{ai}=-h^{[\lambda]}_{ai}. \tag{2.90}$$

Eq. 2.84 differs for real and imaginary perturbations as can be shown by resolving the U-coefficients into real and imaginary parts,

$$x^{\lambda}_{ai}(\varepsilon_a-\varepsilon_i)+\sum_{jb}x^{\lambda}_{bj}\Big[\langle ab||ij\rangle+\langle aj||ib\rangle\Big]+\mathbf{i}y^{\lambda}_{ai}(\varepsilon_a-\varepsilon_i)+\sum_{jb}\mathbf{i}y^{\lambda}_{bj}\Big[-\langle ab||ij\rangle+\langle aj||ib\rangle\Big]=B^{\lambda}_{ai}. \tag{2.91}$$

Therefore, different sets of CPHF equations have to be solved for pure real ($\Re$) and pure imaginary ($\Im$) perturbations,

$$x^{\lambda}_{ai}(\varepsilon_a-\varepsilon_i)+\sum_{jb}x^{\lambda}_{bj}\Big[\langle ab||ij\rangle+\langle aj||ib\rangle\Big]\equiv\sum_{jb}A^{(\Re)}_{ai,bj}x^{\lambda}_{bj}=B^{(\Re)\lambda}_{ai} \tag{2.92}$$
$$\mathbf{i}y^{\lambda}_{ai}(\varepsilon_a-\varepsilon_i)+\sum_{jb}\mathbf{i}y^{\lambda}_{bj}\Big[-\langle ab||ij\rangle+\langle aj||ib\rangle\Big]\equiv\mathbf{i}\sum_{jb}A^{(\Im)}_{ai,bj}y^{\lambda}_{bj}=B^{(\Im)\lambda}_{ai}. \tag{2.93}$$

The solution of the CPHF equations is obtained iteratively.

2.4. Derivatives of the Second-Order Møller-Plesset Energy Correction

2.4.1. The MP2 Energy

The expression for the Hylleraas MP2 energy functional is,

$$\mathcal{E}_2[\mathbf{t}]=\left\{\frac{1}{4}\sum_{ijab}\langle ij||ab\rangle t^{ij(1)}_{ab}+\langle ab||ij\rangle t^{ij(1)\star}_{ab}+\sum_{ij}D_{ij}F_{ij}+\sum_{ab}D_{ab}F_{ab}\right\} \tag{2.94}$$

where

$$D_{ij}=-\frac{1}{2}\sum_{kab}t^{ki(1)}_{ab}t^{kj(1)\star}_{ab} \tag{2.95}$$
$$D_{ab}=\frac{1}{2}\sum_{ijc}t^{ij(1)\star}_{ca}t^{ij(1)}_{cb} \tag{2.96}$$

represent the occupied-occupied and virtual-virtual block of the unrelaxed MP2 one-particle density matrix obtained as expectation value of the spin orbital replacement operators over the first-order wave function. In the following the index $^{(1)}$, which indicates the first-order MP2 amplitudes, is skipped, since no higher-order amplitudes are considered.

In the MP2 Hylleraas functional the set of amplitudes **t** represents the variational wave function parameters, whereas the MO coefficients **c** are fixed.

Density Fitting

The Coulomb matrix can be efficiently approximated by expanding products of basis functions in an extended auxiliary basis set that is usually 2–4 times larger than the orbital basis set. [22, 28, 29] In terms of the 'Resolution of the Identity' (RI) approximation, the Coulomb matrix (RI-J) is given as,

$$J_{\mu\nu} = \sum_{\kappa\tau} P_{\kappa\tau} \langle \mu\kappa | \nu\tau \rangle \approx \sum_{K} d_K (\mu\nu | K). \tag{2.97}$$

It is advantageous here to switch to chemists notation for the two-electron repulsion integrals. The 3-index two-electron repulsion integral is,

$$(\mu\nu | K) = \int \mu(\mathbf{r}_1)\nu(\mathbf{r}_1) r_{12}^{-1} K(\mathbf{r}_2) d\mathbf{r}_1 d\mathbf{r}_2 \tag{2.98}$$

where $K(\mathbf{r_2})$ is a member of the Coulomb auxiliary basis set $\{\eta_K\}$. The vector d_K represents the density in the auxiliary basis which is best obtained from the linear equation system $\mathbf{Vd} = \mathbf{g}$, with $V_{KL} = (K|L)$ and $g_K = \sum_{\kappa\tau} P_{\kappa\tau}(\kappa\tau|K)$, containing two- and 3-index repulsion integrals. It has been shown by Vahtras, Almlöf and Feyereisen that the optimal expansion coefficients are obtained by minimizing the residual repulsion. [22] The linear equation system is most efficiently solved by employing the Cholesky decomposition, which takes advantage of the decomposition of a symmetric, positive definite matrix into the product of a lower triangular matrix and its conjugate transpose. The Cholesky decomposition is roughly twice as efficient as the LU decomposition for solving linear equation systems, since the solution of a triangular set of equations is quite trivial.
An improved variant of this method for the calculation of the near-field part of the Coulomb interaction has been implemented in the ORCA program package and has been dubbed 'Split-RI-J'. [30] This algorithm is most suitable for basis sets with many high angular momentum functions for wich a factor of $\sim$2 is gained compared to the standard RI-J implementation. Excellent Coulomb fitting basis sets have been developed by Ahlrichs and co-workers for almost the entire periodic table. [28, 29]

Feyereisen *et al.* [21] proposed the 'Resolution of the Identity' approximation to MP2 energy calculations (RI-MP2) in the mid 1990s. The MP2 energy expression within the RI framework becomes,

$$E_{MP2} = \frac{1}{4} \sum_{ijab} \langle ij || ab \rangle t_{ab}^{ij} \tag{2.99}$$

$$E_{RI-MP2} = \frac{1}{2} \sum_{iaP} (ia|P) \Gamma_{ia}^{\prime P} \tag{2.100}$$

where the 3-index 2-particle density is defined as,

$$\Gamma'^{P}_{ia} = \sum_{jbQ} V^{-1}_{PQ}(Q|jb)t^{ij(RI)}_{ab} \tag{2.101}$$

$$\Gamma'^{P}_{ai} = \sum_{jbQ} V^{-1}_{PQ}(Q|bj)t^{ij\star(RI)}_{ab}. \tag{2.102}$$

The RI-MP2 double excitation amplitudes t^{ij}_{ab} are given as,

$$t^{ij(RI)}_{ab} = -\sum_{P} \frac{B^{P}_{ai}B^{P}_{bj} - B^{P}_{aj}B^{P}_{bi}}{\varepsilon_a + \varepsilon_b - \varepsilon_i - \varepsilon_j} \tag{2.103}$$

with

$$B^{P}_{ai} = \sum_{Q}(ai|Q)V^{-1/2}_{QP}. \tag{2.104}$$

The calculation of the MP2 energy in the RI approximation affords computational savings of at least a factor of ∼20 for medium size molecules compared to conventional MP2, as has been recently reported in Ref. [31]. The error in the total energies calculated with the correlation fitting basis sets [32–34], denoted $P, Q, ...$, is usually below 0.5 kcal/mol. [31]

2.4.2. The First Derivative of the MP2 Energy

The first derivative of the MP2 energy functional with respect to an arbitrary perturbation λ is,

$$\frac{d\mathcal{E}_2}{d\lambda} = \left(\frac{\partial\mathcal{E}_2}{\partial\lambda}\right) + \left(\frac{\partial\mathcal{E}_2}{\partial c}\right)\left(\frac{\partial c}{\partial\lambda}\right) + \left(\frac{\partial\mathcal{E}_2}{\partial t}\right)\left(\frac{\partial t}{\partial\lambda}\right). \tag{2.105}$$

The last term in eq. 2.105 vanishes, since the MP2 Hylleraas functional is stationary with respect to changes in the double excitation amplitudes. Thus, the MP2 gradient becomes,

$$\frac{\partial\mathcal{E}_2}{\partial\lambda} = \frac{1}{4}\sum_{ijab}\left[\langle ij||ab\rangle^{(\lambda)} + \langle ij||ab\rangle^{\langle\lambda\rangle}\right]t^{ij}_{ab} + \left[\langle ab||ij\rangle^{(\lambda)} + \langle ab||ij\rangle^{\langle\lambda\rangle}\right]t^{ij\star}_{ab} + \sum_{pq} D'_{pq}\left[F^{\{\lambda\}}_{pq} + F^{\langle\lambda\rangle}_{pq}\right] \tag{2.106}$$

where D'_{pq} denotes the unrelaxed MP2 density matrix, which contains no elements in its virtual-occupied and occupied-virtual blocks. Considering perturbation independent basis functions, eq. 2.106 simplifies to,

$$\frac{\partial\mathcal{E}_2}{\partial\lambda} = \frac{1}{4}\sum_{ijab}\langle ij||ab\rangle^{\langle\lambda\rangle}t^{ij}_{ab} + \langle ab||ij\rangle^{\langle\lambda\rangle}t^{ij\star}_{ab} + \sum_{pq} D'_{pq}\left[h^{[\lambda]}_{pq} + F^{\langle\lambda\rangle}_{pq}\right]. \tag{2.107}$$

In the framework of the RI approximation the derivative takes the form,

$$\frac{\partial\mathcal{E}^{(RI)}_2}{\partial\lambda} = \sum_{iaP}(ia|P)^{\langle\lambda\rangle}\Gamma'^{P}_{ia} + (ai|P)^{\langle\lambda\rangle}\Gamma'^{P}_{ai} + \sum_{pq} D'_{pq}\left[h^{[\lambda]}_{pq} + F^{\langle\lambda\rangle}_{pq}\right]. \tag{2.108}$$

Orbital Rotations

The derivatives of the MO coefficients are determined by the unitary CPHF coefficient matrix **U**, as discussed in subsection 2.3.2. Since the basis functions are assumed to be independent of the perturbation, the U coefficients fulfill the condition,

$$U_{pq}^{\lambda} = -U_{qp}^{\lambda\star}. \tag{2.109}$$

Dividing the orbital rotation coefficients in its real and imaginary parts,

$$x_{pq}^{\lambda} + \mathbf{i}y_{pq}^{\lambda} = -x_{pq}^{\lambda} + \mathbf{i}y_{qp}^{\lambda} \tag{2.110}$$

$$x_{pq}^{\lambda} = -x_{pq}^{\lambda} \tag{2.111}$$

$$y_{pq}^{\lambda} = y_{qp}^{\lambda} \tag{2.112}$$

shows, that the imaginary part is symmetric under index exchange, whereas the real part is antisymmetric. This property is important for the derivation of the MO coefficient derivatives for real, hermitian and imaginary, hermitian perturbations. As can be seen from the derivative of the SCF density matrix in eq. 2.113, the first-order density matrix is symmetric for real perturbations and antisymmetric for imaginary perturbations.

$$\begin{aligned}
\frac{\partial\rho(\mathbf{r})}{\partial\lambda} &= \sum_{\mu\nu}\frac{\partial P_{\mu\nu}}{\partial\lambda}\varphi_{\mu}^{\star}(\mathbf{r})\varphi_{\nu}(\mathbf{r}) \\
&= \sum_{\mu\nu}\left[\sum_{ip} U_{pi}^{\lambda\star}c_{\mu p}^{\star}c_{\nu i} + U_{pi}^{\lambda}c_{\mu i}^{\star}c_{\nu p}\right]\varphi_{\mu}^{\star}(\mathbf{r})\varphi_{\nu}(\mathbf{r}) \\
&= \sum_{\mu\nu}\left[\sum_{ip} x_{pi}^{\lambda}\left(c_{\mu p}^{\star}c_{\nu i} + c_{\mu i}^{\star}c_{\nu p}\right) + \mathbf{i}y_{pi}^{\lambda}\left(c_{\mu i}^{\star}c_{\nu p} - c_{\mu p}^{\star}c_{\nu i}\right)\right]\varphi_{\mu}^{\star}(\mathbf{r})\varphi_{\nu}(\mathbf{r})
\end{aligned} \tag{2.113}$$

Thus, for purely imaginary perturbations the electron density does not change to first order, if the basis functions are independent of the perturbation.

Derivation of the MP2 Gradient Expression

In this subsection the explicit expression for the MP2 gradient is derived.

Derivative of the Two-Electron Repulsion Integrals The derivative of the two-electron repulsion integrals becomes,

$$\begin{aligned}
\frac{1}{4}\sum_{ijab}\langle ij||ab\rangle^{\langle\lambda\rangle} t_{ab}^{ij} &= \frac{1}{4}\sum_{ijab}\left\{\sum_{c} U_{ci}^{\lambda\star}\langle cj||ab\rangle + U_{cj}^{\lambda\star}\langle ic||ab\rangle + \sum_{k} U_{ka}^{\lambda}\langle ij||kb\rangle + U_{kb}^{\lambda}\langle ij||ak\rangle\right\} t_{ab}^{ij} \\
&= \frac{1}{4}\sum_{ia} U_{ai}^{\lambda\star}\left\{\sum_{jbc}\langle aj||cb\rangle t_{cb}^{ij} + \langle ja||cb\rangle t_{cb}^{ji}\right\} \\
&\quad - \frac{1}{4}\sum_{ia} U_{ai}^{\lambda\star}\left\{\sum_{jkb}\langle kj||ib\rangle t_{ab}^{kj} + \langle kj||bi\rangle t_{ba}^{kj}\right\} \\
&= \frac{1}{2}\sum_{ia} U_{ai}^{\lambda\star}\left\{\sum_{jbc}\langle aj||cb\rangle t_{cb}^{ij} - \sum_{jkb}\langle kj||ib\rangle t_{ab}^{kj}\right\} \qquad (2.114)
\end{aligned}$$

$$\begin{aligned}
\frac{1}{4}\sum_{ijab}\langle ab||ij\rangle^{\langle\lambda\rangle} t_{ab}^{ij\star} &= \frac{1}{4}\sum_{ijab}\left\{\sum_{k} U_{ka}^{\lambda\star}\langle kb||ij\rangle + U_{kb}^{\lambda\star}\langle ak||ij\rangle + \sum_{c} U_{ci}^{\lambda}\langle ab||cj\rangle + U_{cj}^{\lambda}\langle ab||ic\rangle\right\} t_{ab}^{ij\star} \\
&= -\frac{1}{4}\sum_{ia} U_{ai}^{\lambda}\left\{\sum_{jkb}\langle ib||kj\rangle t_{ab}^{kj\star} + \langle bi||kj\rangle t_{ba}^{kj\star}\right\} \\
&\quad + \frac{1}{4}\sum_{ia} U_{ai}^{\lambda}\left\{\sum_{jbc}\langle cb||aj\rangle t_{cb}^{ij\star} + \langle cb||ja\rangle t_{cb}^{ji\star}\right\} \\
&= \frac{1}{2}\sum_{ia} U_{ai}^{\lambda}\left\{-\sum_{jkb}\langle ib||kj\rangle t_{ab}^{kj\star} + \sum_{jbc}\langle cb||aj\rangle t_{cb}^{ij\star}\right\}. \qquad (2.115)
\end{aligned}$$

In the RI formalism, the two-electron integral derivative takes the form,

$$\begin{aligned}
\sum_{iaP}(ia|P)^{\langle\lambda\rangle}\Gamma_{ia}'^{P} + (ai|P)^{\langle\lambda\rangle}\Gamma_{ai}'^{P} &= \sum_{ia} U_{ai}^{\lambda\star}\left\{\sum_{c}(ac|P)\Gamma_{ic}'^{P} - \sum_{k}(ki|P)\Gamma_{ka}'^{P}\right\} \\
&\quad + \sum_{ia} U_{ai}^{\lambda}\left\{-\sum_{k}(ik|P)\Gamma_{ak}'^{P} + \sum_{c}(ca|P)\Gamma_{ci}'^{P}\right\}. \qquad (2.116)
\end{aligned}$$

Fock Matrix Derivative The derivative of the Fock-matrix containing terms is given as,

$$\sum_{pq} D_{pq}'\left[F_{pq}^{\langle\lambda\rangle} + h_{pq}^{[\lambda]}\right] = \sum_{pq} D_{pq}'\left(\sum_{r} U_{rp}^{\lambda\star}F_{rq} + U_{rq}^{\lambda}F_{pr} + \sum_{ia} U_{ai}^{\lambda\star}\langle pa||qi\rangle + U_{ai}^{\lambda}\langle pi||qa\rangle\right) + \sum_{pq} D_{pq}' h_{pq}^{[\lambda]}. \qquad (2.117)$$

Total MP2 Derivative Collecting the derivative terms from eqs. 2.114, 2.115 and 2.117 yields the general expression for the MP2 gradient,

$$\begin{aligned}\frac{d\mathcal{E}_2}{d\lambda} = &\frac{1}{2}\sum_{ia} U_{ai}^{\lambda\star}\left\{\sum_{jbc}\langle aj||cb\rangle t_{cb}^{ij} - \sum_{jkb}\langle kj||ib\rangle t_{ab}^{kj}\right\} + \frac{1}{2}\sum_{ia} U_{ai}^{\lambda}\left\{-\sum_{jkb}\langle ib||kj\rangle t_{ab}^{kj\star} + \sum_{jbc}\langle cb||aj\rangle t_{cb}^{ij\star}\right\} \\ &+ \sum_{kl} D'_{kl}\left[\sum_{c} U_{ck}^{\lambda\star}F_{cl} + U_{cl}^{\lambda}F_{kc} + h_{kl}^{[\lambda]} + \sum_{ia} U_{ai}^{\lambda\star}\langle ak||il\rangle + U_{ai}^{\lambda}\langle ik||al\rangle\right] \\ &+ \sum_{cd} D'_{cd}\left[\sum_{k} U_{kc}^{\lambda\star}F_{kd} + U_{kd}^{\lambda}F_{ck} + h_{cd}^{[\lambda]} + \sum_{ia} U_{ai}^{\lambda\star}\langle ac||id\rangle + U_{ai}^{\lambda}\langle ic||ad\rangle\right] \end{aligned} \tag{2.118}$$

and the RI-MP2 gradient has the form,

$$\begin{aligned}\frac{d\mathcal{E}_2^{(RI)}}{d\lambda} = &\sum_{ia} U_{ai}^{\lambda\star}\left\{\sum_{cP}(ac|P)\Gamma'^{P}_{ic} - \sum_{kP}(ki|P)\Gamma'^{P}_{ka}\right\} + \sum_{ia} U_{ai}^{\lambda}\left\{-\sum_{kP}(ik|P)\Gamma'^{P}_{ak} + \sum_{cP}(ca|P)\Gamma'^{P}_{ci}\right\} \\ &+ \sum_{kl} D'_{kl}\left[\sum_{c} U_{ck}^{\lambda\star}F_{cl} + U_{cl}^{\lambda}F_{kc} + h_{kl}^{[\lambda]} + \sum_{ia} U_{ai}^{\lambda\star}\langle ak||il\rangle + U_{ai}^{\lambda}\langle ik||al\rangle\right] \\ &+ \sum_{cd} D'_{cd}\left[\sum_{k} U_{kc}^{\lambda\star}F_{kd} + U_{kd}^{\lambda}F_{ck} + h_{cd}^{[\lambda]} + \sum_{ia} U_{ai}^{\lambda\star}\langle ac||id\rangle + U_{ai}^{\lambda}\langle ic||ad\rangle\right]. \end{aligned} \tag{2.119}$$

The Fock matrix elements in eqs. 2.118 and 2.119 vanish, since the zero-order wave function is the Hartree-Fock determinant and therefore, Brillouins' theorem is valid.

The Total MP2 Derivative for Real Perturbations The total MP2 derivative in the case of a real hermitian perturbation is,

$$\frac{d\mathcal{E}_2}{d\lambda} = \sum_{ia} x_{ai}^{\lambda}\left\{\sum_{jbc}\langle aj||cb\rangle t_{cb}^{ij} - \sum_{jkb}\langle kj||ib\rangle t_{ab}^{kj}\right\} + \sum_{ia} x_{ai}^{\lambda}\overline{R}(\mathbf{D}')_{ai} + \sum_{pq} D'_{pq}h_{pq}^{[\lambda]} \tag{2.120}$$

and

$$\frac{d\mathcal{E}_2^{(RI)}}{d\lambda} = 2\sum_{ia} x_{ai}^{\lambda}\left\{\sum_{cP}(ac|P)\Gamma'^{P}_{ic} - \sum_{kP}(ki|P)\Gamma'^{P}_{ka}\right\} + \sum_{ia} x_{ai}^{\lambda}\overline{R}(\mathbf{D}')_{ai} + \sum_{pq} D'_{pq}h_{pq}^{[\lambda]} \tag{2.121}$$

where the response operator for real perturbation has been defined as,

$$\begin{aligned}\overline{R}(\mathbf{D}')_{ai} &= \sum_{pq} D'_{pq}\left(\langle ap||iq\rangle + \langle ip||aq\rangle\right) \\ &= \sum_{pq} D'_{pq}\left(2\langle ap|iq\rangle - \langle ap|qi\rangle - \langle ip|qa\rangle\right). \end{aligned} \tag{2.122}$$

The Total MP2 Derivative for Imaginary Perturbations The total MP2 derivative in the case of an imaginary hermitian perturbation differs significantly from the previously derived derivative for real

perturbations, since the first four terms in eq. 2.123 cancel each other.

$$\begin{aligned}\frac{d\mathcal{E}_2}{d\lambda} = & -\frac{1}{2}\sum_{ia}\mathbf{i}y_{ai}^{\lambda}\left\{\sum_{jbc}\langle aj||cb\rangle t_{cb}^{ij} - \sum_{jkb}\langle kj||ib\rangle t_{ab}^{kj}\right\} + \frac{1}{2}\sum_{ia}\mathbf{i}y_{ai}^{\lambda}\left\{-\sum_{jkb}\langle ib||kj\rangle t_{ab}^{kj\star} + \sum_{jbc}\langle cb||aj\rangle t_{cb}^{ij\star}\right\} \\ & + \sum_{ia}\mathbf{i}y_{ai}^{\lambda}\overline{\overline{R}}(\mathbf{D}')_{ai} + \sum_{pq}D'_{pq}h_{pq}^{[\lambda]} \qquad (2.123) \\ = & \sum_{ia}\mathbf{i}y_{ai}^{\lambda}\overline{\overline{R}}(\mathbf{D}')_{ai} + \sum_{pq}D'_{pq}h_{pq}^{[\lambda]} \qquad (2.124)\end{aligned}$$

The definition for the imaginary response operator is also different from the real analogue,

$$\begin{aligned}\overline{\overline{R}}(\mathbf{D}')_{ai} &= \sum_{pq}D'_{pq}\left(-\langle ap||iq\rangle + \langle ip||aq\rangle\right) \\ &= \sum_{pq}D'_{pq}\left(\langle ap|qi\rangle - \langle ip|qa\rangle\right). \qquad (2.125)\end{aligned}$$

By taking the symmetry of the unrelaxed MP2 density matrix into account, it can be shown, that the elements of the response matrix yield zero,

$$\begin{aligned}\overline{\overline{R}}(\mathbf{D}')_{pq} &= \sum_{rs}D'_{rs}\left(\langle pr|sq\rangle - \langle qr|sp\rangle\right) \\ &= \sum_{rs}\underbrace{(D'_{rs} - D'_{sr})}_{=0}\langle pr|sq\rangle. \qquad (2.126)\end{aligned}$$

Thus, the first derivative of the MP2 energy with respect to an arbitrary imaginary perturbation can be calculated as expectation value of the perturbed one-electron operator, assuming the basis functions to be independent of the perturbation.

The Zero-Order z-vector Equation The total derivative of the MP2 energy functional is,

$$\begin{aligned}\frac{d\mathcal{E}_2}{d\lambda} &= \sum_{ai} x_{ai}^{\lambda}\left[\sum_{jbc}\langle cb||aj\rangle t_{cb}^{ij} - \sum_{jkb}\langle ib||kj\rangle t_{ab}^{kj} + \overline{R}\left(\mathbf{D}'\right)_{ai}\right] \\ &\quad + \frac{1}{2}\sum_{ia}\mathbf{i}y_{ai}^{\lambda}\left[-\sum_{jbc}\langle aj||cb\rangle t_{cb}^{ij} + \sum_{jkb}\langle kj||ib\rangle t_{ab}^{kj} - \sum_{jkb}\langle ib||kj\rangle t_{ab}^{kj\star} + \sum_{jbc}\langle cb||aj\rangle t_{cb}^{ij\star} + \overline{\overline{R}}(\mathbf{D}')_{ai}\right] \\ &\quad + \sum_{pq} D'_{pq}h_{pq}^{[\lambda]} \\ &= \sum_{ai} x_{ai}^{\lambda}X_{ai} + \mathbf{i}y_{ai}^{\lambda}Y_{ai} + \sum_{pq} D'_{pq}h_{pq}^{[\lambda]} \end{aligned} \tag{2.127}$$

where the MP2 and RI-MP2 Lagrangians are introduced,

$$X_{ai} = \sum_{jbc}\langle cb||aj\rangle t_{cb}^{ij} - \sum_{jkb}\langle ib||kj\rangle t_{ab}^{kj} + \overline{R}\left(\mathbf{D}'\right)_{ai} \tag{2.128}$$

$$X_{ai}^{(RI)} = 2\sum_{cP}(ac|P)\Gamma_{ic}'^{P} - 2\sum_{kP}(ki|P)\Gamma_{ka}'^{P} + \overline{R}\left(\mathbf{D}'\right)_{ai} \tag{2.129}$$

$$Y_{ai} = \frac{1}{2}\sum_{jbc} -\langle aj||cb\rangle t_{cb}^{ij} + \langle cb||aj\rangle t_{cb}^{ij\star} + \frac{1}{2}\sum_{jkb}\langle kj||ib\rangle t_{ab}^{kj} - \langle ib||kj\rangle t_{ab}^{kj\star} + \overline{\overline{R}}\left(\mathbf{D}'\right)_{ai} \tag{2.130}$$

$$Y_{ai}^{(RI)} = \sum_{cP} -(ac|P)\Gamma_{ic}'^{P} + (ca|P)\Gamma_{ci}'^{P} + \sum_{kP}(ki|P)\Gamma_{ka}'^{P} - (ik|P)\Gamma_{ak}'^{P} + \overline{\overline{R}}\left(\mathbf{D}'\right)_{ai}. \tag{2.131}$$

The z-vector method developed by Handy and Schäfer [14] replaces the set of CP-SCF equations for every perturbation λ by one perturbation independent z-vector equation. This is done by inserting the formal solution of the CPHF equations, eq. 2.92 and 2.93, into the MP2 derivative expression,

$$\begin{aligned}\frac{dE_2}{d\lambda} &= \sum_{ia} x_{ai}^{\lambda}X_{ai} + \mathbf{i}y_{ai}^{\lambda}Y_{ai} + \sum_{pq} D'_{pq}h_{pq}^{[\lambda]} \\ &= \sum_{ia}\left(\left(\mathbf{A}^{(\Re)}\right)^{-1}\mathbf{B}^{(\Re)\lambda}\right)_{ai}X_{ai} + \mathbf{i}\sum_{ia}\left(\left(\mathbf{A}^{(\Im)}\right)^{-1}\mathbf{B}^{(\Im)\lambda}\right)_{ai}Y_{ai} + \sum_{pq} D'_{pq}h_{pq}^{[\lambda]} \\ &= \sum_{ia} B_{ai}^{(\Re)\lambda}\sum_{jb}\left(\mathbf{A}^{(\Re)}\right)^{-1}_{ai,bj}X_{bj} + \mathbf{i}\sum_{ia} B_{ai}^{(\Im)\lambda}\sum_{jb}\left(\mathbf{A}^{(\Im)}\right)^{-1}_{ai,bj}Y_{bj} + \sum_{pq} D'_{pq}h_{pq}^{[\lambda]} \\ &= -\sum_{ia} B_{ai}^{(\Re)\lambda}\overline{z}_{ai} - \mathbf{i}\sum_{ia} B_{ai}^{(\Im)\lambda}\overline{\overline{z}}_{ai} + \sum_{pq} D'_{pq}h_{pq}^{[\lambda]}. \end{aligned} \tag{2.132}$$

The final z-vector equations are given as,

$$\overline{z}_{ai}(\varepsilon_a - \varepsilon_i) + \sum_{jb}\overline{z}_{bj}\left[\langle ab||ij\rangle + \langle aj||ib\rangle\right] = -X_{ai} \tag{2.133}$$

$$\mathbf{i}\overline{\overline{z}}_{ai}(\varepsilon_a - \varepsilon_i) + \mathbf{i}\sum_{jb}\overline{\overline{z}}_{bj}\left[-\langle ab||ij\rangle + \langle aj||ib\rangle\right] = -Y_{ai} \tag{2.134}$$

and the first MP2 derivative becomes,

$$\frac{dE_2}{d\lambda} = \sum_{pq} D'_{pq}h_{pq}^{[\lambda]} + \sum_{ia} z_{ai}h_{ai}^{[\lambda]} = \sum_{pq} D_{pq}h_{pq}^{[\lambda]} \tag{2.135}$$

with the relaxed MP2 density matrix D_{pq} defined as,

$$D_{ij}^{(\Re)} = D_{ij}^{(\Im)} = D'_{ij} \tag{2.136}$$
$$D_{ab}^{(\Re)} = D_{ab}^{(\Im)} = D'_{ab} \tag{2.137}$$
$$D_{ai}^{(\Re)} = \frac{1}{2}\overline{z}_{ai} \qquad D_{ai}^{(\Im)} = 0 \tag{2.138}$$
$$D_{ia}^{(\Re)} = \frac{1}{2}\overline{z}_{ai} \qquad D_{ia}^{(\Im)} = 0. \tag{2.139}$$

In the imaginary case, the relaxed MP2 density is identical to the unrelaxed MP2 density matrix, since the Lagrangian Y_{ai} is zero. Therefore, a magnetic perturbation does not change the electron density to first order as in the SCF case.

The Relaxed Density Matrix The relaxed density matrix in MP2 has been first identified by Bartlett and co-workers [12, 13] as a by-product in analytic gradient calculations. Therefore, the first derivative of the MP2 energy correction w.r.t. an arbitrary real perturbation has been derived and the z-vector equations are formulated, cf. eqs. 2.132, 2.133. Any basis function independent perturbation can then be expressed as,

$$\frac{dE_2}{d\lambda} = \sum_{pq} D_{pq} h_{pq}^{[\lambda]} \tag{2.140}$$

and in the special case of a delta-function perturbation $h_{pq}^{[\lambda]} = \langle p|\delta(\mathbf{r}' - \mathbf{r})|q\rangle = \psi_p^\star(\mathbf{r})\psi_q(\mathbf{r})$, eq. 2.140 becomes,

$$\frac{dE_2}{d\lambda} = \sum_{pq} D_{pq}\psi_p^\star(\mathbf{r})\psi_q(\mathbf{r}). \tag{2.141}$$

The matrix D was then identified as the matrix representation of the correlation correction to the electron density. [12, 13] The relaxed density itself is a response property obtained as energy derivative of the MP2 correlation correction w.r.t. to the delta-function perturbation. Therefore, the response density contains all orbital relaxation effects, in contrast, to the density obtained as an expectation value over the first-order wave function. [13] It has never been pointed out, what is exactly the case for purely imaginary perturbations. But referring to the previously derived equations (eqs. 2.132, 2.134), one would never end up at these z-vector equations.

2.4.3. The Second Derivative of the MP2 Energy

The derivation of the second derivative of the MP2 Hylleraas functional is given as,

$$\begin{aligned}\frac{d^2\mathcal{E}_2}{d\lambda d\kappa} = \frac{\partial}{\partial\kappa}\Bigg\{ &\sum_{ai} U^{\lambda}_{ai}\Bigg[\frac{1}{2}\sum_{jbc}\langle cb||aj\rangle t^{ij\star}_{cb} - \frac{1}{2}\sum_{jkb}\langle ib||kj\rangle t^{kj\star}_{ab} + \sum_{kl} D'_{kl}\langle ik||al\rangle + \sum_{cd} D'_{cd}\langle ic||ad\rangle \\ &+ \sum_{j} D'_{ji}F_{ia} + \sum_{b} D'_{ab}F_{ib}\Bigg] \\ &+ \sum_{ai} U^{\lambda\star}_{ai}\Bigg[\frac{1}{2}\sum_{jbc}\langle aj||cb\rangle t^{ij}_{cb} - \frac{1}{2}\sum_{jkb}\langle kj||ib\rangle t^{kj}_{ab} + \sum_{kl} D'_{kl}\langle ak||il\rangle + \sum_{cd} D'_{cd}\langle ac||id\rangle \\ &+ \sum_{j} D'_{ij}F_{aj} + \sum_{b} D'_{ba}F_{bi}\Bigg] \\ &+ \sum_{pq} D'_{pq}h^{[\lambda]}_{pq}\Bigg\}. \end{aligned} \tag{2.142}$$

The derivatives of the Fock matrix elements vanish, since the zero-order CP-SCF equations are obtained, after expansion of the perturbed MO coefficients in the basis of the zero-order MO coefficients via the orbital rotation coefficients U^{κ}, eqs. 2.92 and 2.93.

$$\begin{aligned}\sum_{ija} U^{\lambda}_{ai}D'_{ji}F^{\kappa}_{ai} &= \sum_{ija} U^{\lambda}_{ai}D'_{ji}\left[\sum_{k} U^{\kappa\star}_{ka}F_{ki} + \sum_{b} U^{\kappa}_{bi}F_{ab} + h^{[\kappa]}_{ai} + \sum_{kc} U^{\kappa\star}_{ck}\langle ac||ik\rangle + U^{\kappa}_{ck}\langle ak||ic\rangle\right] \\ &= \sum_{ia}\left[U^{\kappa}_{ai}(\varepsilon_a - \varepsilon_i) + h^{[\kappa]}_{ai}\right]\sum_{j} U^{\lambda}_{ai}D'_{ji} + \sum_{ija} U^{\lambda}_{ai}D'_{ji}\sum_{kc}\left[U^{\kappa\star}_{ck}\langle ac||ik\rangle + U^{\kappa}_{ck}\langle ak||ic\rangle\right] \\ &= \sum_{ija} x^{\lambda}_{ai}D'_{ji}\underbrace{\left[\sum_{kc} A^{(\Re)}_{ai,ck}x^{\kappa}_{ck} + h^{(\Re)[\kappa]}_{ai}\right]}_{=0} + \mathbf{i}\sum_{ija} y^{\lambda}_{ai}D'_{ji}\underbrace{\left[\mathbf{i}\sum_{kc} A^{(\Im)}_{ai,ck}y^{\kappa}_{ck} + h^{(\Im)[\kappa]}_{ai}\right]}_{=0}\end{aligned} \tag{2.143}$$

Real Perturbations

$$\begin{aligned}\frac{d^2\mathcal{E}_2}{d\lambda d\kappa} &= \frac{\partial}{\partial\kappa}\left\{\sum_{pq} D'_{pq}h^{[\lambda]}_{pq} + \sum_{ai}\overline{z}_{ai}h^{[\lambda]}_{ai}\right\} \\ &= \sum_{pq}\left[D'^{\kappa}_{pq}h^{[\lambda]}_{pq} + D'_{pq}h^{[\lambda,\kappa]}_{pq}\right] + \sum_{ia}\left(\overline{z}^{\kappa}_{ai}h^{[\lambda]}_{ai} + \overline{z}_{ai}h^{[\lambda,\kappa]}_{ai}\right) + \sum_{pq}\left[\sum_{r} U^{\kappa\star}_{rp}D_{rp} + U^{\kappa}_{rq}D_{pr}\right]h^{[\lambda]}_{pq} \\ &= \sum_{pq}\left[D^{\kappa}_{pq} + \sum_{r} x^{\kappa}_{rp}D_{rq} + x^{\kappa}_{rq}D_{pr}\right]h^{[\lambda]}_{pq} + D_{pq}h^{[\lambda,\kappa]}_{pq}\end{aligned} \tag{2.144}$$

The second MP2 derivative requires the calculation of the first-order density matrix D^{κ}_{pq}. The elements of the perturbed density matrix are given in eqs. 2.145 – 2.148.

$$D^{\kappa}_{ij} = -\frac{1}{2}\sum_{kab}\left(t^{ik,\kappa}_{ab}t^{jk\star}_{ab} + t^{ik}_{ab}t^{jk\star,\kappa}_{ab}\right) \tag{2.145}$$

$$D^{\kappa}_{ab} = \frac{1}{2}\sum_{ijc}\left(t^{ij\star,\kappa}_{ac}t^{ij}_{bc} + t^{ij\star}_{ac}t^{ij,\kappa}_{bc}\right) \tag{2.146}$$

$$D^{\kappa}_{ai} = \frac{1}{2}\overline{z}^{\kappa}_{ai} \tag{2.147}$$

$$D^{\kappa}_{ia} = \frac{1}{2}\overline{z}^{\kappa}_{ai} \tag{2.148}$$

In order to calculate the first-order relaxed MP2 density matrix, the knowledge of the perturbed double excitation amplitudes and the solution of the first-order z-vector equations is required.

First-Order MP2 Amplitude Equations The zero-order MP2 amplitudes are real, but the first-order amplitudes might differ for real and imaginary amplitudes. The MP2 amplitude equation can be derived from the variational condition,

$$\begin{aligned}
\frac{\partial\mathcal{E}_2}{\partial t^{ij}_{ab}} &= \frac{\partial}{\partial t^{ij}_{ab}}\left\{\sum_{klcd}\left[\frac{1}{4}t^{kl}_{cd}\langle kl||cd\rangle + \frac{1}{4}t^{kl\star}_{cd}\langle cd||kl\rangle - \frac{1}{2}\sum_{m}F_{kl}t^{km}_{cd}t^{lm\star}_{cd} + \sum_{e}\frac{1}{2}F_{cd}t^{kl\star}_{ce}t^{kl}_{de}\right]\right\} \\
&= \frac{1}{4}\sum_{klcd}\left[\delta_{ik}\delta_{jl}\delta_{ac}\delta_{bd} - \delta_{jk}\delta_{il}\delta_{ac}\delta_{bd} - \delta_{ik}\delta_{jl}\delta_{bc}\delta_{ad} + \delta_{jk}\delta_{il}\delta_{bc}\delta_{ad}\right]\langle kl||cd\rangle \\
&\quad - \frac{1}{2}\sum_{klmcd}\left[\delta_{ik}\delta_{jm}\delta_{ac}\delta_{bd} - \delta_{jk}\delta_{im}\delta_{ac}\delta_{bd} - \delta_{ik}\delta_{jm}\delta_{bc}\delta_{ad} + \delta_{jk}\delta_{im}\delta_{bc}\delta_{ad}\right]t^{km\star}_{cd}F_{kl} \\
&\quad + \frac{1}{2}\sum_{klcde}\left[\delta_{ik}\delta_{jl}\delta_{ad}\delta_{be} - \delta_{jk}\delta_{il}\delta_{ad}\delta_{be} - \delta_{ik}\delta_{jl}\delta_{bd}\delta_{ae} + \delta_{jk}\delta_{il}\delta_{bd}\delta_{ae}\right]t^{kl\star}_{ce}F_{cd} \\
&= \langle ij||ab\rangle - \frac{1}{2}\sum_{k}\left[t^{kj\star}_{ab}F_{ik} - t^{ki\star}_{ab}F_{jk} - t^{kj\star}_{ba}F_{ik} + t^{ki\star}_{ba}F_{jk}\right] \\
&\quad + \frac{1}{2}\sum_{c}\left[t^{ij\star}_{cb}F_{ca} - t^{ji\star}_{cb}F_{ca} - t^{ij\star}_{ca}F_{cb} + t^{ji\star}_{ca}F_{cb}\right] \\
&= \langle ij||ab\rangle - \sum_{k}t^{kj\star}_{ab}F_{ik} + t^{ik\star}_{ab}F_{jk} + \sum_{c}t^{ij\star}_{cb}F_{ca} + t^{ij\star}_{ac}F_{cb} = 0.
\end{aligned} \tag{2.149}$$

Differentiation of eq. 2.149 with respect to the perturbation κ yields the first-order amplitude equation, eq. 2.150.

$$\begin{aligned}
\frac{\partial^2\mathcal{E}_2}{\partial t^{ij}_{ab}\partial\kappa} &= \frac{\partial\langle ab||ij\rangle}{\partial\kappa} - \sum_{k}\left(F_{ik}\frac{\partial t^{kj\star}_{ab}}{\partial\kappa} + \frac{\partial F_{ik}}{\partial\kappa}t^{kj\star}_{ab} + \frac{\partial t^{ik\star}_{ab}}{\partial\kappa}F_{jk} + t^{ik\star}_{ab}\frac{\partial F_{jk}}{\partial\kappa}\right) \\
&\quad + \sum_{c}\left(F_{ca}\frac{\partial t^{ij\star}_{cb}}{\partial\kappa} + \frac{\partial F_{ca}}{\partial\kappa}t^{ij\star}_{cb} + \frac{\partial t^{ij\star}_{ac}}{\partial\kappa}F_{cb} + t^{ij\star}_{ac}\frac{\partial F_{cb}}{\partial\kappa}\right)
\end{aligned} \tag{2.150}$$

The conditional equation for the first-order complex conjugate MP2 amplitudes is,

$$\begin{aligned}\frac{\partial^2 \mathcal{E}_2}{\partial t_{ab}^{ij\star} \partial \kappa} = & \frac{\partial \langle ij||ab\rangle}{\partial \kappa} - \sum_k \left(F_{ki} \frac{\partial t_{ab}^{kj}}{\partial \kappa} + \frac{\partial F_{ki}}{\partial \kappa} t_{ab}^{kj} + \frac{\partial t_{ab}^{ik}}{\partial \kappa} F_{kj} + t_{ab}^{ik} \frac{\partial F_{kj}}{\partial \kappa} \right) \\ & + \sum_c \left(F_{ac} \frac{\partial t_{cb}^{ij}}{\partial \kappa} + \frac{\partial F_{ac}}{\partial \kappa} t_{cb}^{ij} + \frac{\partial t_{ac}^{ij}}{\partial \kappa} F_{bc} + t_{ac}^{ij} \frac{\partial F_{bc}}{\partial \kappa} \right). \end{aligned} \tag{2.151}$$

The complete derivative of the amplitudes reads,

$$\begin{aligned} t_{ab}^{ij,\kappa} \left(\varepsilon_a + \varepsilon_b - \varepsilon_i - \varepsilon_j\right) = & - \left[\sum_k U_{ka}^{\kappa\star} \langle kb||ij\rangle + U_{kb}^{\kappa\star} \langle ak||ij\rangle + \sum_c U_{ci}^{\kappa} \langle ab||cj\rangle + U_{cj}^{\kappa} \langle ab||ic\rangle \right] \\ & + \sum_k \left(t_{ab}^{ik\star} F_{jk}^{\kappa} + F_{ik}^{\kappa} t_{ab}^{kj\star} \right) - \sum_c \left(t_{ac}^{ij\star} F_{cb}^{\kappa} + F_{ca}^{\kappa} t_{cb}^{ij\star} \right) \\ = & \sum_k x_{ak}^{\kappa} \langle kb||ij\rangle + x_{bk}^{\kappa} \langle ak||ij\rangle - \sum_c x_{ci}^{\kappa} \langle ab||cj\rangle + x_{cj}^{\kappa} \langle ab||ic\rangle \\ & + \sum_k \left(t_{ab}^{ik\star} F_{jk}^{\kappa} + F_{ik}^{\kappa} t_{ab}^{kj\star} \right) - \sum_c \left(t_{ac}^{ij\star} F_{cb}^{\kappa} + F_{ca}^{\kappa} t_{cb}^{ij\star} \right) \end{aligned} \tag{2.152}$$

with the perturbed Fock matrix elements given as,

$$F_{pq}^{\kappa} = h_{pq}^{[\kappa]} + \overline{R}(\mathbf{U}^{\kappa})_{pq}.$$

The derivative for the corresponding complex conjugate double excitation amplitudes is the same as for the real MP2 amplitudes. Thus, the first-order MP2 density matrix for real hermitian perturbations is symmetric.

First-Order z-vector Equations The perturbed z-vector, which defines the virtual-occupied block of the first-order relaxed MP2 density, is obtained as solution to the first-order z-vector equations. These necessary equations are easily derived by differentiating the zero-order z-vector equation, eq. 2.133,

$$\mathbf{A}^{(\Re)} \frac{\partial \overline{\mathbf{z}}}{\partial \kappa} = - \frac{\partial \mathbf{X}}{\partial \kappa} - \frac{\partial \mathbf{A}^{(\Re)}}{\partial \kappa} \overline{\mathbf{z}}. \tag{2.153}$$

The derivative of the matrix $\mathbf{A}^{(\Re)}$ for real perturbations is given as,

$$\begin{aligned} \left(\frac{\partial \mathbf{A}^{(\Re)}}{\partial \kappa} \overline{\mathbf{z}} \right)_{ai} = & \left(\frac{\partial \varepsilon_a}{\partial \kappa} - \frac{\partial \varepsilon_i}{\partial \kappa} \right) \overline{z}_{ai} + \sum_{bj} \overline{z}_{bj} \frac{\partial}{\partial \kappa} \left(\langle ab||ij\rangle + \langle aj||ib\rangle \right) \\ = & \left(\frac{\partial \varepsilon_a}{\partial \kappa} - \frac{\partial \varepsilon_i}{\partial \kappa} \right) \overline{z}_{ai} \\ & + \sum_{bj} \overline{z}_{bj} \left\{ \sum_k U_{ka}^{\kappa\star} \langle kb||ij\rangle + U_{ka}^{\kappa\star} \langle kj||ib\rangle + U_{kb}^{\kappa\star} \langle ak||ij\rangle + U_{kb}^{\kappa} \langle aj||ik\rangle \right. \\ & \left. + \sum_c U_{ci}^{\kappa} \langle ab||cj\rangle + U_{ci}^{\kappa} \langle aj||cb\rangle + U_{cj}^{\kappa} \langle ab||ic\rangle + U_{cj}^{\kappa\star} \langle ac||ib\rangle \right\} \\ = & \left(\frac{\partial \varepsilon_a}{\partial \kappa} - \frac{\partial \varepsilon_i}{\partial \kappa} \right) \overline{z}_{ai} - \sum_k x_{ak}^{\kappa} \overline{R}(\overline{\mathbf{z}})_{ki} + \sum_c x_{ci}^{\kappa} \overline{R}(\overline{\mathbf{z}})_{ac} + \overline{R}(\tilde{\mathbf{z}}^{(\Re)})_{ai} \end{aligned} \tag{2.154}$$

with the modified and perturbation dependent z-density,

$$\tilde{z}_{jk}^{(\Re)} = -\sum_{b} \overline{z}_{bj} x_{bk}^{\kappa} \tag{2.155}$$

$$\tilde{z}_{bc}^{(\Re)} = \sum_{j} \overline{z}_{bj} x_{cj}^{\kappa}. \tag{2.156}$$

The derivative of the real Lagrangian is given in eq. 2.157. Exploring the fact, that the MP2 amplitudes and its derivatives are purely real for electric perturbations, the Lagrangian can be simplified by summarizing the amplitude terms.

$$\begin{aligned}
\frac{\partial X_{ai}}{\partial \kappa} &= \frac{\partial}{\partial \kappa} \left(\sum_{jbc} \langle cb||aj\rangle t_{cb}^{ij} - \sum_{jkb} \langle ib||kj\rangle t_{ab}^{kj} + \overline{R}(\mathbf{D}')_{ai} \right) \\
&= \sum_{jbc} \left\{ \sum_{k} U_{kc}^{\kappa\star} \langle kb||aj\rangle + \sum_{k} U_{kb}^{\kappa\star} \langle ck||aj\rangle + \sum_{k} U_{ka}^{\kappa} \langle cb||kj\rangle + \sum_{d} U_{dj}^{\kappa} \langle cb||ad\rangle \right\} t_{cb}^{ij} \\
&\quad - \sum_{jkb} \left\{ \sum_{c} U_{ci}^{\kappa\star} \langle cb||kj\rangle + \sum_{l} U_{lb}^{\kappa\star} \langle il||kj\rangle + \sum_{c} U_{ck}^{\kappa} \langle ib||cj\rangle + \sum_{c} U_{cj}^{\kappa} \langle ib||kc\rangle \right\} t_{ab}^{kj} \\
&\quad + \sum_{jbc} \langle cb||aj\rangle t_{cb}^{ij,\kappa} - \sum_{jkb} \langle ib||kj\rangle t_{ab}^{kj,\kappa} + \frac{\partial \overline{R}(\mathbf{D}')_{ai}}{\partial \kappa} \\
&= \sum_{jb} x_{bj}^{\kappa} \left[-2 \sum_{kc} \left(\langle jc||ak\rangle t_{bc}^{ik} + \langle ic||bk\rangle t_{ac}^{jk} \right) + \underbrace{\sum_{cd} \langle cd||ab\rangle t_{cd}^{ij}}_{2K(\mathbf{t}^{ij})_{ab}} + \underbrace{\sum_{kl} \langle ij||kl\rangle t_{ab}^{kl}}_{2G_{ab}^{ij}} \right] \\
&\quad - \sum_{k} x_{ak}^{\kappa} \sum_{jbc} \langle cb||kj\rangle t_{cb}^{ij} - \sum_{c} x_{ci}^{\kappa} \sum_{jkb} \langle cb||kj\rangle t_{ab}^{kj} \\
&\quad + \sum_{jbc} \langle cb||aj\rangle t_{cb}^{ij,\kappa} - \sum_{jkb} \langle ib||kj\rangle t_{ab}^{kj,\kappa} + \frac{\partial \overline{R}(\mathbf{D}')_{ai}}{\partial \kappa}
\end{aligned} \tag{2.157}$$

The perturbed Lagrangian contains integrals with 4-internal to 4-external indices, which are contracted with the zero- and first-order amplitudes, respectively. Evaluating the derivative of the response operator for real perturbations,

$$\begin{aligned}
\frac{\partial \overline{R}(\mathbf{D}')_{ai}}{\partial \kappa} &= \frac{\partial}{\partial \kappa} \left\{ \sum_{bc} D'_{bc} \left[\langle ab||ic\rangle + \langle ib||ac\rangle \right] + \sum_{jk} D'_{jk} \left[\langle aj||ik\rangle + \langle ij||ak\rangle \right] \right\} \\
&= \sum_{bc} D'^{\kappa}_{bc} \left[\langle ab||ic\rangle + \langle ib||ac\rangle \right] + \sum_{jk} D'^{\kappa}_{jk} \left[\langle aj||ik\rangle + \langle ij||ak\rangle \right] \\
&\quad + \sum_{bc} D'_{bc} \left\{ \sum_{j} U_{ja}^{\kappa\star} \langle jb||ic\rangle + \sum_{j} U_{jb}^{\kappa\star} \langle aj||ic\rangle + \sum_{d} U_{di}^{\kappa} \langle ab||dc\rangle + \sum_{j} U_{jc}^{\kappa} \langle ab||ij\rangle \right. \\
&\quad \left. + \sum_{d} U_{di}^{\kappa\star} \langle db||ac\rangle + \sum_{j} U_{jb}^{\kappa\star} \langle ij||ac\rangle + \sum_{j} U_{ja}^{\kappa} \langle ib||jc\rangle + \sum_{j} U_{jc}^{\kappa} \langle ib||aj\rangle \right\}
\end{aligned}$$

$$
\begin{aligned}
&+\sum_{jk} D'_{jk}\left\{\sum_{l} U^{\kappa\star}_{la}\langle lj||ik\rangle+\sum_{b} U^{\kappa\star}_{bj}\langle ab||ik\rangle+\sum_{b} U^{\kappa}_{bi}\langle aj||bk\rangle+\sum_{b} U^{\kappa}_{bk}\langle aj||ib\rangle\right.\\
&\left.+\sum_{b} U^{\kappa\star}_{bi}\langle bj||ak\rangle+\sum_{b} U^{\kappa\star}_{bj}\langle ib||ak\rangle+\sum_{l} U^{\kappa}_{la}\langle ij||lk\rangle+\sum_{b} U^{\kappa}_{bk}\langle ij||ab\rangle\right\}\\
=&\sum_{bc} D'^{\kappa}_{bc}\left[\langle ab||ic\rangle+\langle ac||ib\rangle\right]+\sum_{jk} D'^{\kappa}_{jk}\left[\langle aj||ik\rangle+\langle ak||ij\rangle\right]\\
&+\sum_{bc} D'_{bc}\left\{-\sum_{j} x^{\kappa}_{aj}\langle jb||ic\rangle-\sum_{j} x^{\kappa}_{bj}\langle aj||ic\rangle+\sum_{d} x^{\kappa}_{di}\langle ab||dc\rangle-\sum_{j} x^{\kappa}_{cj}\langle ab||ij\rangle\right.\\
&\left.+\sum_{d} x^{\kappa}_{di}\langle db||ac\rangle-\sum_{j} x^{\kappa}_{bj}\langle ij||ac\rangle-\sum_{j} x^{\kappa}_{aj}\langle ib||jc\rangle-\sum_{j} x^{\kappa}_{cj}\langle ib||aj\rangle\right\}\\
&+\sum_{jk} D'_{jk}\left\{-\sum_{l} x^{\kappa}_{al}\langle lj||ik\rangle+\sum_{b} x^{\kappa}_{bj}\langle ab||ik\rangle+\sum_{b} x^{\kappa}_{bi}\langle aj||bk\rangle+\sum_{b} x^{\kappa}_{bk}\langle aj||ib\rangle\right.\\
&\left.+\sum_{b} x^{\kappa}_{bi}\langle bj||ak\rangle+\sum_{b} x^{\kappa}_{bj}\langle ib||ak\rangle-\sum_{l} x^{\kappa}_{al}\langle ij||lk\rangle+\sum_{b} x^{\kappa}_{bk}\langle ij||ab\rangle\right\}\\
=&\,\overline{R}(\mathbf{D}'^{\kappa})_{ai}-\sum_{j} x^{\kappa}_{aj}\overline{R}(\mathbf{D}')_{ij}+\sum_{b} x^{\kappa}_{bi}\overline{R}(\mathbf{D}')_{ab}+\overline{R}(\tilde{\mathbf{D}}'^{\kappa})_{ai}
\end{aligned}
\tag{2.158}
$$

with the modified and perturbation dependent unrelaxed density defined as,

$$
\tilde{D}'^{\kappa}_{bj}=-2\sum_{c} D'_{bc}x^{\kappa}_{cj}+2\sum_{k} x^{\kappa}_{bk}D'_{kj}. \tag{2.159}
$$

Comparing the derivative of the response operator with the derivative of the A-matrix in eq. 2.154 displays three similar response operator type terms over the z-vector on the one hand and over the unrelaxed density on the other hand. Recalling the structure of the relaxed MP2 density matrix shows, that these terms can be summarized as response-type operators over the relaxed MP2 density matrix, eq. 2.160.

$$
\begin{aligned}
&-\sum_{j} x^{\kappa}_{aj}\overline{R}(\mathbf{D}')_{ij}+\sum_{b} x^{\kappa}_{bi}\overline{R}(\mathbf{D}')_{ab}+\overline{R}(\tilde{\mathbf{D}}'^{\kappa})_{ai}-\sum_{k} x^{\kappa}_{ak}\overline{R}(\bar{\mathbf{z}})_{ki}+\sum_{c} x^{\kappa}_{ci}\overline{R}(\bar{\mathbf{z}})_{ac}+\overline{R}(\tilde{\mathbf{z}}^{(\Re)})_{ai}\\
=&-\sum_{j} x^{\kappa}_{aj}\overline{R}(\mathbf{D})_{ij}+\sum_{b} x^{\kappa}_{bi}\overline{R}(\mathbf{D})_{ab}+\overline{R}(\tilde{\mathbf{D}}^{\kappa})_{ai}
\end{aligned}
\tag{2.160}
$$

Collecting all terms for the right hand side of the first-order z-vector equations yields,

$$
\begin{aligned}
&-\frac{\partial\mathbf{X}}{\partial\kappa}-\frac{\partial\mathbf{A}^{(\Re)}}{\partial\kappa}\bar{\mathbf{z}}\\
=&-\sum_{jb} x^{\kappa}_{bj}\left[2\sum_{k}\left[\mathbf{J}^{jk}-\mathbf{K}^{jk}\right]\mathbf{t}^{ik}+\mathbf{t}^{jk}\left[\mathbf{J}^{ik}-\mathbf{K}^{ik}\right]+2\mathbf{K}(\mathbf{t}^{ij})_{ab}+2\mathbf{G}^{ij}_{ab}\right]\\
&+2\sum_{jk} x^{\kappa}_{ak}tr(\mathbf{K}^{kj}\mathbf{t}^{ij})+2\sum_{jkc} x^{\kappa}_{ci}(\mathbf{K}^{kj}\mathbf{t}^{kj})_{ac}-2\sum_{j}\mathbf{K}(\mathbf{t}^{ij,\kappa})_{aj}+2\sum_{jkb}\mathbf{K}^{ik}_{bj}\mathbf{t}^{kj,\kappa}_{ab}\\
&-\left(\frac{\partial\varepsilon_a}{\partial\kappa}-\frac{\partial\varepsilon_i}{\partial\kappa}\right)\bar{z}_{ai}-\overline{R}(\mathbf{D}'^{\kappa})_{ai}+\sum_{j} x^{\kappa}_{aj}\overline{R}(\mathbf{D})_{ij}-\sum_{b} x^{\kappa}_{bi}\overline{R}(\mathbf{D})_{ab}-\overline{R}(\tilde{\mathbf{D}}^{\kappa})_{ai}
\end{aligned}
$$

$$
\begin{aligned}
= & -\sum_{jb} x^{\kappa}_{bj}\boldsymbol{\sigma}^{ij(1)}_{ab} + \sum_{j} x^{\kappa}_{aj} tr\left(\boldsymbol{\sigma}^{ij(2)}\right) + \sum_{jb} x^{\kappa}_{bi}\boldsymbol{\sigma}^{jj(3)}_{ab} - 2\sum_{j}\mathbf{K}(\mathbf{t}^{ij,\kappa})_{aj} + 2\sum_{jkb}\mathbf{K}^{ik}_{bj}\mathbf{t}^{kj,\kappa}_{ab} \\
& - \left(\frac{\partial\varepsilon_a}{\partial\kappa} - \frac{\partial\varepsilon_i}{\partial\kappa}\right)\overline{z}_{ai} - \overline{R}(\mathbf{D}'^{\kappa})_{ai} + \sum_{j} x^{\kappa}_{aj}\overline{R}(\mathbf{D})_{ij} - \sum_{b} x^{\kappa}_{bi}\overline{R}(\mathbf{D})_{ab} - \overline{R}(\tilde{\mathbf{D}}^{\kappa})_{ai}
\end{aligned} \tag{2.161}
$$

where the residual vectors $\boldsymbol{\sigma}$ are defined as,

$$
\boldsymbol{\sigma}^{ij(1)}_{ab} = 2\sum_{k}\left[\mathbf{J}^{jk} - \mathbf{K}^{jk}\right]\mathbf{t}^{ik} + \mathbf{t}^{jk}\left[\mathbf{J}^{ik} - \mathbf{K}^{ik}\right] + 2\mathbf{K}(\mathbf{t}^{ij})_{ab} + 2\mathbf{G}^{ij}_{ab} \tag{2.162}
$$

$$
tr(\boldsymbol{\sigma}^{ij(2)}) = 2\sum_{k} tr(\mathbf{t}^{ik}\mathbf{K}^{jk}) \tag{2.163}
$$

$$
\boldsymbol{\sigma}^{jj(3)}_{ab} = 2\sum_{k}(\mathbf{K}^{kj}\mathbf{t}^{kj})_{ab}. \tag{2.164}
$$

Imaginary Perturbations

The formal expression for the second derivative of the MP2 energy functional with respect to an imaginary hermitian perturbations is given in eq. 2.165. Although the zero-order z-vector in the imaginary case is zero, the perturbed z-vector $\overline{\overline{z}}^{\kappa}_{ai}$ might be non-vanishing.

$$
\begin{aligned}
\frac{d^2\mathcal{E}_2}{d\lambda d\kappa} &= \frac{\partial}{\partial\kappa}\left\{\sum_{pq} D'_{pq}h^{[\lambda]}_{pq} + \sum_{ai}\overline{\overline{z}}_{ai}h^{[\lambda]}_{ai}\right\} \\
&= \sum_{pq}\left[D'^{\kappa}_{pq}h^{[\lambda]}_{pq} + D'_{pq}h^{[\lambda,\kappa]}_{pq}\right] + \sum_{ia}\left(\overline{\overline{z}}^{\kappa}_{ai}h^{[\lambda]}_{ai} + \overline{\overline{z}}_{ai}h^{[\lambda,\kappa]}_{ai}\right) + \sum_{pq}\left[\sum_{r} U^{\kappa\star}_{rp}D_{rp} + U^{\kappa}_{rq}D_{pr}\right]h^{[\lambda]}_{pq} \\
&= \sum_{pq}\left[D^{\kappa}_{pq} + \sum_{r} -\mathbf{i}y^{\kappa}_{rp}D_{rq} + \mathbf{i}y^{\kappa}_{rq}D_{pr}\right]h^{[\lambda]}_{pq} + D_{pq}h^{[\lambda,\kappa]}_{pq}
\end{aligned} \tag{2.165}
$$

The occupied-occupied and virtual-virtual subspaces of the perturbed density matrices are analogous to the real case, but the occupied-virtual block differs in sign, in order to account for the skew symmetry of the imaginary part of the hermitian matrix.

$$
D^{\kappa}_{ij} = -\frac{1}{2}\sum_{kab}\left(t^{ik,\kappa}_{ab}t^{jk\star}_{ab} + t^{ik}_{ab}t^{jk\star,\kappa}_{ab}\right) \tag{2.166}
$$

$$
D^{\kappa}_{ab} = \frac{1}{2}\sum_{ijc}\left(t^{ij\star,\kappa}_{ac}t^{ij}_{bc} + t^{ij\star}_{ac}t^{ij,\kappa}_{bc}\right) \tag{2.167}
$$

$$
D^{\kappa}_{ai} = \frac{1}{2}\overline{\overline{z}}^{\kappa}_{ai} \tag{2.168}
$$

$$
D^{\kappa}_{ia} = -\frac{1}{2}\overline{\overline{z}}^{\kappa}_{ai} \tag{2.169}
$$

First-Order MP2 Amplitude Equations The explicit expressions for the first-order MP2 amplitudes and the corresponding complex conjugate amplitudes can be derived from eqs. 2.150 and 2.151.

$$\begin{aligned} t_{ab}^{ij,\kappa}\left(\varepsilon_a+\varepsilon_b-\varepsilon_i-\varepsilon_j\right) = & -\left[\sum_k U_{ka}^{\kappa\star}\langle kb||ij\rangle + U_{kb}^{\kappa\star}\langle ak||ij\rangle + \sum_c U_{ci}^{\kappa}\langle ab||cj\rangle + U_{cj}^{\kappa}\langle ab||ic\rangle\right] \\ & + \sum_k \left(t_{ab}^{ik\star}F_{kj}^{\kappa} + F_{ki}^{\kappa}t_{ab}^{kj\star}\right) - \sum_c \left(t_{ac}^{ij\star}F_{cb}^{\kappa} + F_{ca}^{\kappa}t_{cb}^{ij\star}\right) \\ = & \sum_k \mathbf{i}y_{ak}^{\kappa}\langle ij||kb\rangle + \mathbf{i}y_{bk}^{\kappa}\langle ij||ak\rangle - \sum_c \mathbf{i}y_{ci}^{\kappa}\langle cj||ab\rangle + \mathbf{i}y_{cj}^{\kappa}\langle ic||ab\rangle \\ & + \sum_k \left(t_{ab}^{ik\star}F_{jk}^{\kappa} + F_{ik}^{\kappa}t_{ab}^{kj\star}\right) - \sum_c \left(t_{ac}^{ij\star}F_{cb}^{\kappa} + F_{ca}^{\kappa}t_{cb}^{ij\star}\right) \end{aligned} \tag{2.170}$$

$$\begin{aligned} t_{ab}^{ij\star,\kappa}\left(\varepsilon_a+\varepsilon_b-\varepsilon_i-\varepsilon_j\right) = & -\left[\sum_c U_{ci}^{\kappa\star}\langle cj||ab\rangle + U_{cj}^{\kappa\star}\langle ic||ab\rangle + \sum_k U_{ka}^{\kappa}\langle ij||kb\rangle + U_{kb}^{\kappa}\langle ij||ak\rangle\right] \\ & + \sum_k \left(t_{ab}^{ik}F_{jk}^{\kappa} + F_{ik}^{\kappa}t_{ab}^{kj}\right) - \sum_c \left(t_{ac}^{ij}F_{bc}^{\kappa} + F_{ac}^{\kappa}t_{cb}^{ij}\right) \\ = & \sum_c \mathbf{i}y_{ci}^{\kappa}\langle cj||ab\rangle + \mathbf{i}y_{cj}^{\kappa}\langle ic||ab\rangle - \sum_k \mathbf{i}y_{ak}^{\kappa}\langle ij||kb\rangle + \mathbf{i}y_{bk}^{\kappa}\langle ij||ak\rangle \\ & + \sum_k \left(t_{ab}^{ik}F_{kj}^{\kappa} + F_{ki}^{\kappa}t_{ab}^{kj}\right) - \sum_c \left(t_{ac}^{ij}F_{bc}^{\kappa} + F_{ac}^{\kappa}t_{cb}^{ij}\right) \end{aligned} \tag{2.171}$$

As can be seen from eqs. 2.170 and 2.171 the derivatives of the double excitation amplitudes and its complex conjugate differ in its algebraic signs, considering the anti-symmetry of the perturbed Fock matrix,

$$F_{pq}^{\kappa} = h_{pq}^{[\kappa]} + \overline{\overline{R}}(\mathbf{U}^{\kappa})_{pq} = -F_{qp}^{\kappa}.$$

Therefore, the following relations for the MP2 amplitudes and subspaces of the density matrix are obtained,

$$\Im\mathfrak{m}\left(t_{ab}^{ij,\kappa}\right) = -\Im\mathfrak{m}\left(t_{ab}^{ij\star,\kappa}\right) \tag{2.172}$$

$$\Im\mathfrak{m}\left(t_{ab}^{ij,\kappa}\right) = -\Re\mathfrak{e}\left(t_{ab}^{ij,\kappa}\right) \tag{2.173}$$

$$\Im\mathfrak{m}\left(D_{ij}^{\kappa}\right) = -\Im\mathfrak{m}\left(D_{ji}^{\kappa}\right) \tag{2.174}$$

$$\Im\mathfrak{m}\left(D_{ab}^{\kappa}\right) = -\Im\mathfrak{m}\left(D_{ba}^{\kappa}\right). \tag{2.175}$$

Perturbed z-vector Equations for the Imaginary Case Differentiation of the zero-order z-vector equation for imaginary perturbations yields,

$$\mathbf{A}^{(\Im)}\frac{\partial\overline{\overline{\mathbf{z}}}}{\partial\kappa} = -\frac{\partial\mathbf{Y}}{\partial\kappa} - \frac{\partial\mathbf{A}^{(\Im)}}{\partial\kappa}\overline{\overline{\mathbf{z}}} \tag{2.176}$$

where the derivative of the A-matrix on the right hand side of the equation system is not required, since the zero-order z-vector is zero.

Differentiating the imaginary Lagrangian yields,

$$\frac{\partial Y_{ai}}{\partial\kappa} = \frac{1}{2}\frac{\partial}{\partial\kappa}\left(\sum_{jbc}\langle cb||aj\rangle t_{cb}^{ij\star} - \sum_{jkb}\langle ib||kj\rangle t_{ab}^{kj\star} - \sum_{jbc}\langle aj||cb\rangle t_{cb}^{ij} + \sum_{jkb}\langle kj||ib\rangle t_{ab}^{kj} + 2\overline{\overline{R}}(\mathbf{D}')_{ai}\right)$$

$$
\begin{aligned}
&= \frac{1}{2}\Bigg\{ \sum_{jbc} t_{cb}^{ij\star}\left[\sum_k U_{kc}^{\kappa\star}\langle kb||aj\rangle + \sum_k U_{kb}^{\kappa\star}\langle ck||aj\rangle + \sum_k U_{ka}^{\kappa}\langle cb||kj\rangle + \sum_d U_{dj}^{\kappa}\langle cb||ad\rangle\right] \\
&\quad - \sum_{jkb} t_{ab}^{kj\star}\left[\sum_c U_{ci}^{\kappa\star}\langle cb||kj\rangle + \sum_l U_{lb}^{\kappa\star}\langle il||kj\rangle + \sum_c U_{ck}^{\kappa}\langle ib||cj\rangle + \sum_c U_{cj}^{\kappa}\langle ib||kc\rangle\right] \\
&\quad - \sum_{jbc} t_{cb}^{ij}\left[\sum_k U_{ka}^{\kappa\star}\langle kj||cb\rangle + \sum_d U_{dj}^{\kappa\star}\langle ad||cb\rangle + \sum_k U_{kc}^{\kappa}\langle aj||kb\rangle + \sum_k U_{kb}^{\kappa}\langle aj||ck\rangle\right] \\
&\quad + \sum_{jkb} t_{ab}^{kj}\left[\sum_c U_{ck}^{\kappa\star}\langle cj||ib\rangle + \sum_c U_{cj}^{\kappa\star}\langle kc||ib\rangle + \sum_c U_{ci}^{\kappa}\langle kj||cb\rangle + \sum_l U_{lb}^{\kappa}\langle kj||il\rangle\right] \\
&\quad + \sum_{jbc}\langle cb||aj\rangle t_{cb}^{ij\star,\kappa} - \sum_{jkb}\langle ib||kj\rangle t_{ab}^{kj\star,\kappa} - \sum_{jbc}\langle aj||cb\rangle t_{cb}^{ij,\kappa} + \sum_{jkb}\langle kj||ib\rangle t_{ab}^{kj,\kappa}\Bigg\} + \frac{\partial\overline{\overline{R}}(\mathbf{D}')_{ai}}{\partial\kappa} \\
&= \mathbf{i}\sum_{bj} y_{bj}^{\kappa}\Bigg[-2\sum_{kc}\left\{\langle jc||ak\rangle t_{bc}^{ik} + \langle ic||bk\rangle t_{ac}^{jk}\right\} + \underbrace{\sum_{cd}\langle cd||ab\rangle t_{cd}^{ij}}_{2K(\mathbf{t}^{ij})_{ab}} + \underbrace{\sum_{kl}\langle ij||kl\rangle t_{ab}^{kl}}_{2G_{ab}^{ij}}\Bigg] \\
&\quad + \mathbf{i}\sum_k y_{ak}^{\kappa}\langle cb||kj\rangle t_{cb}^{ij} + \mathbf{i}\sum_c y_{ci}^{\kappa}\langle cb||kj\rangle t_{ab}^{kj} \\
&\quad - \sum_{jbc}\langle aj||cb\rangle t_{cb}^{ij,\kappa} + \sum_{jkb}\langle kj||ib\rangle t_{ab}^{kj,\kappa} + \frac{\partial\overline{\overline{R}}(\mathbf{D}')_{ai}}{\partial\kappa}.
\end{aligned}
\tag{2.177}
$$

Thus, the perturbed imaginary Lagrangian is similar to the first-order Lagrangian in the real case, cf. eq. 2.157, but differs in the sign of the fifth and sixth integral contribution as well as in the definition of the perturbed amplitudes. The derivative of the imaginary response operator is given,

$$
\begin{aligned}
\frac{\partial\overline{\overline{R}}(\mathbf{D}')_{ai}}{\partial\kappa} &= \frac{\partial}{\partial\kappa}\left\{\sum_{bc} D_{bc}'\left[-\langle ab||ic\rangle + \langle ib||ac\rangle\right] + \sum_{jk} D_{jk}'\left[-\langle aj||ik\rangle + \langle ij||ak\rangle\right]\right\} \\
&= \sum_{bc} D_{bc}'^{\kappa}\left[-\langle ab||ic\rangle + \langle ib||ac\rangle\right] + \sum_{jk} D_{jk}'^{\kappa}\left[-\langle aj||ik\rangle + \langle ij||ak\rangle\right] \\
&\quad + \sum_{bc} D_{bc}'\Bigg\{-\sum_j U_{ja}^{\kappa\star}\langle jb||ic\rangle - \sum_j U_{jb}^{\kappa\star}\langle aj||ic\rangle - \sum_d U_{di}^{\kappa}\langle ab||dc\rangle - \sum_j U_{jc}^{\kappa}\langle ab||ij\rangle \\
&\quad + \sum_d U_{di}^{\kappa\star}\langle db||ac\rangle + \sum_j U_{jb}^{\kappa\star}\langle ij||ac\rangle + \sum_j U_{ja}^{\kappa}\langle ib||jc\rangle + \sum_j U_{jc}^{\kappa}\langle ib||aj\rangle\Bigg\} \\
&\quad + \sum_{jk} D_{jk}'\Bigg\{-\sum_l U_{la}^{\kappa\star}\langle lj||ik\rangle - \sum_b U_{bj}^{\kappa\star}\langle ab||ik\rangle - \sum_b U_{bi}^{\kappa}\langle aj||bk\rangle - \sum_b U_{bk}^{\kappa}\langle aj||ib\rangle \\
&\quad + \sum_b U_{bi}^{\kappa\star}\langle bj||ak\rangle + \sum_b U_{bj}^{\kappa\star}\langle ib||ak\rangle + \sum_l U_{la}^{\kappa}\langle ij||lk\rangle + \sum_b U_{bk}^{\kappa}\langle ij||ab\rangle\Bigg\}
\end{aligned}
$$

$$
\begin{aligned}
&= \sum_{bc} D'^{\kappa}_{bc} \left[-\langle ab||ic\rangle + \langle ib||ac\rangle \right] + \sum_{jk} D'^{\kappa}_{jk} \left[-\langle aj||ik\rangle + \langle ij||ak\rangle \right] \\
&\quad + \mathbf{i} \sum_{bc} D'_{bc} \left\{ \sum_{j} y^{\kappa}_{aj} \langle jb||ic\rangle + \sum_{j} y^{\kappa}_{bj} \langle aj||ic\rangle - \sum_{d} y^{\kappa}_{di} \langle ab||dc\rangle - \sum_{j} y^{\kappa}_{cj} \langle ab||ij\rangle \right. \\
&\quad \left. - \sum_{d} y^{\kappa}_{di} \langle db||ac\rangle - \sum_{j} y^{\kappa}_{bj} \langle ij||ac\rangle + \sum_{j} y^{\kappa}_{aj} \langle ib||jc\rangle + \sum_{j} y^{\kappa}_{cj} \langle ib||aj\rangle \right\} \\
&\quad + \mathbf{i} \sum_{jk} D'_{jk} \left\{ \sum_{l} y^{\kappa}_{al} \langle lj||ik\rangle + \sum_{b} y^{\kappa}_{bj} \langle ab||ik\rangle - \sum_{b} y^{\kappa}_{bi} \langle aj||bk\rangle - \sum_{b} y^{\kappa}_{bk} \langle aj||ib\rangle \right. \\
&\quad \left. - \sum_{b} y^{\kappa}_{bi} \langle bj||ak\rangle - \sum_{b} y^{\kappa}_{bj} \langle ib||ak\rangle + \sum_{l} y^{\kappa}_{al} \langle ij||lk\rangle + \sum_{b} y^{\kappa}_{bk} \langle ij||ab\rangle \right\} \\
&= \overline{\overline{R}}(\mathbf{D}'^{\kappa})_{ai} + \mathbf{i} \sum_{j} y^{\kappa}_{aj} \overline{R}(\mathbf{D})_{ij} - \mathbf{i} \sum_{b} y^{\kappa}_{bi} \overline{R}(\mathbf{D})_{ab} + \overline{\overline{R}}(\tilde{\tilde{\mathbf{D}}}^{\kappa})_{\mathbf{ai}}
\end{aligned} \tag{2.178}
$$

with the modified and perturbation dependent relaxed density defined as,

$$
\tilde{\tilde{D}}^{\kappa}_{bj} = 2\mathbf{i} \sum_{c} D_{bc} y^{\kappa}_{cj} + 2\mathbf{i} \sum_{k} y^{\kappa}_{bk} D_{kj} = -\tilde{\tilde{D}}^{\kappa}_{jb}. \tag{2.179}
$$

Collecting all terms, which define the right hand side of the first-order z-vector equation for imaginary perturbations. The final right hand side of the first-order imaginary z-vector equation is given in eq. 2.180, where the residual vectors are defined in eqs. 2.162–2.164.

$$
\begin{aligned}
&- \frac{\partial \mathbf{Y}}{\partial \kappa} - \frac{\partial \mathbf{A}^{(\Im)}}{\partial \kappa} \overline{\overline{\mathbf{z}}} \\
&= - \sum_{jb} \mathbf{i} y^{\kappa}_{bj} \left[2 \sum_{k} \left[\mathbf{J}^{jk} - \mathbf{K}^{jk} \right] \mathbf{t}^{ik} + \mathbf{t}^{jk} \left[\mathbf{J}^{ik} - \mathbf{K}^{ik} \right] + 2\mathbf{K}(\mathbf{t}^{ij})_{ab} + 2\mathbf{G}^{ij}_{ab} \right] \\
&\quad - 2 \sum_{jk} \mathbf{i} y^{\kappa}_{ak} tr(\mathbf{K}^{kj} \mathbf{t}^{ij}) - 2 \sum_{jkc} \mathbf{i} y^{\kappa}_{ci} (\mathbf{K}^{kj} \mathbf{t}^{kj})_{ac} - 2 \sum_{j} \mathbf{K}(\mathbf{t}^{ij,\kappa})_{aj} + 2 \sum_{jkb} \mathbf{K}^{ik}_{bj} \mathbf{t}^{kj,\kappa}_{ab} \\
&\quad - \overline{\overline{R}}(\mathbf{D}'^{\kappa})_{ai} - \sum_{j} \mathbf{i} y^{\kappa}_{aj} \overline{R}(\mathbf{D})_{ij} + \sum_{b} \mathbf{i} y^{\kappa}_{bi} \overline{R}(\mathbf{D})_{ab} - \overline{\overline{R}}(\tilde{\tilde{\mathbf{D}}}^{\kappa})_{\mathbf{ai}} \\
&= - \sum_{jb} \mathbf{i} y^{\kappa}_{bj} \boldsymbol{\sigma}^{ij(1)}_{ab} - \sum_{j} \mathbf{i} y^{\kappa}_{aj} tr\left(\boldsymbol{\sigma}^{ij(2)} \right) - \sum_{jb} \mathbf{i} y^{\kappa}_{bi} \boldsymbol{\sigma}^{jj(3)}_{ab} - 2 \sum_{j} \mathbf{K}(\mathbf{t}^{ij,\kappa})_{aj} + 2 \sum_{jkb} \mathbf{K}^{ik}_{bj} \mathbf{t}^{kj,\kappa}_{ab} \\
&\quad - \overline{\overline{R}}(\mathbf{D}'^{\kappa})_{ai} - \sum_{j} \mathbf{i} y^{\kappa}_{aj} \overline{R}(\mathbf{D})_{ij} + \sum_{b} \mathbf{i} y^{\kappa}_{bi} \overline{R}(\mathbf{D})_{ab} - \overline{\overline{R}}(\tilde{\tilde{\mathbf{D}}}^{\kappa})_{\mathbf{ai}}
\end{aligned} \tag{2.180}
$$

2.5. The Second Derivative of the RI-MP2 Energy

The 'Resolution of the Identity' approximation is only applied to the correlation correction, but not to the Hartree-Fock wave function. Therefore, the Fock and response operators together with its derivatives are calculated via conventional two-electron repulsion integrals. The formal RI-MP2 second derivative can be written as,

$$\begin{aligned}\frac{d^2\mathcal{E}_2^{(RI)}}{d\lambda d\kappa} =& \frac{\partial}{\partial\kappa}\left\{\sum_{ia} x_{ai}^{\lambda}\left[2\sum_{cP}(ac|P)\Gamma_{ic}'^{P} - \sum_{kP}(ki|P)\Gamma_{ka}'^{P} + \overline{R}(\mathbf{D}')_{ai}\right]\right.\\ &+\mathbf{i}\sum_{ia} y_{ai}^{\lambda}\left[-\sum_{cP}(ac|P)\Gamma_{ic}'^{P} + \sum_{cP}(ca|P)\Gamma_{ci}'^{P} + \sum_{kP}(ki|P)\Gamma_{ka}'^{P} - \sum_{kP}(ik|P)\Gamma_{ak}'^{P} + \overline{\overline{R}}(\mathbf{D}')_{ai}\right]\\ &\left.+\sum_{pq} D_{pq}' h_{pq}^{[\lambda]}\right\}. \end{aligned} \tag{2.181}$$

2.5.1. Real Perturbations

The first-order RI-MP2 density matrix differs from its conventional counterpart in the formulation of the unperturbed and perturbed double excitation amplitudes. The zero-order RI-MP2 amplitudes have been already derived in eq. 2.103, and the first-order amplitudes take the from,

$$\begin{aligned}t_{ab}^{ij,\kappa(RI)}\left(\varepsilon_a+\varepsilon_b-\varepsilon_i-\varepsilon_j\right) =& -\sum_{cP} x_{ci}^{\kappa}\left(B_{ca}^P B_{jb}^P - B_{cb}^P B_{ja}^P\right) + x_{cj}^{\kappa}\left(B_{ia}^P B_{cb}^P - B_{ib}^P B_{ca}^P\right)\\ &+\sum_{kP} x_{ak}^{\kappa}\left(B_{ik}^P B_{jb}^P - B_{ib}^P B_{jk}^P\right) + x_{bk}^{\kappa}\left(B_{ia}^P B_{jk}^P - B_{ik}^P B_{ja}^P\right)\\ &+\sum_{k}\left(t_{ab}^{ik\star}F_{jk}^{\kappa} + F_{ik}^{\kappa}t_{ab}^{kj\star}\right) - \sum_{c}\left(t_{ac}^{ij\star}F_{cb}^{\kappa} + F_{ca}^{\kappa}t_{cb}^{ij\star}\right)\end{aligned} \tag{2.182}$$

with the conventional perturbed Fock matrix elements defined in eq. 2.117. The first-order z-vector equations are identical to the conventional case. Thus, the derivative of the real Lagrangian in the RI approximation remains to be derived,

$$\begin{aligned}\frac{\partial X_{ai}}{\partial\kappa} &= \frac{\partial}{\partial\kappa}\left(2\sum_{cP}(ac|P)\Gamma_{ic}'^{P} - 2\sum_{kP}(ki|P)\Gamma_{ka}'^{P} + \overline{R}(\mathbf{D}')_{ai}\right)\\ &= 2\sum_{cP}\left(\sum_{k} U_{ka}^{\kappa\star}(kc|P) + \sum_{k} U_{kc}^{\kappa}(ak|P)\right)\Gamma_{ic}'^{P} + 2\sum_{jbcP}\left(\sum_{d} U_{dj}^{\kappa\star}B_{ac}^P B_{db}^P + \sum_{k} U_{kb}^{\kappa}B_{ac}^P B_{jk}^P\right)t_{cb}^{ij}\\ &\quad - 2\sum_{kP}\left(\sum_{c} U_{ck}^{\kappa\star}(ci|P) + \sum_{c} U_{ci}^{\kappa}(kc|P)\right)\Gamma_{ka}'^{P} - 2\sum_{jkbP}\left(\sum_{c} U_{cj}^{\kappa\star}B_{ki}^P B_{cb}^P + \sum_{l} U_{lb}^{\kappa}B_{ki}^P B_{jl}^P\right)t_{ab}^{kj}\\ &\quad + 2\sum_{cP}(ac|P)\Gamma_{ic}'^{P,\kappa} - 2\sum_{kP}(ki|P)\Gamma_{ka}'^{P,\kappa} + \frac{\partial\overline{R}(\mathbf{D}')_{ai}}{\partial\kappa}\\ &= 2\sum_{jb} x_{bj}^{\kappa}\sum_{P}\left[\sum_{kc}\left\{B_{ac}^P B_{jk}^P - B_{aj}^P B_{bk}^P\right\}t_{bc}^{ik} + \sum_{kc}\left\{B_{ki}^P B_{bc}^P - B_{bi}^P B_{kc}^P\right\}t_{ac}^{jk}\right.\\ &\quad \left.+\sum_{cd} B_{ac}^P B_{bd}^P t_{cd}^{ij} + \sum_{kl} B_{ki}^P B_{lj}^P t_{ab}^{kj}\right] - 2\sum_{k} x_{ak}\sum_{cP}(kc|P)\Gamma_{ic}'^{P} - 2\sum_{c} x_{ci}^{\kappa}\sum_{kP}(kc|P)\Gamma_{ka}'^{P}\\ &\quad + 2\sum_{cP}(ac|P)\Gamma_{ic}'^{P,\kappa} - 2\sum_{kP}(ki|P)\Gamma_{ka}'^{P,\kappa} + \frac{\partial\overline{R}(\mathbf{D}')_{ai}}{\partial\kappa}\end{aligned} \tag{2.183}$$

with the perturbed 3-index 2-particle density matrix given as,

$$\Gamma'^{P,\kappa}_{ia} = \sum_{jbQ} V^{-1}_{PQ}(Q|jb) t^{ij,\kappa}_{ab}. \tag{2.184}$$

2.5.2. Imaginary Perturbations

The perturbed RI-MP2 amplitudes for imaginary perturbations are shown in eq. 2.185 and 2.186.

$$\begin{aligned} t^{ij,\kappa(RI)}_{ab}\left(\varepsilon_a+\varepsilon_b-\varepsilon_i-\varepsilon_j\right) = & \sum_{cP} \mathbf{i} y^{\kappa}_{ci}\left(B^P_{ca}B^P_{jb}-B^P_{cb}B^P_{ja}\right)+\mathbf{i} y^{\kappa}_{cj}\left(B^P_{ia}B^P_{cb}-B^P_{ib}B^P_{ca}\right) \\ & -\sum_{kP} \mathbf{i} y^{\kappa}_{ak}\left(B^P_{ik}B^P_{jb}-B^P_{ib}B^P_{jk}\right)+\mathbf{i} y^{\kappa}_{bk}\left(B^P_{ia}B^P_{jk}-B^P_{ik}B^P_{ja}\right) \\ & +\sum_{k}\left(t^{ik\star}_{ab}F^{\kappa}_{jk}+F^{\kappa}_{ik}t^{kj\star}_{ab}\right)-\sum_{c}\left(t^{ij\star}_{ac}F^{\kappa}_{cb}+F^{\kappa}_{ca}t^{ij\star}_{cb}\right) \end{aligned} \tag{2.185}$$

$$\begin{aligned} t^{ij\star,\kappa(RI)}_{ab}\left(\varepsilon_a+\varepsilon_b-\varepsilon_i-\varepsilon_j\right) = & \sum_{kP} \mathbf{i} y^{\kappa}_{ak}\left(B^P_{ik}B^P_{jb}-B^P_{ib}B^P_{jk}\right)+\mathbf{i} y^{\kappa}_{bk}\left(B^P_{ia}B^P_{jk}-B^P_{ik}B^P_{ja}\right) \\ & -\sum_{cP} \mathbf{i} y^{\kappa}_{ci}\left(B^P_{ca}B^P_{jb}-B^P_{cb}B^P_{ja}\right)+\mathbf{i} y^{\kappa}_{cj}\left(B^P_{ia}B^P_{cb}-B^P_{ib}B^P_{ca}\right) \\ & +\sum_{k}\left(t^{ik}_{ab}F^{\kappa}_{kj}+F^{\kappa}_{ki}t^{kj}_{ab}\right)-\sum_{c}\left(t^{ij}_{ac}F^{\kappa}_{bc}+F^{\kappa}_{ac}t^{ij}_{cb}\right) \end{aligned} \tag{2.186}$$

The derivative of the RI-MP2 imaginary Lagrangian is given as,

$$\begin{aligned} \frac{\partial Y_{ai}}{\partial\kappa} = & \frac{\partial}{\partial\kappa}\left\{-\sum_{cP}(ac|P)\Gamma'^{P}_{ic}+(ca|P)\Gamma'^{P}_{ci}+\sum_{kP}(ki|P)\Gamma'^{P}_{ka}-(ik|P)\Gamma'^{P}_{ak}+\overline{\overline{R}}(\mathbf{D}')_{ai}\right\} \\ = & -\sum_{cP}\sum_{k}\left[U^{\kappa\star}_{ka}(kc|P)+U^{\kappa}_{kc}(ak|P)\right]\Gamma'^{P}_{ic}-\sum_{jbcP}\left(\sum_{d}U^{\kappa\star}_{dj}B^P_{ac}B^P_{db}+\sum_{k}U^{\kappa}_{kb}B^P_{ac}B^P_{jk}\right)t^{ij}_{cb} \\ & +\sum_{cP}\sum_{k}\left[U^{\kappa\star}_{kc}(ka|P)+U^{\kappa}_{ka}(ck|P)\right]\Gamma'^{P}_{ci}+\sum_{jbcP}\left(\sum_{k}U^{\kappa\star}_{kb}B^P_{ca}B^P_{kj}+\sum_{d}U^{\kappa}_{dj}B^P_{ca}B^P_{bd}\right)t^{ij\star}_{cb} \\ & +\sum_{kP}\sum_{c}\left[U^{\kappa\star}_{ck}(ci|P)+U^{\kappa}_{ci}(kc|P)\right]\Gamma'^{P}_{ka}+\sum_{jkbP}\left(\sum_{c}U^{\kappa\star}_{cj}B^P_{ki}B^P_{cb}+\sum_{l}U^{\kappa}_{lb}B^P_{ki}B^P_{jl}\right)t^{kj}_{ab} \\ & -\sum_{kP}\sum_{c}\left[U^{\kappa\star}_{ci}(ck|P)+U^{\kappa}_{ck}(ic|P)\right]\Gamma'^{P}_{ak}-\sum_{jkbP}\left(\sum_{l}U^{\kappa\star}_{lb}B^P_{ik}B^P_{lj}+\sum_{c}U^{\kappa}_{cj}B^P_{ik}B^P_{bc}\right)t^{kj\star}_{ab} \\ & -2\sum_{cP}(ac|P)\Gamma'^{P,\kappa}_{ic}+2\sum_{kP}(ki|P)\Gamma'^{P,\kappa}_{ka}+\frac{\partial\overline{\overline{R}}(\mathbf{D}')_{ai}}{\partial\kappa} \\ = & 2\sum_{jb}\mathbf{i} y^{\kappa}_{bj}\sum_{P}\left[\sum_{kc}\left\{B^P_{ac}B^P_{jk}-B^P_{aj}B^P_{bk}\right\}t^{ik}_{bc}+\sum_{kc}\left\{B^P_{ki}B^P_{bc}-B^P_{bi}B^P_{kc}\right\}t^{jk}_{ac}\right. \\ & \left.+\sum_{cd}B^P_{ac}B^P_{bd}t^{ij}_{cd}+\sum_{kl}B^P_{ki}B^P_{lj}t^{kj}_{ab}\right]+2\sum_{k}\mathbf{i} y_{ak}\sum_{cP}(kc|P)\Gamma'^{P}_{ic}+2\sum_{c}\mathbf{i} y^{\kappa}_{ci}\sum_{kP}(kc|P)\Gamma'^{P}_{ka} \\ & -2\sum_{cP}(ac|P)\Gamma'^{P,\kappa}_{ic}+2\sum_{kP}(ki|P)\Gamma'^{P,\kappa}_{ka}+\frac{\partial\overline{\overline{R}}(\mathbf{D}')_{ai}}{\partial\kappa}. \end{aligned} \tag{2.187}$$

2.6. Validation of the Derived Formulae for MP2 Second Derivatives

In the actual section we refer to the first derivation of MP2 second derivatives for imaginary perturbations pioneered and first implemented by Gauss [17]. Although the derivation was in the context of gauge-including atomic orbitals (GIAOs), which explicitly depend on the external perturbation, this basis function dependence is simply dropped for comparison purposes. The ORCA package upon the present work is based on does not yet feature GIAOs. Hence, numerical comparison would also not be possible. The starting point for the derivation of Gauss is the expression for the MP2 energy expression, which is explicitly formulated in terms of canonical molecular orbitals. By contrast, the Hylleraas functional, as orbital-invariant formulation of the correlation correction is used in the previously presented derivation, cf. eq. 2.49. Of course, both expressions become identical for canonical molecular orbitals.

$$E_{MP2} = \frac{1}{4}\sum_{ijab} t_{ab}^{ij\star}\langle ab||ij\rangle \tag{2.188}$$

The definition of the unrelaxed density is in both derivations identical,

$$D_{ij} = -\frac{1}{2}\sum_{kab} t_{ab}^{ik} t_{ab}^{jk\star} \tag{2.189}$$

$$D_{ab} = \frac{1}{2}\sum_{ijc} t_{ac}^{ij\star} t_{bc}^{ij} \tag{2.190}$$

with the double excitation amplitudes defined as,

$$t_{ij}^{ab} = \frac{\langle ab||ij\rangle}{(\varepsilon_i + \varepsilon_j - \varepsilon_a - \varepsilon_b)}. \tag{2.191}$$

The occupied-virtual block of the relaxed density is obtained as solution of the z-vector equations. In the formulation of the z-vector equations, general discrepancies occur. The z-vector equations presented in Ref. [17] are the ones that arise from a purely real perturbation,

$$\overline{z}_{bj}\left[(\varepsilon_a - \varepsilon_i) + \langle ab||ij\rangle + \langle ib||aj\rangle\right] = -X_{ai}. \tag{2.192}$$

Although, the actual perturbations with respect to which one takes the derivatives in NMR calculations are the orbital-Zeeman and nucleus-orbit interaction operators, both of which are purely imaginary in nature. Thus, the formal derivative is with respect to a purely imaginary perturbation. It appears to the author that the first derivative of the MP2 energy presented in Ref. [17] is the one obtained for a real perturbation.

Since the present thesis arrives at a slightly different result for the same perturbations, it is appropriate to compare the two derivations term by term. The MP2 Lagrangian is identical in both derivations, except for a factor of 2 arising from the Hylleraas functional.

$$\begin{aligned}\frac{d^2E}{d\lambda d\kappa} &= \sum_{pq}\left[\frac{\partial D'_{pq}}{\partial\kappa}h_{pq}^{\lambda} + D'_{pq}h_{pq}^{\lambda,\kappa}\right] + \sum_{ai}\left[\frac{\partial x_{ai}^{\lambda}}{\partial\kappa}X_{ai} + x_{ai}^{\lambda}\frac{\partial X_{ai}}{\partial\kappa}\right] \\ &= \sum_{pq}\left[\frac{\partial D_{pq}}{\partial\kappa}h_{pq}^{\lambda} + D_{pq}h_{pq}^{\lambda,\kappa}\right]\end{aligned} \tag{2.193}$$

The occupied-occupied and virtual-virtual block of the perturbed relaxed density are given as,

$$\frac{\partial D_{ij}}{\partial \kappa} = -\frac{1}{2}\sum_{kab}\left(\frac{\partial t_{ab}^{ik}}{\partial \kappa} t_{ab}^{jk\star} + t_{ab}^{ik}\frac{\partial t_{ab}^{jk\star}}{\partial \kappa}\right) \tag{2.194}$$

$$\frac{\partial D_{ab}}{\partial \kappa} = \frac{1}{2}\sum_{ijc}\left(\frac{\partial t_{ac}^{ij\star}}{\partial \kappa} t_{bc}^{ij} + t_{ac}^{ij\star}\frac{\partial t_{bc}^{ij}}{\partial \kappa}\right) \tag{2.195}$$

$$\tag{2.196}$$

with the off-diagonal elements of the perturbed relaxed density defined as,

$$\frac{\partial D_{ai}}{\partial \kappa} = \frac{1}{2}\frac{\partial \overline{z}_{ai}}{\partial \kappa} \tag{2.197}$$

$$\frac{\partial D_{ia}}{\partial \kappa} = -\frac{1}{2}\frac{\partial \overline{z}_{ai}}{\partial \kappa}. \tag{2.198}$$

The perturbed amplitude equations are identical, and the derivative of the real Lagrangian with regard to an imaginary perturbation is,

$$\begin{aligned}
\frac{\partial X_{ai}}{\partial \kappa} &= \frac{1}{2}\sum_{jbc}\left(\frac{\partial t_{bc}^{ij\star}}{\partial \kappa}\langle bc||aj\rangle + t_{bc}^{ij\star}\frac{\partial \langle bc||aj\rangle}{\partial \kappa}\right) - \frac{1}{2}\sum_{jkb}\left(\frac{\partial t_{ab}^{jk\star}}{\partial \kappa}\langle ib||jk\rangle + t_{ab}^{jk\star}\frac{\partial \langle ib||jk\rangle}{\partial \kappa}\right) \\
&\quad + \sum_{jk}\left(\frac{\partial D_{jk}}{\partial \kappa}\langle ji||ka\rangle + D_{jk}\frac{\partial \langle ji||ka\rangle}{\partial \kappa}\right) + \sum_{bc}\left(\frac{\partial D_{bc}}{\partial \kappa}\langle bi||ca\rangle + D_{bc}\frac{\partial \langle bi||ca\rangle}{\partial \kappa}\right) \\
&= \frac{1}{2}\mathbf{i}\sum_{jb} y_{bj}^{\kappa}\left\{-2\sum_{kc}\left(\langle jc||ak\rangle t_{bc}^{ik\star} + \langle ic||bk\rangle t_{ac}^{jk\star}\right) + \sum_{cd}\langle cd||ab\rangle t_{cd}^{ij\star} + \sum_{kl}\langle ij||kl\rangle t_{ab}^{kl\star}\right\} \\
&\quad + \frac{1}{2}\mathbf{i}\sum_{jkbc} y_{ak}^{\kappa}\langle bc||kj\rangle t_{bc}^{ij\star} + y_{ci}^{\kappa}\langle cb||jk\rangle t_{bc}^{ij\star} + \frac{1}{2}\sum_{jbc}\langle bc||aj\rangle t_{bc}^{ij\star,\kappa} - \frac{1}{2}\sum_{jkb}\langle ib||jk\rangle t_{ab}^{jk\star,\kappa} \\
&\quad + \sum_{jk} D_{jk}^{\kappa}\langle ji||ka\rangle + \sum_{bc} D_{bc}^{\kappa}\langle bi||ca\rangle - \mathbf{i}\sum_{d} y_{di}^{\kappa}\left(\sum_{jk} D_{jk}\langle jd||ka\rangle + \sum_{bc} D_{bc}\langle bd||ca\rangle\right) \\
&\quad + \mathbf{i}\sum_{l} y_{al}^{\kappa}\left(\sum_{jk} D_{jk}\langle ji||kl\rangle + \sum_{bc} D_{bc}\langle bi||cl\rangle\right) + \overline{\overline{R}}\left(\frac{1}{2}\tilde{\tilde{\mathbf{D}}}^{\kappa}\right)_{ai}.
\end{aligned} \tag{2.199}$$

Comparison with eqs. 2.177 and 2.178 shows, that the derivative of the real Lagrangian with respect to an imaginary perturbation is identical to the derivative of the imaginary Lagrangian with regard to an imaginary perturbation. The only difference in the second derivatives arises from the zero-order z-vector, which enters the first-order z-vector equations. Since, the zero-order z-vector is zero in our derivation the construction of the A-matrix (eq. 2.132, 2.134) is not required. Therefore, our Ansatz will be referred to as the 'imaginary' approach ($\mathfrak{Im}/\mathfrak{Im}$) in the following, whereas the derivation of Ref. [17] is referred to as ($\mathfrak{Re}/\mathfrak{Im}$) approach for comparison purposes.

In Table 2.1 the similiar and the differing terms (highlighted in blue and red) in both derivations are listed. The comparison in Table 2.1 reveals that in our derivation the imaginary z-vector equations with a vanishing imaginary Lagrangian are solved to obtain the zero-order relaxed density. The well-known real z-vector equations employing a non-zero Lagrangian are solved instead in the approach of Ref. [17]. The derivative of the corresponding Lagrangian w.r.t. a purely imaginary perturbation yields the corresponding expressions for the first-order Lagrangian. They only differ by a factor of 2 between the original and the present formulation. This factor arises from the Hylleraas functional. The first-order z-vector equations

differ significantly in the two derivations because of the derivative of the real A-matrix, which is not required in the '$\Im\mathfrak{m}/\Im\mathfrak{m}$' case, since the zero-order z-vector is zero.

Table 2.1.: Comparison of the '$\Im\mathfrak{m}/\Im\mathfrak{m}$' and '$\Re\mathfrak{e}/\Im\mathfrak{m}$' approach to MP2 second derivatives.

term	$\Im\mathfrak{m}/\Im\mathfrak{m}$	$\Re\mathfrak{e}/\Im\mathfrak{m}$
energy correction	$\mathcal{E}_2[\mathbf{t}] = \left\{ \frac{1}{4}\sum_{ijab}\langle ij\|\|ab\rangle t_{ab}^{ij(1)} + \langle ab\|\|ij\rangle t_{ab}^{ij(1)\star} + \sum_{pq} D'_{pq} F_{pq} \right\}$	$E^{(2)} = \frac{1}{4}\sum_{ijab} t_{ab}^{ij\star}\langle ab\|\|ij\rangle$
0^{th} order amplitudes	$t_{ij}^{ab} = -\frac{\langle ab\|\|ij\rangle}{(\varepsilon_a + \varepsilon_b - \varepsilon_i - \varepsilon_j)}$	$t_{ij}^{ab} = \frac{\langle ab\|\|ij\rangle}{(\varepsilon_i + \varepsilon_j - \varepsilon_a - \varepsilon_b)}$
0^{th} order density D'	$D_{ij} = -\frac{1}{2}\sum_{kab} t_{ab}^{ik} t_{ab}^{jk\star}$ $D_{ab} = \frac{1}{2}\sum_{ijc} t_{ac}^{ij\star} t_{bc}^{ij}$	$D_{ij} = -\frac{1}{2}\sum_{kab} t_{ab}^{ik} t_{ab}^{jk\star}$ $D_{ab} = \frac{1}{2}\sum_{ijc} t_{ac}^{ij\star} t_{bc}^{ij}$
0^{th} order Lagrangian	$Y_{ai} = 0$	$X_{ai} = \frac{1}{2}\sum_{jbc}\langle cb\|\|aj\rangle t_{cb}^{ij\star} - \frac{1}{2}\sum_{jkb}\langle ib\|\|kj\rangle t_{ab}^{kj\star} + \sum_{jk} D_{jk}\langle ij\|\|ak\rangle + \sum_{bc} D_{bc}\langle ib\|\|ac\rangle$
0^{th} order z-vector	$\bar{\bar{z}}_{ai} = -\sum_{jb}\left(A^{(\Im)}\right)^{-1}_{ai,bj} Y_{bj}$	$\bar{z}_{ai} = -\sum_{jb}\left(A^{(\Re)}\right)^{-1}_{ai,bj} X_{bj}$
0^{th} order CP-SCF eqs.	$U_{ai}^{\kappa} = -\sum_{jb}\left(A^{(\Im)}\right)^{-1}_{ai,bj} h_{bj}^{[\kappa]}$	$U_{ai}^{\kappa} = -\sum_{jb}\left(A^{(\Im)}\right)^{-1}_{ai,bj} h_{bj}^{[\kappa]}$

Continued.

term	$\Im\mathfrak{m}/\Im\mathfrak{m}$	$\Re\mathfrak{e}/\Im\mathfrak{m}$
1st order amplitudes	$t_{ab}^{ij,\kappa} = \Bigg[\sum_k \mathbf{i} y_{ak}^{\kappa} \langle ij\|\|kb\rangle + \mathbf{i} y_{bk}^{\kappa} \langle ij\|\|ak\rangle - \sum_c \mathbf{i} y_{ci}^{\kappa} \langle cj\|\|ab\rangle + \mathbf{i} y_{cj}^{\kappa} \langle ic\|\|ab\rangle + \sum_k \left(t_{ab}^{ik\star} F_{jk}^{\kappa} + F_{ik}^{\kappa} t_{ab}^{kj\star} \right) - \sum_c \left(t_{ac}^{ij\star} F_{cb}^{\kappa} + F_{ca}^{\kappa} t_{cb}^{ij\star} \right) \Bigg] \times \left(\varepsilon_a + \varepsilon_b - \varepsilon_i - \varepsilon_j \right)^{-1}$	$t_{ab}^{ij,\kappa} = \Bigg[- \sum_k \mathbf{i} y_{ak}^{\kappa} \langle ij\|\|kb\rangle + \mathbf{i} y_{bk}^{\kappa} \langle ij\|\|ak\rangle + \sum_c \mathbf{i} y_{ci}^{\kappa} \langle cj\|\|ab\rangle + \mathbf{i} y_{cj}^{\kappa} \langle ic\|\|ab\rangle - \sum_k \left(t_{ab}^{ik\star} F_{jk}^{\kappa} + F_{ik}^{\kappa} t_{ab}^{kj\star} \right) + \sum_c \left(t_{ac}^{ij\star} F_{cb}^{\kappa} + F_{ca}^{\kappa} t_{cb}^{ij\star} \right) \Bigg] \times \left(\varepsilon_i + \varepsilon_j - \varepsilon_a - \varepsilon_b \right)^{-1}$
1st order density D'^{κ}	$D_{ij}^{\kappa} = -\frac{1}{2} \sum_{kab} \left(t_{ab}^{ik,\kappa} t_{ab}^{jk\star} + t_{ab}^{ik} t_{ab}^{jk\star,\kappa} \right)$ $D_{ab}^{\kappa} = \frac{1}{2} \sum_{ijc} \left(t_{ac}^{ij\star,\kappa} t_{bc}^{ij} + t_{ac}^{ij\star} t_{bc}^{ij,\kappa} \right)$	$D_{ij}^{\kappa} = -\frac{1}{2} \sum_{kab} \left(t_{ab}^{ik,\kappa} t_{ab}^{jk\star} + t_{ab}^{ik} t_{ab}^{jk\star,\kappa} \right)$ $D_{ab}^{\kappa} = \frac{1}{2} \sum_{ijc} \left(t_{ac}^{ij\star,\kappa} t_{bc}^{ij} + t_{ac}^{ij\star} t_{bc}^{ij,\kappa} \right)$
1st order Lagrangian	$\frac{\partial Y_{ai}}{\partial \kappa} = \mathbf{i} \sum_{bj} y_{bj}^{\kappa} \Bigg\{ -2 \sum_{kc} \left(\langle jc\|\|ak\rangle t_{bc}^{ik} + \langle ic\|\|bk\rangle t_{ac}^{jk} \right) + \sum_{cd} \langle cd\|\|ab\rangle t_{cd}^{ij} + \sum_{kl} \langle ij\|\|kl\rangle t_{ab}^{kl} \Bigg\} + \mathbf{i} \sum_k y_{ak}^{\kappa} \langle cb\|\|kj\rangle t_{cb}^{ij} + \mathbf{i} \sum_c y_{ci}^{\kappa} \langle cb\|\|kj\rangle t_{ab}^{kj} - \sum_{jbc} \langle aj\|\|cb\rangle t_{cb}^{ij,\kappa} + \sum_{jkb} \langle kj\|\|ib\rangle t_{ab}^{kj,\kappa} + \sum_{jk} D_{jk}'^{\kappa} \left[-\langle aj\|\|ik\rangle + \langle ij\|\|ak\rangle \right] + \sum_{bc} D_{bc}'^{\kappa} \left[-\langle ab\|\|ic\rangle + \langle ib\|\|ac\rangle \right] + \overline{\overline{R}} \left(\tilde{\tilde{\mathbf{D}}}^{\kappa} \right)_{ai} - \mathbf{i} \sum_d y_{di}^{\kappa} \left(\sum_{jk} D_{jk} \left[\langle aj\|\|dk\rangle + \langle dj\|\|ak\rangle \right] + \sum_{bc} D_{bc} \left[\langle ab\|\|dc\rangle + \langle db\|\|ac\rangle \right] \right) + \mathbf{i} \sum_l y_{al}^{\kappa} \left(\sum_{jk} D_{jk} \left[\langle lj\|\|ik\rangle + \langle ij\|\|lk\rangle \right] + \sum_{bc} D_{bc} \left[\langle lb\|\|ic\rangle + \langle ib\|\|lc\rangle \right] \right)$	$\frac{\partial X_{ai}}{\partial \kappa} = \frac{1}{2} \mathbf{i} \sum_{jb} y_{bj}^{\kappa} \Bigg\{ -2 \sum_{kc} \left(\langle jc\|\|ak\rangle t_{bc}^{ik\star} + \langle ic\|\|bk\rangle t_{ac}^{ik\star} \right) + \sum_{cd} \langle cd\|\|ab\rangle t_{cd}^{ij\star} + \sum_{kl} \langle ij\|\|kl\rangle t_{ab}^{kl\star} \Bigg\} + \frac{1}{2} \mathbf{i} \sum_{jkbc} y_{ak}^{\kappa} \langle bc\|\|kj\rangle t_{bc}^{ij\star} + \mathbf{i} y_{ci}^{\kappa} \langle cb\|\|jk\rangle t_{bc}^{ij\star} + \frac{1}{2} \sum_{jbc} \langle bc\|\|aj\rangle t_{bc}^{ij\star,\kappa} - \frac{1}{2} \sum_{jkb} \langle ib\|\|jk\rangle t_{ab}^{jk\star,\kappa} + \sum_{jk} D_{jk}^{\kappa} \langle ji\|\|ka\rangle + \sum_{bc} D_{bc}^{\kappa} \langle bi\|\|ca\rangle + \overline{\overline{R}} \left(\frac{1}{2} \tilde{\tilde{\mathbf{D}}}^{\kappa} \right)_{ai} - \mathbf{i} \sum_d y_{di}^{\kappa} \left(\sum_{jk} D_{jk} \langle jd\|\|ka\rangle + \sum_{bc} D_{bc} \langle bd\|\|ca\rangle \right) + \mathbf{i} \sum_l y_{al}^{\kappa} \left(\sum_{jk} D_{jk} \langle ji\|\|kl\rangle + \sum_{bc} D_{bc} \langle bi\|\|cl\rangle \right)$

Continued.

term	$\Im\mathfrak{m}/\Im\mathfrak{m}$	$\Re\mathfrak{e}/\Im\mathfrak{m}$
1st order z-vector	$\overline{\overline{z}}^{\kappa}_{ai} = -\sum_{jb}\left(A^{(\Im)}\right)^{-1}_{ai,bj}\frac{\partial Y_{bj}}{\partial\kappa}$ with $\overline{\overline{z}}_{ai}=0$	$\overline{z}^{\kappa}_{ai} = -\sum_{jb}\left(A^{(\Im)}\right)^{-1}_{ai,bj}\frac{\partial X_{bj}}{\partial\kappa} + \left(A^{(\Im)}\right)^{-1}_{ai,bj}\frac{\partial A^{(\Re)}_{ai,bj}}{\partial\kappa}\overline{z}_{bj}$

It has to be pointed out, that from the point of view taken in this thesis the collection of terms in the zero-order real Lagrangian is only possible, if the derivative w.r.t. purely real perturbations is required. In the above derivation a mixture of real and imaginary perturbations is on hand. In general, the real Lagrangian should be written in the following form,

$$\begin{aligned} X_{ai} = {} & \frac{1}{4}\sum_{jbc}\langle cb||aj\rangle t^{ij\star}_{cb} + \langle aj||cb\rangle t^{ij}_{cb} - \frac{1}{4}\sum_{jkb}\langle ib||kj\rangle t^{kj\star}_{ab} + \langle kj||ib\rangle t^{kj}_{ab} \\ & + \frac{1}{2}\sum_{jk} D_{jk}\left[\langle ij||ak\rangle + \langle aj||ik\rangle\right] + \frac{1}{2}\sum_{bc} D_{bc}\left[\langle ib||ac\rangle + \langle ab||ic\rangle\right]. \end{aligned} \tag{2.200}$$

Formulating the derivative of eq. 2.200 w.r.t. a purely imaginary perturbation will not yield the expression for the perturbed Lagrangian in eq. 2.199, but instead,

$$\begin{aligned} \frac{\partial X_{ai}}{\partial\kappa} = {} & \frac{1}{4}\mathbf{i}\sum_{jb} y^{\kappa}_{bj}\left\{2\sum_{kc}\left[-\langle jc||ak\rangle t^{ik\star}_{bc} + \langle ak||jc\rangle t^{ik}_{bc} + \langle ic||bk\rangle t^{jk\star}_{ac} - \langle bk||ic\rangle t^{jk}_{ac}\right]\right. \\ & \left. + \sum_{cd}\langle cd||ab\rangle t^{ij\star}_{cd} - \langle ab||cd\rangle t^{ij}_{cd} + \sum_{kl} -\langle ij||kl\rangle t^{kl\star}_{ab} + \langle kl||ij\rangle t^{kl}_{ab}\right\} \\ & + \frac{1}{4}\mathbf{i}\sum_{jkbc} y^{\kappa}_{ak}\left[\langle cb||kj\rangle t^{ij\star}_{cb} - \langle kj||cb\rangle t^{ij}_{cb}\right] + y^{\kappa}_{ci}\left[-\langle cb||kj\rangle t^{kj\star}_{ab} + \langle kj||cb\rangle t^{kj}_{ab}\right] \\ & + \frac{1}{4}\sum_{jbc}\langle cb||aj\rangle t^{ij\star,\kappa}_{cb} + \langle aj||cb\rangle t^{ij,\kappa}_{cb} - \frac{1}{4}\sum_{jkb}\langle ib||kj\rangle t^{kj\star,\kappa}_{ab} + \langle kj||ib\rangle t^{kj,\kappa}_{ab} \\ & + \frac{1}{2}\overline{R}(\mathbf{D}^{\kappa})_{ai} + \frac{1}{2}\mathbf{i}\sum_{l} y^{\kappa}_{al}\overline{\overline{R}}(\mathbf{D})_{li} + \frac{1}{2}\mathbf{i}\sum_{b} y^{\kappa}_{bi}\overline{\overline{R}}(\mathbf{D})_{ba} + \overline{R}\left(\frac{1}{2}\check{\mathbf{D}}^{\kappa}\right)_{ai} \end{aligned} \tag{2.201}$$

with

$$\begin{aligned} \check{D}^{\kappa}_{bj} &= \mathbf{i}\sum_{k}\left(D_{jk}y^{\kappa}_{kb} - y^{\kappa}_{bk}D_{kj}\right) + \mathbf{i}\sum_{c}\left(D_{bc}y^{\kappa}_{cj} - y^{\kappa}_{jc}D_{cb}\right) \\ &= \mathbf{i}\sum_{k} y^{\kappa}_{kb}\underbrace{\left(D_{jk} - D_{kj}\right)}_{=0} + \mathbf{i}\sum_{c} y^{\kappa}_{cj}\underbrace{\left(D_{bc} - D_{cb}\right)}_{=0}. \end{aligned} \tag{2.202}$$

The first twelve terms in eq. 2.201 vanish, due to the real nature of the two-electron repulsion integrals and the zero-order amplitudes. The terms containing the first-order amplitudes cancel each other, due to the relation between the perturbed real and complex conjugate amplitudes (cf. eqs. 2.170 and 2.171). The derivative of the real response operator w.r.t. an imaginary perturbation vanishes, since the real response operator over an antisymmetric density matrix is zero and similarly the imaginary response operator over

a symmetric density matrix as well. The contracted density matrix $\check{\mathbf{D}}^{\kappa}$ itself is zero, due to the symmetry properties of the matrices involved. In summary, the derivative of the real zero-order Lagrangian w.r.t. an imaginary perturbation is zero and hence, the first-order z-vector gives no contribution to the first-order relaxed density matrix.

2.7. The RIJCOSX Approximation to MP2

In RI-MP2 energy calculations the computation time for the evaluation of the RI-MP2 energy correction exceeds by far the time required for the solution of the SCF equations. Despite the unfavourable scaling of the MP2 step, which scales with $\mathcal{O}(N^5)$, the SCF calculation with a practically observed scaling of $\mathcal{O}(N^{1.5})$ dominates the total wall clock time. In order to overcome the drawbacks of Coulomb and exchange formation algorithms, which proceed via the generation of traditional four-index two-electron integrals, the best approximations for each contribution should be selected. [35, 36]
The 'Resolution of the Identity' approximation to the Coulomb matrix (RI-J) was first invented in the framework of density functional theory (DFT) [37, 38] and has been discussed in detail in section 2.4.1. The error introduced by the incompleteness of the fitting bases could be shown to be negligible, whereas the speedups obtained are of a factor of $10-100$. [28,29] Thus, as long as exact exchange is not required, the Coulomb fitting gives rise to SCF calculations that are $1-2$ orders of magnitude more efficient than traditional Hartree-Fock calculations.
The RIJCOSX approximation combines the advantages of the Split-RI-J variant of the Coulomb density fitting approximation with a semi-numeric exchange treatment, which is efficiently implemented via the 'chain of spheres exchange' (COSX) algorithm [39] into the ORCA program package. Hence, this algorithm is termed RIJCOSX-MP2. COSX is closely related to Friesners pioneering pseudo-spectral techniques but is conceptually simpler as discussed in detail in Ref. [39]. In this section this concept is extended to the first and second derivatives of the RIJCOSX-MP2 energy. Substantial savings compared to the standard MP2 and also to the RI-MP2 method arise from the more efficient SCF step, the more efficient treatment of AO derivative integrals and the accelerated solution of the z-vector equations. [14]

2.7.1. The Semi-Numeric Exchange Matrix

The basic idea for the efficient evaluation of exchange-type matrices is to combine a numeric integration in the physical space with an analytic integration over the Coulomb singularity. The original pseudospectral method has been developed by Friesner and co-workers since the mid 1980s. [40–43] Recently, Neese and co-workers presented a semi-numeric exchange formation on the basis of Friesners' pseudospectral method, but with conceptual simplifications. [39] The conventional exchange-type matrix is given as,

$$K_{\mu\nu} = \sum_{\kappa\tau} P_{\kappa\tau} \, (\mu\kappa|\nu\tau) \tag{2.203}$$

where $P_{\kappa\tau}$ is any density-type matrix. The exchange integrals can be approximated as,

$$\begin{aligned}(\mu\kappa|\nu\tau) = & \int d\mathbf{r}' \varphi_{\mu}(\mathbf{r}')\varphi_{\kappa}(\mathbf{r}') \int d\mathbf{r} \frac{\varphi_{\nu}(\mathbf{r})\varphi_{\tau}(\mathbf{r})}{|\mathbf{r}-\mathbf{r}'|} \\ \approx & \sum_{g} w_g \varphi_{\mu}(\mathbf{r}_g)\varphi_{\kappa}(\mathbf{r}_g) \int d\mathbf{r} \frac{\varphi_{\nu}(\mathbf{r})\varphi_{\tau}(\mathbf{r})}{|\mathbf{r}-\mathbf{r}_g|}\end{aligned} \tag{2.204}$$

where the first analytical integration over the coordinates $\mathbf{r}'$ is replaced by a numerical integration over grid points $\mathbf{r}_g$. The corresponding grid weights w_g are determined by Becke's weighting scheme. [44] The exchange-type matrix can then be efficiently evaluated as,

$$\begin{aligned} K_{\mu\nu} &\approx \sum_g R_{\mu g} \sum_\tau A_{\nu\tau}(\mathbf{r}_g) \sum_\kappa R_{\kappa g} P_{\kappa\tau} \\ &= tr\left(\mathbf{R}\mathbf{G}^+\right)_{\mu\nu}. \end{aligned} \tag{2.205}$$

with

$$R_{\mu g} = w_g^{\frac{1}{2}} \varphi_\mu(\mathbf{r}_g) \tag{2.206}$$

$$F_{\tau g} = (\mathbf{P}\mathbf{R})_{\tau g} \tag{2.207}$$

$$A_{\nu\tau}(\mathbf{r}_g) = \int \frac{\varphi_\nu(\mathbf{r})\varphi_\tau(\mathbf{r})}{|\mathbf{r} - \mathbf{r}_g|} d\mathbf{r} \tag{2.208}$$

$$G_{\nu g} = \sum_\tau F_{\tau g} A_{\nu\tau}(\mathbf{r}_g). \tag{2.209}$$

Note, the absence of least-square fitting operators or any of the advanced features that characterize the pseudospectral approach. [45]

Semi-Numeric Exchange Gradient

The exchange gradient can be written as,

$$\frac{\partial K_{\mu\nu}}{\partial \lambda} = \sum_{\kappa\tau} P_{\kappa\tau} \frac{\partial(\mu\kappa|\nu\tau)}{\partial\lambda}. \tag{2.210}$$

Due to the permutational symmetry of the exchange integrals, the derivative expression can be rearranged as follows,

$$\sum_{\kappa\tau} P_{\kappa\tau} \left(\mu\kappa|\nu\tau^\lambda\right) \approx \sum_g R_{\mu g} \sum_\tau A_{\nu\tau^\lambda}(\mathbf{r}_g) \sum_\kappa R_{\kappa g} P_{\kappa\tau} \tag{2.211}$$

$$= \sum_{\kappa\tau} P_{\kappa\tau} \left(\nu\tau^\lambda|\mu\kappa\right) \approx \sum_g R_{\nu g} \sum_\kappa A_{\mu\kappa}(\mathbf{r}_g) \sum_\tau R_{\tau^\lambda g} P_{\kappa\tau} \tag{2.212}$$

where $R_{\tau^\lambda g}$ is defined by,

$$R_{\tau^\lambda g} = w_g^{\frac{1}{2}} \frac{\partial \varphi_\tau(\mathbf{r}_g)}{\partial\lambda}. \tag{2.213}$$

The formulation of the exchange gradient differs only slightly from the derivation of the semi-numeric exchange itself. Due to the rearrangement of the two-electron exchange gradient integrals only the derivatives of the basis functions on the grid are needed instead of the derivatives of the analytic integrals.

2.7.2. RIJCOSX-MP2 Derivatives

The RIJCOSX approximation to the total RI-MP2 energy is given as,

$$\begin{aligned}\mathcal{E} &\approx \mathcal{E}_0^{(RIJCOSX)} + \mathcal{E}_2^{(RI)} \\ &= \sum_{\mu\nu} P_{\mu\nu} h_{\mu\nu} + \frac{1}{2} \sum_{\mu\nu\kappa\tau} P_{\mu\nu} P_{\kappa\tau} \sum_K B^K_{\mu\nu} B^K_{\kappa\tau} - \frac{1}{2} \sum_{\mu\nu} tr(\mathbf{FG}^+)_{\mu\nu} + \frac{1}{2} \sum_{\mu\nu P} (\mu\nu|P) \Gamma'^P_{\mu\nu}\end{aligned} \tag{2.214}$$

where the Hartree-Fock Coulomb contribution is approximated by the RI-J technique with the Coulomb fitting basis set $\{\eta_K\}$, and the MP2 energy correction is calculated employing the RI approximation with the correlation fitting basis set $\{\eta_P\}$. In contrast, the exchange contribution to the Hartree-Fock energy is evaluated via the COSX algorithm. In principle, only the Fock matrix is approximated via the RIJCOSX algorithm, whereas the RI-MP2 energy correction is evaluated in the conventional way.

The First RIJCOSX-MP2 Derivative

In the first derivative of the RIJCOSX-MP2 energy the RIJCOSX approximation goes into the terms originating from the Fock matrix derivatives, i.e. the response-type operator in the Lagrangian (eqs. 2.129, 2.131) and the left-hand side of the z-vector equations (eqs. 2.133, 2.134). Thus, the RIJCOSX-MP2 Lagrangians become,

$$X^{(RIJCOSX)}_{ai} = 2 \sum_{cP} (ac|P) \Gamma'^P_{ic} - 2 \sum_{kP} (ki|P) \Gamma'^P_{ka} + \tilde{\tilde{R}} (\mathbf{D}')_{ai} \equiv \tilde{X}_{ai} \tag{2.215}$$

$$Y^{(RIJCOSX)}_{ai} = \sum_{cP} -(ac|P) \Gamma'^P_{ic} + (ca|P) \Gamma'^P_{ci} + \sum_{kP} (ki|P) \Gamma'^P_{ka} - (ik|P) \Gamma'^P_{ak} + \bar{\bar{\tilde{R}}} (\mathbf{D}')_{ai} \equiv \tilde{Y}_{ai} \tag{2.216}$$

with

$$\tilde{\tilde{R}} (\mathbf{D}')_{ai} = 2 \sum_{pq} D'_{pq} \sum_K B^K_{ai} B^K_{pq} - \sum_g R_{ag} G^{\mathbf{D}'}_{ig} + R_{ig} G^{\mathbf{D}'}_{ag} \tag{2.217}$$

$$\bar{\bar{\tilde{R}}} (\mathbf{D}')_{ai} = \sum_g R_{ag} G^{\mathbf{D}'}_{ig} - R_{ig} G^{\mathbf{D}'}_{ag} \tag{2.218}$$

and

$$G^{\mathbf{D}'}_{pg} = \sum_r F^{\mathbf{D}'}_{rg} A_{pr}(\mathbf{r}_g) \tag{2.219}$$

$$F^{\mathbf{D}'}_{rg} = (\mathbf{D}' \tilde{\mathbf{X}})_{rg}. \tag{2.220}$$

The z-vector equations in the RIJCOSX approximation are given by,

$$\bar{z}_{ai}(\varepsilon_a - \varepsilon_i) + 2 \sum_{jb} \bar{z}_{bj} \sum_K B^K_{ai} B^K_{bj} - \sum_g R_{ag} \sum_b A_{bi}(\mathbf{r}_g) F^{\bar{\mathbf{z}}}_{bg} - \sum_g R_{ag} \sum_j A_{ji}(\mathbf{r}_g) F^{\bar{\mathbf{z}}}_{jg} = -\tilde{X}_{ai} \tag{2.221}$$

$$\mathbf{i} \bar{\bar{z}}_{ai}(\varepsilon_a - \varepsilon_i) + \mathbf{i} \sum_g R_{ag} \sum_b A_{bi}(\mathbf{r}_g) F^{\bar{\bar{\mathbf{z}}}}_{bg} - \mathbf{i} \sum_g R_{ag} \sum_j A_{ji}(\mathbf{r}_g) F^{\bar{\bar{\mathbf{z}}}}_{jg} = -\tilde{Y}_{ai} \tag{2.222}$$

where the generation of traditional four-index two-electron repulsion integrals can be avoided.

The RIJCOSX-MP2 Gradient

The general form of the MP2 gradient is given as,

$$\frac{\partial \mathcal{E}}{\partial \lambda} = \sum_{pq} D_{pq} h_{pq}^{\{\lambda\}} + \sum_{pq} W_{pq} S_{pq}^{(\lambda)} + \sum_{pqrs} \Gamma_{pqrs} (pq|rs)^{(\lambda)} \tag{2.223}$$

where the additional terms arise from the perturbation dependence of the basis functions. The energy weighted density matrix within the RIJCOSX approximation $\tilde{W}$ is defined as,

$$\tilde{W}_{ij} = -\sum_{kabP} B_{ia}^{P} B_{kb}^{P} t_{ab}^{jk} - \frac{1}{2} D_{ij} (\varepsilon_i + \varepsilon_j) - \frac{1}{2} \tilde{\tilde{R}} (\mathbf{D})_{ij} \tag{2.224}$$

$$\tilde{W}_{ab} = -\sum_{ijcP} B_{ia}^{P} B_{kc}^{P} t_{bc}^{ij} - \frac{1}{2} D_{ab} (\varepsilon_a + \varepsilon_b) \tag{2.225}$$

$$\tilde{W}_{ai} = -2 \sum_{kP} (ik|P) \Gamma'^{P}_{ak} \tag{2.226}$$

and the separable (S) and non-separable (NS) parts of the 2-particle 4-index density matrix $\tilde{\Gamma}$ are,

$$\begin{aligned}
\tilde{\Gamma}^{S}_{pqrs} (pq|rs)^{(\lambda)} &= \big(D_{pq} - D_{pr}\big)(pq|rs)^{(\lambda)} \\
&= D_{pq} \Big((pq|rs)^{(\lambda)} - (ps|rq)^{(\lambda)} \Big) \\
&= D_{pq} \Bigg[2 \sum_{KL} (pq|K)^{(\lambda)} V_{KL}^{-1} (L|rs) - \sum_{KLMN} (pq|M) V_{MK}^{-1} V_{KL}^{(\lambda)} V_{LN}^{-1} (N|rs) \Bigg] \\
&\quad - 2 \sum_{g} \frac{\partial F_{pg}}{\partial \lambda} G_{qg}^{MP2} - 2 \sum_{g} \frac{\partial F_{pg}^{MP2}}{\partial \lambda} G_{qg}
\end{aligned} \tag{2.227}$$

$$\begin{aligned}
\tilde{\Gamma}^{NS}_{iajb} (ia|jb)^{(\lambda)} &= \frac{1}{2} t_{ab}^{ij} \Bigg[\sum_{RS} \Big\{ (ia|R)^{(\lambda)} V_{RS}^{-1} (S|jb) + (ia|R) V_{RS}^{-1} (S|jb)^{(\lambda)} \Big\} \\
&\quad - \sum_{RSTU} (ia|T) V_{TR}^{-1} V_{RS}^{(\lambda)} V_{SU}^{-1} (U|jb) \Bigg].
\end{aligned} \tag{2.228}$$

A detailed derivation of the working equations for the RIJCOSX-MP2 gradient has been reported in Ref. [31].

The Second RIJCOSX-MP2 Derivative

In the second MP2 derivative the calculation of the perturbed double excitation amplitudes which incorporate the derivative Fock matrix elements is required. Therefore, the RIJCOSX approximation implicitly affects the computation of the first-order amplitudes by accelerating the formation of the first-order Fock matrix.

$$\tilde{F}_{pq}^{(\Re),\kappa} = h_{pq}^{[\lambda]} + \tilde{\tilde{R}} (\mathbf{U})_{ai} \tag{2.229}$$

$$\tilde{F}_{pq}^{(\Im),\kappa} = h_{pq}^{[\lambda]} + \tilde{\tilde{R}} (\mathbf{U})_{ai} \tag{2.230}$$

Furthermore, the derivative of the response-type operators as contributions to the perturbed Lagrangians are also approximated via the RIJCOSX technique according to the first-order response-type operators in eqs. 2.217 and 2.218.

The Four-External Contribution to the First-Order Lagrangian The most expensive term in the calculation of the real as well as of the imaginary second MP2 derivative is the 4-external contribution $K(\mathbf{t}^{ij})_{ab}$ to the first-order Lagrangian, cf. eqs. 2.183 and 2.187. The evaluation of this term takes at least about 20% of the total wall clock time and hence, represents the rate limiting step. Therefore, efficient algorithms have to be developed to overcome this bottleneck. Since, there exist no efficient implementations of the four-external contribution to the perturbed Lagrangian within the RI approximation the standard implementation proceeds via traditional AO four-index integrals and uses large-scale BLAS level 3 matrix multiplications in the inner loops. An alternative Ansatz is to calculate this contribution via the 'chain of spheres exchange' algorithm, as,

$$\sigma_{ab}^{ij(4-ext)} = \sum_{cd}(ac|bd)t_{cd}^{ij} \approx \sum_{cd}\sum_{g} w_g \psi_a(\mathbf{r}_g)\psi_c(\mathbf{r}_g) \int d\mathbf{r} \frac{\psi_b(\mathbf{r})\psi_d(\mathbf{r})}{|\mathbf{r}-\mathbf{r}_g|} t_{cd}^{ij} \equiv \tilde{K}(\mathbf{t}^{ij})_{ab}. \tag{2.231}$$

The performance of the two alternative approaches will be numerically compared in Section 4.1.3.

2.8. Derivatives of Double-Hybrid Density Functionals

2.8.1. Density Functional Theory

The basis of density functional theory (DFT) is built on the two Hohenberg-Kohn theorems. [46] The first Hohenberg-Kohn theorem demonstrates that the electronic ground state energy is fully determined by the electron density ρ. Therefore, the energy becomes a unique functional of the electron density and depends only on three spatial coordinates. The second Hohenberg-Kohn theorem states, that the ground state energy can be obtained variationally. The exact ground state electron density is the one, that minimizes the total energy.
The break through of DFT was due to Kohn-Sham theory. [47] The basic idea is to relate a system of non-interacting electrons moving in an effective potential to the real system of interacting electrons in a static potential. The effective potential includes the external potential (V_{eN}) and the electronic exchange and correlation interactions. Thus, the energy becomes,

$$E[\rho] = T_S[\rho] + \int v_{ext}(\mathbf{r})\rho(\mathbf{r})d\mathbf{r} + \int\int \frac{\rho(\mathbf{r})\rho(\mathbf{r}')}{|\mathbf{r}-\mathbf{r}'|} d\mathbf{r}d\mathbf{r}' + E_{XC}[\rho] \tag{2.232}$$

where $T_S[\rho]$ is the Kohn-Sham kinetic energy calculated from the Kohn-Sham orbitals. Unfortunately, the exact energy functional is only known for the free electron gas. Thus, the major problem of DFT is to mimic the exact density functional as exact as possible. The density functionals are best classified by its ingredients, refered to as 'Jacob's ladder', [48]

- Local-Spin-Density Approximation (LSDA): $E^{XC} = \int f(\rho_\alpha, \rho_\beta)d\mathbf{r}$
- Generalized Gradient Approximation (GGA): $E^{XC} = \int f(\rho_\alpha, \rho_\beta, \gamma_{\alpha\alpha}, \gamma_{\alpha\beta}, \gamma_{\beta\beta})d\mathbf{r}$
- Meta-Generalized Gradient Approximation (meta-GGA): $E^{XC} = \int f(\rho_\alpha, \rho_\beta, \gamma_{\alpha\alpha}, \gamma_{\alpha\beta}, \gamma_{\beta\beta}, \tau_\alpha, \tau_\beta)d\mathbf{r}$
- Hybrid- and Hyper-Generalized Gradient Approximation (hyper-GGA): $E^{XC} = \int f(\rho_\alpha, \rho_\beta, \gamma_{\alpha\alpha}, \gamma_{\alpha\beta}, \gamma_{\beta\beta}, (\tau_\alpha, \tau_\beta), \varepsilon_X)d\mathbf{r}$
- Random Phase Approximation (RPA): $E^{XC} = \int f(\rho_\alpha, \rho_\beta, \gamma_{\alpha\alpha}, \gamma_{\alpha\beta}, \gamma_{\beta\beta}, \varepsilon_X, \{\psi_a^\sigma\})d\mathbf{r}$

with the density gradient $\gamma_{\sigma\sigma'} = \nabla\rho_\sigma\nabla\rho_{\sigma'}$, the kinetic energy density $\tau_\sigma = \frac{1}{2}\sum_i |\psi_i^\sigma|^2$, the exact exchange ε_X and the inclusion of virtual Kohn-Sham molecular orbitals $\{\psi_a^\sigma\}$.

2.8.2. Double-Hybrid Density Functionals

Double-hybrid density functionals supplement the well-known hybrid density functionals by a semiempirically scaled second-order perturbation correction. Thus, the solution of the Kohn-Sham SCF equations serves as zero-order reference for the perturbation expansion. Since, the DFT Hamiltonian already partially accounts for electron correlation effects through the exchange-correlation potential, the perturbation correction has to be scaled. The double-hybrid functionals replace part of the semi-local correlation present in gradient corrected functionals by nonlocal, orbital-dependent dynamic correlation. In Perdew's [48] concept of 'Jacobs's ladder', double-hybrid functionals occupy the 'fifth rung' of the metaphorical ladder, which leads from the 'Hartee World' to the 'Heaven of Chemical Accuracy'. Density functionals of the 'fifth rung' include non-local correlation by involving virtual Kohn-Sham [47] molecular orbitals.

The energy expression for perturbatively and gradient corrected hybrid functionals is, [49]

$$E = V_{NN} + \sum_{\mu\nu} P_{\mu\nu} h_{\mu\nu} + \frac{1}{2}\int\int \frac{\rho(\mathbf{r}_1)\rho(\mathbf{r}_2)}{|\mathbf{r}_1 - \mathbf{r}_2|} - \frac{1}{2} a_x \sum_{\mu\nu\kappa\tau\sigma} P^{\sigma}_{\mu\kappa} P^{\sigma}_{\nu\tau} (\mu\nu|\kappa\tau) + c_{DF} E^{XC}[\rho_\alpha, \rho_\beta] + c_{PT2} E_{PT2} \tag{2.233}$$

with V_{NN} representing the nuclear repulsion energy and $h_{\mu\nu}$ is a matrix element of the one-electron operator. The Coulombic interaction is represented by the third term in eq. 2.233 and the fourth term is the Hartree-Fock exchange. The global scaling parameters allow to procced from Hartree-Fock ($a_x = 1, c_{DF} = 0, c_{PT2} = 0$) to MP2 theory ($a_x = 1, c_{DF} = 0, c_{PT2} = 1$), from pure DFT ($a_x = 0, c_{DF} = 1, c_{PT2} = 0$) to hybrid DFT ($0 < a_x < 1, c_{DF} = 1, c_{PT2} = 0$) and finally to the double-hybrid functionals ($0 < a_x < 1, c_{DF} = 1, 0 < c_{PT2} < 1$). The molecular spin orbitals are expanded in atomic centered basis functions with MO coefficients $c_{\mu p}$ as ($\sigma = \alpha, \beta$),

$$\psi^{\sigma}_{p}(\mathbf{r}) = \sum_{\mu} c^{\sigma}_{\mu i} \varphi_\mu(\mathbf{r}). \tag{2.234}$$

with the electron density given as,

$$\rho(\mathbf{r}) = \sum_{i\sigma} |\psi^{\sigma}_{i}(\mathbf{r})|^2 = \sum_{\mu\nu\sigma} P^{\sigma}_{\mu\nu} \varphi_\mu(\mathbf{r}) \varphi_\nu(\mathbf{r}) = \rho_\alpha(\mathbf{r}) + \rho_\beta(\mathbf{r}) \tag{2.235}$$

and the σ-spin density matrix $P^{\sigma}_{\mu\nu} = \sum_i c^{\sigma}_{\mu i} c^{\sigma}_{\nu i}$. The exchange-correlation contribution to the total energy is,

$$E^{XC} = \int f(\rho_\alpha, \rho_\beta, \gamma_{\alpha\alpha}, \gamma_{\alpha\beta}, \gamma_{\beta\beta}) d\mathbf{r}. \tag{2.236}$$

The Fock matrix is defined as,

$$F^{\sigma}_{\mu\nu} = h_{\mu\nu} + \sum_{\kappa\tau} P_{\kappa\tau} (\mu\nu|\kappa\tau) - a_x P^{\sigma}_{\kappa\tau} (\mu\kappa|\nu\tau) + c_{DF} V^{XC}_{\mu\nu} \tag{2.237}$$

with the exchange-correlation potential V^{XC} defined as,

$$V^{XC,\sigma}_{\mu\nu} = \frac{\delta f}{\delta \rho_\sigma} (\varphi_\mu(\mathbf{r}) \varphi_\nu(\mathbf{r})) + 2 \frac{\delta f}{\delta \gamma_{\sigma\sigma}} \vec{\nabla} \rho_\sigma \vec{\nabla} (\varphi_\mu(\mathbf{r}) \varphi_\nu(\mathbf{r})) + \frac{\delta f}{\delta \gamma_{\sigma\sigma'}} \vec{\nabla} \rho_{\sigma'} \vec{\nabla} (\varphi_\mu(\mathbf{r}) \varphi_\nu(\mathbf{r})). \tag{2.238}$$

The derivative of the Fock operator is given as,

$$\begin{aligned}\frac{\partial F_{pq}}{\partial\lambda} &= F_{pq}^{(\lambda)} + h_{pq}^{[\lambda]} + \sum_r U_{rp}^{\lambda\star} F_{rq} + U_{rq}^{\lambda} F_{pr} \\ &\quad + \sum_{kr} U_{rk}^{\lambda\star}\big[(pq|rk) - a_x(pk|rq)\big] + U_{rk}^{\lambda}\big[(pq|kr) - a_x(pr|kq)\big] + c_{DF}\left(\frac{\delta V_{pq}^{XC}}{\delta\zeta}\frac{\partial\zeta}{\partial\lambda}\right) \\ &= F_{pq}^{(\lambda)} + h_{pq}^{[\lambda]} + \sum_r U_{rp}^{\lambda\star} F_{rq} + U_{rq}^{\lambda} F_{pr} + R(\mathbf{U}^{\lambda})_{pq}\end{aligned} \tag{2.239}$$

with the response-type operator defined as,

$$\begin{aligned}R(\mathbf{U}^{\lambda})_{pq\sigma} &= \sum_{kr} U_{rk}^{\lambda\star}\big[(pq|rk) - a_x(pk|rq)\big] + U_{rk}^{\lambda}\big[(pq|kr) - a_x(pr|kq)\big] + c_{DF}\underbrace{\left(\frac{\delta V_{pq}^{XC}}{\delta\zeta}\frac{\partial\zeta}{\partial\lambda}\right)}_{R^{XC}(\mathbf{U}^{\lambda})_{pq}} \\ &= \sum_{kr} U_{rk}^{\lambda\star}\big[(pq|rk) - a_x(pk|rq)\big] + U_{rk}^{\lambda}\big[(pq|kr) - a_x(pr|kq)\big] \\ &\quad + c_{DF}\int\Bigg\{\sum_{\zeta}\frac{\partial^2 f}{\partial\rho_\sigma\partial\zeta}\zeta^{\mathbf{U}^{\lambda}}(\mathbf{r})(\psi_p^\sigma(\mathbf{r})\psi_q^\sigma(\mathbf{r})) \\ &\quad + \sum_{\zeta}\left[2\frac{\partial^2 f}{\partial\gamma_{\sigma\sigma}\partial\zeta}\vec{\nabla}\rho_\sigma(\mathbf{r}) + \frac{\partial^2 f}{\partial\gamma_{\sigma\sigma'}\partial\zeta}\vec{\nabla}\rho_{\sigma'}(\mathbf{r})\right]\zeta^{\mathbf{U}^{\lambda}}(\mathbf{r})\vec{\nabla}(\psi_p^\sigma(\mathbf{r})\psi_q^\sigma(\mathbf{r})) \\ &\quad + \left[2\frac{\partial f}{\partial\gamma_{\sigma\sigma}}\vec{\nabla}\rho_\sigma^{\mathbf{U}^{\lambda}}(\mathbf{r}) + \frac{\partial f}{\partial\gamma_{\sigma\sigma'}}\vec{\nabla}\rho_{\sigma'}^{\mathbf{U}^{\lambda}}(\mathbf{r})\right]\vec{\nabla}(\psi_p^\sigma(\mathbf{r})\psi_q^\sigma(\mathbf{r}))\Bigg\}d\mathbf{r}\end{aligned} \tag{2.240}$$

with

$$\zeta = \rho_\alpha, \rho_\beta, \gamma_{\alpha\alpha}, \gamma_{\alpha\beta}, \gamma_{\beta\beta} \tag{2.241}$$

$$\zeta^{\mathbf{U}^{\lambda}} = \rho_\alpha^{\mathbf{U}^{\lambda}}, \rho_\beta^{\mathbf{U}^{\lambda}}, \gamma_{\alpha\alpha}^{\mathbf{U}^{\lambda}}, \gamma_{\alpha\beta}^{\mathbf{U}^{\lambda}}, \gamma_{\beta\beta}^{\mathbf{U}^{\lambda}} \tag{2.242}$$

$$\rho_\sigma^{\mathbf{U}^{\lambda}} = \sum_{pqr} U_{rp\sigma}^{\lambda\star}\psi_r^\sigma(\mathbf{r})\psi_q^\sigma(\mathbf{r}) + U_{rq\sigma}^{\lambda}\psi_p^\sigma(\mathbf{r})\psi_r^\sigma(\mathbf{r}) \tag{2.243}$$

$$\gamma_{\sigma\sigma}^{\mathbf{U}^{\lambda}} = 2\vec{\nabla}\rho_\sigma^{\mathbf{U}^{\lambda}}\vec{\nabla}\rho_\sigma. \tag{2.244}$$

As can be seen from eq. 2.243 the XC contribution to the response operator vanishes for imaginary perturbation, due to the symmetry of the U-coefficients. The derivative of the response operators in the real and imaginary cases are given as,

$$\frac{\partial\overline{R}(\mathbf{D}')_{ai}}{\partial\kappa} = \overline{R}(\mathbf{D}'^{\kappa})_{ai} + \overline{R}^{XC}(\mathbf{D}'^{\kappa})_{ai} - \sum_j x_{aj}^{\kappa}\overline{R}(\mathbf{D}')_{ij} + \sum_b x_{bi}^{\kappa}\overline{R}(\mathbf{D}')_{ab} + \overline{R}(\tilde{\mathbf{D}}')_{ai} + \overline{R}^{XC,\kappa}(\mathbf{D}')_{ai} \tag{2.245}$$

$$\frac{\partial\overline{\overline{R}}(\mathbf{D}')_{ai}}{\partial\kappa} = \overline{\overline{R}}(\mathbf{D}'^{\kappa})_{ai} + \overline{\overline{R}}^{XC}(\mathbf{D}'^{\kappa})_{ai} + \mathbf{i}\sum_j y_{aj}^{\kappa}\overline{R}(\mathbf{D})_{ij} - \mathbf{i}\sum_b y_{bi}^{\kappa}\overline{R}(\mathbf{D})_{ab} + \overline{\overline{R}}(\tilde{\mathbf{D}})_{ai} \tag{2.246}$$

with the derivative of the zero-order XC response operator defined as,

$$
\begin{aligned}
\overline{R}^{XC,\kappa}(\mathbf{D}')_{ai\alpha} = \frac{\partial}{\partial\kappa}\Bigg(\int\Bigg\{&\Bigg[\frac{\partial^2 f}{\partial\rho_\alpha\partial\rho_\alpha}\rho_\alpha^{\mathbf{D}'}(\mathbf{r})\frac{\partial^2 f}{\partial\rho_\alpha\partial\rho_\beta}\rho_\beta^{\mathbf{D}'}(\mathbf{r}) + \frac{\partial^2 f}{\partial\gamma_{\alpha\alpha}\partial\rho_\alpha}\gamma_{\alpha\alpha}^{\mathbf{D}'}(\mathbf{r}) + \frac{\partial^2 f}{\partial\gamma_{\alpha\beta}\partial\rho_\alpha}\gamma_{\alpha\beta}^{\mathbf{D}'}(\mathbf{r}) + \frac{\partial^2 f}{\partial\gamma_{\beta\beta}\partial\rho_\beta}\gamma_{\beta\beta}^{\mathbf{D}'}(\mathbf{r})\Bigg]\\
&\times(\psi_a^\alpha(\mathbf{r})\psi_i^\alpha(\mathbf{r}))\\
&+2\Bigg[\frac{\partial^2 f}{\partial\rho_\alpha\partial\gamma_{\alpha\alpha}}\rho_\alpha^{\mathbf{D}'}(\mathbf{r}) + \frac{\partial^2 f}{\partial\rho_\beta\partial\gamma_{\alpha\alpha}}\rho_\beta^{\mathbf{D}'}(\mathbf{r}) + \frac{\partial^2 f}{\partial\gamma_{\alpha\alpha}\partial\gamma_{\alpha\alpha}}\gamma_{\alpha\alpha}^{\mathbf{D}'}(\mathbf{r}) + \frac{\partial^2 f}{\partial\gamma_{\alpha\beta}\partial\gamma_{\alpha\alpha}}\gamma_{\alpha\beta}^{\mathbf{D}'}(\mathbf{r}) + \frac{\partial^2 f}{\partial\gamma_{\beta\beta}\partial\gamma_{\alpha\alpha}}\gamma_{\beta\beta}^{\mathbf{D}'}(\mathbf{r})\Bigg]\\
&\vec{\nabla}\rho_\alpha(\mathbf{r})\vec{\nabla}(\psi_a^\alpha(\mathbf{r})\psi_i^\alpha(\mathbf{r}))\\
&+\Bigg[\frac{\partial^2 f}{\partial\rho_\alpha\partial\gamma_{\alpha\beta}}\rho_\alpha^{\mathbf{D}'}(\mathbf{r}) + \frac{\partial^2 f}{\partial\rho_\beta\partial\gamma_{\alpha\beta}}\rho_\beta^{\mathbf{D}'}(\mathbf{r}) + \frac{\partial^2 f}{\partial\gamma_{\alpha\alpha}\partial\gamma_{\alpha\beta}}\gamma_{\alpha\alpha}^{\mathbf{D}'}(\mathbf{r}) + \frac{\partial^2 f}{\partial\gamma_{\alpha\beta}\partial\gamma_{\alpha\beta}}\gamma_{\alpha\beta}^{\mathbf{D}'}(\mathbf{r}) + \frac{\partial^2 f}{\partial\gamma_{\beta\beta}\partial\gamma_{\alpha\beta}}\gamma_{\beta\beta}^{\mathbf{D}'}(\mathbf{r})\Bigg]\\
&\vec{\nabla}\rho_\beta(\mathbf{r})\vec{\nabla}(\psi_a^\alpha(\mathbf{r})\psi_i^\alpha(\mathbf{r}))\\
&+\Bigg[2\frac{\partial f}{\partial\gamma_{\alpha\alpha}}\vec{\nabla}\rho_\alpha^{\mathbf{D}'}(\mathbf{r}) + \frac{\partial f}{\partial\gamma_{\alpha\beta}}\vec{\nabla}\rho_\beta^{\mathbf{D}'}(\mathbf{r})\Bigg]\vec{\nabla}(\psi_a^\alpha(\mathbf{r})\psi_i^\alpha(\mathbf{r}))\Bigg\}d\mathbf{r}\Bigg)\\
=\int\Bigg\{&\sum_\zeta\sum_\xi\frac{\partial^3 f}{\partial\rho_\alpha\partial\zeta\partial\xi}\xi^{\mathbf{U}^\kappa}\zeta^{\mathbf{D}'}(\psi_a^\alpha\psi_i^\alpha) + \Bigg[\frac{\partial^2 f}{\partial\rho_\alpha\partial\gamma_{\alpha\alpha}}\gamma_{\alpha\alpha}^{\mathbf{U}^\kappa\mathbf{D}'} + \frac{\partial^2 f}{\partial\rho_\alpha\partial\gamma_{\alpha\beta}}\gamma_{\alpha\beta}^{\mathbf{U}^\kappa\mathbf{D}'} + \frac{\partial^2 f}{\partial\rho_\alpha\partial\gamma_{\beta\beta}}\gamma_{\beta\beta}^{\mathbf{U}^\kappa\mathbf{D}'}\Bigg](\psi_a^\alpha\psi_i^\alpha)\\
&+2\sum_\zeta\sum_\xi\frac{\partial^3 f}{\partial\gamma_{\alpha\alpha}\partial\zeta\partial\xi}\xi^{\mathbf{U}^\kappa}\zeta^{\mathbf{D}'}\vec{\nabla}\rho_\alpha\vec{\nabla}(\psi_a^\alpha\psi_i^\alpha)\\
&+2\Bigg[\frac{\partial^2 f}{\partial\gamma_{\alpha\alpha}\partial\rho_\alpha}\rho_\alpha^{\mathbf{D}'}\vec{\nabla}\rho_\alpha^{\mathbf{U}^\kappa} + \frac{\partial^2 f}{\partial\gamma_{\alpha\alpha}\partial\rho_\beta}\rho_\beta^{\mathbf{D}'}\vec{\nabla}\rho_\alpha^{\mathbf{U}^\kappa} + \frac{\partial^2 f}{\partial\gamma_{\alpha\alpha}\partial\gamma_{\alpha\alpha}}\left(\gamma_{\alpha\alpha}^{\mathbf{D}'}\vec{\nabla}\rho_\alpha^{\mathbf{U}^\kappa} + \gamma_{\alpha\alpha}^{\mathbf{U}^\kappa\mathbf{D}'}\vec{\nabla}\rho_\alpha\right)\\
&+\frac{\partial^2 f}{\partial\gamma_{\alpha\alpha}\partial\gamma_{\alpha\beta}}\left(\gamma_{\alpha\beta}^{\mathbf{D}'}\vec{\nabla}\rho_\alpha^{\mathbf{U}^\kappa} + \gamma_{\alpha\beta}^{\mathbf{U}^\kappa\mathbf{D}'}\vec{\nabla}\rho_\alpha\right) + \frac{\partial^2 f}{\partial\gamma_{\alpha\alpha}\partial\gamma_{\beta\beta}}\left(\gamma_{\beta\beta}^{\mathbf{D}'}\vec{\nabla}\rho_\alpha^{\mathbf{U}^\kappa} + \gamma_{\beta\beta}^{\mathbf{U}^\kappa\mathbf{D}'}\vec{\nabla}\rho_\alpha\right)\Bigg]\vec{\nabla}(\psi_a^\alpha\psi_i^\alpha)\\
&+\sum_\zeta\sum_\xi\frac{\partial^3 f}{\partial\gamma_{\alpha\beta}\partial\zeta\partial\xi}\xi^{\mathbf{U}^\kappa}\zeta^{\mathbf{D}'}\vec{\nabla}\rho_\beta\vec{\nabla}(\psi_a^\alpha\psi_i^\alpha)\\
&+\Bigg[\frac{\partial^2 f}{\partial\gamma_{\alpha\beta}\partial\rho_\alpha}\rho_\alpha^{\mathbf{D}'}\vec{\nabla}\rho_\beta^{\mathbf{U}^\kappa} + \frac{\partial^2 f}{\partial\gamma_{\alpha\beta}\partial\rho_\beta}\rho_\beta^{\mathbf{D}'}\vec{\nabla}\rho_\beta^{\mathbf{U}^\kappa} + \frac{\partial^2 f}{\partial\gamma_{\alpha\beta}\partial\gamma_{\alpha\alpha}}\left(\gamma_{\alpha\alpha}^{\mathbf{D}'}\vec{\nabla}\rho_\beta^{\mathbf{U}^\kappa} + \gamma_{\alpha\alpha}^{\mathbf{U}^\kappa\mathbf{D}'}\vec{\nabla}\rho_\beta\right)\\
&+\frac{\partial^2 f}{\partial\gamma_{\alpha\beta}\partial\gamma_{\alpha\beta}}\left(\gamma_{\alpha\beta}^{\mathbf{D}'}\vec{\nabla}\rho_\beta^{\mathbf{U}^\kappa} + \gamma_{\alpha\beta}^{\mathbf{U}^\kappa\mathbf{D}'}\vec{\nabla}\rho_\beta\right) + \frac{\partial^2 f}{\partial\gamma_{\alpha\beta}\partial\gamma_{\beta\beta}}\left(\gamma_{\beta\beta}^{\mathbf{D}'}\vec{\nabla}\rho_\beta^{\mathbf{U}^\kappa} + \gamma_{\beta\beta}^{\mathbf{U}^\kappa\mathbf{D}'}\vec{\nabla}\rho_\beta\right)\Bigg]\vec{\nabla}(\psi_a^\alpha\psi_i^\alpha)\\
&+\sum_\zeta 2\frac{\partial^2 f}{\partial\gamma_{\alpha\alpha}\partial\zeta}\zeta^{\mathbf{U}^\kappa}\vec{\nabla}\rho_\alpha^{\mathbf{D}'}\vec{\nabla}(\psi_a^\alpha\psi_i^\alpha) + \frac{\partial^2 f}{\partial\gamma_{\alpha\beta}\partial\zeta}\zeta^{\mathbf{U}^\kappa}\vec{\nabla}\rho_\beta^{\mathbf{D}'}\vec{\nabla}(\psi_a^\alpha\psi_i^\alpha)\Bigg\}d\mathbf{r}
\end{aligned}
\tag{2.247}
$$

and

$$\zeta^{\mathbf{D}'} = \rho_\alpha^{\mathbf{D}'}, \rho_\beta^{\mathbf{D}'}, \gamma_{\alpha\alpha}^{\mathbf{D}'}, \gamma_{\alpha\beta}^{\mathbf{D}'}, \gamma_{\beta\beta}^{\mathbf{D}'} \tag{2.248}$$

$$\xi^{\mathbf{U}^\lambda} = \rho_\alpha^{\mathbf{U}^\lambda}, \rho_\beta^{\mathbf{U}^\lambda}, \gamma_{\alpha\alpha}^{\mathbf{U}^\lambda}, \gamma_{\alpha\beta}^{\mathbf{U}^\lambda}, \gamma_{\beta\beta}^{\mathbf{U}^\lambda} \tag{2.249}$$

$$\gamma_{\sigma\sigma}^{\mathbf{U}^\lambda\mathbf{D}'} = 2\vec{\nabla}\rho_\sigma^{\mathbf{U}^\lambda}\vec{\nabla}\rho_\sigma^{\mathbf{D}'}. \tag{2.250}$$

A detailed derivation of the derivative of the zero-order XC response operator is given in Appendix A.

2.9. The Orbital-Optimized RI-MP2 Method

The second-order Møller-Plesset correlation energy [2] can be regarded as being stationary with respect to the MP2 amplitudes, since the latter can be considered as having been optimized through minimization of the Hylleraas functional [24, 26].

$$\mathcal{E}_2[\mathbf{t}] = 2\Re\mathfrak{e}\langle\Psi_0^{(1)}|\mathcal{H}|\Psi_0^{(0)}\rangle + \langle\Psi_0^{(1)}|\mathcal{H}_0 - \mathcal{E}_0^{(0)}|\Psi_0^{(1)}\rangle \tag{2.251}$$

$\mathcal{H}_0$ is the 0^{th} order Hamiltonian as proposed by Møller and Plesset, $\Psi_0^{(0)}$ is the reference determinant, $\Psi_0^{(1)}$ is the first-order wave function and $\mathcal{E}_0^{(0)} = E_{HF} = \langle\Psi_{HF}|\mathcal{H}|\Psi_{HF}\rangle$ corresponds to the HF energy. The first-order MP2 amplitudes are collectively denoted $\mathbf{t}$.

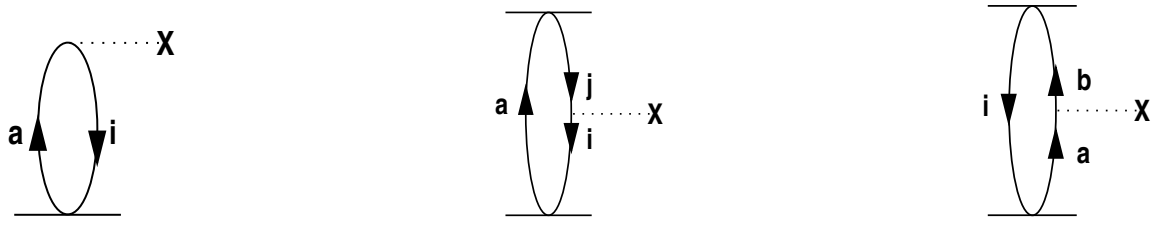

(a) $\sum_{ia} t_a^i F_{ia}$ (b) $-\sum_{ia}\sum_{j} t_a^i t_a^j F_{ij}$ (c) $\sum_{ia}\sum_{b} t_a^i t_b^i F_{ba}$

Figure 2.3.: Constructed diagrams corresponding to eq. 2.255.

Since the MP2 energy is not variational with respect to the molecular orbital (MO) coefficients, no orbital relaxation due to the additional dynamic correlation field is taken into account. In order to allow for orbital relaxation, a new Hylleraas functional can be formulated, which does no longer depend on the MP2 amplitudes alone but becomes also a functional of the orbital rotation parameters, which parametrize the changes in the MO coefficients. The total MP2 energy will then become stationary with respect to the MP2 molecular orbital coefficients and with respect to the MP2 double excitation amplitudes. The extended Hylleraas functional to be minimized, is

$$\mathcal{E}_2[\mathbf{t},\mathbf{R}] = \mathcal{E}_0^{(0)}[\mathbf{R}] + 2\Re\mathfrak{e}\langle\Psi_0^{(1)}|\mathcal{H}|\Psi_0^{(0)}\rangle + \langle\Psi_0^{(1)}|\mathcal{H}_0 - \mathcal{E}_0^{(0)}|\Psi_0^{(1)}\rangle. \tag{2.252}$$

$\mathbf{R}$ are the orbital rotation coefficients that are used to update the MO coefficients $\mathbf{c}$ by means of a unitary transformation. [50] If a spin-unrestricted scheme is desired, different orbitals for different spins are used throughout the entire orbital optimization.

$$\mathbf{c}^{new} = \exp(\mathbf{R})\mathbf{c}^{old} \tag{2.253}$$

$|\Psi_0^{(0)}\rangle$ is the reference determinant, but unlike eq. 2.251 the reference determinant does no longer correspond to the Hartree-Fock determinant. By minimizing the total energy with respect to the MP2 MO coefficients the reference determinant changes with every variation step. The reference energy $\mathcal{E}_0^{(0)}[\mathbf{R}]$ changes simultaneously and therefore it is no longer stationary with respect to the HF MO coefficients. Consequently, Brillouin's theorem [51] is no longer valid and the off-diagonal blocks of the Fock matrix do not vanish. Hence, the first-order wave function would contain contributions from single excitations.

$$|\Psi_0^{(1)}\rangle = \sum_{ia} t_a^i|\Phi_i^a\rangle + \frac{1}{4}\sum_{ijab} t_{ab}^{ij}|\Phi_{ij}^{ab}\rangle \tag{2.254}$$

Thus, the orbital-optimized MP2 Hylleraas functional takes the form,

$$\begin{aligned}\mathcal{E}_2[\mathbf{t},\mathbf{R}] = \mathcal{E}_0^{(0)}[\mathbf{R}] &+ 2\sum_{ia} t_a^i\langle\Phi_i^a|\mathcal{H}|\Phi_0\rangle + \frac{1}{2}\sum_{ijab} t_{ab}^{ij}\langle\Phi_{ij}^{ab}|\mathcal{H}|\Phi_0\rangle \\ &+ \sum_{ijab} t_a^i t_b^j\langle\Phi_i^a|\mathcal{H}_0 - \mathcal{E}_0^{(0)}[\mathbf{R}]|\Phi_j^b\rangle + \sum_{ijklabcd} t_{ab}^{ij}t_{cd}^{kl}\langle\Phi_{ij}^{ab}|\mathcal{H}_0 - \mathcal{E}_0^{(0)}[\mathbf{R}]|\Phi_{kl}^{cd}\rangle \\ &+ \sum_{ijkabc} t_a^i t_{bc}^{jk}\langle\Phi_i^a|\mathcal{H}_0 - \mathcal{E}_0^{(0)}[\mathbf{R}]|\Phi_{jk}^{bc}\rangle + \sum_{ijkabc} t_{ab}^{ij}t_c^k\langle\Phi_{ij}^{ab}|\mathcal{H}_0 - \mathcal{E}_0^{(0)}[\mathbf{R}]|\Phi_k^c\rangle.\end{aligned} \tag{2.255}$$

Evaluating the matrix elements according to the diagrams shown in Fig. 2.3 and applying the 'Resolution

of the Identity' approximation [22, 32, 52] to the MP2 correction, yields,

$$\begin{aligned}\mathcal{E}_2[\mathbf{t},\mathbf{R}] = &\sum_i h_{ii} + \frac{1}{2}\sum_{ij}\langle ij||ij\rangle + 2\sum_{ia} t_a^i F_{ia} + \frac{1}{2}\sum_{iaP}\left[(ia|P)\Gamma'^P_{ia} + (ai|P)\Gamma'^P_{ai}\right] \\ &- \sum_{ija} t_a^i t_a^j F_{ij} + \sum_{iab} t_a^i t_b^i F_{ba} - \frac{1}{2}\sum_{ijkab} t_{ab}^{ij} t_{ab}^{ik} F_{kj} + \frac{1}{2}\sum_{ijabc} t_{ab}^{ij} t_{ac}^{ij} F_{cb}. \end{aligned} \tag{2.256}$$

Since orbital optimization introduces all important effects of the single excitations, we prefer to leave them out of the treatment. Any attempt to the contrary has been found to destroy the convergence properties. Hence, the explicit form of the orbital-optimized MP2 Hylleraas functional within the density fitting approximation (OO-RI-MP2) including only double excitations becomes,

$$\mathcal{E}_2[\mathbf{t},\mathbf{R}] = \sum_i h_{ii} + \frac{1}{2}\sum_{ij}\big\langle ij||ij\big\rangle + \sum_{iaP}(ia|P)\Gamma'^P_{ia} + \sum_{ij} D_{ij}F_{ij} + \sum_{ab} D_{ab}F_{ab}. \tag{2.257}$$

The MP2 like density blocks and the double excitation amplitudes, are defined according to conventional MP2 theory. The orbital changes are parameterized by the anti-Hermitian matrix $\mathbf{R}$ such that no Lagrangian multipliers are required to ensure orbital orthonormality. The Fock operator is expanded to first order in the orbital rotations as,

$$F_{pq} = \sum_r R_{rp}F_{rq} + R_{rq}F_{pr} + \overline{R}(\mathbf{R})_{pq} \tag{2.258}$$

$$\overline{R}(\mathbf{R})_{pq} = \sum_{kc} R_{ck}\Big\{\langle pc||qk\rangle + \langle pk||qc\rangle\Big\}. \tag{2.259}$$

Thus, the first-order energy change becomes ($g_{pqrs} \equiv \langle pq||rs\rangle$),

$$\begin{aligned}\mathcal{L}_{\mathrm{OO}}[\mathbf{t},\mathbf{R}] = &\sum_{ic} R_{ci}\big(h_{ci} + h_{ic}\big) + \frac{1}{2}\sum_{ijc} R_{ci}\big(g_{cjij} + g_{ijcj}\big) + R_{cj}\big(g_{icij} + g_{ijic}\big) \\ &+ 2\sum_{iacP} R_{ci}(ac|P)\Gamma'^P_{ia} - 2\sum_{ikaP} R_{ak}(ik|P)\Gamma'^P_{ia} \\ &- \sum_{ij} D_{ij}\Big(\overline{R}(\mathbf{R})_{ij} + \sum_c \big\{R_{ci}F_{cj} + R_{cj}F_{ic}\big\}\Big) \\ &+ \sum_{ab} D_{ab}\Big(\overline{R}(\mathbf{R})_{ab} - \sum_k \big\{R_{ak}F_{kb} + R_{bk}F_{ak}\big\}\Big). \end{aligned} \tag{2.260}$$

The condition for the energy functional to be stationary with respect to the orbital rotations $\left(\frac{\partial \mathcal{L}_{\mathrm{OO}}[\mathbf{t},\mathbf{R}]}{\partial R_{ai}} = 0\right)$, yields the expression for the orbital gradient and hence, the expression for the OO-RI-MP2 Lagrangian.

$$\begin{aligned}\frac{\partial \mathcal{L}_{\mathrm{OO}}[\mathbf{t},\mathbf{R}]}{\partial R_{ai}} \equiv g_{ai} = &2F_{ai} + 2\sum_j D_{ij}F_{aj} - 2\sum_b D_{ab}F_{ib} + \overline{R}(\mathbf{D})_{ai} \\ &+ 2\sum_{cP}(ac|P)\Gamma'^P_{ia} - 2\sum_{kP}(ik|P)\Gamma'^P_{ia} \end{aligned} \tag{2.261}$$

In order to implement a practical orbital optimization scheme we have chosen a simple DIIS method. [53] A matrix $\mathbf{B}$ that contains the orbital gradient in its off-diagonal blocks and the orbital energies in its

diagonal is repeatedly diagonalized and provides the orbital rotation coefficients directly, eq. 2.262.

$$\mathbf{B} = \begin{pmatrix} \varepsilon_0 & & \mathbf{g}_{ia} \\ & \varepsilon_1 & \\ \mathbf{g}_{ai} & & \ddots \end{pmatrix} \tag{2.262}$$

The whole procedure is carried out self-consistently until both $||g_{ai}||$ and ΔE fall below predefined thresholds. The orbital energies are obtained by diagonalizing the Fock operator in the occupied/occupied and virtual/virtual subspaces of the current orbital set. A flowchart of the optimization procedure is shown in Fig. 2.4.

At convergence, the relaxed density matrix and the one obtained as an expectation value over the first-order wave function become identical. The entire density is given by the sum of the reference density and the correlation contribution,

$$D_{pq}^{OO} = P_{pq}^{ref} + D_{pq} \tag{2.263}$$

$$P_{\mu\nu}^{ref} = \sum_i c_{\mu i} c_{\nu i}. \tag{2.264}$$

In an infinite basis set, the Hellmann-Feynman theorem [54,55] becomes valid and the OO-RI-MP2 density matrix can be used for the calculation of expectation values and to calculate the OO-RI-MP2 gradient, respectively.
Consider a one-electron perturbation of the form λh_λ, e.g. an external electric field, and assume the basis functions to be independent of the perturbation. The first derivative of the OO-RI-MP2 energy w.r.t. the perturbation λ, corresponds to the expectation value of h_λ, if the OO-RI-MP2 equations have converged, eq. 2.265.

$$\frac{\partial E_{OO}}{\partial \lambda} = \sum_{pq} D_{pq} h_{pq}^{\lambda} \tag{2.265}$$

2.9.1. The OO-RI-MP2 Gradient

The general gradient expression is,

$$\frac{dE}{d\lambda} = \sum_{pq} \gamma_{pq} h_{pq}^{\{\lambda\}} + \sum_{pq} W_{pq} S_{pq}^{(\lambda)} + \sum_{pqrs} \Gamma_{pqrs} (pq|rs)^{(\lambda)} \tag{2.266}$$

with the first-order reduced density matrix corresponds to the OO-RI-MP2 density matrix, and the second-order reduced density matrix is defined as,

$$\Gamma_{pqrs}^{S} = D_{pq} - D_{pr} \tag{2.267}$$

$$\Gamma_{iajb}^{NS} = \frac{1}{2} t_{ab}^{ij}. \tag{2.268}$$

The difference of the OO-RI-MP2 gradient compared to the conventional MP2 gradient arises in the formulation of the energy weighted density,

$$W_{ij} = -\sum_{kabP} B_{ia}^{P} B_{kb}^{P} t_{ab}^{jk} - \frac{1}{2} D_{ij}(\epsilon_i + \epsilon_j) - \frac{1}{2}\overline{R}(\mathbf{D})_{ij} \tag{2.269}$$

$$W_{ab} = -\sum_{ijcP} B_{ia}^{P} B_{kc}^{P} t_{bc}^{ij} - \frac{1}{2} D_{ab}(\epsilon_a + \epsilon_b) \tag{2.270}$$

$$W_{ai} = -2\sum_{kP}(ik|P)\Gamma'^{P}_{ak} - 2\sum_{b} D_{ab} F_{ib} \tag{2.271}$$

where an additional Fock matrix element appears in eq. 2.271. However, obviously the calculation of the OO-RI-MP2 gradient is of the same computational effort as the conventional MP2 gradient, once the OO-MP2 equations have converged.

2.9.2. The OO-MP2 Second Derivatives

In this section the second derivatives for the orbital-optimized MP2 method with respect to real perturbations are derived. The RI approximation is neglected for simplicity. Following the general derivative theory for variational wave functions, the perturbed wave function parameters, which are absent in the first derivative have to be determined for the second derivative. In OO-MP2 theory the wave function depends on two sets of parameters, i.e. the molecular orbital coefficients and the double excitation amplitudes. Thus, the following equation system (CP-OO-MP2) is obtained,

$$\begin{pmatrix} \frac{\partial g_{ai}}{\partial \mathbf{U}^{\kappa}} & \frac{\partial g_{ai}}{\partial \mathbf{t}^{ij,\kappa}} \\ \frac{\partial^2 \mathcal{E}_2}{\partial \mathbf{t}^{ij} \partial \mathbf{U}^{\kappa}} & \frac{\partial^2 \mathcal{E}_2}{\partial \mathbf{t}^{ij} \partial \mathbf{t}^{ij,\kappa}} \end{pmatrix} \begin{pmatrix} \mathbf{U}^{\kappa} \\ \mathbf{t}^{ij,\kappa} \end{pmatrix} = \begin{pmatrix} g_{oo} & g_{ot} \\ a_{to} & a_{tt} \end{pmatrix} \begin{pmatrix} \mathbf{U}^{\kappa} \\ \mathbf{t}^{ij,\kappa} \end{pmatrix} = \begin{pmatrix} \mathbf{b}_0^{\kappa} \\ \mathbf{b}_1^{\kappa} \end{pmatrix} \tag{2.272}$$

with the orbital gradient given as,

$$g_{ai} = \sum_{jbc}\langle aj||cb\rangle t_{cb}^{ij} - \sum_{jkb}\langle ib||kj\rangle t_{ab}^{kj} + \overline{R}(\mathbf{D})_{ai} + 2\sum_{j} D_{ij} F_{aj} - 2\sum_{b} D_{ab} F_{ib} + 2F_{ai}. \tag{2.273}$$

The derivative of the orbital gradient becomes,

$$\begin{aligned}
\frac{\partial g_{ai}}{\partial \kappa} = & -2\sum_{j} U_{aj}^{\kappa} F_{ji} + 2\sum_{b} U_{bi}^{\kappa} F_{ab} + 2h_{ai}^{[\kappa]} + 2\sum_{jb} U_{bj}^{\kappa}\left[\langle ab||ij\rangle + \langle aj||ib\rangle\right] \\
& + \sum_{jb} U_{bj}^{\kappa}\left[-2\sum_{kc}\left\{\langle ak||jc\rangle t_{bc}^{ik} + \langle bk||ic\rangle t_{ac}^{kj}\right\} + \sum_{cd}\langle ab||cd\rangle t_{cd}^{ij} + \sum_{kl}\langle kl||ij\rangle t_{ab}^{kl}\right] \\
& - \sum_{jkbc} U_{aj}^{\kappa}\langle jk||cb\rangle t_{cb}^{ik} - \sum_{jkbc} U_{bi}^{\kappa}\langle kj||bc\rangle t_{ac}^{kj} \\
& + \sum_{jbc}\langle aj||cb\rangle t_{cb}^{ij,\kappa} - \sum_{jkb}\langle kj||ib\rangle t_{ab}^{kj,\kappa} \\
& + \sum_{j} D_{ij}^{\kappa} F_{aj} - \sum_{jk} D_{ik} U_{aj}^{\kappa} F_{jk} + \sum_{jb} D_{ij} U_{bj}^{\kappa} F_{ab} + \sum_{j} D_{ij} h_{aj}^{[\kappa]} + \sum_{jkb} D_{ik} U_{bj}^{\kappa}\left[\langle ab||kj\rangle + \langle aj||kb\rangle\right] \\
& + \sum_{b} D_{ab}^{\kappa} F_{ib} - \sum_{bc} D_{ac} U_{bi}^{\kappa} F_{bc} + \sum_{jb} D_{ab} U_{bj}^{\kappa} F_{ij} + \sum_{b} D_{ab} h_{ib}^{[\kappa]} + \sum_{jbc} D_{ac} U_{bj}^{\kappa}\left[\langle ib||cj\rangle + \langle ij||cb\rangle\right] \\
& + \sum_{bc} D_{bc}^{\kappa}\left[\langle ab||ic\rangle + \langle ib||ac\rangle\right] + \sum_{jk} D_{jk}^{\kappa}\left[\langle aj||ik\rangle + \langle ij||ak\rangle\right]
\end{aligned}$$

$$
\begin{aligned}
&+\sum_{bc} D_{bc}\left[-2\sum_{j} U^{\kappa}_{bj}\left\{\langle aj||ic\rangle+\langle ac||ij\rangle\right\}-\sum_{j} U^{\kappa}_{aj}\left\{\langle jb||ic\rangle+\langle ib||jc\rangle\right\}\right]\\
&+\sum_{cd} D_{dc}\left[\sum_{b} U^{\kappa}_{bi}\left\{\langle ad||bc\rangle+\langle bd||ac\rangle\right\}\right]\\
&+\sum_{jk} D_{jk}\left[2\sum_{b} U^{\kappa}_{bj}\left\{\langle ab||ik\rangle+\langle ak||ib\rangle\right\}+\sum_{b} U^{\kappa}_{bi}\left\{\langle aj||bk\rangle+\langle bj||ak\rangle\right\}\right]\\
&-\sum_{kl} D_{lk}\left[\sum_{j} U^{\kappa}_{aj}\left\{\langle jl||ik\rangle+\langle il||jk\rangle\right\}\right].
\end{aligned}
\tag{2.274}
$$

Form the derivative of the perturbed orbital gradient (eq. 2.274) w.r.t. the U-coefficients,

$$
\begin{aligned}
\frac{\partial g^{orb}_{ai}}{\partial U^{\kappa}_{bj}} \equiv g_{oo} = &-2\delta_{ab}F_{ji}+2\delta_{ij}F_{ab}+2\left[\langle ab||ij\rangle+\langle aj||ib\rangle\right]\\
&-2\sum_{kc}\left\{\langle ak||jc\rangle t^{ik}_{bc}+\langle bk||ic\rangle t^{kj}_{ac}\right\}+\sum_{cd}\langle ab||cd\rangle t^{ij}_{cd}+\sum_{kl}\langle kl||ij\rangle t^{kl}_{ab}\\
&-\delta_{ab}\sum_{kc}\langle jk||cb\rangle t^{ik}_{cb}-\delta_{ij}\sum_{kc}\langle kj||bd\rangle t^{kj}_{ac}\\
&-\delta_{ab}\sum_{k} D_{ik}F_{jk}+D_{ij}F_{ab}+\sum_{k} D_{ik}\left\{\langle ab||kj\rangle+\langle aj||kb\rangle\right\}\\
&-\delta_{ij}\sum_{c} D_{ac}F_{bc}+D_{ab}F_{ij}+\sum_{c} D_{ac}\left\{\langle ib||cj\rangle+\langle ij||cb\rangle\right\}\\
&+\sum_{c} D_{bc}\left[-2\left\{\langle aj||ic\rangle+\langle ac||ij\rangle\right\}-\delta_{ab}\left\{\langle jb||ic\rangle+\langle ib||jc\rangle\right\}\right]\\
&+\delta_{ij}\sum_{cd} D_{dc}\left\{\langle ad||bc\rangle+\langle bd||ac\rangle\right\}\\
&+\sum_{k} D_{jk}\left[2\left\{\langle ab||ik\rangle+\langle ak||ib\rangle\right\}+\delta_{ij}\left\{\langle aj||bk\rangle+\langle bj||ak\rangle\right\}\right]\\
&-\delta_{ab}\sum_{kl} D_{lk}\left\{\langle jl||ik\rangle+\langle il||jk\rangle\right\}
\end{aligned}
\tag{2.275}
$$

and form the derivative of the perturbed orbital gradient (eq. 2.274) w.r.t. the perturbed amplitudes,

$$
\begin{aligned}
\frac{\partial g^{orb}_{ai}}{\partial t^{jk,\kappa}_{bc}} \equiv g_{ot} = \frac{\partial}{\partial t^{jk,\kappa}_{bc}}\Bigg\{&\sum_{lde}\langle al||ed\rangle t^{il,\kappa}_{ed}-\sum_{lmd}\langle ml||id\rangle t^{ml,\kappa}_{ad}\\
&+\sum_{de}\left[\frac{1}{2}\sum_{lmf} t^{lm,\kappa}_{df}t^{lm}_{ef}+t^{lm}_{df}t^{lm,\kappa}_{ef}\right]\left[\langle ad||ie\rangle+\langle id||ae\rangle\right]\\
&+\sum_{lm}\left[-\frac{1}{2}\sum_{nde} t^{ln,\kappa}_{de}t^{mn}_{de}+t^{ln}_{de}t^{mn,\kappa}_{de}\right]\left[\langle al||im\rangle+\langle il||am\rangle\right]\Bigg\}
\end{aligned}
$$

$$
\begin{aligned}
&= 2\sum_{lde}\delta_{ij}\delta_{kl}\delta_{be}\delta_{cd}\langle al||ed\rangle - 2\sum_{lmd}\delta_{jm}\delta_{kl}\delta_{ab}\delta_{cd}\langle ml||id\rangle \\
&\quad + \frac{1}{2}\sum_{de}\left[2\sum_{lmf}\delta_{jl}\delta_{km}\delta_{bd}\delta_{cf}t_{ef}^{lm} + \delta_{kl}\delta_{jm}\delta_{cd}\delta_{bf}t_{ef}^{lm} + \delta_{jl}\delta_{km}\delta_{be}\delta_{cf}t_{df}^{lm} + \delta_{kl}\delta_{jm}\delta_{ce}\delta_{df}t_{df}^{lm}\right] \\
&\quad [\langle ad||ie\rangle + \langle id||ae\rangle] \\
&\quad - \frac{1}{2}\sum_{lm}\left[2\sum_{nde}\delta_{bd}\delta_{ce}\delta_{jl}\delta_{kn}t_{de}^{mn} + \delta_{cd}\delta_{be}\delta_{kl}\delta_{jn}t_{de}^{mn} + \delta_{bd}\delta_{ce}\delta_{jm}\delta_{kn}t_{de}^{ln} + \delta_{cd}\delta_{be}\delta_{km}\delta_{jn}t_{de}^{ln}\right] \\
&\quad [\langle al||im\rangle + \langle il||am\rangle] \\
&= 2\delta_{ij}\langle ak||bc\rangle - 2\delta_{ab}\langle jk||ic\rangle \\
&\quad + \sum_{e}t_{ec}^{jk}\left[\langle ab||ie\rangle + \langle ib||ae\rangle\right] + t_{eb}^{kj}\left[\langle ac||ie\rangle + \langle ic||ae\rangle\right] \\
&\quad + \sum_{d}t_{dc}^{jk}\left[\langle ad||ib\rangle + \langle id||ab\rangle\right] + t_{db}^{kj}\left[\langle ad||ic\rangle + \langle id||ac\rangle\right] \\
&\quad - \sum_{m}t_{bc}^{mk}\left[\langle aj||im\rangle + \langle ij||am\rangle\right] + t_{cb}^{mj}\left[\langle ak||im\rangle + \langle ik||am\rangle\right] \\
&\quad - \sum_{l}t_{bc}^{lk}\left[\langle al||ij\rangle + \langle il||aj\rangle\right] + t_{cb}^{lj}\left[\langle al||ik\rangle + \langle il||ak\rangle\right] \\
&= 2\delta_{ij}\langle ak||bc\rangle - 2\delta_{ab}\langle jk||ic\rangle \\
&\quad + 2\sum_{d}t_{dc}^{jk}\left[\langle ad||ib\rangle + \langle id||ab\rangle\right] + t_{db}^{kj}\left[\langle ad||ic\rangle + \langle id||ac\rangle\right] \\
&\quad - 2\sum_{l}t_{bc}^{lk}\left[\langle al||ij\rangle + \langle il||aj\rangle\right] + t_{cb}^{lj}\left[\langle al||ik\rangle + \langle il||ak\rangle\right]. \qquad (2.276)
\end{aligned}
$$

The derivative of the amplitude equation is,

$$
\begin{aligned}
\frac{\partial^2\mathcal{E}_2[\mathbf{t},\mathbf{U}]}{\partial t_{ab}^{ij}\partial\kappa} \equiv a_t &= \frac{\partial}{\partial\kappa}\left\{\langle ij||ab\rangle - \sum_{k}t_{ab}^{ik}F_{jk} + t_{ab}^{kj}F_{ik} + \sum_{c}t_{ac}^{ij}F_{cb} + t_{cb}^{ij}F_{ca}\right\} \\
&= \sum_{c}U_{ci}^{\kappa}\langle cj||ab\rangle + U_{cj}^{\kappa}\langle ic||ab\rangle - \sum_{k}U_{ak}^{\kappa}\langle ij||kb\rangle + U_{bk}^{\kappa}\langle ij||ak\rangle \\
&\quad - \sum_{k}t_{ab}^{ik,\kappa}F_{jk} + t_{ab}^{kj,\kappa}F_{ik} - \sum_{kc}t_{ab}^{ik}U_{cj}^{\kappa}F_{ck} + t_{ab}^{ik}U_{ck}^{\kappa}F_{jc} + t_{ab}^{kj}U_{ci}^{\kappa}F_{ck} + t_{ab}^{kj}U_{ck}^{\kappa}F_{ic} \\
&\quad - \sum_{k}t_{ab}^{ik}h_{jk}^{[\kappa]} + t_{ab}^{kj}h_{ik}^{[\kappa]} + t_{ab}^{ik}R(\mathbf{U}^{\kappa})_{jk} + t_{ab}^{kj}R(\mathbf{U}^{\kappa})_{ik} \\
&\quad + \sum_{c}t_{ac}^{ij,\kappa}F_{cb} + t_{cb}^{ij,\kappa}F_{ca} - \sum_{kc}t_{ac}^{ij}U_{ck}^{\kappa}F_{kb} + t_{ac}^{ij}U_{bk}^{\kappa}F_{ck} + t_{cb}^{ij}U_{ck}^{\kappa}F_{ka} + t_{cb}^{ij}U_{ca}^{\kappa}F_{ck} \\
&\quad + \sum_{c}t_{ac}^{ij}h_{cb}^{[\kappa]} + t_{cb}^{ij}h_{ca}^{[\kappa]} + t_{ac}^{ij}R(\mathbf{U}^{\kappa})_{cb} + t_{cb}^{ij}R(\mathbf{U}^{\kappa})_{ca}. \qquad (2.277)
\end{aligned}
$$

Form the derivative of the perturbed amplitude equation (eq. 2.277) w.r.t. the U-coefficients,

$$
\begin{aligned}
\frac{\partial a_t}{\partial U_{ck}^{\kappa}} \equiv a_{to} = \frac{\partial}{\partial U_{ck}^{\kappa}}\Big\{ &\sum_{c}U_{ci}^{\kappa}\langle cj||ab\rangle + U_{cj}^{\kappa}\langle ic||ab\rangle - \sum_{k}U_{ak}^{\kappa}\langle ij||kb\rangle + U_{bk}^{\kappa}\langle ij||ak\rangle \\
&- \sum_{lc}t_{ab}^{il}\left[U_{cj}^{\kappa}F_{cl} + U_{cl}^{\kappa}F_{jc}\right] + t_{ab}^{lj}\left[U_{ci}^{\kappa}F_{cl} + U_{cl}^{\kappa}F_{ic}\right] - \sum_{l}t_{ab}^{il}R(\mathbf{U}^{\kappa})_{jl} + t_{ab}^{lj}R(\mathbf{U}^{\kappa})_{il} \\
&- \sum_{kd}t_{ad}^{ij}\left[U_{dk}^{\kappa}F_{kb} + U_{bk}^{\kappa}F_{dk}\right] + t_{db}^{ij}\left[U_{dk}^{\kappa}F_{ka} + U_{ak}^{\kappa}F_{dk}\right] + \sum_{d}t_{ad}^{ij}R(\mathbf{U}^{\kappa})_{db} + t_{db}^{ij}R(\mathbf{U}^{\kappa})_{da}\Big\}
\end{aligned}
$$

$$
\begin{aligned}
&= \frac{\partial}{\partial U^{\kappa}_{ck}} \Bigg\{ \sum_{kc} U^{\kappa}_{ck} \Big[\delta_{ik}\langle cj||ab\rangle + \delta_{jk}\langle ic||ab\rangle - \delta_{ac}\langle ij||kb\rangle - \delta_{bc}\langle ij||ak\rangle \\
&\quad - \sum_{l} t^{il}_{ab} \left[\delta_{jk}F_{cl} + \delta_{lk}F_{jc}\right] - \sum_{l} t^{lj}_{ab} \left[\delta_{ik}F_{cl} + \delta_{lk}F_{ic}\right] \\
&\quad - \sum_{l} t^{il}_{ab} \left[\langle jc||lk\rangle + \langle jk||lc\rangle\right] + t^{lj}_{ab} \left[\langle ic||lk\rangle + \langle ik||lc\rangle\right] \\
&\quad - \sum_{d} t^{ij}_{ad} \left[\delta_{dc}F_{kb} + \delta_{bc}F_{dk}\right] - \sum_{d} t^{ij}_{db} \left[\delta_{ac}F_{kd} + \delta_{dc}F_{ak}\right] \\
&\quad + \sum_{d} t^{ij}_{ad} \left[\langle dc||bk\rangle + \langle dk||bc\rangle\right] + t^{ij}_{bd} \left[\langle dc||ak\rangle + \langle dk||ac\rangle\right] \Big] \Bigg\} \\
&= \delta_{ik}\langle cj||ab\rangle + \delta_{jk}\langle ic||ab\rangle - \delta_{ac}\langle ij||kb\rangle - \delta_{bc}\langle ij||ak\rangle \\
&\quad - \sum_{l} t^{il}_{ab} \left[\delta_{jk}F_{cl} + \delta_{lk}F_{jc}\right] - \sum_{l} t^{lj}_{ab} \left[\delta_{ik}F_{cl} + \delta_{lk}F_{ic}\right] \\
&\quad - \sum_{l} t^{il}_{ab} \left[\langle jc||lk\rangle + \langle jk||lc\rangle\right] + t^{lj}_{ab} \left[\langle ic||lk\rangle + \langle ik||lc\rangle\right] \\
&\quad - \sum_{d} t^{ij}_{ad} \left[\delta_{dc}F_{kb} + \delta_{bc}F_{dk}\right] - \sum_{d} t^{ij}_{db} \left[\delta_{ac}F_{kd} + \delta_{dc}F_{ak}\right] \\
&\quad + \sum_{d} t^{ij}_{ad} \left[\langle dc||bk\rangle + \langle dk||bc\rangle\right] + t^{ij}_{bd} \left[\langle dc||ak\rangle + \langle dk||ac\rangle\right]
\end{aligned} \tag{2.278}
$$

and form the derivative of the perturbed amplitude equation (eq. 2.277) w.r.t. the perturbed amplitudes,

$$
\begin{aligned}
\frac{\partial a^{\kappa}_{t}}{\partial t^{ij,\kappa}_{ab}} \equiv a_{tt} &= \frac{\partial}{\partial t^{ij,\kappa}_{ab}} \left\{ - \sum_{k} t^{ik,\kappa}_{ab} F_{jk} + t^{kj,\kappa}_{ab} F_{ik} + \sum_{c} t^{ij,\kappa}_{ac} F_{cb} + t^{ij,\kappa}_{cb} F_{ca} \right\} \\
&= - \sum_{k} \delta_{jk} F_{jk} + \delta_{ik} F_{ik} + \sum_{c} \delta_{bc} F_{cb} + \delta_{ac} F_{ca} \\
&= - \varepsilon_j - \varepsilon_i + \varepsilon_b + \varepsilon_a .
\end{aligned} \tag{2.279}
$$

The right-hand sides of the CP-OO-MP2 equations are given,

$$
b^{\kappa}_{0} = 2h^{[\kappa]}_{ai} + \sum_{j} D_{ij} h^{[\kappa]}_{aj} + \sum_{b} D_{ab} h^{[\kappa]}_{ib} \tag{2.280}
$$

$$
b^{\kappa}_{1} = - \sum_{k} t^{ik}_{ab} h^{[\kappa]}_{kj} + t^{kj}_{ab} h^{[\kappa]}_{ki} + \sum_{c} t^{ij}_{ac} h^{[\kappa]}_{cb} + t^{ij}_{cb} h^{[\kappa]}_{ca} \tag{2.281}
$$

and the total 2nd derivative of the OO-MP2 energy becomes,

$$
\begin{aligned}
\frac{\partial^2 \mathcal{E}_2}{\partial\lambda\partial\kappa} = \frac{\partial}{\partial\kappa} \Bigg\{ & 2 \sum_{ia} F_{ai} + \sum_{i} h^{[\lambda]}_{ii} + \sum_{ijabc} \langle aj||cb\rangle t^{ij}_{cb} - \sum_{ijkab} \langle kj||ib\rangle t^{kj}_{ab} \\
& + 2 \sum_{ija} D_{ij} F_{aj} - 2 \sum_{iab} D_{ab} F_{ib} + \sum_{ij} D_{ij} h^{[\lambda]}_{ij} + \sum_{ab} D_{ab} h^{[\lambda]}_{ab} + \sum_{ia} R(\mathbf{D})_{ai} \Bigg\}
\end{aligned}
$$

$$
\begin{aligned}
&= -2\sum_{ija} U^{\kappa}_{aj} F_{ji} + 2\sum_{iab} U^{\kappa}_{bi} F_{ab} + 2\sum_{ai} h^{[\kappa]}_{ai} + 2\sum_{ai} R(\mathbf{U}^{\kappa})_{ai} \\
&\quad + 2\sum_{ai} U^{\kappa}_{ai} h^{[\lambda]}_{ai} + \sum_{i} h^{[\lambda,\kappa]}_{ii} \\
&\quad + \sum_{jb} U^{\kappa}_{bj} \left[-2\sum_{kc} \left\{ \langle ak||jc\rangle t^{ik}_{bc} + \langle bk||ic\rangle t^{kj}_{ac} \right\} + \sum_{cd} \langle ab||cd\rangle t^{ij}_{cd} + \sum_{kl} \langle kl||ij\rangle t^{kl}_{ab} \right] \\
&\quad - \sum_{jkbc} U^{\kappa}_{aj} \langle jk||cb\rangle t^{ik}_{cb} - \sum_{jkbc} U^{\kappa}_{bi} \langle kj||bc\rangle t^{kj}_{ac} \\
&\quad + \sum_{jbc} \langle aj||cb\rangle t^{ij,\kappa}_{cb} - \sum_{jkb} \langle kj||ib\rangle t^{kj,\kappa}_{ab} \\
&\quad + 2\sum_{ija} D^{\kappa}_{ij} F_{aj} + 2\sum_{ijab} U^{\kappa}_{bj} D_{ij} F_{ab} - 2\sum_{ijka} U^{\kappa}_{ak} D_{ij} F_{kj} + 2\sum_{ija} D_{ij} h^{[\kappa]}_{aj} + 2\sum_{ija} D_{ij} R(\mathbf{U}^{\kappa})_{aj} \\
&\quad - 2\sum_{iab} D^{\kappa}_{ab} F_{ib} - 2\sum_{iabc} U^{\kappa}_{ci} D_{ab} F_{cb} + 2\sum_{ijab} U^{\kappa}_{bj} D_{ij} F_{ij} - 2\sum_{iab} D_{ab} h^{[\kappa]}_{ib} - 2\sum_{iab} D_{ab} R(\mathbf{U}^{\kappa})_{ib} \\
&\quad + \sum_{ij} D_{ij} h^{[\lambda,\kappa]}_{ij} + \sum_{ij} D^{\kappa}_{ij} h^{[\lambda]}_{ij} + \sum_{ija} U^{\kappa}_{ai} D_{ij} h^{[\lambda]}_{aj} + U^{\kappa}_{aj} D_{ij} h^{[\lambda]}_{ia} \\
&\quad + \sum_{ab} D_{ab} h^{[\lambda,\kappa]}_{ab} + \sum_{ab} D^{\kappa}_{ab} h^{[\lambda]}_{ab} - \sum_{iab} U^{\kappa}_{ai} D_{ab} h^{[\lambda]}_{ib} + U^{\kappa}_{bi} D_{ab} h^{[\lambda]}_{ai} \\
&\quad + \sum_{ia} R^{\kappa}(\mathbf{D})_{ai} \\
&= 2\sum_{ai} U^{\kappa}_{ai} h^{[\lambda]}_{ai} + \sum_{i} h^{[\lambda,\kappa]}_{ii} + \mathbf{g}_{oo}\mathbf{U}^{\kappa} + \mathbf{g}_{ot}\mathbf{t}^{ij,\kappa} \\
&\quad + \sum_{ij} D_{ij} h^{[\lambda,\kappa]}_{ij} + \sum_{ij} D^{\kappa}_{ij} h^{[\lambda]}_{ij} + \sum_{ija} U^{\kappa}_{ai} D_{ij} h^{[\lambda]}_{aj} + U^{\kappa}_{aj} D_{ij} h^{[\lambda]}_{ia} \\
&\quad + \sum_{ab} D_{ab} h^{[\lambda,\kappa]}_{ab} + \sum_{ab} D^{\kappa}_{ab} h^{[\lambda]}_{ab} - \sum_{iab} U^{\kappa}_{ai} D_{ab} h^{[\lambda]}_{ib} + U^{\kappa}_{bi} D_{ab} h^{[\lambda]}_{ai}. \qquad (2.282)
\end{aligned}
$$

The CP-OO-MP2 equations to solve have the form,

$$
\begin{aligned}
&\mathbf{g}_{oo}\mathbf{U}^{\kappa} + \mathbf{g}_{ot}\mathbf{t}^{\kappa} = \mathbf{b}^{\kappa}_{0} && (2.283)\\
&\mathbf{a}_{to}\mathbf{U}^{\kappa} + \mathbf{a}_{tt}\mathbf{t}^{\kappa} = \mathbf{b}^{\kappa}_{1} && (2.284)\\
\Longleftrightarrow\ &\mathbf{t}^{\kappa} = \left(\mathbf{b}^{\kappa}_{1} - \mathbf{a}_{to}\mathbf{U}^{\kappa}\right)\left(\mathbf{a}_{tt}\right)^{-1} \\
\Longleftrightarrow\ &\mathbf{g}_{oo}\mathbf{U}^{\kappa} + \mathbf{g}_{ot}\left[\mathbf{b}^{\kappa}_{1} - \mathbf{a}_{to}\mathbf{U}^{\kappa}\right]\left(\mathbf{a}_{tt}\right)^{-1} = \mathbf{b}^{\kappa}_{0} \\
\Longleftrightarrow\ &\left[\mathbf{g}_{oo} - \mathbf{g}_{ot}\mathbf{a}_{to}\left(\mathbf{a}_{tt}\right)^{-1}\right]\mathbf{U}^{\kappa} = \mathbf{b}^{\kappa}_{0} - \mathbf{g}_{ot}\mathbf{b}^{\kappa}_{1}\left(\mathbf{a}_{tt}\right)^{-1} && (2.285)\\
\Longleftrightarrow\ &\sum_{jb}\left[g^{oo}_{ai,bj} - \sum_{klcd} g^{ot}_{ai,ck,dl} a^{to}_{ck,dl,bj}\left(a^{tt}_{ck,dl}\right)^{-1}\right] U^{\kappa}_{bj} = b^{0,\kappa}_{ai} - \sum_{klcd} g^{ot}_{ai,ck,dl} b^{1,\kappa}_{ck,dl}\left(a^{tt}_{ck,dl}\right)^{-1}. && (2.286)
\end{aligned}
$$

Apparently, the CP-OO-MP2 equations are substantially more complex than the well-known CP-SCF equations. In Section 3.3 a very preliminary algorithm for the solution of the these equations is proposed.

2.9.3. Spin Contamination

The expectation value of the total spin operator $\hat{S}^2$ is regarded as a diagnostic tool to measure the spin contamination in the UHF reference determinant [56–58]. In post-Hartree-Fock methods $\langle \hat{S}^2 \rangle$ can be evaluated by means of response theory [56]. The perturbation λS^2 is added to the Hamiltonian, and the

derivative of the perturbation dependent energy yields the desired expectation value, eq. 2.287.

$$\langle \hat{S}^2 \rangle = \left. \frac{dE(\lambda)}{d\lambda} \right|_{\lambda=0} \tag{2.287}$$

Note, that the perturbation expansion only corresponds to the exact expectation value of $\hat{S}^2$ in the case of variational methods. $\langle \hat{S}^2 \rangle$ for the OO-RI-MP2 can be expressed as [57],

$$\langle \hat{S}^2 \rangle_{\mathrm{OO}} = \langle \hat{S}^2 \rangle_{\mathrm{ref}} + 2\langle \Psi_0 | \hat{S}^2 | \Psi_1 \rangle. \tag{2.288}$$

The correlation correction to the expectation value of the total spin operator over the reference determinant has the explicit form [59],

$$2\langle \Psi_0 | \hat{S}^2 | \Psi_1 \rangle = -\frac{1}{2} \sum_{ia}^{\alpha} \sum_{jb}^{\beta} S_{ib}^{\alpha\beta} S_{ja}^{\beta\alpha} t_{ab}^{ij} \tag{2.289}$$

where $S_{ib}^{\alpha\beta} = \int \Phi_i^{\alpha} s_+ \Phi_b^{\beta} d\tau$ and $S_{ja}^{\beta\alpha} = \int \Phi_j^{\beta} s_- \Phi_a^{\alpha} d\tau$. [57] $\Phi_i^{\alpha}, \Phi_j^{\beta}$ denote internal and $\Phi_a^{\alpha}, \Phi_b^{\beta}$ represent virtual α-/β-spin orbitals, respectively.

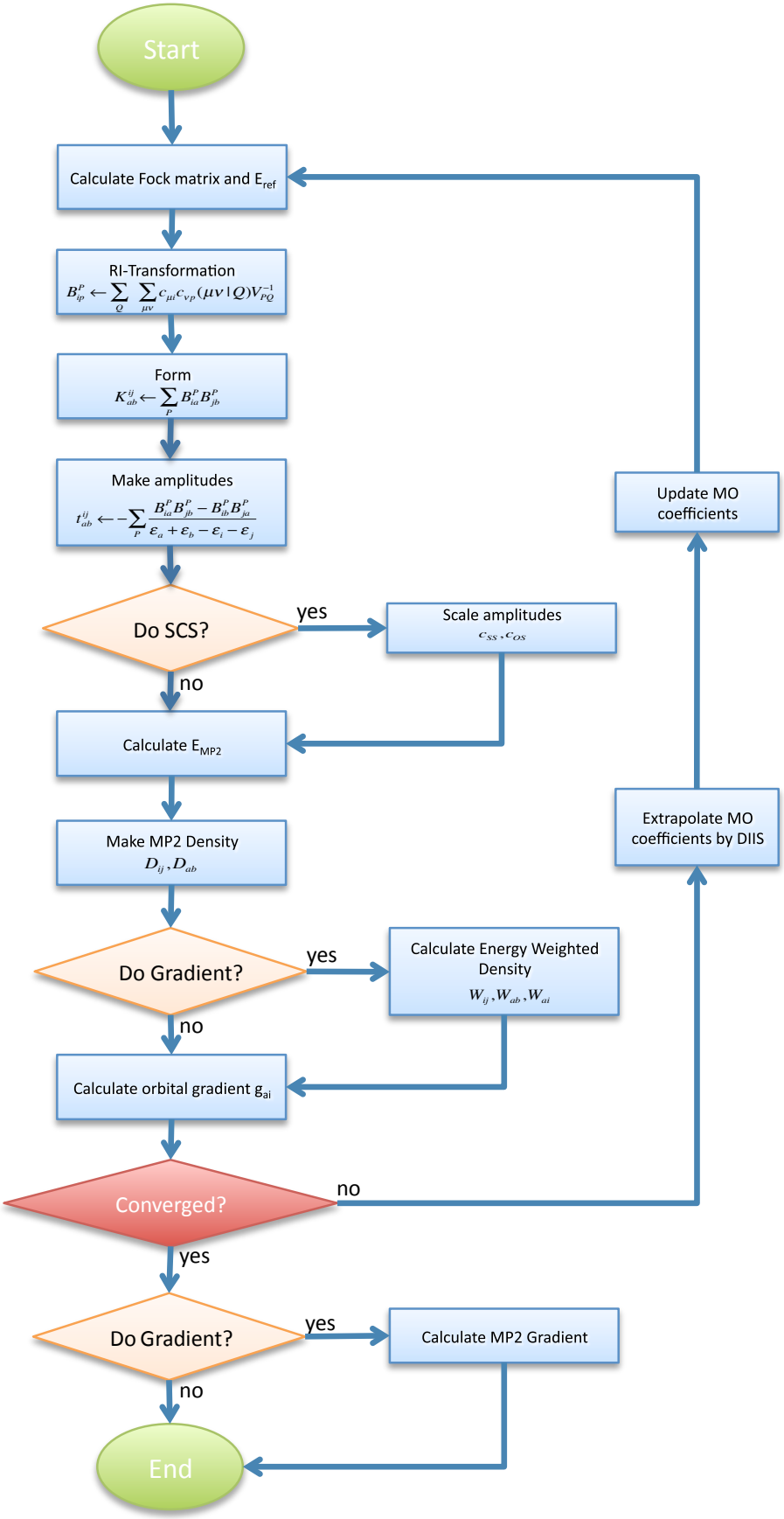

Figure 2.4.: Flowchart of the OO-RI-MP2 module.

3. Computational Details

3.1. Implementation of RI-MP2 First and Second Derivatives

In this section the implementation of RI-MP2 derivatives is described. The algorithm is divided into two major parts, i.e. a part, in which the zero-order relaxed RI-MP2 density matrix is calculated and a second part, in which the first-order relaxed RI-MP2 density matrix is constructed.

3.1.1. First Derivatives

The first part for the calculation of first-order properties proceeds as demonstrated in Listing 3.1.

```
Form V_pq^-1/2
Perform RI-transformation of B_ip^P ← c_μi c_νp (μν|P) V_PQ^-1/2
   store I^ij(P,1), I^i(a,P) on disc
// Calculate additional RI-integrals, if second derivatives are requested
if (DerivMode == _SECOND_)
   if (StoreABV)
      Perform RI-transformation of B_ab^P ← c_μa c_νb (μν|P) V_PQ^-1/2
        store I^ab(P,1) on disc
      Calculate the Coulomb-type integrals J^ij(a,b) ← B_ij^P B_ab^P
        store J^ij on disc
        remove B_ab^P from disc
   else
      Direct transformation of B^P_{a_ib b_ib} ← c_{μ a_ib} c_{ν b_ib} (μν|P) V_PQ^-1/2 in a loop over batches ib of ab-pairs
      Calculate the Coulomb-type integrals J^ij(a_ib, b_ib) ← B_ij^P B^P_{a_ih b_ih} for the current batch
        store J^ij on disc
   endif StoreABV
endif DerivMode
Loop over op1
   Loop over batches of i
     Loop over op2
       Loop over j
         form K^ij(a,b) ← B_ia^P B_jb^P
              t^ij(a,b) ← −[K^ij(a,b) − K^ij(b,a)] × (ε_a + ε_b − ε_i − ε_j)^-1
              Γ^i(P,a) ← t_ab^ij B_jb^P
              D^sym(a,b) ← ½ (t^ij t^ij+)_ab
         store t^ij(a,b) for the actual batch only
         if (DerivMode == _SECOND_)
           store K^ij(a,b), t^ij(a,b) on disc
         endif DerivMode
       end loop j
       Loop over j
         Loop over k
           read t^ij, t^ik
           form D^sym(j,k) ← −½ tr(t^ij t^ik+)
         end loop k
       end loop j
     end loop op2
   end loop i
   // Construct 3-interal and 3-external contribution
```

```
   // to the real Lagrangian
41 if (PertMode == _REAL_)
     Loop over i
43     Loop over a
         form X^sym(a,i) ← Γ^i(P,a)B^P_ip
45     end loop a
     end loop i
47 endif PertMode
end loop op1
49 // Store unrelaxed density matrix
Transform D^sym(μ,ν) ← c_μp c_νq D^sym(p,q)
51 Store D^sym(μ,ν) on disc
// Finalize the real Lagrangian and
53 // solve the zero-order z-vector equations
if (PertMode == _REAL_)
55 form X^sym(a,i) ← R̄(D)(a,i)
   solve A^ℜ_ai,bj z̄^sym(a,i) = −X^sym(a,i)
57 form D^sym(a,i) ← −½ z̄^sym(a,i)
   // Store relaxed density matrix
59 transform D^sym(μ,ν) ← c_μp c_νq D^sym(p,q)
   store D^sym(μ,ν) on disc
61 endif PertMode
// Finalize first derivative
63 Form E^λ_MP2 ← tr(D^sym · h^[λ])
```

Listing 3.1: Algorithm for RI-MP2 first derivatives.

Starting with the calculation of the negative square root of the V-matrix by using the Cholesky decomposition of the inverse V-matrix, the 2- and 3-index two-electron repulsion integrals and its contraction to the corresponding $B^P_{\mu\nu}$ intermediates are calculated and the RI-integrals in the AO basis are transformed to the requested MO-basis integrals.

If second derivatives are required, the 2-internal/2-external Coulomb integrals are calculated and stored on disc. This can be done either in the MO basis requiring the temporary storage of the 2-external RI-integrals B^P_{ab}, or using an AO-direct algorithm in which the storage of B^P_{ab} can be avoided. The latter version is strongly recommended for larger systems.

In a loop over the number of operators, i.e. spin cases, and a loop over batches of internal orbitals, the 2-external/2-internal exchange integrals are calculated on the fly and directly contracted to the double excitation amplitudes. Additionally, the 3-index 2-particle density is constructed and the virtual-virtual block of the symmetric MP2 unrelaxed density matrix is formed via BLAS level 3 matrix multiplications. The MP2 amplitudes are temporarily stored for the actual batch. The internal-internal block of the unrelaxed density matrix is built from the prestored amplitudes by employing BLAS level 3 matrix operations. In the case of real perturbations the 3-external and 3-internal contributions to the MP2 Lagrangian are formed and stored in the symmetric matrix X. The unrelaxed MP2 density matrix is transformed to the AO basis and stored on disc.

For real perturbations the Lagrangian is finalized and the zero-order z-vector equations are solved. The resulting z-vector is added to the unrelaxed density forming the relaxed density matrix, which is transformed to the AO basis and stored on disc. The MP2 density matrices are then used to calculate the total first derivative of the MP2 energy correction.

3.1.2. Second Derivatives

The implementation of the second RI-MP2 derivative starts with the precalculation of the 3-/4-internal integrals from the previously stored RI-integrals. The formation of the $\boldsymbol{\sigma}$-vectors is also performed using the prestored MO-integrals, except for the 4-external contribution, which is calculated in the AO basis with either the AOBLAS algorithm or via the semi-numeric exchange treatment (COSX).
In the loop over perturbations, the CP-SCF equations are solved for the actual perturbation and the perturbed Fock matrix is formed with the resulting U-coefficients. The response-type operator $R(\mathbf{U})$ is calculated in the AO basis and then transformed to the MO basis. The 3-external contribution to the first-order RI-MP2 amplitudes is partially precalculated by transforming the external index of the U-coefficients to the AO basis and contracting them with the 3-index RI-AO-integrals. These intermediates are temporarily stored on disc.
In a loop over operators and batches of internal orbitals, the first-order double excitation amplitudes are formed and stored for the actual batch. Furthermore, the first-order 2-particle 3-index density is constructed and the perturbed amplitudes are contracted to form the unrelaxed first-order MP2 density matrix using BLAS level 3 matrix operations. In the case of imaginary perturbations, the perturbed MP2 density matrix is antisymmetric.
Subsequently, the 3-external and 3-internal contributions to the first-order Lagrangian are calculated from the first-order 2-particle 3-index density and the corresponding integrals. The 3-external contribution is calculated in the AO basis and then transformed to the MO basis.

The contributions to the first-order Lagrangian containing the derivatives of the two-electron integrals are computed from the prestored $\boldsymbol{\sigma}$-matrices by contraction with the corresponding U-coefficients.
The derivative of the response-type operator is calculated in the AO basis and subsequently back transformed to the MO basis. In the case of double-hybrid functionals, the contribution $R(\mathbf{D}'^{\kappa})_{ai}$ already contains the scaled contribution from the XC kernel, and the functional derivatives of the XC kernel $R^{XC,\kappa}(\mathbf{D}'^{\kappa})_{ai}$ are added separately to the first-order Lagrangian. The real perturbed Lagrangian is finalized by adding the perturbed orbital energies contracted with the zero-order z-vector.
The solution of the first-order z-vector equations yields the first-order z-vector, which is required to finalize the first-order relaxed density matrix. The resulting MP2 density matrix is transformed to the AO basis and stored on disc. The entire algorithm for the calculation of the first-order relaxed RI-MP2 density matrix is shown in Listing 3.2.

```
Calculate I^ij(k,p) ← B^P_ik B^P_jp from the stored RI-integrals
  store I^ij(k,l), I^ij(k,a) on disc
Calculate the σ^ij(a,b)-matrices
  σ^ij(1)(a,b) ← t^ik(a,c) [J^kj(c,b) − K^kj(c,b)] + [J^ik(a,c) − K^ik(a,c)] t^kj(c,b) + K^ij(k,l) t^kl
  if (KCOpt == _AOBLAS_)
    σ^ij(1)(a,b) ← c_μa c_κb (μν|κτ) t^ij(ν,τ)
  elsif (KCOpt == _COSX_)
    σ^ij(1)(a,b) ← c_μa c_κb w_g φ_μ(r_g) φ_ν(r_g) (κ|τ) t^ij(ν,τ)
  endif KCOpt
  tr(σ^ij(2)(a,b)) ← tr(t^ik K^jk)
  σ^ij(3)(a,b) ← (K^kj t^kj)_ab
  store σ^ij(1), tr(σ^ij(2)), σ^j(3) on disc
/* ********************************************************** */
/* Loop over perturbations                                    */
/* ********************************************************** */
Loop over ipert
  // ---------------------------------------------------------
  // Solve the CP-SCF equations for appropriate perturbation
```

```
19  // ------------------------------------------------------------------
    Solve A_{ai,bj} U^κ_{bj} = -h^κ_{ai}
21
    // ------------------------------------------------------------------
23  //  Calculate the perturbed Fock operator
    // ------------------------------------------------------------------
25  R(U^κ)(p,q) ← c_{μp} c_{νq} U^κ(η,τ) [(μν||ητ) ± (μν||τη)]
    FX(p,q) ← h^κ(p,q) + R(U^κ)(p,q)
27
    // ------------------------------------------------------------------
29  //  Precalculate 3-external contribution to the
    //  perturbed amplitudes
31  // ------------------------------------------------------------------
    TX^i(a,P) ← -c_{νa} U^κ_{μi} B^P_{μν}
33  store TX^i on disc

35  // ------------------------------------------------------------------
    //  Start batching over internal orbitals
37  // ------------------------------------------------------------------
    Loop over op1
39    Loop over batches of i
        Loop over op2
41        Loop over j
            form tx^{ij}(a,b) ← -U^κ(k,a) I^{ij}(k,b) - U^κ(k,b) I^{ij}(k,a) - TX^i(b,P) I^j(a,P) - TX^j(a,P) I^i(b,P)
43               tx^{ij}(a,b) ← t^{ik}(a,b) FX(j,k) + FX(i,k) t^{kj}(a,b) - t^{ij}(a,c) FX(b,c) - FX(a,c) t^{ij}(c,b)
                 Γx^i(P,a) ← I^j(b,P) tx^{ij}_{ab}
45               if (PertMode == _REAL_)
                   DX(a,b) ← 1/2 ( tx^{ij} t^{ij+} + t^{ij} tx^{ij+} )_{ab}
47               elsif (PertMode == _IMAG_)
                   DX(a,b) ← 1/2 ( tx^{ij} t^{ij+} - t^{ij} tx^{ij+} )_{ab}
49          store tx^{ij}(a,b) for the actual batch
          end loop j
51        Loop over j
            Loop over k
53            read t^{ij}, t^{ik} from disc
              read tx^{ij}, tx^{ik}
55            if (PertMode == _REAL_)
                DX(j,k) ← -1/2 ( tr(tx^{ij} t^{ik+}) + tr(t^{ij} tx^{ik+}) )
57            elsif (PertMode == _IMAG_)
                DX(j,k) ← -1/2 ( -tr(tx^{ij} t^{ik+}) + tr(t^{ij} tx^{ik+}) )
59          end loop k
          end loop j
61      end loop op2
      end loop i
63    // ------------------------------------------------------------------
      // Form 3-internal and 3-external contribution to the perturbed
65    // Lagrangian LMP2X
      // ------------------------------------------------------------------
67    Loop over i
        Loop over a
69        if (PertMode == _REAL_)
            Xx^{sym}(a,i) ← -2 B^P_{ki} Γ'^{P,κ}_{ka}
71          Xx^{sym}(a,i) ← 2 B^P_{μν} Γ'^{P,κ}_{iν}
          elsif (PertMode == _IMAG_)
73          Yx^{asym}(a,i) ← 2 B^P_{ki} Γ'^{P,κ}_{ka}
            Yx^{asym}(a,i) ← -2 c_{μa} B^P_{μν} Γ'^{P,κ}_{iν}
75        endif PertMode
        end loop a
77    end loop i
  end loop op1
79  // ------------------------------------------------------------------
    //  Contract the precalculated sigma-vectors with the
81  //  corresponding U-coefficients
    // ------------------------------------------------------------------
83  if (PertMode == _REAL_)
```

```
    Xx^sym(a,i) ← x^κ_bj σ^ij(1)_ab − x^κ_ja tr(σ^ij(2)) − x^κ_bi σ^ij(3)_ab
  elsif (PertMode == _IMAG_)
    Yx^asym(a,i) ← i y^κ_bj σ^ij(1)_ab + i y^κ_ja tr(σ^ij(2)) + i y^κ_bi σ^ij(3)_ab
  endif PertMode

  // ------------------------------------------------------------------
  //  Calculate the derivative of the response operator
  // ------------------------------------------------------------------
  if (PertMode == _REAL_)
    Xx^sym(a,i) ← R̄(D'^κ)_ai − x^κ_ai R̄(D)_ij + x^κ_bi R̄(D)_ab + R̄(D̃)_ai
  if (PertMode == _IMAG_)
    Yx^asym(a,i) ← R̿(D'^κ)_ai + i y^κ_aj R̄(D)_ij − i y^κ_bi R̄(D)_ab + R̿(D̃)_ai
  endif PertMode

  //  In the case of double-hybrid functionals add the contribution
  //  containing the third functional derivatives
  if (DHDF && (PertMode == _REAL_) )
    Xx^sym(a,i) ← R̄^{XC,κ}(D)_ai
  endif DHDF

  // ------------------------------------------------------------------
  // Add perturbed orbital energies to the Lagrangian
  // ------------------------------------------------------------------
  if (PertMode == _REAL_)
    Xx^sym(a,i) ← (∂ε_a/∂κ − ∂ε_i/∂κ) z̄_ai
  endif PertMode

  // ------------------------------------------------------------------
  // Solve first-order z-vector equations
  // ------------------------------------------------------------------
  if (PertMode == _REAL_)
    Solve A^ℜ_ai,bj ∂z̄_bj/∂κ = −Xx^sym(a,i) − ∂A^ℜ_ai,bj/∂κ z̄_bj
  elsif (PertMode == _IMAG_)
    Solve A^ℑ_ai,bj ∂z̿_bj/∂κ = −Yx^asym(a,i)
  endif PertMode

  // ------------------------------------------------------------------
  // Finalize the perturbed relaxed density
  // ------------------------------------------------------------------
  if (PertMode == _REAL_)
    DX^sym(a,i) ← −½ z̄^κ(a,i)
    DX^sym(p,q) ← x^κ_rp D_rq + x^κ_rq D_pr
  elsif (PertMode == _IMAG_)
    DX^asym(i,a) ← ½ z̿^κ(a,i)
    DX^asym(a,i) ← −½ z̿^κ(a,i)
    DX^asym(p,q) ← −i y^κ_rp D_rq + i y^κ_rq D_pr
  endif PertMode

  transform DX(μ,ν) ← c_μp c_νq DX(p,q)
  store DX(μ,ν) on disc

end loop ipert
```

Listing 3.2: Algorithm for RI-MP2 second derivatives.

3.2. The 'Chain of Spheres Exchange' Algorithm

The semi-numeric exchange treatment is efficiently implemented via the 'chain of spheres exchange' (COSX) algorithm. [39] In this algorithm each contracted basis function is surrounded by a sphere outside

of which its contribution to the exchange matrix is assumed to be negligible. Practically, this basis function cutoff is 10^{-10} which corresponds roughly to a radius of $\sim$3Å for a valence basis function. Given these spheres, a list of partners for each basis function with a non-negligible differential overlap (S-junction) is constructed. Likewise, a list of partners which are connected via a non-negligible density matrix element (P-junction) is built. These lists are expected to become asymptotically constant, as long as Kohn's conjecture holds, i.e. the absolute values of the density or overlap matrix elements, respectively, drop asymptotically with the distance of the corresponding orbital shells. The structure of the COSX algorithm as it is implemented is shown is Listing 3.3.

```
Preselect interacting pairs of basis functions
Loop ig over grid points
 Calculate basis function values R_μg                                  // O(N)
 if (DoGrad)
   Calculate basis function derivatives R_μλg                          // O(N)
 Construct secondary (and tertiary) shell lists                        // O(N)
 Perform BLAS level 3 matrix multiplication F_τg = Σ_κ R_κg P_κτ       // O(N)
 Calculate analytic integrals G_νg = Σ_τ F_τg A_ντ(r_g)                // O(N)
 Perform BLAS level 3 matrix multiplication K_μν = Σ_g R_μg G_νg       // O(N)
 if (DoGrad)
   Perform BLAS level 3 matrix multiplication K^λ_μν = Σ_g R_μλg G_νg  // O(N)
end
```

Listing 3.3: Schematic diagram of the COSX algorithm.

First, the interacting pairs of basis functions which interact via S- or P-junction are preselected. In the loop over batches of grid points the surviving basis function values and, if requested, its derivatives are calculated. Then a secondary shell list is constructed with basis functions, which interact with the primary list of shells via the density matrix. The tertiary shell list is not required for the evaluation of the semi-numeric exchange gradient, due to the permutational symmetry of the two-electron derivative integrals. The $F_{\tau g}$-intermediate is built via large scale BLAS Level 3 matrix routines. The analytical integration represents the rate limiting step, and in the formation semi-numeric exchange matrix and its gradient, respectively, use of BLAS level 3 routines is made again. The COSX algorithm is potentially linear scaling, but due to the small decay constant of the exponential functions the secondary shell list only becomes constant for fairly large systems, i.e. $\sim$25Å.

3.2.1. COSX integration grids

The integration grids employed for the numerical integration within the COSX algorithm are derived from standard DFT grids included in the ORCA program package, but are considerably smaller. The accuracy of the integration grids is controlled by the radial resolution parameter ε together with the largest Lebedev grid used in constructing the atomic grid. ε defines the number of radial shells n_r for a given atom and is calculated as $n_r = 15\varepsilon + 5r - 40$ [60], where r is the row of the periodic table to which the atom belongs. For a radial integration accuracy of ε=$\{$3.34;4.01;4.34;5.01$\}$ the number of radial grid points for the 1st to 3rd row of the periodic table is $\{$(15,20,25);(25,30,35);(30,35,40);(40,45,50)$\}$. The pruning algorithm of Gill *et al.* is used to reduce the number of points in the inner and outer regions. [61] In order to investigate the influence of the employed integration grids on the accuracy of the resulting first- and second-order properties, different angular grids in combination with several radial resolution parameters have been tested for diverse molecules and varying basis sets.

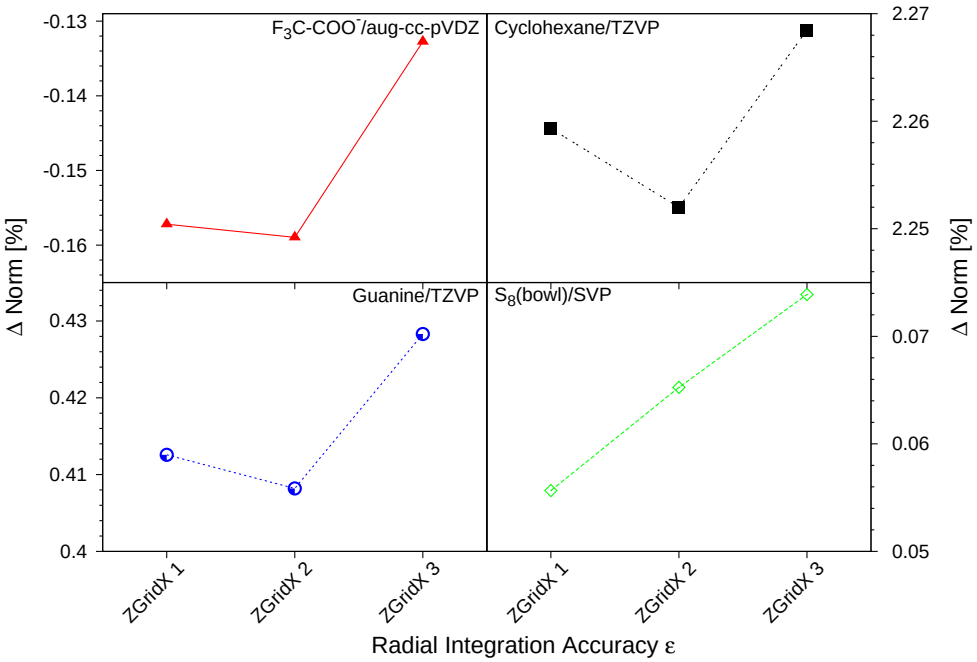

Figure 3.1.: Deviation of the RIJCOSX-MP2 gradient norm [%] depending on the SCF grids with regard to the original MP2 method. ZGridX 1-3 refer to Lebedev-50/3.34, Lebedev-50/4.01 and Lebedev-194/4.34.

RIJCOSX-MP2 Gradient For comparison, the same four representative molecules with the same diverse basis sets, as for the earlier evaluation of the SCF grids have been chosen. [39]
The grids used for the calculation of the response-type operators are dependent on the chosen SCF grids, since they originate from the HF equations. Therefore, the influence of the employed integration grids for the solution of the z-vector equations on the quality of the calculated gradient norm compared to the original MP2 gradient norm has been tested. As shown in Fig. 3.1, the deviations of the gradient norm are very small (<3%) and the very limited deviations follow no general trend. We therefore have considered the smallest SCF grid as being appropriate for the present purpose.
The calculation of the derivative of the basis functions on the grid required for the RIJCOSX-MP2 gradient is independent of the employed SCF grids. Therefore, we tested different angular grids in combination with several radial integration accuracies. In Fig. 3.2 the deviation of the norm calculated with the RIJCOSX approximation compared to the norm of the original MP2 method is presented.
The trend of the norm deviation changes between different molecules but is almost independent of the angular grid. The maximum deviation of the gradient norm is 3.5% for the cyclohexane molecule, but is considerably smaller for the other molecules in this test suite (<1%). The curves corresponding to the large 302 and 434 point Lebedev grid nearly coincide and even the deviations obtained with the smaller 194 point Lebedev grid are still reasonable. However, extended test calculations have shown, that best convergence in geometry optimizations is obtained with the Lebedev-302 radial grid in combination with a radial integration accuracy of 4.43. Hence we choose this very conservative scheme as our default setting.

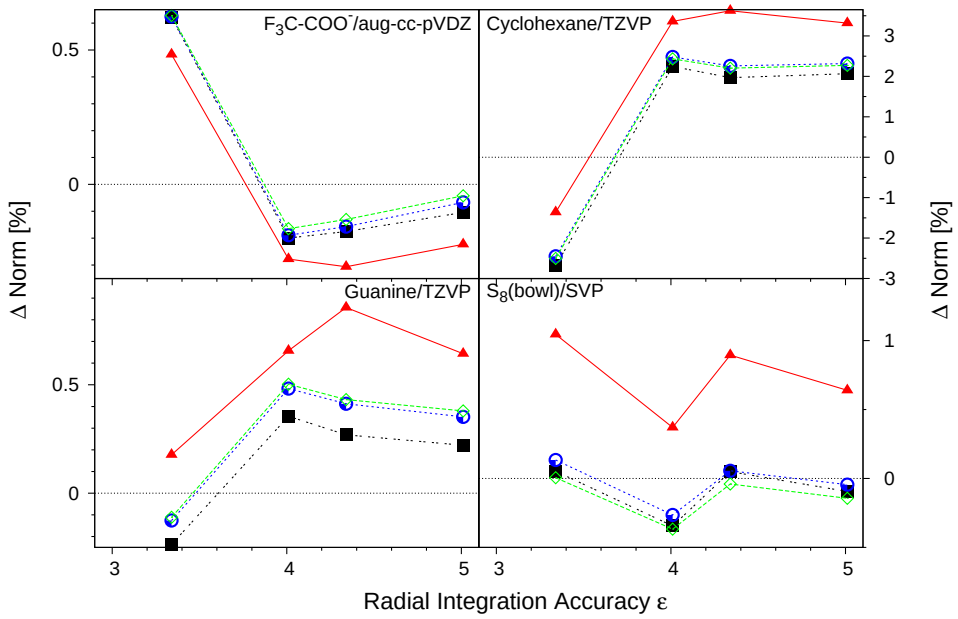

Figure 3.2.: Deviation of the RIJCOSX-MP2 gradient norm [%] depending on the grids used for the evaluation of the basis function derivatives with regard to the original MP2 method. Triangles=110 point Lebedev grid, filled squares=195 point Lebedev grid, circles=302 point Lebedev grid and empty squares=434 point Lebedev grid.

RIJCOSX-MP2 Second-Order Properties The COSX grids used for the solution of the first-order z-vector equations as well as for the evaluation of the perturbed response-type operators depend on the chosen SCF grids. As it has already turned out for the calculated gradient, the second-order properties are almost unaffected by the grid choice as well. Therefore, the only grid to be determined, is the one used in the calculation of the 4-external contribution to the σ-vector. In Fig. 3.3 the deviation of the isotropic polarizability calculated with the COSX approximation compared to the one calculated with the conventional AO-based algorithm is presented. The error is usually $<$0.001 au and both Lebedev-195 and Lebedev-302 grids show negligible errors, which are almost independent on the radial integration accuracy. The deviation is for each molecule and all grids $<$0.01%. The error introduced by the COSX approximation in the calculated isotropic g-shifts is shown in Fig. 3.4. The deviations in the g-tensor are one order of magnitude larger ($<$0.1%) compared to the error in the polarizabilities. Overall, it turned out that the Lebedev-110 angular grid in combination with a radial resolution parameter of 3.34 represents a good compromise between efficiency and accuracy.

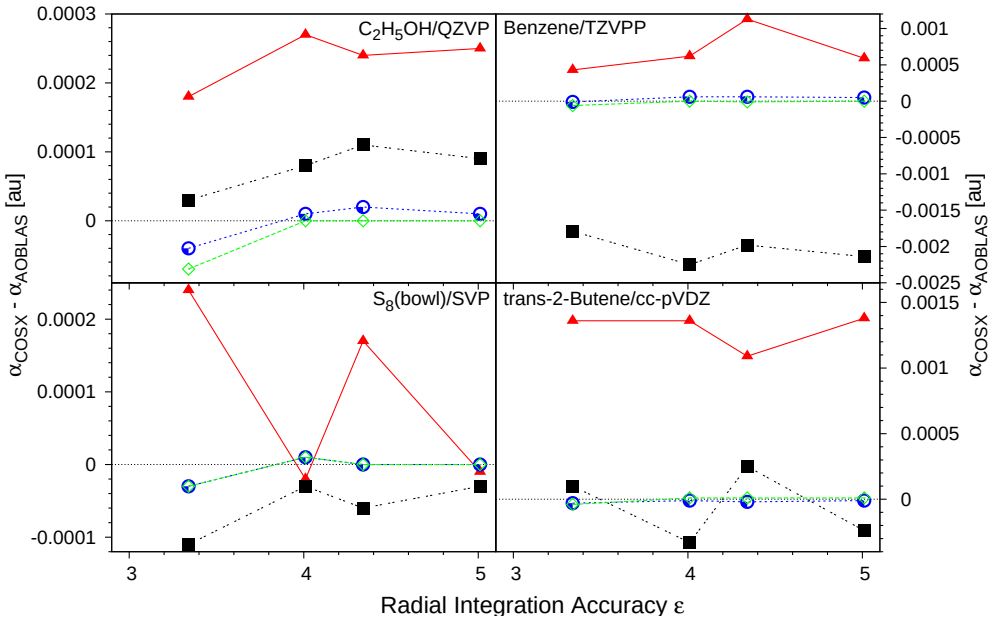

Figure 3.3.: Deviation of the isotropic polarizability [au] calculated with the COSX algorithm (COSX) from the direct AO treatment (AOBLAS) depending on the grids used for the evaluation of the $K(\mathbf{t}^{ij})_{ab}$ term. Triangles=50 point Lebedev grid, filled squares=110 point Lebedev grid, circles=194 point Lebedev grid and empty squares=302 point Lebedev grid.

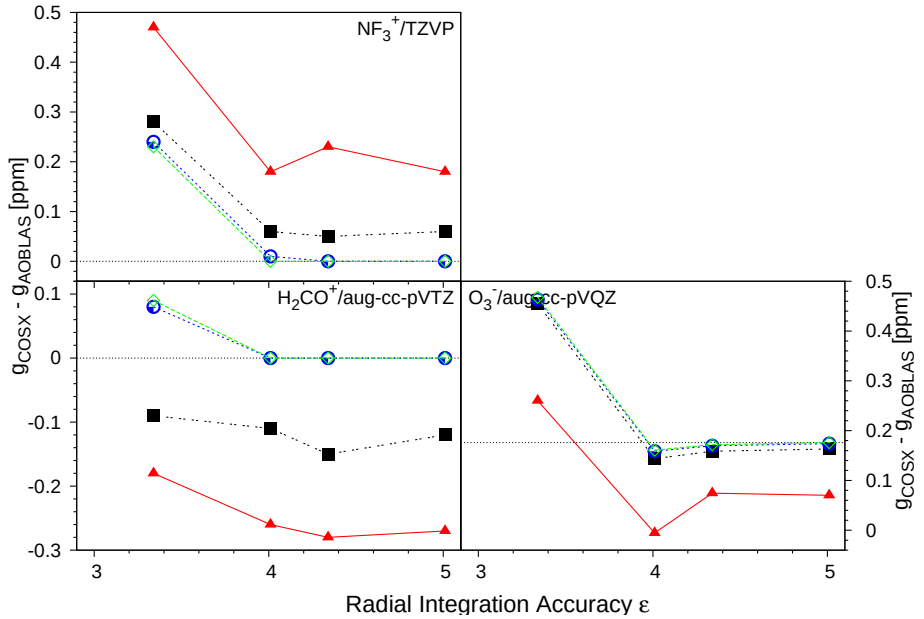

Figure 3.4.: Deviation of the isotropic g-shift [ppm] calculated with the COSX algorithm (COSX) from the direct AO treatment (AOBLAS) depending on the grids used for the evaluation of the $K(\mathbf{t}^{ij})_{ab}$ term. Triangles=50 point Lebedev grid, filled squares=110 point Lebedev grid, circles=194 point Lebedev grid and empty squares=302 point Lebedev grid.

3.3. Proposed Algorithm for the Calculation of Second Derivatives

In this section a preliminary algorithm for the solution of the coupled-perturbed OO-MP2 equations, derived in Section 2.9.2, is proposed. Listing 3.4 presents the construction of the right-hand side of the CP-OO-MP2 equations. The first step is to contract the one-electron perturbation matrix $h^{[\kappa]}$ with the corresponding zero-order double excitation amplitudes and the orbital energy denominator $a^{tt}_{ck,dl}$. The resulting four-index quantity is saved on disc and later used for the formation of the 3-internal/3-external contributions to the Lagrangian.

Further contraction with another set of zero-order amplitudes leads to a matrix $ttxh$ with which the response-type operator $R(ttxh)_{ai}$ can be calculated and added to the first-order Lagrangian LX_{ai}. The 3-external contribution to the Lagrangian can be efficiently evaluated in the AO-basis, whereas the 3-internal contribution is calculated with prestored integrals. The Lagrangian is finalized by adding the contracted and uncontracted $h^{[\kappa]}_{ai}$ terms. The first-order Lagrangian is then used to solve of the CP-OO-MP2 equations.

```
/* ***************************************************************************
     Form the right-hand side of the OO-MP2 equations for each perturbation κ
   *************************************************************************** */
// Construct auxiliary matrix for the contraction in ttxh ← t^kl b^{1,κ}_{ck,dl} · (a^tt_{ck,dl})^-1
loop over k
  loop over l
    Get stored amplitudes t^kl
    loop over m
      // Form the internal part of the txh-matrix
      Get stored amplitudes t^km, t^ml
      Form txh^kl ← −t^km h^[κ]_ml − h^[κ]_km t^ml
    end loop m
    // Form the virtual part of txh-matrix
    BLAS_Add_Mat_x_Mat(txh^kl, t^kl, hV^[κ])
    BLAS_Add_Mat_x_Mat(txh^kl, hV^[κ],†, t^kl)
    loop over c
      loop over d
        // Finalize txh-matrix
        txh^kl(c, d) ← txh^kl(c, d) · (−ε_k − ε_l + ε_c + ε_d)^−1
      end loop d
    end loop c
    Store txh^kl on disc

    // Form virtual part of the ttxh-matrix
    BLAS_Add_Mat_x_Mat(ttxhV, 2 · t^kl, txh^kl,†)
    BLAS_Add_Mat_x_Mat(ttxhV, 2 · t^lk, txh^kl)
    loop over m
      Get stored amplitudes t^ml, t^mk
      // Form internal part of the ttxh-matrix
      ttxh(m, k) ← −2 · BLAS_Trace(t^ml, txh^kl,†)
      ttxh(m, l) ← −2 · BLAS_Trace(t^mk, txh^kl)
    end loop m
  end loop l
end loop k

// Construct the first-order Lagrangian
loop over batches of i
  loop over a
    LX(a, i) ← 2 · h^[κ]_ai
    loop over j
      LX(a, i) ← D_ij h^[κ]_aj
    end loop j
```

```
    loop over b
44    LX(a,i) ← D_ab h_ib^[κ]
    end loop b
46  end loop a
  loop over AOs
48    loop over l
        // Form 3-external contribution to LX
50      LX(a,i) ← 4 · c_μa c_κl (μν|κτ) txh_ντ^il
      end loop l
52  end loop AOs

54  loop over l
      Get stored 3-internal integrals I^il ← (ik|ld)
56    loop over a
        // Form 3-internal contribution to LX
58      LX(a,k) ← −4 · (ik|ld) txh_ad^il
      end loop a
60  end loop l
end loop ibatch
62
// Calculate response-type contribution to LX
64 LX(a,i) ← 2 · R(ttxh)_ai

66 // ----------------------------------------
// Solve the OO-MP2 equations
68 // ----------------------------------------
Call function Solve_OOMP2Eqs()
```

Listing 3.4: Proposed algorithm for the construction of the right-hand side of the CP-OO-MP2 equations.

In Listing 3.5 a potential algorithm for the solution of the CP-OO-MP2 equations is presented. Several terms which occur in the first-order Lagrangian for the conventional MP2 method appear on the left-hand side of the CP-OO-MP2 equations. First, a $\boldsymbol{\sigma}$-vector is calculated and stored on disc just like in the canonical MP2 case. Then an adequate initial guess has to be made for the U-coefficients. Afterwards, the well-known left-hand side of the CP-SCF equations is formulated as one contribution to the CP-OO-MP2 left-hand side. Then the formal derivative of the response-type operator similar to the MP2 case is built. Several Fock-matrix terms are added and finally, to complete the G_{ai} intermediate the $\boldsymbol{\sigma}$-vector is contracted with the corresponding orbital rotation coefficients.

In a second step a four-index quantity is formed, which contains a response-type operator over the U-coefficients contracted with the zero-order amplitudes, several Fock-matrix elements contracted with the double excitation amplitudes and the U-coefficients as well as 3-external and 3-internal two-electron repulsion integrals multiplied by the actual U-coefficients. The $R_{ck,dl}$ quantity is scaled by the denominator $a^{tt}_{ck,dl}$ and stored on disc.

The intermediate four-index quantity is first contracted with the OO-MP2 amplitudes to calculate a response-type operator, and subsequently used for the contraction with 3-external/3-internal two-electron integrals.

The left-hand side of the OO-MP2 equations is finalized and convergence is checked. If convergence has not been achieved yet, the U-coefficients are updated, e.g. by a DIIS procedure.

At convergence, the U-coefficients are used to calculate the first-order OO-MP2 amplitudes and the entire second derivative.

```
/* ****************************************************
     Solve the CP-OO-MP2 equations
   **************************************************** */

Calculate the σ^ij(a,b)-matrices
  σ^ij(1)(a,b) ← t^ik(a,c) [J^kj(c,b) − K^kj(c,b)] + [J^ik(a,c) − K^ik(a,c)] t^kj(c,b) + K^ij(k,l)t^kl
  if (KCOpt == _AOBLAS_)
    σ^ij(1)(a,b) ← c_μa c_κb (μν|κτ) t^ij(ν,τ)
  elsif (KCOpt == _COSX_)
    σ^ij(1)(a,b) ← c_μa c_κb w_g φ_μ(r_g) φ_ν(r_g) (κ|τ) t^ij(ν,τ)
  endif KCOpt
  tr(σ^ij(2)(a,b)) ← tr(t^ik K^jk)
  σ^ij(3)(a,b) ← (K^kj t^kj)_ab
  store σ^ij(1), tr(σ^ij(2)), σ^j(3) on disc

// ----------------------------------------
// INITIAL GUESS
// ----------------------------------------
U^κ_bj = − LX / (ε_a − ε_i)

loop over CP-Iter
  // ----------------------------------------
  // Generate Σ_jb U^κ_bj g^oo_ai,bj
  // ----------------------------------------
  Calculate Σ_jb U^κ_bj g^oo(ai,bj) ← Σ_jb U^κ_bj A^(ℜ)_ai,bj

  // Add response-type terms to the left-hand side of OO-CP-MP2 equations
  G_ai ← Σ_jb −δ_ab U^κ_bj R(D)_ij + δ_ij U^κ_bj R(D)_ab + Σ_k D_ik R(U^κ)_ak + Σ_c D_ac R(U^κ)_ic + R(D̃)_ai

  // Add Fock-matrix terms
  G_ai ← Σ_jb U^κ_bj [D_ij F_ab + D^ij_ab − δ_ab Σ_k D_ik F_jk − δ_ij Σ_c D_ac F_bc]

  // Add σ-terms
  G_ai ← U^κ_bj σ^ij(1)_ab − U^κ_ja tr(σ^ij(2)) − U^κ_bi σ^ij(3)_ab

  // ----------------------------------------
  // Generate Σ_jb U^κ_bj Σ_klcd g^ot_ai,ck,dl a^to_ck,dl,bj (a^tt_ck,dl)^−1
  // ----------------------------------------
  Form the contraction R_ck,dl ← Σ_jb U^κ_bj a^to_ck,dl,bj (a^tt_ck,dl)^−1
    Calculate response-type contribution
        R_ck,dl ← − Σ_m R(U^κ)_lm · t^km_cd + R(U^κ)_km · t^ml_cd − Σ_e R(U^κ)_ed · t^kl_ce + R(U^κ)_ec · t^kl_de
    Add Fock-matrix terms
        R_ck,dl ← Σ_jb U^κ_bj [ − Σ_m t^km_cd [δ_lj F_bm + δ_mj F_lb] + t^ml_cd [δ_kj F_bm + δ_mj F_kb] − Σ_e t^kl_ce [δ_eb F_jd + δ_db F_ej] + t^kl_ed [δ_cb F_je + δ_db F_ej] ]
    Add 2-electron repulsion integrals
        R_ck,dl ← Σ_jμ δ_kj U^κ_μj ⟨μl||cd⟩ + Σ_jν δ_lj U^κ_νj ⟨kν||cd⟩ − Σ_jb U^κ_bj [δ_cb ⟨kl||jd⟩ + δ_db ⟨kl||cj⟩]
    Multiply with the denominator R_ck,dl ← R_ck,dl · (a^tt_ck,dl)^−1
    store R_ck,dl on disc

  Form the contraction O_ai ← Σ_ck,dl g^ot_ai,ck,dl R_ck,dl
    Calculate response-type contribution O_ai ← 2R(t · R)_ai
    Add 2-electron integral contribution O_ai ← 2 Σ_klκτ δ_ik ⟨μl||κτ⟩ R_κk,τl − 2 Σ_klcd δ_ac ⟨kl||id⟩ R_ck,dl

  Finalize the left-hand side of the CP-OO-MP2 equations O_ai ← G_ai − O_ai

  if (CP-Iter > 0) CheckConvergence()

  if (NotConverged) UpdateUCoefficients()
  else break

end loop CP-Iter
```

Listing 3.5: Algorithm for the solution of CP-OO-MP2 equations.

By analyzing the individual terms occurring on the left-hand side of the CP-OO-MP2 equations, it appears that the solution of the CP-OO-MP2 equations is of the similar computational effort as the calculation of the first-order MP2 Lagrangian in conventional MP2 theory. However, the CP-OO-MP2 equations have to be solved iteratively, and thus the computational costs scale with the number of iterations. Thus, the solution of the first-order z-vector equations in general MP2 theory is replaced by the solution of the CP-OO-MP2 equations in the OO-MP2 method.

4. Validation

In the present section the validation of our implementation of second RI-MP2 derivatives is presented. Therefore, the calculated electric and magnetic properties are compared to MP2 results obtained with the CFOUR program package [62]. A numerical check for the imaginary second MP2 derivatives could not be performed, because the use of complex molecular orbital coefficients is not available in the ORCA program package.

4.1. Polarizabilities

4.1.1. Calculation of Polarizabilities

Static polarizabilities can be considered as second-order response of the molecular system with regard to an external electric field $\vec{\mathcal{E}}$. Therefore, the energy can be expanded in a Taylor series around $|\mathcal{E}| = 0$,

$$E(\vec{\mathcal{E}}) = E^{(0)} + \sum_{\alpha} \left(\frac{\partial E}{\partial \mathcal{E}_\alpha} \right)_{|\mathcal{E}|=0} \mathcal{E}_\alpha + \frac{1}{2} \sum_{\alpha\beta} \left(\frac{\partial^2 E}{\partial \mathcal{E}_\alpha \partial \mathcal{E}_\beta} \right)_{|\mathcal{E}|=0} \mathcal{E}_\alpha \mathcal{E}_\beta + \frac{1}{3!} \sum_{\alpha\beta\gamma} \left(\frac{\partial^3 E}{\partial \mathcal{E}_\alpha \partial \mathcal{E}_\beta \partial \mathcal{E}_\gamma} \right)_{|\mathcal{E}|=0} \mathcal{E}_\alpha \mathcal{E}_\beta \mathcal{E}_\gamma + \dots . \tag{4.1}$$

with $\alpha, \beta, \gamma, \ldots = x, y, z$. Comparing eq. 4.1 with the expression for the energy of a molecule in an electric field in classical physics, eq. 4.2,

$$E(\vec{\mathcal{E}}) = E^{(0)} - \sum_{\alpha} \mu_\alpha \mathcal{E}_\alpha - \frac{1}{2} \sum_{\alpha\beta} \alpha_{\alpha\beta} \mathcal{E}_\alpha \mathcal{E}_\beta - \frac{1}{3!} \sum_{\alpha\beta\gamma} \beta_{\alpha\beta\gamma} \mathcal{E}_\alpha \mathcal{E}_\beta \mathcal{E}_\gamma + \ldots \tag{4.2}$$

shows, that the polarizability tensor α can be expressed as second derivative of the energy w.r.t. an external electric field.

$$\alpha_{\alpha\beta} = -\frac{1}{2} \sum_{\alpha\beta} \left(\frac{\partial^2 E}{\partial \mathcal{E}_\alpha \partial \mathcal{E}_\beta} \right)_{|\mathcal{E}|=0} \tag{4.3}$$

Analogously, the dipole moment μ corresponds to the first and the hyperpolarizability to the third energy derivative.

4.1.2. Validation of Polarizabilities as Implemented in the ORCA Program Package

In Table 4.1 the calculated isotropic polarizabilities for a series of small organic compounds are listed. The polarizabilities have been calculated employing a triple-ζ basis set (TZVP [63, 64]) and Dunning's quadruple-ζ basis set (cc-pVQZ [65]). For the 'Resolution of the Identity' approximation the corresponding correlation fitting basis sets from the Turbomole library [32, 33] were used. The energies were converged

to 10^{-10} E_h. The results maintained with the ORCA program package are compared to the CFOUR results. The error introduced by the RI approximation is assumed to be negligible, since the error in the total energies is usually <1 mE_h. This is confirmed by the numbers presented in Table 4.1, where the deviations in the isotropic polarizabilities are typically $\leq$0.005 au for the TZVP basis and $\leq$0.02 au for the cc-pVQZ basis compared to the conventional MP2 reference. The error ranges from -0.003 to 0.006 au and from -0.004 to 0.037 au, respectively. Since, the error is in the interval of the typical error introduced by the RI approximation, we consider the correct implementation of the RI-MP2 second derivatives as proven for real perturbations.

Table 4.1.: Calculated isotropic polarizabilities for a series of small organic compounds in [au]. Comparison of CFOUR and ORCA implementation. Structures have been optimized at the RI-MP2/TZVP level.

molecule	TZVP				cc-pVQZ			
	CFOUR		ORCA		CFOUR		ORCA	
	HF	MP2	HF	RI-MP2	HF	MP2	HF	RI-MP2
CH_4	13.701	13.847	13.700	13.849	15.274	15.582	15.274	15.583
C_2H_2	18.276	17.278	18.277	17.277	21.450	20.574	21.450	20.574
C_2H_4	24.212	23.020	24.212	23.021	25.800	24.936	25.800	24.936
C_2H_6	25.008	25.484	25.008	25.487	26.702	27.400	26.702	27.402
C_3H_4[a]	30.484	29.892	30.484	29.894	33.818	33.453	33.818	33.455
cyclo-C_3H_6	33.026	33.768	33.026	33.774	34.021	34.911	34.029	34.920
C_3H_8	36.201	37.159	36.201	37.165	38.073	39.322	38.081	39.332
1-Butyne[a]	42.243	42.125	42.244	42.128	45.663	45.799	45.678	45.795
1-Butene	47.165	46.686	47.165	46.689	49.416	49.420	49.419	49.442
trans-2-Butene	47.150	46.735	47.150	46.741	49.660	49.727	49.675	49.744
C_6H_6[a]	61.914	62.303	61.914	62.300	64.700	65.202	64.735	65.239
cyclo-C_6H_{12}	64.545	66.821	64.545	66.832	—[b]	—[b]	66.600	69.247
CH_3OH	16.825	17.396	16.825	17.399	18.681	19.481	18.681	19.482
CH_3CHO	25.093	26.202	25.093	26.202	26.965	28.273	26.977	28.284
C_2H_5OH	28.085	29.157	28.085	29.162	30.135	31.483	30.145	31.495
MD			0.0000	0.0025			0.0076	0.0086
MAD			0.0002	0.0030			0.0076	0.0091

4.1.3. RIJCOSX Error

In this section the accuracy of the RIJCOSX approximation is benchmarked. Therefore, isotropic polarizabilities have been calculated with three different basis sets up to quintuple-ζ quality [65] with the corresponding auxiliary basis functions [66]. The standard COSX integration grids analyzed in Section 3.2.1 have been employed. The RIJCOSX approximation becomes more efficient with increasing angular momenta and increasing system size. Therefore, the largest speedup is achieved for the cc-pV5Z basis set. For systems with $\sim$500 basis functions an overall speedup in the total wall clock time of a factor of 10 could be achieved. For the cyclohexane molecule with a basis dimension of 1206 even a factor of 15 has been reached.

[a] CFOUR energy convergence criterion decreased to 10^{-8} E_h.
[b] CFOUR calculation could not been finished.

Table 4.2.: Calculated isotropic HF polarizabilities for a series of small organic compounds in [au]. Estimation of the RIJCOSX error. Structures have been optimized at the RI-MP2/TZVP level.[d]

molecule	cc-pVTZ		cc-pVQZ		cc-pV5Z	
	HF	RIJCOSX-HF	HF	RIJCOSX-HF	HF	RIJCOSX-HF
CH_4	14.657	14.667	15.274	15.279	15.582	15.600
C_2H_2	19.650	19.674	21.450	21.560	22.407	22.647
C_2H_4	24.305	24.280	25.800	25.791	27.007	27.114
C_2H_6	26.019	25.980	26.702	26.668	27.033	26.995
C_3H_4	31.826	31.836	33.818	33.920	34.851	35.079
cyclo-C_3H_6	33.112	33.077	34.029	34.002	35.267	35.231
C_3H_8	37.220	37.187	38.081	38.058	38.900	38.855
1-Butyne	43.559	43.636	45.678	45.795	47.239	47.500
1-Butene	47.671	47.612	49.419	49.418	50.784	50.952
trans-2-Butene	48.032	48.005	49.675	49.700	51.188	51.403
C_6H_6	61.618	61.621	64.735	64.930	68.481	68.953[e]
cyclo-C_6H_{12}	65.516	65.474	66.600	66.580	69.484	69.791
CH_3OH	17.725	17.729	18.681	18.682	19.224	19.240
CH_3CHO	25.769	25.783	26.977	26.988	28.371	28.348
C_2H_5OH	29.064	29.075	30.145	30.164	31.402	31.401
MD		−0.0071		0.0314		0.1259
MAD		0.0275		0.0466		0.1450

In Tables 4.2 and 4.3 the calculated isotropic polarizabilities at the Hartree-Fock and MP2 level are presented. The error in the static polarizabilities grows with increasing basis dimension. This behaviour is also observed for single point energies and has been analyzed in detail in Refs. [39] and [31]. Therefore, the use of larger integration grids has been recommended for calculations with extended basis sets. Nevertheless, a mean absolute error of 0.1–0.15 au in isotropic polarizabilities for the cc-pV5Z basis set is still satisfactory. Except for the benzene molecule, for which the SCF failed to converge on the standard COSX grids, no outliers have been observed. Thus, the RIJCOSX approximation demonstrates again its robustness and high efficiency.

[d] Errors in final RIJCOSX-SCF energies are for cc-pVTZ=0.02.0.01.0.17.0.07.0.02.0.08.0.10.0.09.0.26.0.19.0.08.0.35.0.01.−0.01.0.01 kcal/mol and for cc-pVQZ=0.25.−0.03.0.33.0.54.0.26.0.41.0.67.0.27.0.98.0.95.0.83.1.40.0.43.0.25.0.39 kcal/mol and for cc-pV5Z=0.60.0.22.0.90.1.07.0.73.1.19.1.44.1.05.2.09.2.11.2.43.−0.03.0.95.0.75.1.02 kcal/mol.

[e] Due to SCF convergence problems the following COSX grids were employed: small SCF grid Lebedev-50/3.67, medium SCF grid Lebedev-110/4.01, final SCF grid Lebedev-194/4.34 and if so COSX $K(\mathbf{t}^{ij})_{ab}$ grid Lebedev-302/4.34.

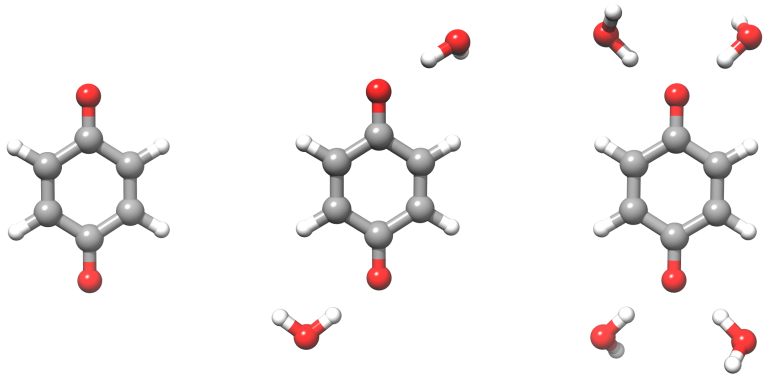

(a) $BQ^{\bullet-}$ (b) $BQ^{\bullet-}\times 2H_2O$ (c) $BQ^{\bullet-}\times 4H_2O$

Figure 4.1.: Structures of the *p*-benzosemiquinone anion radical ($BQ^{\bullet-}$) coordinated with up to four water molecules.

Table 4.3.: Calculated isotropic MP2 polarizabilities for a series of small organic compounds in [au]. Estimation of the RIJCOSX error. Structures have been optimized at the RI-MP2/TZVP level.[f]

molecule	cc-pVTZ		cc-pVQZ		cc-pV5Z	
	RI-MP2	RIJCOSX-MP2	RI-MP2	RIJCOSX-MP2	RI-MP2	RIJCOSX-MP2
CH_4	14.844	14.855	15.583	15.591	15.965	15.987
C_2H_2	18.801	18.824	20.574	20.674	21.509	21.719
C_2H_4	23.376	23.344	24.936	24.915	26.129	26.206
C_2H_6	26.529	26.478	27.402	27.356	27.838	27.787
C_3H_4	31.418	31.422	33.455	33.545	34.519	34.712
cyclo-C_3H_6	33.691	33.646	34.920	34.884	36.431	36.386
C_3H_8	38.199	38.159	39.332	39.303	40.301	40.250
1-Butyne	43.565	43.646	45.795	45.934	47.484	47.729
1-Butene	47.433	47.348	49.442	49.384	50.902	51.004
trans-2-Butene	47.825	47.774	49.744	49.728	51.452	51.608
C_6H_6	62.008	62.007	65.239	65.410	69.272	69.663[e]
cyclo-C_6H_{12}	67.731	67.674	69.247	69.217	72.632	72.925
CH_3OH	18.286	18.290	19.482	19.483	20.237	20.257
CH_3CHO	26.824	26.838	28.284	28.294	29.891	29.870
C_2H_5OH	30.103	30.116	31.495	31.519	33.005	33.013
MD		−0.0141		0.0205		0.1106
MAD		0.0341		0.0519		0.1346

COSX Timings The speedup obtained by employing the RIJCOSX approximation to RI-MP2 second derivative calculations is analyzed in the present paragraph. Therefore, the structures of the *para*-benzosemiquinone anion radicals ($BQ^{\bullet-}$) coordinated with up to four water molecules (Fig. 4.1) have been optimized with the TPSS [67] meta-GGA density functional and a TZVP [64, 68] basis set under

[f] Errors in final RIJCOSX-MP2 energies are for cc-pVTZ=0.04.−0.13.0.08.0.17.−0.01.0.01.0.23.−0.10.0.37.0.29.0.43.−0.64.0.22.0.04.0.02 kcal/mol and for cc-pVQZ=0.25.−0.03.0.33.0.54.0.26.0.41.0.67.0.27.0.98.0.95.0.83.1.40.0.43.0.25.0.39 kcal/mol and for cc-pV5Z=0.60.0.22.0.90.1.07.0.73.1.19.1.44.1.05.2.09.2.11.2.76.0.07.0.95.0.75.1.02 kcal/mol.

tight optimization criteria. The structure of the $BQ^{\bullet-}\times 4H_2O$ anion radical was taken from Ref. [69]. The static isotropic polarizabilities have been calculated with Ahlrichs' TZVPP [66,70] basis set together with the corresponding auxiliary basis sets.

Table 4.4.: Timings in [s] for the formation of the 4-external contribution to the σ-vector $K(\mathbf{t}^{ij})_{ab}$ and total wall clock times for one polarizability calculation in a TZVPP basis set with the RIJCOSX-MP2 method.

Molecule	N_{Basis}	$N_{AuxBasisJ}$	$N_{AuxBasisC}$	Time $K(\mathbf{t}^{ij})_{ab}$		Total Time	
				AOBLAS	COSX	AOBLAS	COSX
$BQ^{\bullet-}$	304	436	728	5523 (47.6%)	1790 (21.5%)	11603	8312
$BQ^{\bullet-}\times 2H_2O$	422	578	1000	33690 (53.2%)	7161 (18.6%)	63318	38495
$BQ^{\bullet-}\times 4H_2O$	540	720	1272	130721 (56.2%)	20311 (16.5%)	232611	122988

In Table 4.4 the speedup achieved by calculating the 4-external contribution $K(\mathbf{t}^{ij})_{ab}$ to the σ-vector semi-numerically with the 'chain of spheres exchange' algorithm is tabulated. The total wall clock times listed in Table 4.4 refer to the formation of the first-order relaxed MP2 density matrix employing the RIJCOSX approximation. Whereas in the default AOBLAS algorithm the calculation of $K(\mathbf{t}^{ij})_{ab}$ is the time determining step, which takes $\sim$50% of the total wall clock time, the COSX treatment reduces the computational effort drastically to $\leq$20%. The speedup for the entire calculation is $\sim$1.5 for the smallest compound and $\sim$2 for the solvated $BQ^{\bullet-}\times 4H_2O$ radical.

Table 4.5.: Timings in [s] for the formation of the perturbed response operator $\overline{R}^{\kappa}(\mathbf{D})_{ai}$ and the solution of the first-order z-vector equations $\overline{z}_{ai}$ for one polarizability calculation in a TZVPP basis set.

Molecule	N_{Basis}	$N_{AuxBasisJ}$	$N_{AuxBasisC}$	Time $\overline{R}^{\kappa}(\mathbf{D})_{ai}$		Time $\overline{z}_{ai}$	
				AO (direct)	RIJCOSX	AO (direct)	RIJCOSX
$BQ^{\bullet-}$	304	436	728	1082 (6.0%)	241 (2.1%)	6255 (35.0%)	1553 (13.4%)
$BQ^{\bullet-}\times 2H_2O$	422	578	1000	2224 (2.8%)	438 (0.7%)	16610 (20.7%)	3978 (6.3%)
$BQ^{\bullet-}\times 4H_2O$	540	720	1272	3815 (1.4%)	685 (0.3%)	20775 (7.9%)	4304 (1.9%)

In Table 4.5 the timings for the formation of the perturbed response operator $\overline{R}^{\kappa}(\mathbf{D})_{ai}$ and for the solution of the first-order z-vector equations are shown. The formation of $\overline{R}^{\kappa}(\mathbf{D})_{ai}$ can be accelerated by a factor $\sim$5 if the Coulomb-type integrals are approximated by the 'Resolution of the Identity' approximation and the exchange-type integrals are evaluated semi-numerically. But this speedup has almost no effect on the total wall clock time, since the step is by far not rate limiting. The situation changes for the solution of the z-vector equations, which account for $\sim$35% of the entire wall clock time for the smallest *p*-benzosemiquinone anion radical, but becomes less expensive for growing systems. Nevertheless, a factor of $\sim$4–5 can be gained by employing the RIJCOSX approximation to the solution of the z-vector equations. An overall speedup of $\sim$2 could be achieved even for these small systems by employing the RIJCOSX approximation throughout and by treating the 4-external contribution semi-numerically.

4.1.4. Numeric versus Analytic Polarizabilities

In this section the numeric calculation of isotropic polarizabilities is compared to the analytic evaluation. Therefore, the structures of the nitropyridine compounds shown in Fig. 4.2 have been optimized with

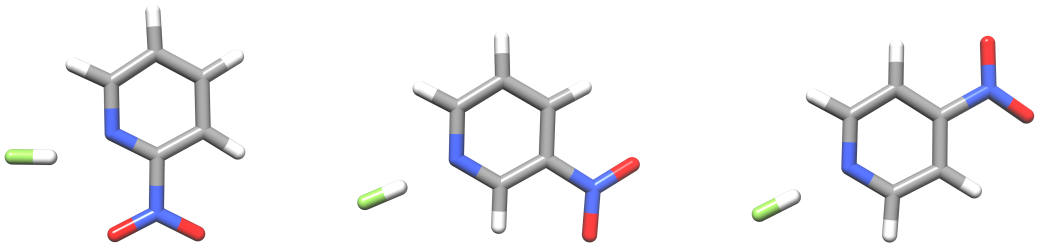

(a) **I** (b) **II** (c) **III**

Figure 4.2.: Structures of (a) 2-nitropyridine, (b) 3-nitropyridine and (c) 4-nitropyridine coordinated by hydrogen fluoride.

the BP86 [71, 72] GGA density functional in a polarized triple-ζ basis set (TZVPP [66, 70]) under tight optimization conditions. The static polarizabilities have been calculated at the RI-MP2 [21] level with Dunning's cc-pVTZ [65] basis set and the corresponding auxiliary basis functions [66]. The numeric polarizabilities have been evaluated either by first finite differences of dipole moments (POLAR2) or by second finite differences of energies (POLAR3). In order to speedup the analytic calculation of isotropic polarizabilities (POLAR1) the COSX approximation has been applied for the calculation of the 4-external term in the first-order Lagrangian 'COSX' (cf. eq. 2.231) or the RIJCOSX approximation has been employed throughout 'RIJCOSX'. The standard COSX integration grids analyzed in Section 3.2.1 have been used.

The timings listed in Table 4.6 refer to total wall clock times for a polarizability calculation subsequent to a single point and relaxed RI-MP2 density calculation for the SCF, the RI-MP2 unrelaxed and relaxed densities. The difference in the total time required to perform one numeric polarizability calculation using the POLAR2 approach compared to an analytic evaluation with conventional RI-MP2 is almost negligible, due to the small system size (15 first row atoms) and basis set. The second finite differences of energies technique (POLAR3) is roughly a factor 2 more slower compared to the analytic derivative evaluation, due to the larger number of displacements. Calculating the 4-external contribution to the first-order Lagrangian semi-numerically (COSX) gains ∼20–25% in computation time. The application of the RIJCOSX approximation to the analytical computation thus saves ∼60% of the total wall clock time.

Table 4.6.: Total wall clock times for numeric versus analytic isotropic polarizabilities [au] for 2-/3-/4-nitropyridine compounds in [s] for a cc-pVTZ basis set (N_{Bas}=370, N_{BasJ}=545, N_{BasC}=960).

	POLAR1			POLAR2	POLAR3
		COSX	RIJCOSX		
I	68 445.9 ($\alpha_{iso} = 78.80$)	54 744.5	28 544.1	71 052.4 ($\alpha_{iso} = 78.78$)	150 614.6
II	71 026.3 ($\alpha_{iso} = 79.74$)	54 634.8	30 435.9	73 200.4 ($\alpha_{iso} = 79.78$)	152 946.1
III	68 763.0 ($\alpha_{iso} = 78.80$)	52 248.3	28 449.0	71 261.2 ($\alpha_{iso} = 78.80$)	152 163.9

Benchmark Study In order to benchmark the implementation of second analytic RI-MP2 derivatives the 16-annulene molecule, shown in Fig. 4.3, has been chosen. The structure of the 16-annulene compound has been optimized at the RIJCOSX-MP2 level with a TZVP [66,70] basis set. The static polarizabilities have been calculated with triple-ζ and quadruple-ζ basis sets (cc-pVTZ, cc-pVQZ [65]).

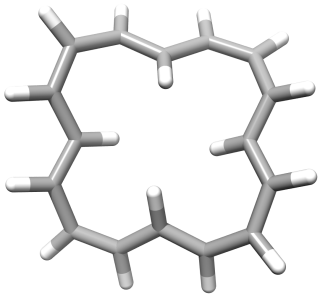

Figure 4.3.: Structure of 16-annulene optimized at RIJCOSX-MP2/TZVP level.

For the cc-pVTZ basis set (N_{Bas}=704, N_{BasJ}=960, N_{BasC}=1776) the total wall clock time for the analytic polarizability calculation is roughly ∼3 days 23 hours 2 minutes (∼1 day 11 hours 16 minutes with RIJCOSX) on a Intel(R) Xeon(R) CPU with 2.4GHz and 6GB RAM. The same calculation using the finite differences technique of dipole moments took ∼4 days 8 hours 14 minutes (∼1 day 8 hours 43 minutes with RIJCOSX) on the same machine. The polarizability calculation employing the cc-pVQZ basis set (N_{Bas}=1360, N_{BasJ}=960, N_{BasC}=2992) took roughly 17 days 9 hours employing the RIJCOSX approximation on a Quad-Core AMD Opteron Processor with 2.2GHz and 8GB of main memory. The computation time is dominated by the calculation of the 4-internal contribution to the $\boldsymbol{\sigma}$-vector, which is somewhat surprising. It has to be checked whether this is an artifact of load balancing on the computer or if the routine itself has to be further optimized for large-scale applications. By contrast, the evaluation of the 4-external contribution to the $\boldsymbol{\sigma}$-vector took only ∼6% of the overall time required for the calculation of the relaxed RIJCOSX-MP2 density matrix. For comparison, the MP2 polarizability calculation of the benzene molecule in a cc-pVQZ basis set (N_{Bas}=510) took ∼8 days 20 hours with the CFOUR program package on an identical machine.

4.2. Chemical Shieldings

4.2.1. Calculation of Chemical Shielding Tensors

In magnetic resonance spectroscopy the concept of effective spin Hamiltonians plays a fundamental role in the understanding of experimental data. [73] The effective spin Hamiltonian used to resemble the nuclear magnetic resonance (NMR) spectra for closed-shell compounds is given as,

$$\mathcal{H}_S^{NMR} = -\sum_A \gamma_A \hbar \vec{\mathcal{B}}^T (1 - \boldsymbol{\sigma}^A) \vec{\mathcal{I}}^A + \frac{1}{2} \sum_{A \neq B} \gamma_A \gamma_B \hbar^2 \vec{\mathcal{I}}^{AT} (\mathbf{D}^{AB} + \mathbf{K}^{AB}) \vec{\mathcal{I}}^B \tag{4.4}$$

where γ_A is the nuclear magnetogyric ratio for nucleus A and $\vec{\mathcal{I}}^A$ represents the nuclear spin operator. The nuclear magnetic dipole moment $\vec{\mathcal{M}}^A$ is related to the nuclear spin operators via

$$\vec{\mathcal{M}}^A = \gamma_A \hbar \vec{\mathcal{I}}^A. \tag{4.5}$$

In eq. 4.4 $\boldsymbol{\sigma}^A$ is the nuclear magnetic shielding tensor, which describes the magnetic shielding effects of the electrons; $\mathbf{D}^{AB}$ indicates the classical dipolar interaction between nuclear magnetic dipole moments and $\mathbf{K}^{AB}$ denotes the reduced indirect nuclear spin-spin coupling between nuclear dipoles induced by the surrounding electrons. [74] The effective NMR spin Hamiltonian reproduces the nuclear magnetic energy levels in a molecular system without explicitly accounting for the electrons. [74] Expanding the electronic energy in the magnetic field $\vec{\mathcal{B}}$ and in the nuclear magnetic moments $\{\vec{\mathcal{M}}^A\}$ yields,

$$E(\vec{\mathcal{B}}, \{\vec{\mathcal{M}}^A\}) = E_0 + \frac{1}{2}\sum_{\alpha\beta} \mathcal{B}_\alpha^T \left.\frac{\partial^2 E}{\partial \mathcal{B}_\alpha \partial \mathcal{B}_\beta}\right|_{|\mathcal{B}|=0} \mathcal{B}_\beta + \sum_A \sum_{\alpha\beta} \mathcal{B}_\alpha^T \left.\frac{\partial^2 E}{\partial \mathcal{B}_\alpha \partial \mathcal{M}_\beta^A}\right|_{|\mathcal{B}|=0,|\mathcal{M}|=0} \mathcal{M}_\beta^A + \frac{1}{2}\sum_{A\neq B} \vec{\mathcal{M}}_\alpha^{AT} \left.\frac{\partial^2 E}{\partial \mathcal{M}_\alpha^A \partial \mathcal{M}_\beta^B}\right|_{|\mathcal{M}|=0} \mathcal{M}_\beta^B \tag{4.6}$$

with $\alpha, \beta, \gamma, ... = x, y, z$. In eq. 4.6 the first-order terms vanish for closed-shell systems, either due to the imaginary nature of the operator or because the spin operators generate triplet wave functions. [74] The second energy derivatives in eq. 4.6 can be identified by comparison with the spin Hamiltonian in eq. 4.4 as,

$$\xi_{\alpha\beta} = -\left.\frac{\partial^2 E}{\partial \mathcal{B}_\alpha \partial \mathcal{B}_\beta}\right|_{|\mathcal{B}|=0} \tag{4.7}$$

$$\sigma_{\alpha\beta}^A = \left.\frac{\partial^2 E}{\partial \mathcal{B}_\alpha \partial \mathcal{M}_\beta^A}\right|_{|\mathcal{B}|=0,|\mathcal{M}|=0} + 1 \tag{4.8}$$

$$K_{\alpha\beta}^{AB} = \left.\frac{\partial^2 E}{\partial \mathcal{M}_\alpha^A \partial \mathcal{M}_\beta^B}\right|_{|\mathcal{M}|=0} - D_{\alpha\beta}^{AB}. \tag{4.9}$$

The second energy derivative w.r.t. two components of the magnetic field in eq. 4.7 is the molecular magnetizability $\xi_{\alpha\beta}$, which corresponds to the polarizability in the electric case. The magnetizability tensor does not enter the NMR spin Hamiltonian. The chemical shielding tensor $\sigma_{\alpha\beta}^A$ can be expressed as mixed second energy derivative w.r.t. the magnetic field and nuclear magnetic moment of nucleus A (eq. 4.8), and the reduced indirect spin-spin coupling tensor $K_{\alpha\beta}^{AB}$ corresponds to the second energy derivative w.r.t. the components of the nuclear magnetic moments (eq. 4.9). The second-order molecular properties can be generally expressed by means of time-independent perturbation theory as, [75]

$$\frac{\partial^2 E(\lambda,\kappa)}{\partial\lambda\partial\kappa} = \left\langle \Psi_n^{(0)} \middle| \frac{\partial^2 \mathcal{H}}{\partial\lambda\partial\kappa} \middle| \Psi_n^{(0)} \right\rangle - \sum_{n\neq k} \frac{\left\langle \Psi_n^{(0)} \middle| \frac{\partial\mathcal{H}}{\partial\lambda} \middle| \Psi_k^{(0)} \right\rangle \left\langle \Psi_k^{(0)} \middle| \frac{\partial\mathcal{H}}{\partial\kappa} \middle| \Psi_n^{(0)} \right\rangle}{E_n^{(0)} - E_k^{(0)}} + \frac{\left\langle \Psi_n^{(0)} \middle| \frac{\partial\mathcal{H}}{\partial\kappa} \middle| \Psi_k^{(0)} \right\rangle \left\langle \Psi_k^{(0)} \middle| \frac{\partial\mathcal{H}}{\partial\lambda} \middle| \Psi_n^{(0)} \right\rangle}{E_n^{(0)} - E_k^{(0)}} \tag{4.10}$$

where the second energy derivative in eq. 4.10 consists of a ground-state expectation value over the second-order Hamiltonian (diamagnetic contribution) and a sum-over-states contribution over all excited states of the molecular system and transition moments between ground and excited states with the first-order Hamiltonian (paramagnetic contribution). [74, 75] The nonrelativistic molecular Hamiltonian in the

presence of an external homogeneous magnetic field and nuclear magnetic moments is given as,

$$\mathcal{H}(\vec{\mathcal{B}}, \{\vec{\mathcal{M}}^A\}) = \frac{1}{2}\sum_i \boldsymbol{\pi}_i^2 + \sum_i \mathbf{m}_i \mathbf{B}^{tot}(\mathbf{r}_i) - \sum_{iA} \frac{Z_A}{\mathbf{r}_{iA}} + \frac{1}{2}\sum_{i\neq j} \frac{1}{\mathbf{r}_{ij}} + \frac{1}{2}\sum_{A\neq B} \frac{Z_A Z_B}{\mathbf{R}_{AB}} - \sum_A \mathbf{M}_A \mathbf{B}^{tot}(\mathbf{R}_A) + \sum_{A>B} \mathbf{M}_A^T \mathbf{D}_{AB} \mathbf{M}_B. \tag{4.11}$$

The kinetic momentum operator is defined as,

$$\boldsymbol{\pi}_i = -\mathbf{i}\nabla_i + \mathbf{A}^{tot}(\mathbf{r}_i) \tag{4.12}$$

and the magnetic field is uniquely determined by the vector potential $\mathbf{A}^{tot}(\mathbf{r}_i)$ through the following relation,

$$\mathbf{B}^{tot}(\mathbf{r}_i) = \nabla_i \times \mathbf{A}^{tot}(\mathbf{r}_i) \tag{4.13}$$

where the superscript 'tot' indicates, that the total magnetic field is considered, i.e. the external magnetic field and the magnetic field due to the magnetic moments of the nuclei. The diamagnetic contributions to the nuclear magnetic properties are obtained by formulating the corresponding second derivatives of the Hamiltonian in eq. 4.11. Therefore, the operator describing the nuclear contribution to the chemical shielding tensor in atomic units is obtained as second derivative of the nuclear Zeeman interaction, [74,76]

$$\frac{\partial^2 \mathcal{H}}{\partial \mathcal{B}_\alpha \partial \mathcal{M}_\beta^A} = -1 + \frac{\alpha^2}{2} \frac{\mathbf{r}(\mathbf{r}-\mathbf{R}_A)\delta_{\alpha\beta} - r_\beta(\mathbf{r}-\mathbf{R}_A)_\alpha}{|\mathbf{r}-\mathbf{R}_A|^3}. \tag{4.14}$$

The Gauge-Origin Problem The gauge-origin problem can be traced back to the use of the vector potential $\mathbf{A}$ for defining the magnetic field, since the choice of $\mathbf{A}$ is not unique. [76] This does not affect the exact solution to the Schrödinger equation, but since gauge-invariance can not be enforced for the wave function itself, approximate solutions do not necessarily satisfy the requirement of gauge-invariance, due to the finite-basis set representation. [76, 77] While the nucleus represents the natural gauge origin for atoms, there exists no such intuitive choice for molecules. The use of distributed gauges has proven to be the best alternative to ensure gauge-invariance in molecular property calculations. The most popular approaches are the individual gauges for localized orbitals (IGLO) approach by Kutzelnigg [78,79], and the gauge-including atomic orbital (GIAO) approach [80–84], which is based on individual gauges for atomic orbitals. In present day computational chemistry the GIAO approach is the one that is dominantly used.

4.2.2. Validation of Chemical Shielding Tensors as Implemented in the ORCA Program Package

The implementation of RI-MP2 second derivatives for magnetic perturbations in the ORCA program package is compared to the CFOUR implementation on the example of chemical shielding tensors. All structures have been optimized at the MP2 level of theory employing the RI approximation and the TZVP [63, 64] basis set with the corresponding auxiliary basis functions [32, 33] under tight convergence criteria. The chemical shielding tensors were calculated employing the split-valence basis set SVP [64,85] as well as the triple-ζ basis set TZVP [64, 68] with the appropriate auxiliary basis sets [66]. The energy convergence was chosen to be 10^{-10} E_h and the threshold for the residuum norm in the CP-SCF equations was set to 10^{-10}. Due to the dependence of the calculated magnetic properties on the gauge origin, the

point of origin {0.0, 0.0, 0.0} has been chosen for this purpose throughout.

Table 4.7.: Calculated isotropic chemical shieldings for a series of small organic compounds in [ppm]. Comparison of CFOUR and ORCA implementation for SVP basis set. Structures have been optimized at the RI-MP2/TZVP level.

molecule	CFOUR			ORCA			
	HF	MP2	CCSD	HF	RI-MP2		RI-B2PLYP
					$\mathfrak{Im}/\mathfrak{Im}$	$\mathfrak{Re}/\mathfrak{Im}$	$\mathfrak{Im}/\mathfrak{Im}$
				^{1}H			
C**H**$_4$	31.149	30.935	31.032	31.149	30.931	30.930	30.876
C$_2$**H**$_4$	22.753	22.809	22.970	22.753	22.617	22.820	22.569
C$_2$**H**$_6$	29.914	29.572	29.708	29.914	29.540	29.566	29.451
C$_3$**H**$_8$	19.901	19.194	19.359	19.901	19.044	19.166	19.457
	33.011	32.777	32.929	33.011	32.783	32.775	32.507
	34.422	34.121	34.286	34.422	34.092	34.128	33.723
C$_5$**H**$_{12}$	30.896	30.550	30.730	30.893	30.507	30.548	30.322
C$_6$**H**$_6$	8.937	8.382	—	8.937	7.866	8.384	8.657
cyclo-C$_6$**H**$_{12}$	18.780	17.917	—	18.780	17.694	17.892	18.111
	40.173	40.093	—	40.173	40.125	40.102	39.380
				^{13}C			
CH$_4$	204.134	207.890	206.180	204.134	208.242	208.515	202.415
C$_2$H$_4$	86.817	103.554	103.664	86.817	105.451	105.759	91.589
C$_2$H$_6$	206.981	208.807	208.087	206.981	209.401	209.634	201.558
C$_3$H$_8$	202.024	203.023	202.983	202.024	203.710	203.944	195.762
	215.712	215.931	216.104	215.711	216.894	217.084	207.371
C$_5$H$_{12}$	195.647	195.645	196.698	195.647	196.536	196.755	188.323
	243.736	241.147	242.756	243.736	242.552	242.678	231.044
C$_6$H$_6$	103.066	117.968	—	103.066	120.781	121.030	107.548
cyclo-**C**$_6$H$_{12}$	214.501	213.257	—	214.501	214.243	214.427	204.530

In Tables 4.7 and 4.8 the isotropic chemical shieldings for two different basis sets are listed. The approach derived in Section 2.5 is referred to as '$\mathfrak{Im}/\mathfrak{Im}$' approach, whereas the derivation of Gauss [17] (Section 2.6) is dubbed '$\mathfrak{Re}/\mathfrak{Im}$' Ansatz. The Hartree-Fock chemical shielding tensors are identical for the CFOUR and the ORCA program package. For the majority of the test suite the differences between the MP2 and RI-MP2 implementations are reasonable: $\sim$0.1 ppm for ^{1}H and $\sim$1 ppm for the ^{13}C chemical shieldings (Table 4.9). An error of this magnitude can be traced back to the error introduced by the RI approximation. The RI error in the final energies is in the range of 0.005–0.5 mE$_h$ ($\sim$10–30μE$_h$/Atom). Hence, the implementation of analytic second RI-MP2 derivatives in the ORCA program package was shown to be consistent with the CFOUR implementation.

Furthermore, isotropic chemical shieldings calculated with the double-hybrid density functional B2PLYP [1] are presented in Tables 4.7 and 4.8. In order to benchmark the results obtained with the B2PLYP functional CCSD [86] calculations for the smaller organic compounds have been performed with the CFOUR program package. As can be seen from the error statistics in Table 4.9 the B2PLYP functional performs poorly for the chemical shielding tensors of the organic compounds in the present test set. The hydrogen shielding constants are worse by a factor of 2 compared to MP2/RI-MP2 and for carbon it is even a factor

of 3–4. Thus, the performance of B2PLYP for the prediction of chemical shielding constants appears to be disappointing.

Table 4.8.: Calculated isotropic chemical shieldings for a series of small organic compounds in [ppm]. Comparison of CFOUR and ORCA implementation for TZVP basis set. Structures have been optimized at the RI-MP2/TZVP level.

molecule	CFOUR			ORCA			
	HF	MP2	CCSD	HF	RI-MP2		RI-B2PLYP
					$\mathfrak{Im}/\mathfrak{Im}$	$\mathfrak{Re}/\mathfrak{Im}$	$\mathfrak{Im}/\mathfrak{Im}$
				^{1}H			
CH_4	31.279	31.103	31.193	31.279	31.080	31.097	31.132
C_2H_4	23.326	23.376	23.544	23.326	23.170	23.388	23.194
C_2H_6	29.871	29.529	29.666	29.871	29.482	29.520	29.509
C_3H_8	21.749	21.010	21.184	21.479	20.858	20.980	21.299
	32.317	32.070	32.219	32.317	32.056	32.061	31.909
	33.062	32.740	32.930	33.062	32.702	32.744	32.461
C_5H_{12}	30.231	29.850	30.045	30.231	29.795	29.840	29.736
C_6H_6	11.935	11.365	—	11.935	10.871	11.371	11.643
cyclo-C_6H_{12}	20.846	19.873	—	20.846	19.663	19.847	20.131
	37.343	37.206	—	37.343	37.208	37.198	36.671
				^{13}C			
CH_4	197.459	201.811	199.510	197.459	202.184	202.526	197.130
C_2H_4	71.723	85.995	85.889	71.722	88.249	88.654	74.094
C_2H_6	193.182	196.188	194.708	193.183	196.758	197.082	189.071
C_3H_8	185.695	187.877	187.026	185.696	188.589	188.897	180.609
	195.838	197.181	196.734	195.838	198.052	198.336	188.802
C_5H_{12}	177.725	178.560	178.803	177.726	179.488	179.774	171.156
	213.590	211.985	213.240	213.590	213.250	213.467	202.175
C_6H_6	80.665	92.510	—	80.665	95.726	96.081	82.095
cyclo-C_6H_{12}	189.819	189.915	—	189.819	190.892	191.163	181.396

Table 4.9.: Error statistics for isotropic chemical shielding tensors compared to MP2 and to CCSD. Errors are given in [ppm].

	CFOUR	ORCA		
	MP2	RI-MP2		RI-B2PLYP
		$\mathfrak{Im}/\mathfrak{Im}$	$\mathfrak{Re}/\mathfrak{Im}$	$\mathfrak{Im}/\mathfrak{Im}$
SVP				
	^{1}H			
Mean Deviation (MP2 reference)		−0.1151	−0.0039	
Mean Absolute Deviation (MP2 reference)		0.1227	0.0097	
Mean Deviation (CCSD reference)	−0.1509	−0.2143	−0.1544	−0.3013
Mean Absolute Deviation (CCSD reference)	0.1509	0.2143	0.1544	0.3293

Continued.

		CFOUR	ORCA		
		MP2	RI-MP2		RI-B2PLYP
			$\mathfrak{Im}/\mathfrak{Im}$	$\mathfrak{Re}/\mathfrak{Im}$	$\mathfrak{Im}/\mathfrak{Im}$
		^{13}C			
	Mean Deviation (MP2 reference)		1.1764	1.4004	
	Mean Absolute Deviation (MP2 reference)		1.1764	1.4004	
	Mean Deviation (CCSD reference)	−0.0679	0.9020	1.1281	−8.3443
	Mean Absolute Deviation (CCSD reference)	0.7736	1.0066	1.1504	8.3443
TZVP					
		^{1}H			
	Mean Deviation (MP2 reference)		−0.1237	−0.0076	
	Mean Absolute Deviation (MP2 reference)		0.1241	0.0120	
	Mean Deviation (CCSD reference)	−0.1576	−0.2340	−0.1644	−0.2201
	Mean Absolute Deviation (CCSD reference)	0.1576	0.2340	0.1644	0.2530
		^{13}C			
	Mean Deviation (MP2 reference)		1.2407	1.5509	
	Mean Absolute Deviation (MP2 reference)		1.2407	1.5509	
	Mean Deviation (CCSD reference)	0.5267	1.8322	1.5229	−7.5533
	Mean Absolute Deviation (CCSD reference)	0.9547	1.8322	1.5229	7.5533

5. Results

5.1. Comparison of Two Efficient Approximate Hartree-Fock Approaches

5.1.1. Introduction

Non-hybrid density functional theory can be very efficiently implemented in quantum chemical and solid state computer codes due to the fact that only local potentials enter the Kohn-Sham operator. This allows for the very efficient calculation of the two-electron Coulomb contributions by the 'Resolution of the Identity' [22, 37], Fourier transform [87] or pseudospectral [40] techniques. For the calculation of the exchange-correlation contributions efficient numerical integration techniques have been devised. [44, 88] Any other quantum chemical method requires the calculation of the nonlocal Hartree-Fock (HF) exchange term. Despite the fact that this term is inherently linear scaling [89, 90], the effort to evaluate it often dominates the computational effort in calculations on medium sized molecules (30-100 atoms) that form the subject of most contemporary quantum chemical investigations. Hence, it is necessary to develop efficient exact or approximate techniques to compute the HF exchange contributions.

In a recent paper, Weigend and co-workers [91] have compared the performance of the RI approximation for the computation of the Coulomb and exchange parts [92] with that of the Cholesky decomposition technique. [93, 94] The two techniques are closely related. In the RI approach one introduces an auxiliary basis set that needs to be optimized in some way while in the Cholesky decomposition technique the significant part of the orbital product space is determined. The 3-index electron-electron repulsion integrals that characterize the RI approach or the 3-index Cholesky vectors that result from the decomposition are then employed to construct approximations to the Coulomb and exchange contributions of the HF or KS matrices. Depending on the cut-off for the Cholesky decomposition, almost arbitrarily accurate results can be obtained. In the RI technique there always remains an, albeit smooth, basis set incompleteness error. It could be shown that at a given target accuracy of better than 1 Millihartree (mE_h) for the total energy of a medium sized molecule the RI approach is more efficient than the Cholesky decomposition technique. [91] In this section, the efficiency of the RI-JK algorithm proposed and discussed by Weigend and co-workers [91] is compared to the recently developed RIJCOSX approximation [39], which has been already discussed in detail in section 2.7. The focus is set to the comparison of the efficiency as well as the strengths and weaknesses of the RI-JK and RIJCOSX techniques.

5.1.2. Methods

The relevant equations for the RI-JK and RIJCOSX techniques as implemented in the ORCA program [25] are briefly recalled for the sake of completness. Our RI-JK implementation is essentially identical to the one proposed by Weigend *et al.* [91] and greatly improves upon an early attempt to achieve an efficient

RI-JK approximation. [95] The two-electron part of the closed-shell Fock matrix is given by,

$$G_{\mu\nu} = J_{\mu\nu} - \frac{1}{2}K_{\mu\nu} = \sum_{\kappa\tau} P_{\kappa\tau}\left((\mu\nu|\kappa\tau) - \frac{1}{2}(\mu\kappa|\nu\tau)\right) \tag{5.1}$$

$$= \sum_{\kappa\tau} P_{\kappa\tau}(\mu\nu|\kappa\tau) - \sum_{i}(\mu i|\nu i). \tag{5.2}$$

Eq. 5.1 is used in the formulation of the RIJCOSX approximation while the simplicity of the HF-density matrix ($P_{\mu\nu} = 2\sum_i c_{\mu i}c_{\nu i}$) leads to eq. 5.2 that is exploited in the RI-JK approach. Introducing an auxiliary basis set $\{\eta_K\}$, the Coulomb term is computed via the standard RI-J sequence as,

$$g_K = \sum_{\mu\nu} P_{\mu\nu}(\mu\nu|K) \tag{5.3}$$

$$d_K = \sum_{L} V^{-1}_{KL} g_L \tag{5.4}$$

$$J^{RI-J}_{\mu\nu} \approx \sum_{K} d_K(\mu\nu|K) \tag{5.5}$$

$$(\mu\nu|K) = \int \mu(\mathbf{r}_1)\nu(\mathbf{r}_1)r_{12}^{-1}K(\mathbf{r}_2)d\mathbf{r}_1 d\mathbf{r}_2 \tag{5.6}$$

$$V_{KL} = \int K(\mathbf{r}_1)r_{12}^{-1}L(\mathbf{r}_2)d\mathbf{r}_1 d\mathbf{r}_2. \tag{5.7}$$

In the RIJCOSX approximation the Split-RI-J [30] sequence is employed. In RI-JK, the calculation of the exchange matrix proceeds as, [92]

$$X^K_{\mu i} = \sum_{\nu} c_{\nu i}(\mu\nu|K) \tag{5.8}$$

$$Y^K_{\mu i} = \sum_{L} V^{-1/2}_{KL} X^L_{\mu i} \tag{5.9}$$

$$K^{RI-JK}_{\mu\nu} \approx \sum_{iK} Y^K_{\mu i} Y^K_{\nu i}. \tag{5.10}$$

If properly organized all three steps can be done as matrix multiplications making use of the extremely high efficiency of the basic linear algebra subroutine (BLAS) level 3 library functions that are available for all modern computers. Since the memory requirements for the intermediate quantities scale cubically with molecular size it will often be necessary to perform the calculation in batches and generate the 3-index integrals repeatedly.

Formally, the calculation of the Coulomb term scales as $\mathcal{O}(N^3)$ and that of the RI-JK exchange term as $\mathcal{O}(N^4)$. Prescreening of negligible 3-index integrals reduces the Coulomb term to $\mathcal{O}(N^2)$ while sparsity is not exploited in the RI-JK exchange approximation which remains at $\mathcal{O}(N^4)$ scaling. The requirements for the auxiliary basis sets are modest for the Coulomb part but more stringent for the exchange part. Ahlrichs, Weigend and co-workers have developed suitable basis sets for either Coulomb alone [28, 96, 97] or simultaneous Coulomb and exchange fitting. [92, 98] The COSX approximation to the exchange term is written as the following sequence, [39]

$$K^{COSX}_{\mu\nu} \approx \sum_{g} R_{\mu g} G_{\nu g} \tag{5.11}$$

$$R_{\mu g} = w_g^{\frac{1}{2}} \varphi_\mu(\mathbf{r}_g) \tag{5.12}$$

$$F_{\tau g} = (\mathbf{PR})_{\tau g} \tag{5.13}$$

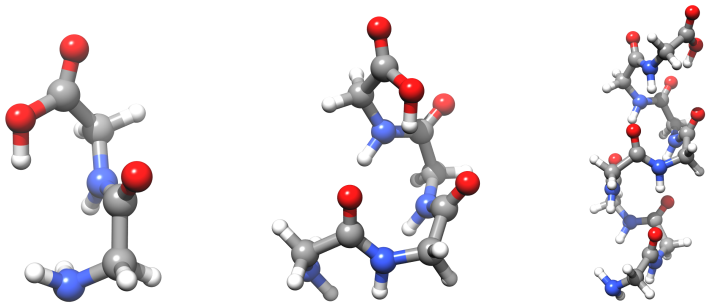

(a) $(gly)_2$ (b) $(gly)_4$ (c) $(gly)_8$

Figure 5.1.: Glycine chains.

$$A_{\nu\tau}(\mathbf{r}_g) = \int \frac{\varphi_\nu(\mathbf{r})\varphi_\tau(\mathbf{r})}{|\mathbf{r}-\mathbf{r}_g|} d\mathbf{r} \tag{5.14}$$

$$G_{\nu g} = \sum_\tau F_{\tau g} A_{\nu\tau}(\mathbf{r}_g). \tag{5.15}$$

With proper thresholding the formal scaling of this procedure is $\mathcal{O}(N)$ but due to the relatively slow decay of the density matrix elements one typically observes quadratic scaling in practice. [39] A detailed consideration of the RIJCOSX approximation is given in section 2.7.

5.1.3. Results

In order to compare the efficiency of the RI-JK and RIJCOSX approximations calculations were carried out with a number of basis sets on glycine helices $(gly)_2$, $(gly)_4$ and $(gly)_8$ shown in Fig. 5.1. Our conclusions are independent of this choice. The orbital basis sets of the Karlsruhe group were used [28, 92, 96, 97]. The def2-TZVP(-df) basis was constructed by replacing the 2d1f polarization part for the main group elements by the 1d polarization functions of the older TZVP basis set. While this basis set is not recommended [99], there are still many calculations being done with basis sets of this size and quality. The 'def2' Coulomb fitting bases '/J' have been used for RIJCOSX and the '/JK' Coulomb and exchange auxiliary bases for RI-JK. After completion of the work, we became aware of new fitting basis sets that would reduce the cost for RI-JK calculations further by 20-30% for the largest basis sets. [98] Calculations were carried out on a single CPU of a MacPro 3.1, operating system OS X 10.5, 2 quad-core Intel XEON 3.0 GHZ CPUs that have 12 MB level 2 cache. For the COSX approximation the default grids described in Ref. [39] were used except for the def2-QZVPP calculations where a slightly larger grid was employed as discussed previously. [39] All calculations were carried out with a development version of the ORCA program (version 2.7.0). [25]

The results collected in Table 5.1 show some interesting features:

1. The absolute error of the two methods is similar and both reproduce the canonical results within the chemical accuracy of ∼1 kcal/mol. Interestingly, both methods show the largest errors for the smallest basis set (def2-SVP). However, the error of the RI-JK approximation is always positive while that of the RIJCOSX approximation can have either sign. The error of the RI-JK approximation is therefore seen to be more smooth and energy differences will be slightly more accurate. However, both methods yield errors that are smaller than the typical uncertainties in computational chemistry applications that are due to errors in the structures, the treatment of the environment, the intrinsic errors in density functionals or the basis set incompleteness errors.

Table 5.1.: Comparison of RI-JK and RIJCOSX for RHF calculations on glycine chains. Total wall clock times are given in [min] and the error in the final energies is listed in [mE_h].

molecule	Basis	N_{Basis}	T_{Wall}	$SpeedUp_{RI-JK}$	$Error_{RI-JK}$	$SpeedUp_{RIJCOSX}$	$Error_{RIJCOSX}$
$(gly)_2$	def2-SVP	166	1.8	2.4	0.4	1.5	−0.6
	def2-TZVP(-df)	219	5.3	4.5	0.2	2.6	−0.4
	def2-TZVPP	391	42.9	7.9	0.3	4.9	−0.2
	def2-QZVPP	753	464.3	9.1	0.3	4.5	0.5
$(gly)_4$	def2-SVP	308	10.2	1.8	0.8	2.2	−1.1
	def2-TZVP(-df)	407	32.0	2.8	0.5	3.4	−0.5
	def2-TZVPP	723	232.8	5.1	0.5	5.8	−0.1
	def2-QZVPP	1389	2684.1	5.8	0.6	6.6	0.9
$(gly)_8$	def2-SVP	592	57.2	1.0	1.5	2.9	−1.7
	def2-TZVP(-df)	783	208.4	2.3	0.9	5.6	−0.8
	def2-TZVPP	1387	1379.6	5.0	1.0	9.7	−0.1
	def2-QZVPP	2661	12262.7	6.2	1.2	8.4	1.4

2. Both approximations perform best for large and accurate basis sets. As discussed earlier [39], this is related to the much better scaling of the both approximations with the highest angular momentum in the basis set. In the standard calculation of four index integrals this scaling is $16/9L^{10} + \cdots$ for the Davidson algorithm. [100] In the case of RI-JK this reduces to $2/9L^9 + \cdots$ due to the 3-index nature of the electron-electron repulsion integrals. In COSX the scaling is even reduced to $\mathcal{O}(L^6)$. [39]
3. For the small $(gly)_2$ molecule, the RI-JK approximation is more efficient than RIJCOSX, for $(gly)_4$ the performance of both approximations is comparable while for $(gly)_8$ RIJCOSX performs better. This result is, of course, not unexpected due to the less favorable scaling of RI-JK compared to RIJCOSX. However, low-order scaling variants of RI-JK can and have been developed. [101]
4. This behavior is typical and not affected by the choice of glycine chains as the test systems. For example, for cholesterol a more or less 2 dimensional molecule the times required for RI-JK and RIJCOSX for a RHF calculation with the def2-TZVP basis set (74 atoms, 1144 basis functions) require 16900 sec (RI-JK) and 7300 sec (RIJCOSX), in line with the $(gly)_n$ results. The total energies differ by only 0.3 mE_h.

5.1.4. Discussion

In this section the efficiency of the RI-JK and RIJCOSX approximations to the calculation of the Fock matrix was examined and illustrated by some test calculations. The comparison reveals that both approximations are efficient and accurate while their performance is overall comparable. For large-scale calculations on smaller molecules RI-JK is probably preferable while RIJCOSX is the method of choice for larger molecules. Several points are noted:

1. RI-JK achieves its efficiency through the formulation of the density matrix in the MO basis. This implies that for other exchange-type matrices, for example those that arise in electric and magnetic

linear response calculations, the approximation is less beneficially employed. In this respect RIJCOSX, that is formulated entirely in the AO basis, is the more general technique for simultaneously approximating Coulomb and exchange-type contributions.

2. For spin unrestricted calculations the cost of the RI-JK method doubles since the rate limiting step is the first contraction of the MO coefficients with the 3-index integrals. This is not true for the COSX approximation where the rate limiting step is the calculation of the integrals which is independent on the number of spin cases.
3. Energy derivatives are more readily and more efficiently formulated in the RIJCOSX approximation compared to RI-JK. [39, 43]
4. RI-JK requires much more main memory than RIJCOSX due to the structure of the intermediate quantities. Thus, if memory becomes limiting many passes through the integral list may be necessary in RI-JK with concomitant penalties in the overall performance. However, this is not much of an issue if about 4 GB of main memory are available.
5. Since RI-JK is dominated by matrix multiplications it will strongly benefit from the latest hardware developments where matrix operations can be extremely efficiently performed on graphics cards. This will further increase the attractiveness of RI-JK.

In summary, both, the RI-JK and RIJCOSX approximations are attractive tools in quantum chemistry. Their efficiency, accuracy, robustness and availability could be proven.

5.2. Efficient Structure Optimization with Second-Order Many-Body Perturbation Theory: The RIJCOSX-MP2 Method

5.2.1. Introduction

In the last two decades many attempts have been undertaken in the improvement of the quality and efficiency of MP2 calculations. On the one hand, empirical parameters have been determined to individually scale the parallel and antiparallel spin components in MP2 theory, e.g. Grimme's 'spin-component scaled' MP2 (SCS-MP2 [102, 103]) or the simplified approach of Head-Gordon *et al.* 'scaled opposite-spin' MP2 (SOS-MP2 [58, 104, 105]) that also leads to reduced computational scaling from $\mathcal{O}(N^5)$ to $\mathcal{O}(N^4)$. On the other hand the development of double-hybrid functionals has introduced semi-local dynamic correlation effects by adding a perturbative second-order correction in the framework of density functional theory. [1, 49]

Substantial progress to improve the efficiency of MP2 calculations was made by Almlöf and Saebøby introducing an integral direct MP2 algorithm to avoid storage of $\mathcal{O}(N^4)$ intermediates. [106] Further modifications to the original algorithm have been reported by Head-Gordon and Pople [107] as well as by Ahlrichs. [108] Probably, the most efficient semi-direct Ansatz without avoiding the storage of $\mathcal{O}(N^4)$ quantities on disk, was proposed by Pulay and co-workers [109–112], who presented very large MP2 calculations with more than 2000 basis functions. [113] A linear scaling integral direct MP2 code based on the Laplace transformation technique introduced by Almlöf [114] and discussed by various authors [115–117] has been developed by Ochsenfeld and co-workers. [118–121] Amongst others Werner, Schütz and co-workers have developed efficient approximate linear scaling approaches [122–126] which employed the

correlation domain concept of Pulay and Saebø. [127–129]
The most popular approximation used in combination with the MP2 method is the 'Resolution of the Identity' (RI) approximation, in which products of orbitals are expanded in an auxiliary basis set. [20] The RI-MP2 method was first reported by Feyereisen *et al.* [21] and was based on the results of Vahtras, Feyereisen and Almlöf who showed that the RI technique performs best in the Coulomb metric. [22] The outstanding performance of the RI-MP2 method is indisputable. The speedup of one to two orders of magnitude for large basis sets in comparison to the canonical result with errors in energies usually smaller than 0.1 mE_h/atom demonstrates the impressive efficiency of the RI-MP2 method.
The first derivation and implementation of the MP2 gradient was reported by Pople at the end of the 1970s. [11] Direct and semi-direct variants of the MP2 gradient implementation have been developed by Frisch, Head-Gordon and Pople more than ten years later. [130,131] Ahlrichs implemented a modification of the semi-direct MP2 gradient with reduced disk storage requirements and the exploit of nonabelian point group symmetry in the well-known MPGRAD program that is part of the TuboMole program suite. [108]
Weigend and Häser demonstrated the efficient use of the 'Resolution of the Identity' approximation in MP2 gradient calculations. [52] Further refinement was made by Head-Gordon and co-workers who first presented the restricted open shell MP2 gradient within the RI approximation [132] and later on proposed a more efficient RI-MP2 gradient algorithm by utilizing a semi-direct batching approach. [133] Analytic derivatives associated with the recently developed double-hybrid functionals have been reported by Neese, Schwabe and Grimme [49], who also demonstrated the efficient application of the RI approximation to the incorporated MP2 correction.
Like any other wave function based electron correlation theory, the basis set requirements for MP2 calculations are much more stringent than for SCF calculations. Hence, in order to obtain results that properly reflect the intrinsic accuracy of the MP2 method rather than basis set incompleteness artifacts one needs to employ at least a triple-ζ basis with at least two or three sets of polarization functions. [134] However, in order to obtain truly converged results much larger basis sets are necessary. Fortunately, basis set extrapolation techniques are known that allow one to extrapolate to the MP2 basis set limit. However, the preferred level for a reliable extrapolation still involves triple- and quadruple-ζ basis sets. In this case, traditional SCF and MP2 calculations become very expensive and highly time consuming. Thus, it is desirable to search for algorithms that perform efficiently with such extended basis sets for at least medium sized molecules that are described by 500–2000 basis functions. In this respect, the RI-MP2 method is a great achievement since it performs much better than the standard MP2 algorithms for extended basis sets. In fact, in calculations with extended basis sets the SCF calculation, despite its more favorable computational scaling, usually strongly dominates over the RI-MP2 step in terms of execution time. Neese and co-workers have recently shown, that great speedups by up to an order of magnitude can be obtained with negligible loss of accuracy, if the SCF step is performed in an approximate way that involves the RI approximation for the Coulomb integrals, while performing a semi-analytic integration of the exchange term in the HF equations. [39] This concept can be easily adopted for RI-MP2 energy calculations, since the employed approximations to the HF equations do not enter the familiar calculation of the RI-MP2 energy correction. The semi-numeric algorithm used to approximate the exchange term is called 'chain of spheres' (COSX), hence, this algorithm is termed RIJCOSX-MP2. It could be demonstrated, that the computational savings immediatly carry over to the case of double-hybrid density functional theory that inherits from RI-MP2 the significant basis set dependence. The working equations for the RIJCOSX-MP2 gradient have been already derived in Section 2.7.

5.2.2. Calculations

Computational Details

All calculations were performed with a development version of the ORCA program package. [25] The split-valence ((def2-)SV [85]), triple-ζ valence ((def2-)TZV [68]) and quadruple-ζ valence ((def2-)QZV [135]) basis sets developed by the Karlsruhe group together with the appropriate polarization functions from the TurboMole library were used throughout. [64] In order to obtain optimum results, different auxiliary basis sets should be used for the approximation of the Coulomb term [97] (/J in ORCA notation) and the MP2 energy [32–34, 136] (/C in ORCA notation). Alternatively, the larger Coulomb plus exchange [98] (/JK in ORCA notation) auxiliary basis sets can be used for the entire calculation, although the MP2 energies obtained with these fitting bases are noticeable inferior to the ones obtained with the C-bases. Nevertheless, the non-completeness errors in the RI approximation are so smooth that the choice of the auxiliary basis set does play a minor role for chemical applications and an unbalanced or erroneous behaviour was never observed with any of the tested auxiliary basis sets.
Calculations labeled RI-MP2 used the RI [22] approximation only for the calculation of the MP2 correction. In RIJ-DX-MP2 calculations exact analytic integration of the exchange contribution and the RI approximation [38, 137] for the Coulomb terms in combination with conventional RI-MP2 were employed. The label RIJCOSX-MP2 refers to a RI-MP2 calculation where the COSX approximation [39] in conjunction with Split-RI-J (in the SCF part) and the standard RI approximation (in the MP2 part) was employed. In RIJCOSX-MP2 calculations the default SCF grids [39] were used to obtain the HF energy. For the calculation of the response operator (eq. 2.217) and for the solution of the z-vector equations (eq. 2.221) a Lebedev-50 angular integration grid with an integration accuracy of 3.34 has been determined to be sufficient in extended test calculations. However, for the calculation of the derivatives of the basis functions on the grid (eq. 2.227), a large Lebedev-302 angular grid with a radial integration accuracy of 4.34 is required to prevent the buildup of numerical noise. The double-hybrid density functional calculations have been performed with the B2PLYP functional developed by Grimme. [1]
Total energies were generally converged to 10^{-8} E_h. To benchmark the optimized structures, energy convergence tolerances of 10^{-10} E_h and tight optimization criteria were enforced. The Frozen-Core approximation [138] was employed throughout, and the time savings compared to the all-electron treatment are about $\sim$10% for the RIJCOSX-MP2 treatment, determined on the example of the D-glucose molecule in combination with the TZVPP or QZVP basis set. Calculations were carried out on Quad-Core AMD Opteron(tm) 2.2 GHz CPUs with 512 KB level 2 cache and 16 GB RAM.

5.2.3. Results

In this section, the RIJCOSX-MP2 method is benchmarked against the conventional MP2 as well as the RI-MP2 method in terms of accuracy and efficiency. In order to not mix up the different approximations employed, an overview of the abbreviations used, is given in Table 5.2. Whenever the original or conventional MP2 method is mentioned, no approximations are involved. For RI-, RIJ-DX- and RIJCOSX-MP2, the MP2 energy correction is identically calculated applying the RI approximation.

Table 5.2.: Overview of the different approximations employed for the SCF and MP2 parts. Indices 'J' and 'K' refer to the Coulomb and Exchange contributions, respectively, 'RI' indicates the original 'Resolution of the Identity' approximation and 'COSX' denotes the semi-numeric exchange treatment.

	approximations				
	SCF		**MP2**		
methods	Coulomb	exchange	correction	separable gradient	non-separable gradient
MP2 energy	exact	exact	exact	—	—
MP2 gradient	exact	exact	exact	exact	exact
RI-MP2 energy	exact	exact	RI	—	—
RI-MP2 gradient	exact	exact	RI	exact	RI
RIJ-DX-MP2 energy	RI	exact	RI	—	—
RIJ-DX-MP2 gradient	RI	exact	RI	J-RI/K-exact	RI
RIJCOSX-MP2 energy	Split-RI-J	COSX	RI	—	—
RIJCOSX-MP2 gradient	Split-RI-J	COSX	RI	J-RI/K-COSX	RI

Efficiency and Accuracy of RIJCOSX-MP2 Energy Calculations

In order to demonstrate the efficiency and accuracy of the RIJCOSX approximation for MP2 energy calculations, we have calculated single point energies of seven medium sized molecules consisting of 15–57 atoms, employing two large basis sets with up to ∼1200 basis functions. The speedups listed in Table 5.3 are classified in terms of speedups in the SCF calculation and in the evaluation of the MP2 correction. Due to the fact that neither the RIJ-DX nor the RIJCOSX approximation has any influence on the calculation of the RI-MP2 energy correction, the speedups displayed in the last column of Table 5.3 are identical for RI, RIJ-DX and RIJCOSX. The speedups for the evaluation of the MP2 correction in terms of the RI approximation range from ∼18.5–33.5, which again demonstrates the high efficiency of the density fitting technique.

Whereas the RIJ-DX treatment represents generally no improvement over the original RI approximation, the benefit in computation time for the RIJCOSX approximation originates from the immense speedup during the SCF calculation. The Hartree-Fock equations in the RIJCOSX framework are solved about ∼4–11 times faster compared to the approximation-free RHF method. Since MP2 energy calculations are strongly dominated by the solution of the HF equations, the overall speedup, that can be achieved with several approximations corresponds roughly to the speedup obtained in the SCF iterations (∼1–2 for RIJ-DX, ∼5–14 for RIJCOSX). The speedups in the SCF module are considerably lower, than the speedups reported in Ref. [39]. This is due to the fact that the integral generation package of ORCA was recently replaced with the LIBINT package designed by Valeev and Ferman that is inherently more efficient, in particular for high angular momentum basis functions. [139] Hence, the favorable scaling of the COSX approximation with respect to higher angular momenta becomes less pronounced than previously reported. In general, the speedups obtained with the RIJCOSX approximation during the SCF iterations decrease by roughly a factor of 4 for the TZVPP basis set, and by a factor of ∼6 for the QZVP basis set (cf. speedup for the menthol molecule in QZVP basis: with LIBINT package – 11.6, without LIBINT package – 61.2).

The speedups listed in Table 5.3 concerning the MP2 energy correction obtained with the RI approximation compared to the conventional MP2 correction generally decrease with larger basis sets. This is caused by the higher angular momenta in the auxiliary basis set and the associated generation of the 3-index

Table 5.3.: Efficiency and accuracy of the RIJ-DX and RIJCOSX algorithms for MP2 energy calculations on medium size molecules with different basis sets. The speedup refers to the ratio of wall clock times of the SCF module or the RI-MP2 module (RI-MP2) required to finish one energy calculation. The speedups are given relative to the original MP2 method without any approximations. The deviation of the single point energies to the MP2 reference is denoted ΔE_{RI}, ΔE_{RIJ-DX} and $\Delta E_{RIJCOSX}$ in [kcal/mol].

molecule	N_{Atoms}	Basis	N_{Basis}	ΔE			SpeedUp SCF		SpeedUp
				RI	RIJ-DX	RIJCOSX	RIJ-DX	RIJCOSX	RI-MP2
adenine	15	TZVPP	150	0.1	−0.1	0.7	1.0	3.9	29.8
		QZVP	220	0.1	−0.1	1.1	1.0	6.9	18.7
beclometahsone	57	TZVPP	1277	0.4	−0.1	0.8	1.1	7.7	20.2
D-glucose	24	TZVPP	540	0.2	−0.2	0.0	1.1	4.5	26.3
		QZVP	1044	0.1	−0.3	0.8	1.1	7.9	21.6
dibenzo-crown-18-6	50	TZVPP	1142	0.3	−0.3	0.6	1.3	6.1	18.5
epinephrine	26	TZVPP	585	0.2	−0.2	0.5	1.1	4.4	27.2
		QZVP	1131	0.1	−0.3	1.3	1.0	7.7	24.2
menthol	31	TZVPP	621	0.2	−0.1	0.2	1.2	5.8	33.5
		QZVP	1227	0.1	−0.2	1.6	1.1	11.4	29.2
tyrosine	24	TZVPP	557	0.2	−0.1	0.6	1.1	4.9	26.0
		QZVP	1071	0.1	−0.2	1.4	1.1	7.4	22.9

integrals in the atomic orbital basis. Replacing the QZVP/C auxbasis by the smaller TZVPP/C auxbasis set, i.e. reducing the highest angular momentum from 'h' to 'g', yields roughly a speedup of ∼35 in the RI-MP2 module compared to conventional MP2 for the adenine molecule in a QZVP orbital basis.
The deviation in total single point energies introduced by the different approximations is on the same order of magnitude with absolute errors amounting to 0.1–0.4 kcal/mol with RI and RIJ-DX. The error for the RIJ-DX approximation is overall negative, which results from the well-known variational nature of Coulomb energy by the RI approximation. [28, 38, 137] The error in total single point energies introduced by the RIJCOSX approximation is about one order of magnitude larger than what is obtained with RIJ-DX and is overall positive. The errors are larger for the extended QZVP basis set, which has also been reported for the RIJCOSX-HF energy in Ref. [39]. These errors can be reduced by applying a larger Lebedev final grid.

Accuracy of the RIJCOSX-MP2 Gradient

In order to prove the accuracy of the geometries predicted with the RI, RIJ-DX and RIJCOSX approximations in restricted MP2 (RMP2) calculations, we performed structure optimizations on some representative medium sized molecules (Fig. 5.2).

In Table 5.4 deviations of the structural parameters relative to the original MP2 method are collected. The RIJ-DX approximation introduces no noticeable error compared to the original RI-MP2 method. The deviations introduced by the 'Resolution of the Identity' approximation are in average less than or equal to 0.01 pm in bond distances and 0.005 degrees in bond angles. The maximum absolute errors are 0.03 pm in bond lengths and 0.02 degrees in bond angles. The RIJCOSX approximation introduces deviations, which are about one order of magnitude larger. Bond distances deviate by about 0.1 pm from their parent values, whereas bond angles differ typically by less than 0.2 degrees. The largest error in bond lengths is

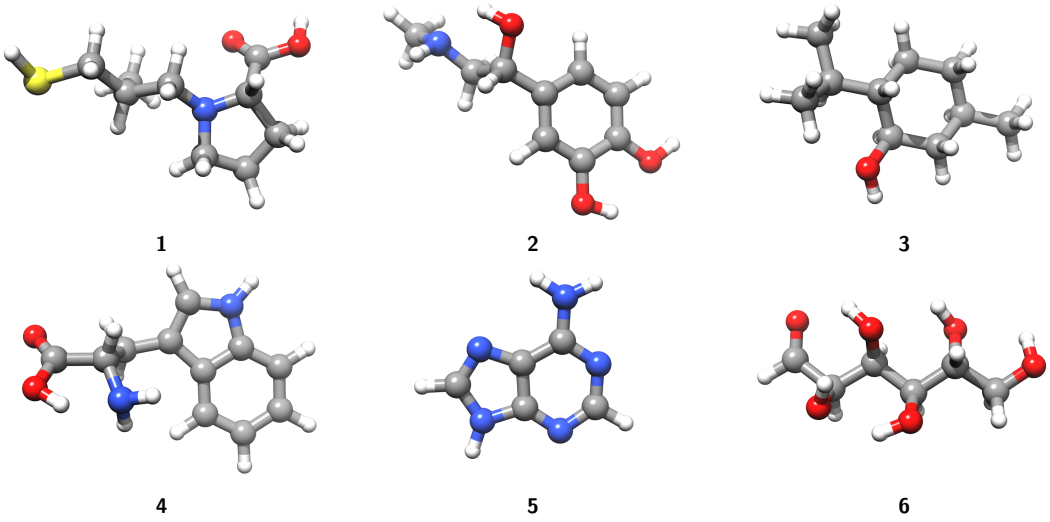

Figure 5.2.: Systems used for testing the accuracy of geometry optimizations (**1**=Captopril, **2**=Epinephrine, **3**=Menthol, **4**=Tryptophane, **5**=Adenine, **6**=D-Glucose).

up to 0.4 pm, the corresponding error in bond angles is 0.7 degrees. The mean absolute deviations for the RIJCOSX-MP2 method are in the same range observed previously for the RIJCOSX-HF method. [39] The deviations of the final total energies from the canonical values remain below 2 kcal/mol, and are significantly smaller when compared to the RI-MP2 method (<1 kcal/mol).

Table 5.4.: Statistical analysis of errors in the optimized geometries of molecules **1**-**6** from the RI, RIJ-DX and RIJCOSX approximations compared to the parent RMP2 method. Errors are given relative to the parent MP2 method. All calculations were done with the TZVP basis set (distances in pm, angles in degrees).[a]

		$\Delta^{\text{mean}}_{\text{distances}}$	$\Delta^{\text{mean absolute}}_{\text{distances}}$	$\Delta^{\text{max}}_{\text{distances}}$	$\Delta^{\text{mean}}_{\text{angles}}$	$\Delta^{\text{mean absolute}}_{\text{angles}}$	$\Delta^{\text{max}}_{\text{angles}}$
1	RI-MP2	−0.011	0.011	0.020	−0.001	0.003	0.020
	RIJ-DX-MP2	−0.013	0.013	0.020	−0.001	0.004	0.020
	RIJCOSX-MP2	−0.001	0.102	0.400	−0.005	0.145	0.400
2	RI-MP2	−0.007	0.007	0.020	0.001	0.002	0.020
	RIJ-DX-MP2	−0.008	0.008	0.030	0.000	0.002	0.010
	RIJCOSX-MP2	−0.031	0.075	0.170	−0.014	0.139	0.380
3	RI-MP2	−0.012	0.012	0.020	0.000	0.001	0.010
	RIJ-DX-MP2	−0.013	0.013	0.030	0.000	0.002	0.010
	RIJCOSX-MP2	−0.036	0.077	0.240	−0.001	0.133	0.400
4	RI-MP2	−0.004	0.004	0.020	0.000	0.002	0.010
	RIJ-DX-MP2	−0.005	0.006	0.020	0.000	0.005	0.010
	RIJCOSX-MP2	−0.001	0.075	0.220	0.001	0.164	0.730
5	RI-MP2	−0.004	0.004	0.020	0.003	0.004	0.020
	RIJ-DX-MP2	−0.004	0.004	0.020	0.003	0.004	0.020
	RIJCOSX-MP2	−0.031	0.044	0.130	0.015	0.073	0.280

[a] N(distances) for molecules 1-6=30.26.31.38.16.23, N(angles) for molecules 1-6=56.42.61.46.24.28. Errors in final total energies are for RI=0.7.0.3.0.9.0.3.0.1.0.2 kcal/mol, RIJ-DX=0.5.0.2.0.7.0.1.−0.1.0.1 kcal/mol, RIJ-COSX=0.6.0.9.1.6.0.8.0.4.0.4 kcal/mol.

Continued.

		$\Delta^{\text{mean}}_{\text{distances}}$	$\Delta^{\text{mean absolute}}_{\text{distances}}$	$\Delta^{\text{max}}_{\text{distances}}$	$\Delta^{\text{mean}}_{\text{angles}}$	$\Delta^{\text{mean absolute}}_{\text{angles}}$	$\Delta^{\text{max}}_{\text{angles}}$
6	RI-MP2	−0.006	0.006	0.020	0.000	0.002	0.010
	RIJ-DX-MP2	−0.007	0.007	0.020	0.000	0.002	0.010
	RIJCOSX-MP2	−0.011	0.086	0.310	0.004	0.106	0.360

Efficiency of the RIJCOSX-MP2 Method

In Table 5.5 and Table 5.6 the efficiency of the RIJ-DX-MP2 and RIJCOSX-MP2 methods is demonstrated compared to the original MP2 as well as to the already very efficient RI-MP2 method.
The speedups listed in Table 5.5 show the efficiency of the RI, RIJ-DX and RIJCOSX approximations for 13 medium sized molecules for three different basis sets with up to ∼620 basis functions. The RIJ-DX approximation shows speedups up to a factor of 2.4 in the gradient calculations, but represents no major improvement over the original RI approximation. In general, the speedup becomes noticeable for ∼200 basis functions. The speedups tend to become more remarkable with larger basis sets, but the enhancements are almost not observable.
The RIJCOSX approximation shows only minor speedups for the smallest employed basis set SV(P). For the smallest molecules in our test suite the RIJCOSX approximation even slows down the MP2 gradient calculations. For the next larger basis set TZVP, the RIJCOSX approximation accelerates the calculations by a factor of ∼3 for molecules with around 300 basis functions. The speedup increases noticeably with basis set and system size. In the case of the menthol molecule a factor of ∼7.5 in computation time is gained, if the RIJCOSX approximation is applied. For comparison, the speedup reduces to ∼4 when RI-MP2 serves as reference.
The deviation of the gradient norm shows a deviation for RIJCOSX-MP2, which is naturally somewhat larger than for the RIJ-DX approximation, but as has been shown in the previous subsection, this has almost no influence on the resulting structures.

Table 5.5.: Efficiency of the RIJ-DX and RIJCOSX algorithms for MP2 calculations on medium sized molecules with different basis sets. The speedup refers to the ratio of total wall clock times required to finish one gradient calculation. The speedups are given relative to the original MP2 method without any approximations. The deviation of the gradient norm w.r.t. the MP2 reference is denoted $\Delta_{\text{RIJ}-\text{DX}}$ and Δ_{RIJCOSX} in [E_h/bohr].

molecule	N_{Atoms}	Basis	N_{Basis}	$\Delta_{\text{RIJ}-\text{DX}}$	Δ_{RIJCOSX}	SpeedUp		
						RI	RIJ-DX	RIJCOSX
adenine	15	SV(P)	150	−0.0001	−0.0009	1.3	1.3	1.3
		TZVP	220	−0.0001	−0.0004	1.4	1.4	2.3
		TZVPP	380	0.0001	−0.0009	1.3	1.3	4.1
cysteine	14	SV(P)	116	−0.0002	−0.0010	1.2	1.2	0.8
		TZVP	178	−0.0002	−0.0013	1.2	1.4	1.7
		TZVPP	318	0.0000	−0.0011	1.4	1.4	3.7
cytosine	13	SV(P)	122	−0.0001	−0.0017	1.2	1.2	1.1
		TZVP	182	−0.0002	−0.0015	1.2	1.4	1.8
		TZVPP	318	0.0001	−0.0016	1.2	1.3	3.6

Continued.

molecule	N_{Atoms}	Basis	N_{Basis}	Δ_{RIJ-DX}	$\Delta_{RIJCOSX}$	SpeedUp		
						RI	RIJ-DX	RIJCOSX
D-glucose	24	SV(P)	192	0.0004	−0.0001	1.5	1.5	1.2
		TZVP	300	0.0004	0.0002	1.6	1.8	2.8
		TZVPP	540	−0.0002	−0.0002	1.6	2.0	5.6
epinephrine	26	SV(P)	208	0.0000	0.0000	1.4	1.4	1.3
		TZVP	325	0.0002	0.0014	1.6	1.9	3.0
		TZVPP	585	0.0000	0.0011	1.7	1.9	5.6
ferrocene	21	SV(P)	184	−0.0002	−0.0008	1.2	1.3	1.6
		TZVP	283	−0.0005	−0.0012	1.3	1.3	3.0
		TZVPP	490	0.0002	−0.0009	1.3	1.7	5.3
glycine	10	SV(P)	80	−0.0002	−0.0007	1.2	1.0	0.7
		TZVP	125	−0.0003	−0.0002	1.2	1.1	1.1
		TZVPP	225	0.0000	0.0000	1.3	1.2	2.8
guanine	16	SV(P)	164	0.0000	−0.0015	1.4	1.3	1.5
		TZVP	239	0.0000	−0.0017	1.4	1.5	2.5
		TZVPP	411	0.0001	−0.0014	1.3	1.4	4.4
histidine	20	SV(P)	172	−0.0003	−0.0003	1.4	1.3	1.2
		TZVP	263	−0.0003	−0.0002	1.5	1.7	2.6
		TZVPP	467	0.0000	0.0001	1.6	1.8	5.1
menthol	31	SV(P)	194	0.0002	0.0003	1.3	1.6	1.0
		TZVP	329	0.0003	0.0000	1.6	1.8	2.9
		TZVPP	621	0.0002	−0.0001	1.9	2.4	7.5
nitroglycerine	17	SV(P)	178	0.0001	−0.0005	1.4	1.4	1.3
		TZVP	258	0.0001	−0.0002	1.5	1.7	2.9
		TZVPP	442	0.0001	−0.0004	1.5	1.7	5.2
thymine	15	SV(P)	138	0.0000	−0.0008	1.2	1.1	1.0
		TZVP	207	0.0000	−0.0011	1.4	1.4	2.0
		TZVPP	363	0.0001	−0.0012	1.4	1.5	4.3
tyrosine	24	SV(P)	204	−0.0003	−0.0006	1.6	1.6	1.3
		TZVP	313	−0.0002	−0.0006	1.5	1.7	3.0
		TZVPP	557	0.0000	−0.0005	1.6	1.9	5.8

In Table 5.6 the speedup of the RIJ-DX and RIJCOSX approximations to the MP2 gradient is related to the very efficient RI-MP2 gradient. Therefore, we studied 24 molecules in the range of 10–86 atoms with ∼100-1900 basis functions. The speedup obtained with the RIJ-DX-MP2 method compared to RI-MP2 is about a factor of ∼1.2. The inclusion of the SCF wall clock time has almost no consequence on the overall speedup.

For the smallest basis set in our test set SV(P) the speedup for the RIJCOSX approximation in the MP2 module is almost negligible, and the inclusion of the SCF wall clock times has no influence on the entire performance. The speedup of the RIJCOSX approximation becomes more observable for the triple-ζ basis set TZVP and for molecules with $\geq$300 basis functions (∼1.5–2.3).

For the TZVPP basis set the speedup varies from a factor of 2 to 3 for the MP2 module, and even reaches a factor of 4.2 for the morphin molecule when the SCF calculation is taken into account. Excellent speedups

are obtained with the more extended QZVP basis set. Speedups of a factor ∼4.5–6 are obtained for the MP2 module and even a factor of 9.2 is achieved for the NiTrenNCS2 molecule when the SCF wall clock time is included in the comparison. This behaviour has to be expected, due to the favourable scaling of the RIJCOSX approximation with respect to higher angular momenta.

In order to verify the quality of the calculated gradients, we also listed the errors in the norm of the MP2 gradient in Table 5.6.

Table 5.6.: Efficiency of the RIJ-DX and RIJCOSX algorithms for RI-MP2 calculations on medium sized molecules with different basis sets. The speedup refers to the ratio of wall clock times of either the RI-MP2 module (RI-MP2) or the total wall clock time (total) required to finish one gradient calculation. The deviation of the gradient norm w.r.t. the RI-MP2 reference is denoted $\Delta_{\mathrm{RIJ-DX}}$ and $\Delta_{\mathrm{RIJCOSX}}$ in $[\mathrm{E_h/bohr}]$.

molecule	N_{Atoms}	Basis	N_{Basis}	Δ_{RIJ-DX}	$\Delta_{RIJCOSX}$	SpeedUp (RIJ-DX)		SpeedUp (RIJCOSX)	
						RI-MP2	total	RI-MP2	total
adenine	15	SV(P)	150	0.0000	−0.0009	1.0	1.0	1.0	1.0
		TZVP	220	0.0000	−0.0004	1.1	1.0	1.5	1.7
		TZVPP	380	0.0001	−0.0009	1.0	1.0	2.9	3.1
		QZVP	720	0.0001	−0.0010	1.1	1.1	5.9	6.3
beclometahsone	57	SV(P)	454	0.0004	0.0007	1.2	1.2	1.1	1.3
		TZVP	709	0.0003	0.0004	1.3	1.4	2.0	2.5
		TZVPP	1277	0.0000	0.0001	1.2	1.3	2.4	3.3
captopril	30	SV(P)	220	0.0002	0.0008	1.1	1.1	0.8	0.9
		TZVP	352	0.0001	0.0005	1.3	1.3	1.6	2.0
		TZVPP	644	0.0002	0.0006	1.2	1.2	2.9	3.4
		QZVP	1264	0.0002	0.0005	1.4	1.4	4.9	6.2
cholesterole	74	SV(P)	484	0.0004	0.0001	1.1	1.1	1.0	1.1
		TZVP	808	0.0003	−0.0004	1.4	1.4	1.7	2.2
		TZVPP	1512	0.0002	−0.0001	1.4	1.4	2.1	2.9
CO-heme	86	SV(P)	782	0.0000	−0.0001	1.2	1.2	1.1	1.3
		TZVP	1180	0.0000	−0.0002	1.2	1.3	1.6	2.2
cysteine	14	SV(P)	116	−0.0002	−0.0009	1.0	1.0	0.6	0.7
		TZVP	178	−0.0002	−0.0013	1.2	1.2	1.2	1.3
		TZVPP	318	0.0000	−0.0011	1.0	1.0	2.6	2.7
		QZVP	622	0.0000	−0.0010	1.2	1.2	5.1	5.5
cytosine	13	SV(P)	122	−0.0001	−0.0016	1.0	1.0	0.8	0.9
		TZVP	182	−0.0002	−0.0014	1.1	1.2	1.4	1.5
		TZVPP	318	0.0001	−0.0016	1.0	1.0	2.7	2.9
		QZVP	606	0.0001	−0.0016	1.1	1.1	5.6	6.0
D-glucose	24	SV(P)	192	0.0003	−0.0002	1.0	1.0	0.8	0.8
		TZVP	300	0.0003	0.0001	1.1	1.1	1.4	1.7
		TZVPP	540	−0.0002	−0.0002	1.3	1.3	3.1	3.6
		QZVP	1044	0.0000	−0.0002	1.4	1.3	4.5	5.5
dibenzo-crown-18-6	50	SV(P)	412	−0.0001	0.0000	1.2	1.2	1.0	1.1
		TZVP	638	0.0003	0.0001	1.3	1.3	1.6	2.0
		TZVPP	1142	0.0002	0.0000	1.3	1.3	2.1	2.7

Continued.

molecule	N_{Atoms}	Basis	N_{Basis}	Δ_{RIJ-DX}	$\Delta_{RIJCOSX}$	SpeedUp (RIJ-DX)		SpeedUp (RIJCOSX)	
						RI-MP2	total	RI-MP2	total
epinephrine	26	SV(P)	208	−0.0001	0.0000	1.1	1.0	0.9	0.9
		TZVP	325	0.0002	0.0014	1.2	1.2	1.5	1.8
		TZVPP	585	0.0000	0.0011	1.1	1.1	2.7	3.4
		QZVP	1131	0.0000	0.0008	1.4	1.4	5.2	6.7
ferrocene	21	SV(P)	184	−0.0001	−0.0007	1.1	1.1	1.4	1.3
		TZVP	283	−0.0005	−0.0012	1.1	1.0	2.0	2.4
		TZVPP	490	0.0003	−0.0009	1.0	1.3	3.5	4.0
		QZVP	954	0.0003	−0.0020	1.0	1.0	4.5	5.7
flutamide	30	SV(P)	288	0.0004	0.0016	1.1	1.1	1.0	1.1
		TZVP	427	0.0001	0.0014	1.2	1.2	1.6	2.0
		TZVPP	743	0.0000	0.0013	1.1	1.1	2.5	3.0
		QZVP	1413	0.0000	0.0013	1.4	1.4	4.5	5.8
glycine	10	SV(P)	80	−0.0002	−0.0007	0.8	0.9	0.5	0.6
		TZVP	125	−0.0002	−0.0002	1.0	0.9	0.9	0.9
		TZVPP	225	0.0000	0.0000	1.0	0.9	2.2	2.2
		QZVP	435	0.0000	−0.0003	1.1	1.0	4.6	4.7
guanine	16	SV(P)	164	0.0001	−0.0013	0.9	0.9	1.0	1.1
		TZVP	239	0.0001	−0.0015	1.1	1.1	1.6	1.8
		TZVPP	411	0.0001	−0.0013	1.0	1.0	3.1	3.3
		QZVP	777	0.0001	−0.0017	1.2	1.2	5.9	6.6
histidine	20	SV(P)	172	−0.0002	−0.0002	0.9	0.9	0.8	0.9
		TZVP	263	−0.0002	−0.0001	1.1	1.1	1.4	1.7
		TZVPP	467	0.0001	0.0001	1.2	1.1	2.8	3.2
		QZVP	897	0.0000	0.0001	1.3	1.2	5.3	6.2
menthol	31	SV(P)	194	0.0001	0.0002	1.2	1.2	0.6	0.7
		TZVP	329	0.0003	0.0000	1.3	1.1	1.5	1.8
		TZVPP	621	0.0001	−0.0002	1.3	1.2	3.2	3.9
		QZVP	1227	0.0000	0.0001	1.4	1.4	5.3	7.3
morphin	40	SV(P)	332	0.0001	0.0002	1.2	1.2	1.3	1.4
		TZVP	513	0.0001	0.0005	1.3	1.2	2.3	2.9
		TZVPP	917	0.0001	0.0008	1.3	1.3	3.1	4.2
		QZVP	1767	0.0001	0.0004	1.3	1.3	5.1	7.0
NiTrenNCS2	35	SV(P)	292	0.0000	0.0006	1.1	1.1	1.3	1.5
		TZVP	451	0.0001	0.0005	1.1	1.4	1.7	2.6
		TZVPP	794	0.0000	0.0002	1.3	1.3	2.9	4.0
		QZVP	1562	0.0000	0.0005	1.4	1.4	5.1	9.2
nitroglycerine	17	SV(P)	178	0.0001	−0.0005	1.1	1.0	0.9	0.9
		TZVP	258	0.0001	−0.0002	1.1	1.1	1.7	1.9
		TZVPP	442	0.0001	−0.0004	1.1	1.1	3.0	3.4
		QZVP	834	0.0001	−0.0003	1.3	1.2	4.8	5.6

Continued.

molecule	N_{Atoms}	Basis	N_{Basis}	Δ_{RIJ-DX}	$\Delta_{RIJCOSX}$	SpeedUp (RIJ-DX)		SpeedUp (RIJCOSX)	
						RI-MP2	total	RI-MP2	total
penicilin	42	SV(P)	376	0.0000	0.0007	1.1	1.1	1.1	1.2
		TZVP	567	0.0001	−0.0002	1.2	1.2	1.6	1.9
		TZVPP	999	0.0001	0.0010	1.3	1.3	2.3	2.9
		QZVP	1921	0.0001	0.0007	1.5	1.5	3.6	4.7
tetracycline	56	SV(P)	496	0.0001	0.0019	1.2	1.2	1.2	1.4
		TZVP	752	0.0001	0.0022	1.2	1.3	1.8	2.2
		TZVPP	1328	0.0000	0.0019	1.2	1.3	2.2	2.9
thymine	15	SV(P)	138	0.0000	−0.0007	0.9	0.9	0.8	0.8
		TZVP	207	0.0001	−0.0011	1.0	1.0	1.3	1.5
		TZVPP	363	0.0001	−0.0012	1.1	1.1	2.2	2.9
		QZVP	693	0.0001	−0.0014	1.1	1.1	5.3	5.8
tryptophane	27	SV(P)	234	−0.0002	0.0000	1.1	1.1	1.0	1.1
		TZVP	357	−0.0002	−0.0001	1.1	1.1	1.6	2.0
		TZVPP	633	0.0001	0.0001	1.2	1.2	2.9	3.6
		QZVP	1215	0.0001	0.0000	1.4	1.4	5.2	6.7
tyrosine	24	SV(P)	204	−0.0003	−0.0006	1.0	1.0	0.8	0.9
		TZVP	313	−0.0002	−0.0006	1.1	1.1	1.7	1.9
		TZVPP	557	0.0000	−0.0004	1.1	1.1	3.1	3.6
		QZVP	1071	0.0000	−0.0003	1.3	1.3	4.8	5.9

In Table 5.7 the speedups introduced by the RIJ-DX and RIJCOSX approximations in double-hybrid functional calculations for four representative molecules are listed. The speedups with respect to the conventional RI treatment are almost identical to the pure MP2 case. Thus, the speedups of the investigated approximations are comparably efficient for double-hybrid functional calculations.

Table 5.7.: Efficiency of the RIJ-DX and RIJCOSX algorithms for RI-B2PLYP calculations on medium sized molecules with different basis sets. The speedup refers to the ratio of wall clock times of either the RI-MP2 module (RI-MP2) or the total wall clock time (total) required to finish one gradient calculation. The deviation of the gradient norm w.r.t. the RI-B2PLYP reference is denoted Δ_{RIJ-DX} and $\Delta_{RIJCOSX}$ in [E_h/bohr].

molecule	N_{Atoms}	Basis	N_{Basis}	Δ_{RIJ-DX}	$\Delta_{RIJCOSX}$	SpeedUp (RIJ-DX)		SpeedUp (RIJCOSX)	
						RI-MP2	total	RI-MP2	total
beclometahsone	57	SV(P)	454	0.0006	0.0006	1.2	1.2	1.5	1.6
		TZVP	709	0.0004	0.0002	1.2	1.3	1.9	2.3
		TZVPP	1277	0.0000	0.0000	1.3	1.3	2.3	2.8
dibenzo-crown-18-6	50	SV(P)	412	−0.0001	0.0000	1.2	1.2	1.4	1.3
		TZVP	638	0.0003	0.0002	1.3	1.3	1.7	1.9
		TZVPP	1142	0.0002	0.0000	1.3	1.3	2.1	2.4
morphin	40	SV(P)	332	0.0003	0.0003	1.2	1.2	1.8	1.7
		TZVP	513	0.0001	0.0003	1.3	1.3	2.7	2.9
		TZVPP	917	0.0001	0.0004	1.3	1.2	3.4	3.9
		QZVP	1767	0.0001	0.0002	1.5	1.4	5.4	6.3

Continued.

molecule	N_{Atoms}	Basis	N_{Basis}	Δ_{RIJ-DX}	$\Delta_{RIJCOSX}$	SpeedUp (RIJ-DX)		SpeedUp (RIJCOSX)	
						RI-MP2	total	RI-MP2	total
tetracycline	56	SV(P)	496	0.0002	0.0011	1.2	1.2	1.5	1.5
		TZVP	752	0.0002	0.0011	1.2	1.2	1.7	2.0
		TZVPP	1328	0.0000	0.0009	1.3	1.3	2.0	2.4

Timing Analysis of the RIJCOSX-MP2 Method

A detailed analysis of the timings for the different parts of the MP2 gradient is presented in this subsection. For the comparison of the original MP2 with the RIJCOSX-MP2 method, the menthol molecule in a TZVPP basis serves as an example. The calculation of one MP2 gradient takes about ∼18 hours. The time spent in the the MP2 module is ∼14 hours (80% of the total wall clock time).

A detailed analysis of the different components of the MP2 gradient is given in Table 5.8. The integral transformation in the original MP2 method corresponds to a 3/4 transformation of AO integrals to the MO basis, and is besides the calculation of separable and non-separable gradient contributions the most time consuming step. The evaluation of the internal part of the unrelaxed density matrix D(internal) is more expensive than in the RI-MP2 variants, due to the generation of the required integrals containing one Frozen-Core index on the fly. The formation of the 3-external part of the Lagrangian L(3-ext), eq. 2.215 is also more costly in terms of computation time, due to the large AO↔MO transformations. The calculation of the non-separable and separable gradient, is done simultaneously in the original MP2 code and the time determining step is the calculation of the derivative of the two-electron repulsion integrals.

The situation changes drastically when going to the RI-MP2 variants. The time required for the integral transformation is negligible, since in RI-MP2 methods only 3-index integrals are needed, which can be calculated very efficiently. The formation of the exchange integrals becomes somewhat more expensive, due to the larger matrix multiplications, but the effect on the overall timing is insignificant. The evaluation of D(internal) is more effcient, due to prestored Frozen-Core integrals and the 3-external part of the Lagrangian only requires the transformation of one virtual index. The calculation of the separable gradient is done analogously to the parent MP2 method, but the non-separable part is very efficiently calculated employing 3- and 2-index derivative integrals, eq. 2.228.

The speedup achieved with the RIJ-DX approximation results from the more efficient calculation of the response-type operators, and as a consequence, the accelerated solution of the z-vector equations. The separable gradient profits from the application of the RI approximation to the Coulomb contribution, whereas the non-separable gradient saves computation time through storage of the 3-index 2-particle density and the use of large BLAS level 2 operations.

The RIJCOSX approximation introduces a highly efficient treatment of the exchange-type contributions to the MP2 gradient. The calculation of the response-type operators, eq. 2.217, and the solution of the z-vector equations is highly dominated by the formation of the exchange-type contributions. The employment of the RIJCOSX approximation speeds the calculation of these contributions up by a factor of ∼7–8. A speedup of ∼2 is gained by exploiting the efficient calculation of the basis function derivatives on the grid, as ingredient to the separable gradient.

Table 5.8.: Timings in [s] of the individual contributions to the MP2 gradient depending on the employed approximation obtained for the menthol molecule (31 atoms) in a TZVPP basis set.

Gradient Components	MP2	RI-MP2	RIJ-DX-MP2	RIJCOSX-MP2
Integral Transformation	18061	133	129	136
K^{ij}(a,b)	65	145	144	148
T^{ij}(a,b)	27	17	16	17
D(virtual)	60	61	60	60
D(internal)	1537	124	117	122
W(virtual)	120	121	119	121
W(internal)	191	217	194	201
L(3-ext)	1510	260	250	257
L(3-int)	16	6	6	6
R(D)	1170	1209	949	146
R(z)	1209	1213	969	148
z-vector solution	5410	5497	4062	773
Separable Gradient (S)		10918	8937	3733
Non-separable Gradient (NS)		582	325	327
Gradient (S + NS)	20290	11500	9262	4060
Total Time	49689	20732	16533	6460

Parallelization

The separable COSX-MP2 gradient, eq. 2.227, is parallelized over batches of grid points. A reasonable load balancing is achieved by distributing the batches of grid points over the processors such, that all processors work on all parts of the molecular system to nearly the same extent. A single gather operation is then performed at the end of the COSX integration loop, in order to keep the communication overhead negligible. The same strategy has been followed for the parallel exchange treatment in the SCF module. In Fig. 5.3 the efficiency of the parallel implementation is demonstrated for a medium sized molecule (dibenzo-crown-18-6/QZVP, 50 atoms, 2202 basis functions). The scaling behaviour is excellent for up to 16 processors, although the example is not really large. However, the evaluation of the basis function derivatives on the grid requires the large Lebedev-302 angular grid with an integration accuracy of 4.34, which yields about 185000 grid points that are divided among the processors. Some of the plotted speedups in Fig. 5.3 seem to be better than the linear speedup, which is mainly due to the inaccuracy in the time measurement, since no statistics have been performed.

The parallelization of the entire MP2 gradient module, presented in Fig. 5.4, is less efficient, than that for the separable COSX-MP2 gradient contribution. However, up to at least 10 processors reasonable speedups are achieved. The reason for the apparent stagnation of the speedup with 12 processors, is the poor scaling of the 3-external part to the MP2 Lagrangian and of the separable gradient calculated in the RI approximation with the number of processors employed. The speedup of the evaluation of the 3-external Lagrangian contribution achieves a factor 4.4 speedup for 10 processors and decreases to a factor of 3.8 for 12 and 16 processors. A similar situation is found for the separable gradient calculated within the RI approximation. Although not rate determining, the speedup amounts to only a factor of $\sim$3. The scaling of the internal part of the energy weighted density matrix is also reduced to a factor of 10 for 16 processors. All three contributions together determine 30% of the total wall clock time needed

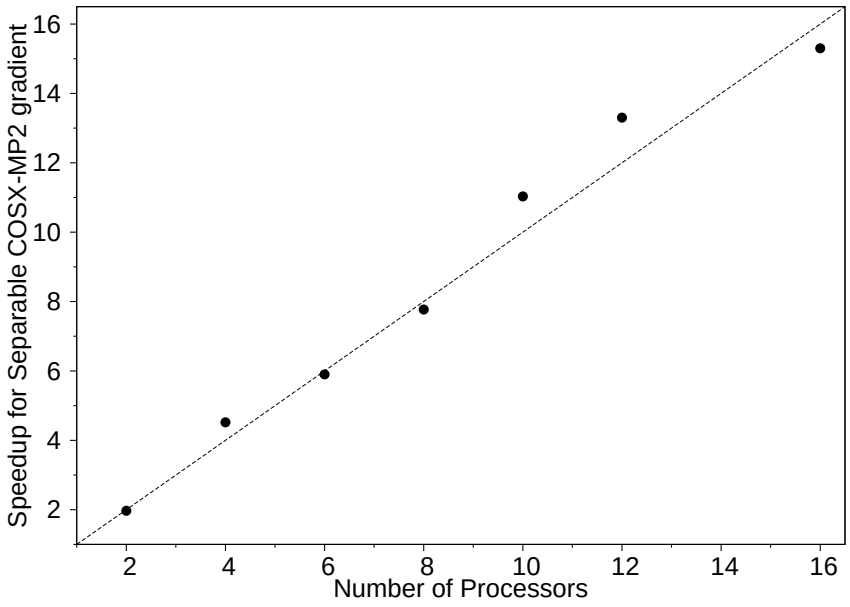

Figure 5.3.: Parallelization efficiency of the COSX gradient algorithm with Dibenzo-crown-18-6/QZVP as example. Plotted is the wall clock time required for formation of the entire separable COSX-MP2 gradient relative to the time taken for the same operation by a single process.

for the calculation on 16 processors. Furthermore, some smaller parts of the parallel MP2 gradient do not scale ideally with the number of used processors. Taken together, these factors are responsible for the worsened scaling starting with 10–12 employed processors.

5.2.4. Application

In order to demonstrate the high efficiency of the RIJCOSX-MP2 approach geometry optimizations on DNA base tetramers are presented. The nomenclature is shown in Fig. 5.5 and the timings for the structure optimizations with a TZVPP basis set and tight convergence criteria are listed in Table 5.9. The time required for one optimization step for a closed-shell system with ∼1500 basis functions and ∼2000 and ∼3500 auxiliary basis functions, respectively, takes about 10 hours on 8 CPUs. These timings impressively confirm the outstanding efficiency of the RIJCOSX-MP2 method.

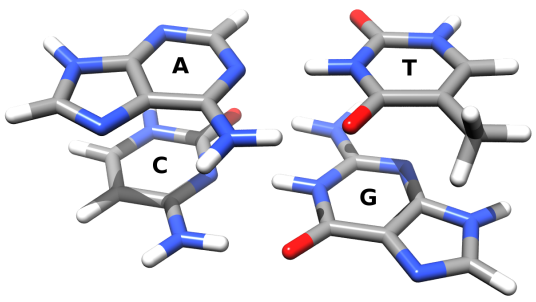

Figure 5.5.: Stacked DNA base pairs (GCTA), (G) Guanine, (C) Cytosine, (T) Thymine, (A) Adenine.

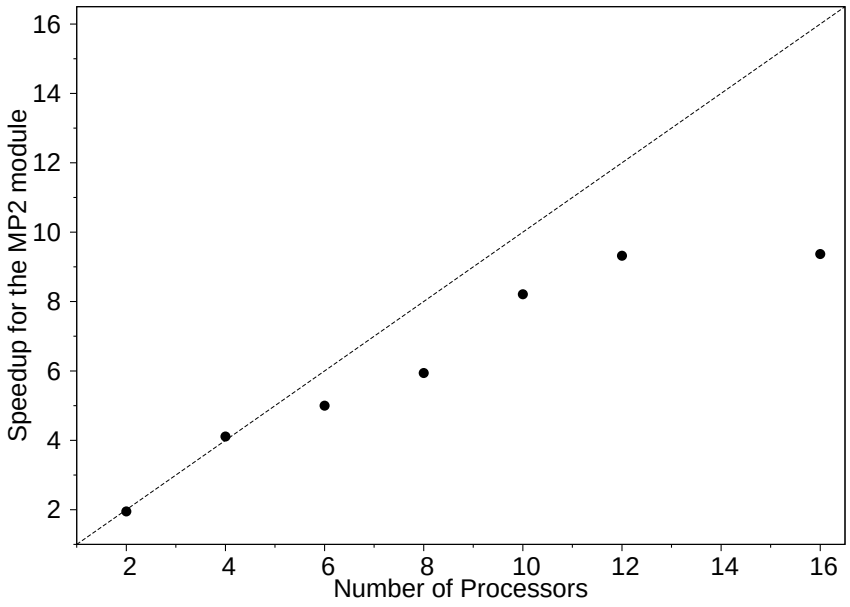

Figure 5.4.: Parallelization efficiency of the MP2 gradient algorithm with Dibenzo-crown-18-6/QZVP as example. Plotted is the wall clock time required for formation of the entire COSX-MP2 gradient relative to the time taken for the same operation by a single process.

Table 5.9.: Total wall clock times for gradient calculations on 8 CPUs of DNA base pairs with the RIJCOSX-MP2/TZVPP method.

Molecule	N_{Atoms}	N_{Basis}	$N_{AuxBasisJ}$	$N_{AuxBasisC}$	N_{Cycles}	Time	
						1 Opt Step	total
GCTA	59	1472	2093	3518	20	9h 30m	7d 21h 12m
GCCG	58	1458	2082	3488	39	9h 42m	15d 21h 16m
ATTA	60	1486	2104	3548	21	11h 10m	9d 19h 05m

5.2.5. Discussion

In the present section, the applicability of the semi-numeric exchange treatment via the COSX approximation to the exchange-type contributions of the MP2 gradient has been presented. The entire RIJCOSX-MP2 gradient algorithm fulfills all important requirements necessitated by a reliable approximate method. The optimized structures show only negligible deviations from the MP2 structures. The RIJCOSX-MP2 gradient is efficient with observed speedups in wall-clock times of ∼7–7.5 for the TZVPP basis set compared to conventional MP2 regarding one gradient calculation (including the SCF time). RIJCOSX-MP2 versus RI-MP2 yields also speedups of ∼5–9 for one entire energy and gradient calculation with the QZVP basis. The speedups obtained in pure MP2 calculations are immediately carried over to the case of double-hybrid density functional theory.

The RIJCOSX-MP2 method is generally applicable and does neither depend on the molecular system nor on the chosen basis set. The program is parallelized and scales reasonably well with the number of used processors but some more work is required before efficient large scale parallelization on many processors is achieved. Nevertheless, an application of the RIJCOSX-MP2 method to the geometry optimizations of DNA base tetramers with ∼1500 basis functions could be presented. Overall, we believe that the present development adds to the applicability of MP2-type methods such as MP2, SCS-MP2 or double-hybrid density functional theory in large-scale chemical applications.

5.3. Correlated *ab initio* Spin Densities for Larger Molecules: The Orbital-Optimized Spin-Component-Scaled MP2 Method

5.3.1. Introduction

The calculation of the hyperfine structure in electron paramagnetic resonance (EPR) spectra and its high resolution variants such as electron-nuclear double resonance (ENDOR) or hyperfine sublevel correlation spectroscopy (HYSCORE) has been recognized to be a difficult field for theoretical chemistry. Unlike the electron density, that is positive everywhere in space, the spin density is a strongly structured function that can be either positive or negative. This has been realized already by the pioneers of EPR spectroscopy that have referred to the phenomenon as 'spin polarization'. Classical examples are the aromatic protons of benzylic radicals or the proton hyperfine couplings (hfcs) of CH_3 that are known to be negative. McConnel has given an intuitively appealing valence bond interpretation of the spin polarization phenomenon. [140] However, it is difficult to implement valence bond theory rigorously in terms of *ab initio* wave functions. In Hartree-Fock (HF) theory, the spin polarization arises in a rather natural way in the unrestricted HF variant (UHF). However, once calculations with large basis sets became feasible it quickly became clear that the UHF prediction of hyperfine couplings is very poor. Typically, spin polarization contributions are too large by about a factor of three. This has been analyzed in some detail by Hameka [141] and Chipman. [142] Thus, the calculation of accurate first principles spin densities requires the incorporation of a substantial amount of dynamic correlation. The simplest correlation method, second-order Møller-Plesset perturbation theory (MP2), is known to be insufficient and often provides somewhat erratic results when applied to open-shell systems. Provided that basis sets with sufficient flexibility in the core region and adequate polarization functions to cover dynamic correlation are used (e.g. Ref. [143]) the quadratic configuration interaction with single and double excitations (QCISD) or the more rigorous coupled cluster theory with single- and double excitations (CCSD) are known to provide essentially satisfactory results. [144–150] However, these methods involve iterative steps with $\mathcal{O}(N^6)$ scaling with respect to system size. Thus, their routine application to larger molecules is presently not possible.

Density functional theory (DFT), often provides much better results than UHF theory [143,151] and there are many successful applications of DFT to the calculation of EPR hyperfine coupling constants (hfccs). Among the multitude of functionals that could be used, the 'gold standard' B3LYP functional provides good results for organic radicals. [147] For transition metal nuclei all functionals have difficulties since they underestimate the core level spin polarization. [152, 153] This can to some extent be compensated by mixing more HF exchange into hybrid density functionals. This is, however, not a satisfactory solution to the problem since the optimum mixing depends strongly on the investigated system. In a previous study it was found that among the standard functionals, the meta-generalized gradient approximation

based hybrid functional TPSSh [154] provides the best results for transition metal complexes. [155] Other problem cases for DFT include strongly delocalized radicals where the self-interaction error strongly deteriorates the results. [156, 157]

In a recent study, we have investigated the behavior of the new class of double-hybrid density functionals (DHDFs) that have shown in many fields their high potential. [1] In general, excellent results have been obtained for hyperfine couplings with the B2PLYP functional [155], provided that the calculations are based on the relaxed density approach [155], that arises naturally in analytic gradient theory of correlated wave function theories. [12, 49, 158, 159] However, even B2PLYP was found to suffer to some extent from the unstable MP2 component despite the fact that it was found to be greatly superior to MP2 itself.

Despite all recent progress, we feel that it would be desirable to have an affordable wave function based *ab initio* method available that reliably provides results of essentially QCISD or CCSD quality. Most recently, it was shown that the results of MP2 for open-shell molecules can be greatly improved in accuracy and stability if the orbitals are optimized alongside with the double excitation amplitudes. [160, 161] This orbital optimization is based on the well-known Hylleraas functional [24] that has been shown by Saebøand Pulay to lead to an orbital-invariant formulation of MP2 theory. [26] The method has been dubbed OO-MP2 and was further improved by combining it with the concepts of spin-component scaling (SCS-MP2) [102] thus leading to OO-SCS-MP2. The variant with spin-opposite scaling MP2 (SOS-MP2) has been explored by Head-Gordon and co-workers. [104] The computational effort of OO-SCS-MP2 is best characterized as an iterative $\mathcal{O}(N^5)$ process that is substantially cheaper than QCISD or CCSD but also considerably more expensive than MP2. However, if the OO-SCS-MP2 method is combined with the resolution of the identity (RI) approximation [22], it is applicable in reasonable computation times to at least medium sized molecules of contemporary chemical interest that are far too large for QCISD and CCSD to be applicable.

In this section, the performance of the OO-(SCS-)MP2 method for the calculation of hfccs has been investigated. Following a brief description of the theory, the OO-MP2 and OO-SCS-MP2 methods are benchmarked against the results of CCSD and CCSD(T) calculations. The applicability to larger molecules is demonstrated in the final part of the section.

5.3.2. Theory

The theory of the orbital optimized MP2 method has been reviewed in detail in Section 2.9.3. The basic idea is to minimize an extended Hylleraas functional with regard to the MO coefficients as well as to the MP2 double excitation amplitudes. Due to the variational nature of the orbital optimized MP2 Ansatz, the first derivative of the OO-MP2 energy w.r.t. an arbitrary perturbation λ, corresponds to the expectation value of h_λ, if the OO-MP2 equations have converged, eq. 5.16.

$$\frac{\partial E_{OO}}{\partial \lambda} = \sum_{pq} D_{pq} h^{\lambda}_{pq} \tag{5.16}$$

In a spin-unrestricted scheme, the total electron density and the spin density matrices are obtained as the sum and difference of the spin-up and spin-down densities respectively. Thus, the isotropic (c) and

dipolar (d) parts of the hyperfine coupling tensor are calculated as,

$$A_{kl}^{(A;c)} = \delta_{kl}\frac{8\pi}{3}\frac{P_A}{2S}\sum_{\mu\nu} D_{\mu\nu}^{OO(\alpha-\beta)}\langle\varphi_\mu|\delta(\mathbf{R}_A)|\varphi_\nu\rangle \tag{5.17}$$

$$A_{kl}^{(A;d)} = \frac{P_A}{2S}\sum_{\mu\nu} D_{\mu\nu}^{OO(\alpha-\beta)}\langle\varphi_\mu|r_A^{-5}(r_A^2\delta_{kl} - 3r_{A;k}r_{A;l}|\varphi_\nu\rangle. \tag{5.18}$$

Where $D_{\mu\nu}^{OO(\alpha-\beta)}$ is the orbital optimized MP2 spin density matrix, S denotes the total spin and P_A is an atom specific constant, defined in eq. 5.19.

5.3.3. Computational Details

In order to benchmark the performance of the OO-SCS-RI-MP2 and OO-RI-MP2 methods, hyperfine coupling constants (hfccs) of a series of small radicals and transition metal complexes have been calculated. To avoid complicated issues like basis set convergence (that is very slow for singular properties like the isotropic hfccs), vibrational averaging or matrix effects, we choose to initially calibrate the OO-MP2 methods relative to a higher level method, specifically CCSD(T) [162].

All MP2 and DFT calculations were carried out with a development version of the ORCA program package. [25] The application of the 'Resolution of the Identity' approximation [22] in terms of the Split-RI-J algorithm [30] is indicated with the prefix 'RI'. The Coupled Cluster calculations were performed with the ACES II (now CFour) program suite. [163] All electrons were correlated throughout the study.

The small radicals were optimized on the CCSD(T) level [162] employing Dunning's cc-pVTZ basis set. [65] In the case of the OH, NO and NH_2 radicals experimental structures were used. The structures of the transition metal complexes were taken from Ref. [164].

Barone's triple-ζ EPR-III [165] basis set was employed for the calculation of the hyperfine coupling constants, except for the elements Al, S, Cl, and Si, for which Kutzelniggs IGLO-III [166] basis set was used. For the element Mg a modified TZVPP basis set which has been decontracted in the s-part was employed. [98] A triply polarized basis set with additional flexibility in the core region (CP(PPP)) was applied for the transition metal atoms. [167]

In preliminary studies comparing RI-MP2 to conventional MP2 it was ensured that the auxiliary basis sets used in the present study lead to an error of $\leq$1 MHz in the calculated hfccs. The decontracted def2-TZVPP/JK auxiliary basis set of Weigend and co-workers [92] was found suitable to reach this level of accuracy.

All energies were converged to 10^{-9} E_h and the convergence criteria for the orbital gradient was chosen 10^{-3}.

The P_A factor in eqs. 5.17 and 5.18 is the product of the electronic and nuclear g-values and Bohr magnetons, respectively, and specific for each atom type.

$$P_A = g_e g_N \beta_e \beta_N \tag{5.19}$$

The nuclear g-values employed for the calculation of the hfccs were taken from Ref. [168], and are listed in Table 5.10.

Table 5.10.: g_N values and P_A factors employed for the calculation of hfccs.

atom	g_N	P_A [MHz/au^3]
^{1}H	5.5856912	533.5514
^{11}B	1.7924240	171.2143
^{13}C	1.4048200	134.1900
^{14}N	0.4037607	38.5677
^{17}O	−0.7575160	−72.3588
^{19}F	5.2577320	502.2244
^{25}Mg	−0.3421800	−32.6854
^{27}Al	1.4566010	139.1361
^{29}Si	−1.1106000	−106.0857
^{33}S	0.4291100	40.9891
^{35}Cl	0.5479157	52.3375

5.3.4. Numerical Results

Throughout the following subsection $A_{11}^{(A)}$, $A_{22}^{(A)}$ and $A_{33}^{(A)}$ denote the diagonal elements of the total hyperfine coupling tensor, $A^{(A;c)}$ indicates the isotropic Fermi contact contribution to the hfc tensor and the anisotropic spin dipolar contributions are assigned by $A_{11}^{(A;d)}$, $A_{22}^{(A;d)}$ and $A_{33}^{(A;d)}$.

Atoms

In Table 5.11 the isotropic and anisotropic hfccs for the first row main group elements B−F are listed. Denoting the principal values of the anisotropic hfc tensor $2b, -b, -b$, only b is reported. The CCSD(T) results presented in Table 5.11 serve as reference. For these systems the effect of the perturbative triples correction is negligible and the CCSD results are very close to CCSD(T). The RI-MP2 method tends to slightly underestimate the isotropic hfc contribution but performs surprisingly good for atomic hfccs.

Both orbital optimized MP2 methods yield excellent results. They tend to slightly overestimate the hfc contributions in absolute value with OO-RI-MP2 performing marginally better than its spin-component scaled variant. As expected, the errors in the anisotropic hfccs tend to be smaller than the error in the isotropic contributions. Orbital optimization yields almost no improvement for the atomic hfccs compared to conventional MP2.

Compared to CCSD(T), the B2PLYP double-hybrid functional performs reasonably well but certainly worse than the OO-MP2 methods for the dipolar contribution to the hfccs. For the Fermi contact interaction, the results of B2PLYP relative to CCSD(T) are of limited quality. However, relative to the experimental numbers B2PLYP is the most accurate of the tested approaches. This is likely a fortuitous result as basis sets far from the limit are used in this study.

Table 5.11.: Calculated hfccs in [MHz] of first row main group elements.

atom		method						
		RI-MP2	OO-RI-MP2	OO-SCS-RI-MP2	B2PLYP	CCSD	CCSD(T)	Expt.
^{11}B	$A^{(A;d)}$	56.1	56.1	55.9	58.7	55.1	55.1	
	$A^{(A;c)}$	−2.4	2.6	2.7	17.1	3.7	4.2	11.6[a]/18.7[b]
^{13}C	$A^{(A;d)}$	−47.7	−47.7	−47.5	−49.0	−47.4	−47.3	
	$A^{(A;c)}$	8.4	12.7	13.7	24.3	10.9	11.3	(21.4)[c]/(22.5)[a]
^{14}N	$A^{(A;d)}$	0.0	0.0	0.0	0.0	0.0	0.0	
	$A^{(A;c)}$	7.5	8.7	9.5	11.4	7.8	7.9	10.4[d]
^{17}O	$A^{(A;d)}$	72.7	72.6	72.6	74.2	72.4	72.4	
	$A^{(A;c)}$	−23.6	−25.9	−28.5	−31.0	−24.5	−24.5	34.5[e]
^{19}F	$A^{(A;d)}$	1588.9	1588.5	1587.1	1608.8	1581.2	1580.3	
	$A^{(A;c)}$	243.9	259.3	284.6	278.5	247.2	245.8	301.7[e]

Radicals

In Tables 5.12 and 5.13 the hyperfine coupling constants for a variety of small radicals are listed.

Table 5.12.: Hyperfine coupling constants in [MHz] for a variety of small S=1/2 systems.

	$\langle S^2 \rangle$			$A_{11}^{(A)}$	$A_{22}^{(A)}$	$A_{33}^{(A)}$	$A^{(A;c)}$	$A_{11}^{(A;d)}$	$A_{22}^{(A;d)}$	$A_{33}^{(A;d)}$
^{2}BO	0.799945	^{11}B	RI-MP2	973.2	973.2	1067.4	1004.6	−31.4	−31.4	62.8
		^{11}B	SCS-RI-MP2	945.8	945.8	1050.5	980.7	−34.9	−34.9	69.8
	0.758740	^{11}B	OO-RI-MP2	977.3	977.3	1055.4	1003.3	−26.0	−26.0	52.0
	0.755607	^{11}B	OO-SCS-RI-MP2	971.7	971.7	1053.2	998.9	−27.2	−27.2	54.3
		^{11}B	B2PLYP	1033.7	1033.7	1116.9	1061.4	−27.7	−27.7	55.5
		^{11}B	CCSD	1016.3	1016.3	1090.9	1041.1	−24.9	−24.9	49.7
		^{11}B	CCSD(T)	978.9	978.9	1057.3	1005.0	−26.1	−26.1	52.3
			Expt [174]	998	998	1079	1025	−27	−27	54
		^{17}O	RI-MP2	−93.1	−69.5	−69.5	−77.4	−15.8	7.9	7.9
		^{17}O	SCS-RI-MP2	−95.1	−86.8	−86.8	−89.6	−5.6	2.8	2.8
		^{17}O	OO-RI-MP2	−55.4	9.9	9.9	−11.9	−43.5	21.8	21.8
		^{17}O	OO-SCS-RI-MP2	−50.1	11.3	11.3	−9.2	−40.9	20.5	20.5
		^{17}O	B2PLYP	−55.7	5.5	5.5	−14.9	−40.8	20.4	20.4
		^{17}O	CCSD	−55.3	9.7	9.7	−12.0	−43.4	21.7	21.7
		^{17}O	CCSD(T)	−54.3	5.1	5.1	−14.7	−39.6	19.8	19.8
^{2}BS	0.855236	^{11}B	RI-MP2	730.4	730.4	844.0	768.3	−37.8	−37.8	75.7
		^{11}B	SCS-RI-MP2	675.1	675.1	802.0	717.4	−42.3	−42.3	84.6
	0.771530	^{11}B	OO-RI-MP2	769.4	769.4	858.5	799.1	−29.7	−29.7	59.4
	0.763958	^{11}B	OO-SCS-RI-MP2	746.5	746.5	840.2	777.7	−31.2	−31.2	62.5
		^{11}B	B2PLYP	785.7	785.7	883.9	818.4	−32.8	−32.8	65.5
		^{11}B	CCSD	767.0	767.0	852.3	795.5	−28.4	−28.4	56.9
		^{11}B	CCSD(T)	737.2	737.2	826.1	766.8	−29.6	−29.6	59.3
			Expt [175]				796			
		^{33}S	RI-MP2	29.0	29.0	60.0	39.3	−10.3	−10.3	20.6

[a] Ref. [169]
[b] Ref. [170]
[c] Ref. [171]
[d] Ref. [172]
[e] Ref. [173]

Continued.

	$\langle S^2 \rangle$			$A_{11}^{(A)}$	$A_{22}^{(A)}$	$A_{33}^{(A)}$	$A^{(A;c)}$	$A_{11}^{(A;d)}$	$A_{22}^{(A;d)}$	$A_{33}^{(A;d)}$
		^{33}S	SCS-RI-MP2	37.2	37.2	55.6	43.3	−6.1	−6.1	12.2
		^{33}S	OO-RI-MP2	−14.2	−14.2	51.2	7.6	−21.8	−21.8	43.6
		^{33}S	OO-SCS-RI-MP2	−17.3	−17.3	45.2	3.5	−20.8	−20.8	41.6
		^{33}S	B2PLYP	−16.0	−16.0	47.6	5.2	−21.2	−21.2	42.4
		^{33}S	CCSD	−19.1	−19.1	47.7	3.2	−22.3	−22.3	44.5
		^{33}S	CCSD(T)	−13.1	−13.1	47.1	7.0	−20.1	−20.1	40.1
^{2}CN	1.159620	^{13}C	RI-MP2	485.4	485.4	740.7	570.5	−85.1	−85.1	170.2
		^{13}C	SCS-RI-MP2	445.0	445.0	712.6	534.2	−89.2	−89.2	178.4
	0.754597	^{13}C	OO-RI-MP2	434.7	434.7	601.0	490.2	−55.4	−55.4	110.8
	0.754714	^{13}C	OO-SCS-RI-MP2	435.2	435.2	603.2	491.2	−56.0	−56.0	112.0
		^{13}C	B2PLYP	343.3	343.3	555.5	414.1	−70.7	−70.7	141.5
		^{13}C	CCSD	602.4	602.4	761.4	655.4	−53.0	−53.0	106.0
		^{13}C	CCSD(T)	499.4	499.4	669.5	556.1	−56.7	−56.7	113.5
			Expt [176]	543	543	678	588	−45	−45	90
		^{14}N	RI-MP2	1.7	1.7	30.2	11.2	−9.5	−9.5	18.9
		^{14}N	SCS-RI-MP2	5.6	5.6	31.5	14.2	−8.6	−8.6	17.3
		^{14}N	OO-RI-MP2	−13.8	−13.8	46.8	6.4	−20.2	−20.2	40.4
		^{14}N	OO-SCS-RI-MP2	−20.1	−20.1	39.9	−0.1	−20.0	−20.0	40.0
		^{14}N	B2PLYP	−44.1	−44.1	14.0	−24.7	−19.3	−19.3	38.7
		^{14}N	CCSD	−39.8	−39.8	19.7	−20.0	−19.8	−19.8	39.7
		^{14}N	CCSD(T)	−37.4	−37.4	20.0	−18.3	−19.1	−19.1	38.3
			Expt [176]	−28	−28	27	−13	−15	−15	30
^{2}CO$^+$	0.960189	^{13}C	RI-MP2	1331.1	1331.1	1583.7	1415.3	−84.2	−84.2	168.4
		^{13}C	SCS-RI-MP2	1275.5	1275.5	1549.5	1366.8	−91.4	−91.4	182.7
	0.761082	^{13}C	OO-RI-MP2	1413.0	1413.0	1566.3	1464.1	−51.1	−51.1	102.2
	0.758066	^{13}C	OO-SCS-RI-MP2	1411.0	1411.0	1569.0	1463.6	−52.7	−52.7	105.3
		^{13}C	B2PLYP	1497.5	1497.5	1662.7	1552.6	−55.1	−55.1	110.1
		^{13}C	CCSD	1538.2	1538.2	1675.2	1583.9	−45.7	−45.7	91.3
		^{13}C	CCSD(T)	1460.9	1460.9	1611.6	1511.1	−50.3	−50.3	100.5
			Expt [177]	1524	1524	1671	1573	−49	−49	98
		^{17}O	RI-MP2	−103.6	−103.6	−85.1	−97.4	−6.2	−6.2	12.3
		^{17}O	SCS-RI-MP2	−113.3	−113.3	−77.3	−101.3	−12.0	−12.0	24.0
		^{17}O	OO-RI-MP2	−57.8	55.6	55.6	17.8	−75.6	37.8	37.8
		^{17}O	OO-SCS-RI-MP2	−48.6	60.2	60.2	23.9	−72.5	36.3	36.3
		^{17}O	B2PLYP	−45.9	56.3	56.3	22.2	−68.1	34.1	34.1
		^{17}O	CCSD	−55.5	59.2	59.2	21.0	−76.5	38.3	38.3
		^{17}O	CCSD(T)	−49.2	51.8	51.8	18.1	−67.3	33.7	33.7
			Expt [177]	−47	52	52	19	−66	33	33
^{2}NO	0.797337	^{14}N	RI-MP2	−205.6	−23.1	60.1	−56.2	−149.4	33.1	116.3
		^{14}N	SCS-RI-MP2	−200.1	−22.2	63.3	−53.0	−147.1	30.8	116.3
	0.752023	^{14}N	OO-RI-MP2	−18.3	−17.2	88.4	17.6	−36.0	−34.8	70.8
	0.752677	^{14}N	OO-SCS-RI-MP2	−15.5	−12.6	93.3	21.8	−37.2	−34.3	71.6
		^{14}N	B2PLYP	−16.9	−16.7	96.4	20.9	−37.8	−37.7	75.4
		^{14}N	CCSD	−16.7	−12.9	97.3	22.6	−39.3	−35.5	74.8
		^{14}N	CCSD(T)	−23.1	−18.0	92.3	17.1	−40.2	−35.0	75.2
			Expt [168]				22			
		^{17}O	RI-MP2	−630.1	−288.7	19.7	−299.7	−330.4	11.0	319.4
		^{17}O	SCS-RI-MP2	−622.2	−289.4	13.5	−299.4	−322.9	10.0	312.9
		^{17}O	OO-RI-MP2	−155.7	34.7	43.0	−26.0	−129.7	60.7	69.0
		^{17}O	OO-SCS-RI-MP2	−162.9	25.6	36.2	−33.7	−129.2	59.3	69.9
		^{17}O	B2PLYP	−167.6	31.2	35.8	−33.6	−134.0	64.7	69.3
		^{17}O	CCSD	−168.3	23.5	38.8	−35.4	−133.0	58.9	74.1
		^{17}O	CCSD(T)	−169.6	11.5	26.9	−43.7	−125.9	55.2	70.6

Continued.

	$\langle S^2 \rangle$			$A_{11}^{(A)}$	$A_{22}^{(A)}$	$A_{33}^{(A)}$	$A^{(A;c)}$	$A_{11}^{(A;d)}$	$A_{22}^{(A;d)}$	$A_{33}^{(A;d)}$
^{2}OH	0.756733	^{17}O	RI-MP2	−321.9	98.5	98.7	−41.6	−280.4	140.1	140.3
		^{17}O	SCS-RI-MP2	−322.1	98.9	100.6	−40.9	−281.2	139.8	141.4
	0.753177	^{17}O	OO-RI-MP2	−326.5	92.5	93.7	−46.8	−279.7	139.3	140.5
	0.753094	^{17}O	OO-SCS-RI-MP2	−327.0	93.3	93.5	−46.7	−280.3	140.0	140.2
		^{17}O	B2PLYP	−337.5	89.7	91.0	−52.3	−285.2	142.0	143.2
		^{17}O	CCSD	−324.2	92.9	94.5	−45.6	−278.6	138.5	140.1
		^{17}O	CCSD(T)	−322.8	93.8	95.4	−44.5	−278.2	138.3	139.9
			Expt [178]				−51			
		^{1}H	RI-MP2	−142.1	−87.0	18.9	−70.1	−72.1	−16.9	88.9
		^{1}H	SCS-RI-MP2	−133.2	−78.4	26.6	−61.7	−71.5	−16.7	88.3
		^{1}H	OO-RI-MP2	−150.2	−95.1	13.2	−77.4	−72.8	−17.7	90.5
		^{1}H	OO-SCS-RI-MP2	−144.0	−89.2	18.9	−71.4	−72.6	−17.8	90.3
		^{1}H	B2PLYP	−142.0	−87.9	19.2	−70.3	−71.8	−17.7	89.5
		^{1}H	CCSD	−148.1	−93.5	15.1	−75.5	−72.6	−18.0	90.6
		^{1}H	CCSD(T)	−145.6	−91.1	16.8	−73.3	−72.3	−17.8	90.1
			Expt [178]				~ -69			
^{2}MgF	0.750477	^{25}Mg	RI-MP2	−308.1	−296.5	−296.5	−300.4	−7.8	3.9	3.9
		^{25}Mg	SCS-RI-MP2	−303.2	−291.5	−291.5	−295.4	−7.8	3.9	3.9
	0.751211	^{25}Mg	OO-RI-MP2	−306.8	−295.2	−295.2	−299.0	−7.8	3.9	3.9
	0.751017	^{25}Mg	OO-SCS-RI-MP2	−301.7	−290.0	−290.0	−293.9	−7.8	3.9	3.9
		^{25}Mg	B2PLYP	−324.7	−312.7	−312.7	−316.7	−8.0	4.0	4.0
		^{25}Mg	CCSD	−306.8	−295.2	−295.2	−299.0	−7.8	3.9	3.9
		^{25}Mg	CCSD(T)	−305.3	−293.7	−293.7	−297.6	−7.8	3.9	3.9
			Expt [179]	−349	−331	−331	−337	−12	6	6
		^{19}F	RI-MP2	116.2	116.2	302.8	178.4	−62.2	−62.2	124.4
		^{19}F	SCS-RI-MP2	108.9	108.9	291.8	169.9	−61.0	−61.0	121.9
		^{19}F	OO-RI-MP2	118.1	118.1	313.7	183.3	−65.2	−65.2	130.4
		^{19}F	OO-SCS-RI-MP2	105.0	105.0	295.7	168.6	−63.6	−63.6	127.1
		^{19}F	B2PLYP	127.1	127.1	367.6	207.3	−80.2	−80.2	160.3
		^{19}F	CCSD	123.7	123.7	309.3	185.6	−61.8	−61.8	123.7
		^{19}F	CCSD(T)	120.6	120.6	315.6	185.6	−65.0	−65.0	130.0
			Expt [180]	143	143	332	206	−63	−63	126
^{2}AlO	0.808358	^{27}Al	RI-MP2	−135.8	−135.8	85.4	−62.1	−73.7	−73.7	147.5
		^{27}Al	SCS-RI-MP2	−155.0	−155.0	52.2	−85.9	−69.1	−69.1	138.1
	0.762247	^{27}Al	OO-RI-MP2	1034.1	1034.1	1181.9	1083.4	−49.2	−49.2	98.5
	0.765396	^{27}Al	OO-SCS-RI-MP2	970.3	970.3	1118.2	1019.6	−49.3	−49.3	98.6
		^{27}Al	B2PLYP	922.1	922.1	1094.6	979.6	−57.5	−57.5	115.0
		^{27}Al	CCSD	425.3	425.3	596.7	482.4	−57.2	−57.2	114.3
		^{27}Al	CCSD(T)	509.1	509.1	677.8	565.3	−56.2	−56.2	112.4
			Expt [181]	713	713	872	766	−53	−53	106
		^{17}O	RI-MP2	0.7	188.7	188.7	126.0	−125.3	62.7	62.7
		^{17}O	SCS-RI-MP2	−42.5	182.7	182.7	107.6	−150.1	75.1	75.1
		^{17}O	OO-RI-MP2	−89.3	41.8	41.8	−1.9	−87.4	43.7	43.7
		^{17}O	OO-SCS-RI-MP2	−86.5	53.0	53.0	6.5	−93.0	46.5	46.5
		^{17}O	B2PLYP	−70.0	62.9	62.9	18.6	−88.6	44.3	44.3
		^{17}O	CCSD	−109.5	82.0	82.0	18.1	−127.7	63.8	63.8
		^{17}O	CCSD(T)	−98.5	78.2	78.2	19.3	−117.8	58.9	58.9
^{2}HCO	0.765630	^{1}H	RI-MP2	366.1	376.5	401.6	381.4	−15.3	−4.9	20.2
		^{1}H	SCS-RI-MP2	363.6	373.7	400.1	379.1	−15.5	−5.5	21.0
	0.752927	^{1}H	OO-RI-MP2	352.9	361.0	390.9	368.2	−15.4	−7.3	22.6
	0.753275	^{1}H	OO-SCS-RI-MP2	350.1	358.0	389.0	365.7	−15.6	−7.7	23.3
		^{1}H	B2PLYP	366.1	374.2	404.6	381.7	−15.5	−7.4	23.0
		^{1}H	CCSD	372.6	391.8	400.8	388.4	−15.8	3.4	12.4

Continued.

	$\langle S^2 \rangle$			$A_{11}^{(A)}$	$A_{22}^{(A)}$	$A_{33}^{(A)}$	$A^{(A;c)}$	$A_{11}^{(A;d)}$	$A_{22}^{(A;d)}$	$A_{33}^{(A;d)}$
		^{1}H	CCSD(T)	374.6	393.8	402.4	390.3	−15.7	3.5	12.1
			Expt [182]	∼377	∼377	∼343	354	−9	−9	25
						− 381				
		^{17}O	RI-MP2	−152.4	−24.6	5.3	−57.3	−95.2	32.6	62.5
		^{17}O	SCS-RI-MP2	−153.6	−21.7	3.2	−57.4	−96.3	35.6	60.6
		^{17}O	OO-RI-MP2	−136.6	7.5	17.0	−37.4	−99.2	44.9	54.3
		^{17}O	OO-SCS-RI-MP2	−140.3	4.8	15.7	−40.0	−100.4	44.7	55.6
		^{17}O	B2PLYP	−147.8	9.7	17.4	−40.2	−107.6	50.0	57.6
		^{17}O	CCSD	−144.6	−1.8	16.1	−43.4	−101.2	41.6	59.5
		^{17}O	CCSD(T)	−141.7	−0.6	13.5	−42.9	−98.7	42.3	56.4
		^{13}C	RI-MP2	289.4	301.2	429.8	340.1	−50.7	−38.9	89.7
		^{13}C	SCS-RI-MP2	300.3	308.0	439.1	349.1	−48.9	−41.1	90.0
		^{13}C	OO-RI-MP2	325.9	332.9	456.4	371.7	−45.9	−38.8	84.7
		^{13}C	OO-SCS-RI-MP2	332.3	342.2	465.3	379.9	−47.6	−37.7	85.4
		^{13}C	B2PLYP	338.5	345.2	476.0	386.6	−48.0	−41.4	89.4
		^{13}C	CCSD	284.5	291.2	342.7	306.1	−21.6	−15.0	36.6
		^{13}C	CCSD(T)	278.3	286.0	336.2	300.2	−21.9	−14.2	36.0
			Expt [182]	∼337	∼353	∼437	365	−39	−12	50
							− 377	− −48	− −24	− 72
$^{2}H_2CO$	0.785332	^{13}C	RI-MP2	−109.2	−86.2	−81.7	−92.4	−16.8	6.2	10.7
		^{13}C	SCS-RI-MP2	−80.2	−65.8	−59.5	−68.5	−11.7	2.7	9.0
	0.755748	^{13}C	OO-RI-MP2	−137.7	−113.6	−99.6	−117.0	−20.8	3.4	17.4
	0.754596	^{13}C	OO-SCS-RI-MP2	−112.6	−91.6	−84.6	−96.2	−16.3	4.7	11.7
		^{13}C	B2PLYP	−117.9	−89.0	−85.7	−97.5	−20.4	8.5	11.8
		^{13}C	CCSD	−119.5	−88.9	−88.6	−99.0	−20.5	10.1	10.4
		^{13}C	CCSD(T)	−114.7	−87.9	−84.9	−95.9	−18.9	7.9	11.0
			Expt [183]	−124	−105	−99	−109	−15	4	10
		^{17}O	RI-MP2	−316.8	89.1	98.9	−42.9	−273.9	132.1	141.8
		^{17}O	SCS-RI-MP2	−320.4	101.8	108.0	−36.9	−283.5	138.7	144.8
		^{17}O	OO-RI-MP2	−285.3	56.4	75.4	−51.2	−234.1	107.5	126.6
		^{17}O	OO-SCS-RI-MP2	−305.0	62.6	76.0	−55.5	−249.6	118.1	131.5
		^{17}O	B2PLYP	−316.4	61.0	84.3	−57.0	−259.4	118.1	141.3
		^{17}O	CCSD	−318.1	50.0	79.3	−62.9	−255.1	112.9	142.2
		^{17}O	CCSD(T)	−310.3	56.1	78.6	−58.5	−251.8	114.6	137.2
		^{1}H	RI-MP2	272.5	274.9	297.9	281.8	−9.3	−6.9	16.2
		^{1}H	SCS-RI-MP2	243.3	245.3	269.9	252.8	−9.5	−7.6	17.1
		^{1}H	OO-RI-MP2	355.2	357.3	387.6	366.7	−11.5	−9.4	20.9
		^{1}H	OO-SCS-RI-MP2	315.1	317.2	345.6	326.0	−10.8	−8.8	19.6
		^{1}H	B2PLYP	313.7	316.3	341.4	323.8	−10.1	−7.5	17.6
		^{1}H	CCSD	276.7	292.0	313.7	294.1	−17.4	−2.1	19.5
		^{1}H	CCSD(T)	286.5	303.6	326.3	305.5	−19.0	−1.8	20.9
			Expt [183]	363	376	377	372	−9	4	5
$^{2}H_2O^{+}$	0.761586	^{1}H	RI-MP2	−118.3	−88.4	6.3	−66.8	−51.5	−21.6	73.1
		^{1}H	SCS-RI-MP2	−109.2	−79.5	14.2	−58.2	−51.0	−21.3	72.4
	0.754418	^{1}H	OO-RI-MP2	−137.5	−107.6	−9.3	−84.8	−52.7	−22.8	75.5
	0.754004	^{1}H	OO-SCS-RI-MP2	−132.5	−102.9	−4.7	−80.0	−52.5	−22.9	75.4
		^{1}H	B2PLYP	−131.7	−102.4	−4.8	−79.6	−52.0	−22.8	74.8
		^{1}H	CCSD	−174.4	−78.5	5.2	−82.6	−91.8	4.0	87.8
		^{1}H	CCSD(T)	−170.4	−75.0	8.2	−79.1	−91.3	4.0	87.3
			Expt [178]				−73			
		^{17}O	RI-MP2	−366.5	84.4	88.0	−64.7	−301.8	149.1	152.7
		^{17}O	SCS-RI-MP2	−363.8	91.1	93.4	−59.8	−304.0	150.9	153.2
		^{17}O	OO-RI-MP2	−375.7	70.0	75.1	−76.9	−298.8	146.9	152.0

Continued.

	$\langle S^2 \rangle$			$A_{11}^{(A)}$	$A_{22}^{(A)}$	$A_{33}^{(A)}$	$A^{(A;c)}$	$A_{11}^{(A;d)}$	$A_{22}^{(A;d)}$	$A_{33}^{(A;d)}$
		^{17}O	OO-SCS-RI-MP2	−374.2	74.2	78.3	−73.9	−300.3	148.1	152.2
		^{17}O	B2PLYP	−383.1	72.6	77.5	−77.7	−305.5	150.2	155.2
		^{17}O	CCSD	−375.1	68.8	73.9	−77.5	−297.6	146.2	151.4
		^{17}O	CCSD(T)	−372.6	71.0	75.9	−75.2	−297.4	146.2	151.1
			Expt [178]				−83			
$^2CH_3$	0.761614	^{13}C	RI-MP2	−18.2	−18.2	211.5	58.4	−76.6	−76.6	153.1
		^{13}C	SCS-RI-MP2	−33.7	−33.7	197.6	43.4	−77.1	−77.1	154.2
	0.754306	^{13}C	OO-RI-MP2	−4.8	−4.8	224.4	71.6	−76.4	−76.4	152.8
	0.753550	^{13}C	OO-SCS-RI-MP2	−15.1	−15.1	215.1	61.6	−76.8	−76.8	153.5
		^{13}C	B2PLYP	5.2	5.3	241.4	84.0	−78.8	−78.7	157.5
		^{13}C	CCSD	−3.5	−3.5	225.6	72.8	−76.4	−76.4	152.8
		^{13}C	CCSD(T)	−7.2	−7.2	221.6	69.1	−76.2	−76.2	152.5
			Expt [184, 185]	13	13	198	75	~ -62	~ -62	~ 123
		^{1}H	RI-MP2	−111.2	−68.8	−33.9	−71.3	−39.9	2.5	37.4
		^{1}H	SCS-RI-MP2	−95.5	−53.1	−20.4	−56.3	−39.2	3.3	35.9
		^{1}H	OO-RI-MP2	−118.1	−75.9	−39.0	−77.7	−40.4	1.8	38.7
		^{1}H	OO-SCS-RI-MP2	−105.6	−63.5	−28.0	−65.7	−39.9	2.3	37.7
		^{1}H	B2PLYP	−109.5	−67.9	−31.0	−69.5	−40.0	1.6	38.4
		^{1}H	[a]CCSD	−124.4	−66.8	−29.5	−73.6	−50.8	6.8	44.0
		^{1}H	[a]CCSD(T)	−121.4	−64.1	−27.2	−70.9	−50.5	6.8	43.8
			Expt [184, 185]	−105	−69	−35	−70	−35	1	35
$^2SiH_3$	0.769857	^{29}Si	RI-MP2	−390.6	−111.9	−111.9	−204.8	−185.8	92.9	92.9
		^{29}Si	SCS-RI-MP2	−351.0	−70.7	−70.7	−164.1	−186.9	93.5	93.5
	0.764049	^{29}Si	OO-RI-MP2	−402.6	−125.0	−125.0	−217.5	−185.0	92.5	92.5
	0.761726	^{29}Si	OO-SCS-RI-MP2	−373.3	−94.8	−94.8	−187.6	−185.7	92.8	92.8
		^{29}Si	B2PLYP	−386.7	−96.0	−96.0	−192.9	−193.8	96.9	96.9
		^{29}Si	CCSD	−401.5	−124.0	−124.0	−216.5	−185.0	92.5	92.5
		^{29}Si	CCSD(T)	−393.1	−116.3	−116.3	−208.6	−184.5	92.3	92.3
		^{1}H	RI-MP2	−86.7	−67.8	−64.2	−72.9	−13.8	5.1	8.7
		^{1}H	SCS-RI-MP2	−68.2	−49.3	−46.2	−54.6	−13.6	5.3	8.4
		^{1}H	OO-RI-MP2	−93.0	−74.0	−70.0	−79.0	−14.0	5.0	9.0
		^{1}H	OO-SCS-RI-MP2	−78.8	−59.9	−56.1	−65.0	−13.8	5.0	8.8
		^{1}H	B2PLYP	−77.8	−59.2	−54.9	−64.0	−13.8	4.8	9.0
		^{1}H	[a]CCSD	−86.8	−66.4	−59.0	−70.7	−16.1	4.3	11.8
		^{1}H	[a]CCSD(T)	−83.3	−63.0	−55.6	−67.3	−16.0	4.3	11.7
$^2C_3H_5$[b]	0.833312	^{13}C	RI-MP2	−47.4	−24.7	−14.4	−28.9	−18.6	4.1	14.4
		^{13}C	SCS-RI-MP2	−42.2	−18.2	−8.5	−23.0	−19.2	4.8	14.5
	0.760583	^{13}C	OO-RI-MP2	−64.0	−42.8	−31.3	−46.0	−18.0	3.2	14.7
	0.760700	^{13}C	OO-SCS-RI-MP2	−60.8	−38.4	−27.1	−42.1	−18.7	3.7	15.0
		^{13}C	B2PLYP	−61.8	−36.9	−25.2	−41.3	−20.5	4.4	16.1
			Expt [186]				−48			
		^{13}C	RI-MP2	−32.4	−30.9	107.8	14.8	−47.3	−45.8	93.0
		^{13}C	SCS-RI-MP2	−40.7	−39.4	100.8	6.9	−47.6	−46.3	93.9
		^{13}C	OO-RI-MP2	−13.9	−12.3	125.1	32.9	−46.9	−45.3	92.1
		^{13}C	OO-SCS-RI-MP2	−18.3	−16.9	121.6	28.8	−47.1	−45.7	92.9
		^{13}C	B2PLYP	−8.8	−7.2	136.4	40.1	−48.9	−47.3	96.2
			Expt [186]				61			
		^{1}H	RI-MP2	−14.5	−4.0	−3.4	−7.3	−7.2	3.3	3.9
		^{1}H	SCS-RI-MP2	−20.6	−10.1	−8.7	−13.1	−7.5	3.0	4.5
		^{1}H	OO-RI-MP2	1.0	9.5	11.6	7.4	−6.4	2.2	4.2
		^{1}H	OO-SCS-RI-MP2	−1.1	7.8	9.7	5.5	−6.5	2.3	4.2

[a] Dipolar contributions are averaged over the three corresponding atoms.
[b] CCSD and CCSD(T) calculations were not feasible.

Continued.

	$\langle S^2 \rangle$			$A_{11}^{(A)}$	$A_{22}^{(A)}$	$A_{33}^{(A)}$	$A^{(A;c)}$	$A_{11}^{(A;d)}$	$A_{22}^{(A;d)}$	$A_{33}^{(A;d)}$
		^{1}H	B2PLYP	3.0	11.6	14.2	9.6	−6.6	2.0	4.6
			Expt [186]				12			
		^{1}H	RI-MP2	−60.2	−34.7	−14.3	−36.4	−23.8	1.7	22.1
		^{1}H	SCS-RI-MP2	−49.9	−24.5	−5.4	−26.6	−23.3	2.1	21.2
		^{1}H	OO-RI-MP2	−71.2	−45.8	−23.1	−46.7	−24.5	0.9	23.6
		^{1}H	OO-SCS-RI-MP2	−64.6	−39.2	−17.1	−40.3	−24.3	1.1	23.2
		^{1}H	B2PLYP	−68.7	−43.3	−20.3	−44.1	−24.6	0.8	23.8
			Expt [186]				−41			
		^{1}H	RI-MP2	−51.5	−31.6	−10.6	−31.2	−20.2	−0.4	20.7
		^{1}H	SCS-RI-MP2	−41.1	−21.3	−1.6	−21.3	−19.8	−0.0	19.8
		^{1}H	OO-RI-MP2	−62.2	−42.3	−19.1	−41.2	−21.0	−1.1	22.1
		^{1}H	OO-SCS-RI-MP2	−55.5	−35.7	−13.1	−34.8	−20.7	−0.9	21.7
		^{1}H	B2PLYP	−60.0	−40.2	−16.7	−39.0	−21.0	−1.2	22.3
			Expt [186]				−39			
$^{2}O_2H$	0.762838	^{17}O	RI-MP2	−315.7	60.1	76.0	−59.9	−255.9	120.0	135.9
		^{17}O	SCS-RI-MP2	−325.7	57.1	74.3	−64.8	−261.0	121.9	139.1
	0.752418	^{17}O	OO-RI-MP2	−276.2	58.0	60.8	−52.5	−223.7	110.5	113.3
	0.752900	^{17}O	OO-SCS-RI-MP2	−296.8	51.0	52.6	−64.4	−232.4	115.4	117.0
		^{17}O	B2PLYP	−301.5	59.3	63.0	−59.7	−241.7	119.0	122.7
		^{17}O	CCSD	−310.1	58.5	59.0	−64.2	−245.9	122.7	123.2
		^{17}O	CCSD(T)	−299.7	58.9	60.4	−60.1	−239.5	119.0	120.5
		^{17}O	RI-MP2	−146.8	−0.2	7.3	−46.6	−100.2	46.3	53.9
		^{17}O	SCS-RI-MP2	−141.3	−7.9	3.2	−48.7	−92.7	40.8	51.8
		^{17}O	OO-RI-MP2	−139.7	22.0	27.9	−29.9	−109.7	52.0	57.8
		^{17}O	OO-SCS-RI-MP2	−145.4	7.0	13.0	−41.8	−103.6	48.8	54.8
		^{17}O	B2PLYP	−147.7	15.7	20.7	−37.1	−110.6	52.8	57.8
		^{17}O	CCSD	−133.4	9.2	15.3	−36.3	−97.1	45.5	51.6
		^{17}O	CCSD(T)	−136.6	12.6	16.9	−35.7	−100.9	48.3	52.6
		^{1}H	RI-MP2	−56.8	−49.8	1.9	−34.9	−21.9	−14.9	36.8
		^{1}H	SCS-RI-MP2	−53.1	−47.3	2.4	−32.6	−20.4	−14.6	35.0
		^{1}H	OO-RI-MP2	−53.5	−41.7	5.2	−30.0	−23.5	−11.7	35.2
		^{1}H	OO-SCS-RI-MP2	−50.0	−39.6	5.2	−28.1	−21.8	−11.5	33.3
		^{1}H	B2PLYP	−51.3	−42.0	6.6	−28.9	−22.4	−13.1	35.5
		^{1}H	CCSD	−39.8	−34.4	−8.8	−27.7	−12.2	−6.8	18.9
		^{1}H	CCSD(T)	−40.5	−36.3	−7.8	−28.2	−12.3	−8.1	20.4
			Expt [168]					−11	−8	20
$^{2}CO_2^-$	0.763529	^{17}O	RI-MP2	−148.3	−65.0	−55.6	−89.6	−58.6	24.7	34.0
		^{17}O	SCS-RI-MP2	−147.1	−61.4	−53.2	−87.3	−59.9	25.9	34.0
	0.753048	^{17}O	OO-RI-MP2	−158.2	−81.7	−74.4	−104.7	−53.4	23.0	30.4
	0.753120	^{17}O	OO-SCS-RI-MP2	−155.0	−74.4	−67.3	−98.9	−56.1	24.5	31.6
		^{17}O	B2PLYP	−157.3	−67.2	−60.6	−95.0	−62.3	27.9	34.4
		^{17}O	CCSD	−156.3	−64.3	−52.1	−90.9	−65.4	26.6	38.8
		^{17}O	CCSD(T)	−157.9	−68.8	−57.0	−94.6	−63.4	25.8	37.6
		^{13}C	RI-MP2	303.2	311.3	407.5	340.6	−37.5	−29.4	66.8
		^{13}C	SCS-RI-MP2	298.2	306.6	407.2	337.3	−39.1	−30.7	69.8
		^{13}C	OO-RI-MP2	274.7	278.7	360.9	304.8	−30.1	−26.1	56.1
		^{13}C	OO-SCS-RI-MP2	278.2	284.0	372.3	311.5	−33.3	−27.5	60.8
		^{13}C	B2PLYP	297.2	303.3	403.4	334.6	−37.5	−31.3	68.8
		^{13}C	CCSD	290.1	298.5	406.4	331.7	−41.6	−33.1	74.8
		^{13}C	CCSD(T)	275.4	282.5	380.6	312.9	−37.4	−30.4	67.8
$^{2}NH_2$	0.759428	^{14}N	RI-MP2	−18.8	−18.3	109.2	24.0	−42.8	−42.3	85.1
		^{14}N	SCS-RI-MP2	−21.3	−21.0	107.6	21.8	−43.0	−42.8	85.8
	0.753988	^{14}N	OO-RI-MP2	−15.2	−14.5	112.5	27.6	−42.8	−42.1	84.9

Continued.

	$\langle S^2 \rangle$			$A_{11}^{(A)}$	$A_{22}^{(A)}$	$A_{33}^{(A)}$	$A^{(A;c)}$	$A_{11}^{(A;d)}$	$A_{22}^{(A;d)}$	$A_{33}^{(A;d)}$
	0.753602	^{14}N	OO-SCS-RI-MP2	−16.8	−16.3	111.5	26.1	−42.9	−42.5	85.4
		^{14}N	B2PLYP	−12.7	−11.8	118.6	31.4	−44.0	−43.2	87.2
		^{14}N	CCSD	−15.8	−15.0	111.6	26.9	−42.7	−42.0	84.7
		^{14}N	CCSD(T)	−16.7	−16.0	110.4	25.9	−42.6	−41.9	84.5
			Expt [186, 187]	−17	−15	116	28	−45	−43	88
		^{1}H	RI-MP2	−120.3	−70.3	−3.4	−64.7	−55.7	−5.6	61.3
		^{1}H	SCS-RI-MP2	−107.0	−57.1	7.6	−52.2	−54.8	−5.0	59.8
		^{1}H	OO-RI-MP2	−128.5	−78.7	−9.1	−72.1	−56.4	−6.6	63.0
		^{1}H	OO-SCS-RI-MP2	−118.6	−69.1	−0.6	−62.8	−55.9	−6.3	62.1
		^{1}H	B2PLYP	−120.3	−71.3	−2.3	−64.6	−55.7	−6.7	62.3
		^{1}H	CCSD	−155.3	−63.4	9.8	−69.6	−85.6	6.2	79.4
		^{1}H	CCSD(T)	−152.7	−61.3	11.5	−67.5	−85.2	6.2	79.0
			Expt [186, 187]	−123	−72	−1	−67	−56	−5	66
$^{2}NO_2$	0.770946	^{14}N	RI-MP2	129.5	131.9	182.0	147.8	−18.3	−15.8	34.2
		^{14}N	SCS-RI-MP2	132.4	139.2	189.1	153.6	−21.2	−14.4	35.5
	0.751284	^{14}N	OO-RI-MP2	130.6	131.3	177.8	146.6	−16.0	−15.3	31.2
	0.752347	^{14}N	OO-SCS-RI-MP2	134.4	139.4	186.9	153.5	−19.2	−14.2	33.3
		^{14}N	B2PLYP	127.9	130.7	187.2	148.6	−20.7	−17.9	38.6
		^{14}N	CCSD	121.6	126.2	187.3	145.0	−23.5	−18.8	42.3
		^{14}N	CCSD(T)	122.9	126.7	183.3	144.3	−21.4	−17.6	39.0
			Expt [182]	131	138	190	153	−22	−15	37
		^{17}O	RI-MP2	−166.0	−17.3	−10.9	−64.7	−101.3	47.4	53.8
		^{17}O	SCS-RI-MP2	−164.5	−14.5	−4.6	−61.2	−103.3	46.7	56.6
		^{17}O	OO-RI-MP2	−177.6	−33.6	−27.7	−79.7	−98.0	46.0	52.0
		^{17}O	OO-SCS-RI-MP2	−176.0	−28.7	−21.8	−75.5	−100.5	46.8	53.7
		^{17}O	B2PLYP	−171.5	−11.1	−7.4	−63.3	−108.1	52.2	56.0
		^{17}O	CCSD	−169.1	−6.4	1.5	−58.0	−111.1	51.6	59.5
		^{17}O	CCSD(T)	−171.6	−13.6	−5.1	−63.4	−108.2	49.9	58.3
			Expt [182]	∼ −160	∼ −7	∼5	−47	−106	47	59
							– −61			
$^{2}NF_2$	0.764471	^{14}N	RI-MP2	−7.2	−3.8	144.8	44.6	−51.8	−48.4	100.2
		^{14}N	SCS-RI-MP2	−7.2	−3.5	147.1	45.5	−52.7	−49.0	101.6
	0.753535	^{14}N	OO-RI-MP2	−3.8	−1.3	136.6	43.8	−47.7	−45.1	92.8
	0.753792	^{14}N	OO-SCS-RI-MP2	−1.0	1.9	143.1	48.0	−49.0	−46.1	95.1
		^{14}N	B2PLYP	−1.4	1.7	147.5	49.3	−50.7	−47.5	98.2
		^{14}N	CCSD	−1.0	1.8	147.1	49.3	−50.3	−47.5	97.8
		^{14}N	CCSD(T)	−4.3	−1.7	140.5	44.8	−49.1	−46.6	95.7
		^{19}F	RI-MP2	−61.5	−4.0	616.1	183.5	−245.1	−187.5	432.6
		^{19}F	SCS-RI-MP2	−58.7	40.1	595.7	192.4	−251.1	−152.3	403.4
		^{19}F	OO-RI-MP2	−128.1	−90.5	626.1	135.8	−263.9	−226.3	490.2
		^{19}F	OO-SCS-RI-MP2	−71.6	−50.1	631.5	169.9	−241.5	−220.1	461.6
		^{19}F	B2PLYP	−90.6	−65.2	653.6	165.9	−256.5	−231.2	487.7
		^{19}F	CCSD	−91.9	−22.1	612.2	166.1	−258.0	−188.2	446.2
		^{19}F	CCSD(T)	−97.8	−48.1	617.7	157.3	−255.1	−205.4	460.4
$^{2}NF_3^+$	0.784752	^{14}N	RI-MP2	−34.3	−34.3	121.3	17.5	−51.9	−51.9	103.7
		^{14}N	SCS-RI-MP2	−40.2	−40.2	117.7	12.4	−52.6	−52.6	105.3
	0.754225	^{14}N	OO-RI-MP2	33.1	33.1	170.6	78.9	−45.8	−45.8	91.7
	0.754666	^{14}N	OO-SCS-RI-MP2	40.5	40.5	182.2	87.8	−47.2	−47.2	94.4
		^{14}N	B2PLYP	31.5	31.5	176.6	79.8	−48.4	−48.4	96.7
		^{14}N	CCSD	53.6	53.6	201.5	102.9	−49.3	−49.3	98.6
		^{14}N	CCSD(T)	42.7	42.7	186.5	90.6	−47.9	−47.9	95.9
			Expt [168]				276			
		^{19}F	RI-MP2	−134.6	−75.3	659.4	149.8	−284.4	−225.2	509.5

Continued.

	$\langle S^2 \rangle$			$A_{11}^{(A)}$	$A_{22}^{(A)}$	$A_{33}^{(A)}$	$A^{(A;c)}$	$A_{11}^{(A;d)}$	$A_{22}^{(A;d)}$	$A_{33}^{(A;d)}$
		^{19}F	SCS-RI-MP2	−145.3	−53.0	629.4	143.7	−289.0	−196.7	485.7
		^{19}F	OO-RI-MP2	−77.8	25.5	814.9	254.2	−332.0	−228.7	560.7
		^{19}F	OO-SCS-RI-MP2	−24.8	59.4	831.0	288.6	−313.3	−229.1	542.5
		^{19}F	B2PLYP	−82.0	20.7	836.4	258.4	−340.4	−237.7	578.0
		^{19}F	[a]CCSD	−24.3	129.2	853.7	319.6	−343.8	−190.4	534.2
		^{19}F	[a]CCSD(T)	−41.4	76.2	825.9	286.9	−328.3	−210.6	539.0
			Expt [168]				468			
$^2O_3^-$	0.788861	^{17}O	RI-MP2	−39.9	174.2	180.8	105.0	−144.9	69.1	75.8
		^{17}O	SCS-RI-MP2	−87.5	160.3	163.1	78.6	−166.1	81.7	84.5
	0.751039	^{17}O	OO-RI-MP2	−184.7	10.8	14.9	−53.0	−131.7	63.8	67.9
	0.753723	^{17}O	OO-SCS-RI-MP2	−238.9	−29.4	−21.3	−96.6	−142.4	67.1	75.3
		^{17}O	B2PLYP	−205.0	20.5	24.1	−53.4	−151.5	74.0	77.6
		^{17}O	CCSD	−251.8	1.1	5.3	−81.8	−170.0	82.9	87.0
		^{17}O	CCSD(T)	−229.4	7.0	10.9	−70.5	−158.9	77.5	81.4
		^{17}O	RI-MP2	−109.9	60.1	115.5	21.9	−131.8	38.2	93.6
		^{17}O	SCS-RI-MP2	−100.4	48.0	114.1	20.6	−121.0	27.4	93.5
		^{17}O	OO-RI-MP2	−105.9	30.0	33.7	−14.1	−91.8	44.1	47.8
		^{17}O	OO-SCS-RI-MP2	−128.7	4.2	19.3	−35.0	−93.7	39.3	54.4
		^{17}O	B2PLYP	−131.5	27.3	29.6	−24.9	−106.7	52.2	54.5
		^{17}O	CCSD	−136.3	12.6	17.8	−35.3	−101.0	48.0	53.1
		^{17}O	CCSD(T)	−129.7	19.6	21.5	−29.5	−100.2	49.1	51.0
$^2ClO_2$[b]	0.788737	^{17}O	RI-MP2	−111.4	44.9	49.3	−5.7	−105.7	50.6	55.1
		^{17}O	SCS-RI-MP2	−121.0	36.4	44.1	−13.5	−107.5	49.9	57.6
	0.751049	^{17}O	OO-RI-MP2	−120.4	35.6	37.4	−15.8	−104.6	51.4	53.2
	0.757835	^{17}O	OO-SCS-RI-MP2	−141.7	13.3	26.7	−33.9	−107.8	47.2	60.6
		^{17}O	B2PLYP	−143.8	33.0	33.3	−25.8	−118.0	58.8	59.1
		^{25}Cl	RI-MP2	−45.6	−44.0	169.0	26.5	−72.1	−70.4	142.5
		^{25}Cl	SCS-RI-MP2	−10.2	−6.6	213.3	65.5	−75.7	−72.1	147.8
		^{25}Cl	OO-RI-MP2	−38.7	−36.0	155.0	26.8	−65.4	−62.8	128.2
		^{25}Cl	OO-SCS-RI-MP2	2.6	7.7	205.7	72.0	−69.4	−64.3	133.7
		^{35}Cl	B2PLYP	−43.8	−39.6	176.1	30.9	−74.7	−70.5	145.2
			Expt [168]					−83	−77	46

Table 5.13.: Hyperfine coupling constants in [MHz] for a variety of small S>1/2 systems.

	$\langle S^2 \rangle$			$A_{11}^{(A)}$	$A_{22}^{(A)}$	$A_{33}^{(A)}$	$A^{(A;c)}$	$A_{11}^{(A;d)}$	$A_{22}^{(A;d)}$	$A_{33}^{(A;d)}$
^{3}NH	2.016491	^{14}N	RI-MP2	−28.0	37.8	37.8	15.9	−43.8	21.9	21.9
		^{14}N	SCS-RI-MP2	−29.6	37.1	37.1	14.9	−44.5	22.2	22.2
	2.007690	^{14}N	OO-RI-MP2	−25.6	40.0	40.0	18.1	−43.7	21.9	21.9
	2.006912	^{14}N	OO-SCS-RI-MP2	−26.5	39.7	39.7	17.7	−44.2	22.1	22.1
		^{14}N	B2PLYP	−23.4	44.3	44.3	21.7	−45.1	22.6	22.6
		^{13}N	CCSD	−26.6	38.9	38.9	17.1	−43.6	21.8	21.8
		^{14}N	CCSD(T)	−27.0	38.4	38.4	16.6	−43.6	21.8	21.8
			Expt [168]	−26	43	43	20	−46	23	23
		^{1}H	RI-MP2	−98.8	−98.8	−5.5	−67.7	−31.1	−31.1	62.2
		^{1}H	SCS-RI-MP2	−87.0	−87.0	4.7	−56.4	−30.6	−30.6	61.2
		^{1}H	OO-RI-MP2	−103.1	−103.1	−8.6	−71.6	−31.5	−31.5	63.0
		^{1}H	OO-SCS-RI-MP2	−94.2	−94.2	−0.5	−62.9	−31.2	−31.2	62.4
		^{1}H	B2PLYP	−91.8	−91.8	1.1	−60.8	−31.0	−31.0	62.0

[a] Dipolar contributions are averaged over the three corresponding atoms.
[b] CCSD and CCSD(T) calculations were not feasible.

Continued.

	$\langle S^2 \rangle$			$A_{11}^{(A)}$	$A_{22}^{(A)}$	$A_{33}^{(A)}$	$A^{(A;c)}$	$A_{11}^{(A;d)}$	$A_{22}^{(A;d)}$	$A_{33}^{(A;d)}$
		^{1}H	CCSD	−98.9	−98.9	−4.9	−67.6	−31.4	−31.4	62.7
		^{1}H	CCSD(T)	−97.3	−97.3	−3.6	−66.1	−31.2	−31.2	62.4
			Expt [168]	−100	−100	−10	−70	−30	−30	60
$^{3}OH^{+}$	2.014161	^{17}O	RI-MP2	−120.5	−120.5	115.0	−42.0	−78.5	−78.5	157.0
		^{17}O	SCS-RI-MP2	−120.5	−120.5	116.9	−41.4	−79.1	−79.1	158.3
	2.006706	^{17}O	OO-RI-MP2	−123.9	−123.9	110.5	−45.8	−78.1	−78.1	156.2
	2.006180	^{17}O	OO-SCS-RI-MP2	−124.5	−124.5	111.3	−45.9	−78.6	−78.6	157.2
		^{17}O	B2PLYP	−127.5	−127.5	112.8	−47.4	−80.1	−80.1	160.2
		^{17}O	CCSD	−123.6	−123.6	110.3	−45.6	−78.0	−78.0	155.9
		^{17}O	CCSD(T)	−122.9	−122.9	110.9	−45.0	−77.9	−77.9	155.9
		^{1}H	RI-MP2	−120.4	−120.4	9.8	−77.0	−43.4	−43.4	86.8
		^{1}H	SCS-RI-MP2	−115.0	−115.0	15.0	−71.7	−43.3	−43.3	86.7
		^{1}H	OO-RI-MP2	−126.1	−126.1	5.2	−82.3	−43.8	−43.8	87.5
		^{1}H	OO-SCS-RI-MP2	−122.4	−122.4	8.9	−78.6	−43.8	−43.8	87.6
		^{1}H	B2PLYP	−116.0	−116.0	13.7	−72.8	−43.2	−43.2	86.4
		^{1}H	CCSD	−121.4	−121.4	9.6	−77.7	−43.7	−43.7	87.3
		^{1}H	CCSD(T)	−119.5	−119.5	11.1	−76.0	−43.6	−43.6	87.1
$^{3}SH^{+}$	2.020489	^{33}S	RI-MP2	−58.2	82.6	82.6	35.6	−93.8	46.9	46.9
		^{33}S	SCS-RI-MP2	−58.9	83.0	83.0	35.7	−94.6	47.3	47.3
	2.007451	^{33}S	OO-RI-MP2	−53.5	88.7	88.7	41.3	−94.8	47.4	47.4
	2.006436	^{33}S	OO-SCS-RI-MP2	−52.8	90.3	90.3	42.6	−95.3	47.7	47.7
		^{33}S	B2PLYP	−63.8	84.1	84.1	34.8	−98.6	49.3	49.3
		^{33}S	CCSD	−44.9	96.4	96.4	49.3	−94.2	47.1	47.1
		^{33}S	CCSD(T)	−43.4	97.5	97.5	50.5	−93.9	46.9	46.9
		^{1}H	RI-MP2	−89.5	−89.5	−52.3	−77.1	−12.4	−12.4	24.8
		^{1}H	SCS-RI-MP2	−78.5	−78.5	−41.5	−66.2	−12.3	−12.3	24.7
		^{1}H	OO-RI-MP2	−83.4	−83.4	−46.5	−71.1	−12.3	−12.3	24.6
		^{1}H	OO-SCS-RI-MP2	−74.9	−74.9	−38.0	−62.6	−12.3	−12.3	24.6
		^{1}H	B2PLYP	−67.4	−67.4	−30.8	−55.2	−12.2	−12.2	24.4
		^{1}H	CCSD	−77.6	−77.6	−40.9	−65.4	−12.2	−12.2	24.5
		^{1}H	CCSD(T)	−76.4	−76.4	−39.8	−64.2	−12.2	−12.2	24.4
$^{3}O_{2}$	2.048075	^{17}O	RI-MP2	−75.8	−75.8	55.4	−32.1	−43.7	−43.7	87.5
		^{17}O	SCS-RI-MP2	−91.2	−91.2	42.0	−46.8	−44.4	−44.4	88.8
	2.004177	^{17}O	OO-RI-MP2	−84.9	−84.9	46.1	−41.2	−43.7	−43.7	87.3
	2.006328	^{17}O	OO-SCS-RI-MP2	−101.3	−101.3	31.8	−56.9	−44.4	−44.4	88.7
		^{17}O	B2PLYP	−93.3	−93.3	45.0	−47.2	−46.1	−46.1	92.2
		^{17}O	CCSD	−102.0	−102.0	36.7	−55.7	−46.2	−46.2	92.5
		^{17}O	CCSD(T)	−97.0	−97.0	39.3	−51.6	−45.4	−45.4	90.9
			Expt [188]	−102	−102	39	−55	−47	−47	94
$^{3}S_{2}$	2.049667	^{33}S	RI-MP2	−39.9	34.7	34.7	9.8	−49.7	24.9	24.9
		^{33}S	SCS-RI-MP2	−34.4	40.5	40.5	15.5	−49.9	25.0	25.0
	2.015132	^{33}S	OO-RI-MP2	−33.4	41.1	41.1	16.2	−49.6	24.8	24.8
	2.018289	^{33}S	OO-SCS-RI-MP2	−27.8	47.1	47.1	22.1	−49.9	25.0	25.0
		^{33}S	B2PLYP	−36.2	40.9	40.9	15.2	−51.4	25.7	25.7
		^{33}S	CCSD	−26.7	49.8	49.8	24.3	−51.0	25.5	25.5
		^{33}S	CCSD(T)	−26.5	48.6	48.6	23.6	−50.1	25.1	25.1
^{3}SO	2.054070	^{33}S	RI-MP2	−52.0	39.2	39.2	8.8	−60.8	30.4	30.4
		^{33}S	SCS-RI-MP2	−44.0	48.6	48.6	17.7	−61.7	30.9	30.9
	2.012992	^{33}S	OO-RI-MP2	−49.2	42.1	42.1	11.7	−60.9	30.4	30.4
	2.015130	^{33}S	OO-SCS-RI-MP2	−41.5	51.2	51.2	20.3	−61.8	30.9	30.9
		^{33}S	B2PLYP	−50.3	43.8	43.8	12.4	−62.8	31.4	31.4
		^{33}S	CCSD	−42.3	52.0	52.0	20.5	−62.8	31.4	31.4
		^{33}S	CCSD(T)	−40.8	51.5	51.5	20.7	−61.5	30.8	30.8

Continued.

$\langle S^2 \rangle$			$A_{11}^{(A)}$	$A_{22}^{(A)}$	$A_{33}^{(A)}$	$A^{(A;c)}$	$A_{11}^{(A;d)}$	$A_{22}^{(A;d)}$	$A_{33}^{(A;d)}$
	^{17}O	RI-MP2	−38.2	−38.2	48.8	−9.2	−29.0	−29.0	58.0
	^{17}O	SCS-RI-MP2	−43.3	−43.3	42.8	−14.6	−28.7	−28.7	57.4
	^{17}O	OO-RI-MP2	−57.3	−57.3	30.9	−27.9	−29.4	−29.4	58.8
	^{17}O	OO-SCS-RI-MP2	−63.6	−63.6	23.9	−34.4	−29.2	−29.2	58.4
	^{17}O	B2PLYP	−65.8	−65.8	30.8	−33.6	−32.2	−32.2	64.4
	^{17}O	CCSD	−72.3	−72.3	21.2	−41.1	−31.2	−31.2	62.3
	^{17}O	CCSD(T)	−67.9	−67.9	23.9	−37.3	−30.6	−30.6	61.2

In general, the deviations from CCDS(T) that are obtained with OO-RI-MP2 and OO-SCS-RI-MP2 methods do not appear to be systematic. In fact, the orbital optimized MP2 (OO-MP2) methods do not generally tend to either underestimate or overestimate the hfccs neither in magnitude nor in absolute value. This behaviour is well reflected in the mean error statistics presented in Table 5.14. The mean error of the OO-MP2 methods is close to zero and is very similar to the mean error of the CCSD method.

Table 5.14.: Error statistics in [MHz] for a variety of small S≥1/2 systems in comparison to CCSD(T) results.

	$A_{11}^{(A)}$	$A_{22}^{(A)}$	$A_{33}^{(A)}$	$A^{(A;c)}$	$A_{11}^{(A;d)}$	$A_{22}^{(A;d)}$	$A_{33}^{(A;d)}$
Mean error RI-MP2	−24	−27	−19	−24	−1	−4	5
Mean absolute error RI-MP2	49	49	44	45	16	9	16
Mean error SCS-RI-MP2	−26	−26	−21	−24	−2	−2	4
Mean absolute error SCS-RI-MP2	55	53	47	50	16	11	18
Mean error OO-RI-MP2	3	−5	−1	−1	4	−4	0
Mean absolute error OO-RI-MP2	30	30	28	27	7	6	7
Mean error OO-SCS-RI-MP2	5	−3	−0	0	5	−4	−1
Mean absolute error OO-SCS-RI-MP2	24	23	23	21	7	5	5
Mean error B2PLYP	2	−2	6	2	0	−4	4
Mean absolute error B2PLYP	28	26	26	24	7	6	8
Mean error CCSD	−4	−1	−3	−3	−2	2	0
Mean absolute error CCSD	15	17	15	16	3	3	2

Regarding the mean absolute errors, CCSD is the closest to the CCSD(T) reference data. Anyway, not by a large margin. However, the OO-MP2 methods are only worse by about ∼10−15 MHz in the total and isotropic hfccs. The deviations in the dipolar hfccs are small for both the CCSD and OO-MP2 methods. Interestingly, it can be seen from Table 5.14 that the spin component scaled variant of the OO-RI-MP2 method (OO-SCS-RI-MP2) improves upon the results of the initial OO-RI-MP2 method. Though, comparison of individual entries shows, that this improvement is not systematic.

Table 5.15.: Error statistics in [MHz] for a variety of small S≥1/2 systems in comparison to experimental results.

	$A_{11}^{(A)}$	$A_{22}^{(A)}$	$A_{33}^{(A)}$	$A^{(A;c)}$	$A_{11}^{(A;d)}$	$A_{22}^{(A;d)}$	$A_{33}^{(A;d)}$
Mean error RI-MP2	−51	−55	−39	−57	−2	−7	8
Mean absolute error RI-MP2	61	65	56	67	9	8	14
Mean error SCS-RI-MP2	−56	−60	−42	−60	−3	−7	9
Mean absolute error SCS-RI-MP2	72	77	61	77	9	9	14
Mean error OO-RI-MP2	−11	−17	−8	−23	1	−5	3
Mean absolute error OO-RI-MP2	40	41	36	45	7	6	9
Mean error OO-SCS-RI-MP2	−5	−6	2	−19	−2	−3	4
Mean absolute error OO-SCS-RI-MP2	30	32	31	36	4	4	7
Mean error B2PLYP	−4	−3	10	−18	−4	−4	8
Mean absolute error B2PLYP	27	27	28	36	5	6	9
Mean error CCSD	−23	−16	−11	−27	−5	1	4
Mean absolute error CCSD	35	31	33	37	8	5	8
Mean error CCSD(T)	−25	−19	−13	−33	−5	−1	4
Mean absolute error CCSD(T)	30	28	27	39	8	5	8

In Table 5.15 we compare the results of our calculations to experiment. The scaled error statistics in Table 5.17 displays the same overall trends. Obviously, the performance of the OO-MP2 methods is extremely good - in fact as good as what is obtained for CCSD and even CCSD(T). This excellent behavior should certainly be taken with a grain of salt as one is neither close to the basis set limit nor have vibrational effects been included in the calculations.

In Table 5.16 the individual deviations with respect to the CCSD(T) results are scaled with the corresponding P_A factor for each element A. Due to the possibly large magnitude of the P_A factor (e.g. for the hydrogen atom P_H=533.5514 MHz/au^3, cf. Table 5.10), the scaling by P_A offers an element independent insight into the error statistics.

Table 5.16 shows a slight tendency for overestimation of the total and isotropic hfccs by the OO-MP2 methods, which is indicated by the overall positive mean error. The mean absolute error confirms the slightly superior performance of CCSD, when compared to the CCSD(T) reference. Importantly, the OO-MP2 methods reduce the errors of the MP2 method itself by a factor of 2−3 and hence they represent a definite improvement.

Table 5.16.: Error statistics in [au^3] for a variety of small S$\geq$1/2 systems in comparison to CCSD(T) results. Error scaled by the corresponding element-specific factor P_A [MHz/au^3].

	$A_{11}^{(A)}$	$A_{22}^{(A)}$	$A_{33}^{(A)}$	$A^{(A;c)}$	$A_{11}^{(A;d)}$	$A_{22}^{(A;d)}$	$A_{33}^{(A;d)}$
Mean error RI-MP2	−0.1440	−0.1502	−0.2197	−0.1713	0.0273	0.0211	−0.0484
Mean absolute error RI-MP2	0.5025	0.4262	0.3541	0.4108	0.1832	0.0974	0.1771
Mean error SCS-RI-MP2	−0.1316	−0.1391	−0.2166	−0.1624	0.0313	0.0237	−0.0550
Mean absolute error SCS-RI-MP2	0.5236	0.4538	0.3619	0.4329	0.1957	0.1184	0.1951
Mean error OO-RI-MP2	0.0293	0.0375	0.0609	0.0426	−0.0134	−0.0051	0.0186
Mean absolute error OO-RI-MP2	0.1792	0.1742	0.1795	0.1684	0.0557	0.0344	0.0472
Mean error OO-SCS-RI-MP2	0.0739	0.0722	0.0891	0.0784	−0.0046	−0.0064	0.0110
Mean absolute error OO-SCS-RI-MP2	0.1365	0.1508	0.1463	0.1363	0.0429	0.0325	0.0373
Mean error B2PLYP	0.0627	0.0287	0.0783	0.0566	0.0062	−0.0283	0.0220
Mean absolute error B2PLYP	0.1800	0.1605	0.1743	0.1539	0.0559	0.0433	0.0540
Mean error CCSD	0.0453	0.0352	0.0315	0.0373	0.0083	−0.0023	−0.0060
Mean absolute error CCSD	0.0818	0.0840	0.0762	0.0765	0.0230	0.0163	0.0208

Table 5.17.: Error statistics in [au^3] for a variety of small S$\geq$1/2 systems in comparison to experimental results. Error scaled by the corresponding element-specific factor P_A [MHz/au^3].

	$A_{11}^{(A)}$	$A_{22}^{(A)}$	$A_{33}^{(A)}$	$A^{(A;c)}$	$A_{11}^{(A;d)}$	$A_{22}^{(A;d)}$	$A_{33}^{(A;d)}$
Mean error RI-MP2	−0.3488	−0.2950	−0.2067	−0.4179	−0.0641	−0.0146	0.0781
Mean absolute error RI-MP2	0.4852	0.5436	0.4465	0.5444	0.0893	0.0718	0.1132
Mean error SCS-RI-MP2	−0.3622	−0.3085	−0.2276	−0.4365	−0.0616	−0.0123	0.0732
Mean absolute error SCS-RI-MP2	0.5410	0.5943	0.4488	0.5860	0.0838	0.0770	0.1083
Mean error OO-RI-MP2	−0.0259	−0.0283	0.0261	−0.1578	−0.0172	−0.0216	0.0382
Mean absolute error OO-RI-MP2	0.2755	0.2821	0.2790	0.3121	0.0484	0.0327	0.0672
Mean error OO-SCS-RI-MP2	−0.0411	−0.0402	0.0121	−0.1568	−0.0186	−0.0198	0.0377
Mean absolute error OO-SCS-RI-MP2	0.2429	0.2508	0.2572	0.2914	0.0394	0.0303	0.0594
Mean error B2PLYP	−0.0449	−0.0535	0.0332	−0.1570	−0.0235	−0.0340	0.0570
Mean absolute error B2PLYP	0.2144	0.2079	0.2044	0.2753	0.0357	0.0412	0.0615
Mean error CCSD	−0.1463	−0.1514	−0.1217	−0.2378	−0.0067	−0.0142	0.0203
Mean absolute error CCSD	0.2272	0.2148	0.2220	0.2861	0.0505	0.0356	0.0554
Mean error CCSD(T)	−0.1859	−0.1809	−0.1480	−0.2815	−0.0143	−0.0121	0.0258
Mean absolute error CCSD(T)	0.2180	0.2117	0.2056	0.3031	0.0422	0.0302	0.0509

In order to gain more insight into the individual description of different nuclei, the scaled error statistics are broken down into the contributions of H, C, N, O, and F atoms and compared to CCSD(T) results. From the results in Table 5.18 it is seen that the ^{1}H hfccs are well described by all employed MP2 methods. However, for ^{13}C, ^{14}N, ^{17}O and ^{19}F hfccs the orbital optimization leads to large improvements

in the results. This is most clearly seen in the ^{14}N hfccs. In the case of the ^{13}C and ^{19}F hfccs, the OO-SCS-RI-MP2 method even performs almost as well as CCSD.

Table 5.18.: Mean absolute error in [au^3] for H, C, N, O, and F atoms in a variety of small S$\geq$1/2 systems in comparison to CCSD(T) results. Error scaled by the corresponding element-specific factor P_A [MHz/au^3].

	$A_{11}^{(A)}$	$A_{22}^{(A)}$	$A_{33}^{(A)}$	$A^{(A;c)}$	$A_{11}^{(A;d)}$	$A_{22}^{(A;d)}$	$A_{33}^{(A;d)}$
				^{1}H			
RI-MP2	0.0294	0.0189	0.0171	0.0135	0.0216	0.0123	0.0133
SCS-RI-MP2	0.0496	0.0280	0.0226	0.0315	0.0220	0.0123	0.0142
OO-RI-MP2	0.0379	0.0351	0.0336	0.0255	0.0208	0.0132	0.0111
OO-SCS-RI-MP2	0.0318	0.0173	0.0148	0.0113	0.0222	0.0137	0.0124
B2PLYP	0.0302	0.0179	0.0145	0.0091	0.0226	0.0138	0.0129
CCSD	0.0064	0.0066	0.0062	0.0064	0.0007	0.0003	0.0009
				^{13}C			
RI-MP2	0.2474	0.2490	0.2892	0.2386	0.1163	0.1120	0.2238
SCS-RI-MP2	0.4293	0.4155	0.3528	0.3634	0.1371	0.1328	0.2570
OO-RI-MP2	0.2312	0.2376	0.3368	0.2684	0.0440	0.0444	0.0887
OO-SCS-RI-MP2	0.2247	0.2278	0.3144	0.2500	0.0448	0.0414	0.0800
B2PLYP	0.3605	0.3556	0.4326	0.3827	0.0609	0.0621	0.1214
CCSD	0.2603	0.2560	0.2427	0.2531	0.0181	0.0177	0.0311
				^{14}N			
RI-MP2	1.1529	0.4874	0.4263	0.6750	0.4779	0.3177	0.2902
SCS-RI-MP2	1.1944	0.5582	0.4660	0.7283	0.4711	0.3258	0.3061
OO-RI-MP2	0.1817	0.1561	0.2209	0.1608	0.0540	0.0276	0.0811
OO-SCS-RI-MP2	0.1570	0.1589	0.1252	0.1460	0.0286	0.0262	0.0526
B2PLYP	0.1465	0.1358	0.1666	0.1494	0.0311	0.0245	0.0292
CCSD	0.0833	0.0777	0.1066	0.0852	0.0239	0.0175	0.0380
				^{17}O			
RI-MP2	0.6826	0.7025	0.5474	0.6294	0.2976	0.1167	0.2851
SCS-RI-MP2	0.6256	0.6857	0.5297	0.6023	0.3047	0.1517	0.2823
OO-RI-MP2	0.1559	0.1417	0.1388	0.1343	0.1194	0.0606	0.0700
OO-SCS-RI-MP2	0.0581	0.1356	0.1157	0.0911	0.0772	0.0504	0.0478
B2PLYP	0.0851	0.0760	0.0740	0.0484	0.0729	0.0474	0.0454
CCSD	0.0704	0.0660	0.0538	0.0540	0.0470	0.0258	0.0303
				^{19}F			
RI-MP2	0.1182	0.1816	0.1711	0.1562	0.0513	0.0273	0.0497
SCS-RI-MP2	0.1333	0.1911	0.2181	0.1711	0.0431	0.0505	0.0936
OO-RI-MP2	0.0572	0.0794	0.0172	0.0476	0.0096	0.0319	0.0415
OO-SCS-RI-MP2	0.0391	0.0232	0.0208	0.0156	0.0244	0.0286	0.0052
B2PLYP	0.0473	0.0688	0.0514	0.0413	0.0179	0.0490	0.0669
CCSD	0.0221	0.0710	0.0334	0.0460	0.0184	0.0327	0.0164

The OO-MP2 results are now compared to previously published hfccs, calculated with the double-hybrid functional B2PLYP. [1] The B2PLYP functional combines the advantages of hybrid density functional

theory with a scaled MP2 correction to account for semi-local dynamic correlation effects, and has shown to provide excellent results for the prediction of hyperfine structure. [155] All DFT functionals failed to predict the hfccs of the molecules CN, AlO and NF_3^+ properly, and therefore these molecules were excluded from the error statistics in Ref. [155]. However, in this paper we decided to include all molecules in our error analysis, shown in Table 5.14. The B2PLYP mean absolute error compared to the CCSD(T) reference in the total hfccs is ∼27 MHz, which is similar to the deviations of the OO-MP2 methods from CCSD(T). The same is valid for the isotropic (24 MHz) and anisotropic (∼7 MHz) contributions to the hfccs. Thus, the OO-MP2 methods are at least not inferior to B2PLYP and it might be speculated that they could be more reliable in situations where the self-interaction error of DFT becomes important. In comparison to the experimental results, the OO-MP2 methods even outperforms the B2PLYP functional concerning the isotropic hfcc, with a mean absolute error of 58 MHz, whereas the errors in the total and anisotropic hfccs remain unchanged.

The expectation value of the total spin operator is listed in the second column of Tables 5.12 and 5.13. The spin contamination as recalled in Section 2.9.3, i.e. the deviation of $\langle S^2 \rangle$ from the ideal value, is in most cases drastically reduced by the OO-MP2 methods compared to the conventional RI-MP2 methods, that are based on UHF reference determinants. The only exception represents the MgF molecule, for which the spin contamination in the OO-MP2 methods is slightly increased compared to the standard MP2 methods.
The spin contamination often serves as an indicator for the quality of the underlying wave function. In the present context, this would imply an improved wave function, due to orbital relaxation within the dynamic correlation field. However, there is no obvious correlation between the reduced spin contamination and improved hyperfine coupling constants. Regarding the CN molecule, where the spin contamination is drastically reduced (RI-MP2: 0.409724, OO-RI-MP2: 0.010045), the ^{13}C hfccs are even worse for the OO-MP2 methods than for the conventional MP2 methods. Thus, no direct conclusion should be drawn from the decreased spin contamination in the OO-MP2 methods.

In summary, the results assembled here show that the OO-MP2 methods can rival the already excellent B2PLYP results for the prediction of hfccs. Importantly, the results of OO-MP2 predictions are of similar quality than the already excellent CCSD numbers. In general, the OO-SCS-RI-MP2 method represents, at most, a modest improvement of the parent OO-RI-MP2 method.

Transition Metal Hyperfine Coupling Constants

To investigate the description of the spin density in electronically more complicated systems, i.e. when spin polarization effects become large, the hyperfine coupling constants of some small illustrative transition metal compounds are analyzed. In Table 5.19 the total $A^{(A)}$, isotropic $A^{(A;c)}$ and dipolar $A^{(A;d)}$ hfccs are listed for the OO-(SCS-)RI-MP2 and CCSD(T) methods as well as for the double-hybrid functional B2PLYP, which was found to perform best under all tested functionals in Ref. [155]. Taking the CCSD(T) results as reference shows excellent agreement with the OO-RI-MP2 hfccs. Spin-component scaling does generally not improve the calculated hfccs. As shown in Fig. 5.6 the OO-RI-MP2 spin densities at the metal nuclei are almost of CCSD(T) quality. The B2PLYP functional tend to overestimate the spin density at the metal center compared to the CCSD(T) method, but agrees best with the experimental data. This is likely fortuitous, since the basis sets employed are far from being complete.

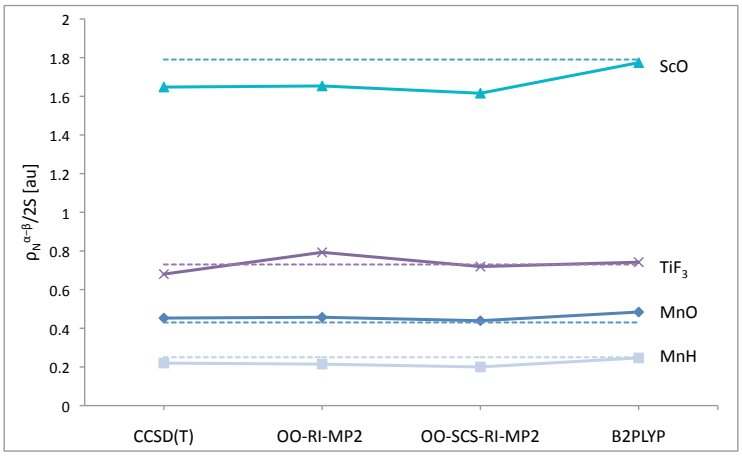

Figure 5.6.: Spin density $\rho_N^{\alpha-\beta}$ at the metal nucleus in ^{2}ScO, $^2TiF_3$, ^{6}MnO, and ^{7}MnH normalized to the number of unpaired electrons dependent on the method employed. The dashed lines represent the experimentally determined spin density.

Table 5.19.: Hyperfine coupling constants in [MHz] for a variety of small transition metal compounds.

			$A_{11}^{(A)}$	$A_{22}^{(A)}$	$A_{33}^{(A)}$	$A^{(A;c)}$	$A_{11}^{(A;d)}$	$A_{22}^{(A;d)}$	$A_{33}^{(A;d)}$
^{2}ScO	OO-RI-MP2	^{45}Sc	1778.3	1778.3	1837.8	1798.1	−19.8	−19.8	39.7
	OO-SCS-RI-MP2	^{45}Sc	1736.6	1736.6	1797.7	1757.0	−20.4	−20.4	40.7
	B2PLYP	^{45}Sc	1908.1	1908.1	1971.4	1929.2	−21.1	−21.1	42.2
	CCSD(T)	^{45}Sc	1767.8	1767.8	1840.1	1791.9	−24.1	−24.1	48.2
		Expt [189]	1922	1922	1997	1947	−25	−25	50
	OO-RI-MP2	^{17}O	−26.5	−26.5	−26.0	−26.3	−0.2	−0.2	0.3
	OO-SCS-RI-MP2	^{17}O	−23.6	−23.6	−22.0	−23.1	−0.5	−0.5	1.1
	B2PLYP	^{17}O	−24.4	−24.4	−23.7	−24.2	−0.2	−0.2	0.5
	CCSD(T)	^{17}O	−24.2	−24.2	−24.0	−24.0	−0.2	−0.2	0.1
		Expt [189]				−20	−0.4	−0.4	0.8
$^2TiF_3$	OO-RI-MP2	^{47}Ti	−209.6	−188.8	−187.9	−195.4	−14.2	6.6	7.6
	OO-SCS-RI-MP2	^{47}Ti	−192.2	−169.7	−168.3	−176.7	−15.4	7.0	8.4
	B2PLYP	^{47}Ti	−205.4	−178.1	−178.1	−187.2	−18.2	9.1	9.1
	CCSD[a]	^{47}Ti	−185.5	−163.0	−163.0	−170.5	−15.0	7.5	7.5
		Expt [190]	−199	−178	−178	−185	−14	7	7
	OO-RI-MP2	^{19}F	−55.2	−15.8	−1.9	−24.3	−30.9	8.5	22.4
	OO-SCS-RI-MP2	^{19}F	−45.0	−23.8	−1.8	−23.5	−21.5	−0.3	21.7
	B2PLYP	^{19}F	−36.5	−14.4	1.8	−16.4	−20.2	1.9	18.2
	CCSD[a]	^{19}F	−59.7	−29.2	−16.4	−35.1	−24.6	5.9	18.7
		Expt [190]				8			
	OO-RI-MP2	^{19}F	−57.2	−17.8	−1.4	−25.5	−31.8	7.6	24.1
	OO-SCS-RI-MP2	^{19}F	−46.0	−25.1	−0.1	−23.7	−22.2	−1.4	23.6
	B2PLYP	^{19}F	−36.5	−14.4	1.8	−16.4	−20.2	1.9	18.2
	CCSD[a]	^{19}F	−59.7	−29.2	−16.4	−35.1	−24.6	5.9	18.7
		Expt [190]				8			

[a] CCSD results employing a (15s11p6d)/[9s7p4d] basis set are taken from Ref. [164]

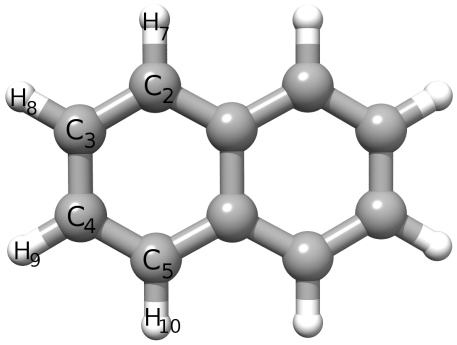

Figure 5.7.: Numbering of the atoms in the naphthalene anion radical.

Continued.

			$A_{11}^{(A)}$	$A_{22}^{(A)}$	$A_{33}^{(A)}$	$A^{(A;c)}$	$A_{11}^{(A;d)}$	$A_{22}^{(A;d)}$	$A_{33}^{(A;d)}$
^{7}MnH	OO-RI-MP2	^{55}Mn	224.3	224.3	260.3	236.3	−12.0	−12.0	24.0
	OO-SCS-RI-MP2	^{55}Mn	209.1	209.1	244.1	220.8	−11.7	−11.7	23.3
	B2PLYP	^{55}Mn	261.7	261.7	294.6	272.7	−11.0	−11.0	21.9
	CCSD(T)[b]	^{55}Mn	230.8	230.8	268.6	243.4	−12.6	−12.6	25.2
		Expt [191]	267	267	303	279	−12	−12	24
	OO-RI-MP2	^{1}H	0.2	0.2	36.0	12.1	−11.9	−11.9	23.8
	OO-SCS-RI-MP2	^{1}H	1.9	1.9	37.7	13.8	−11.9	−11.9	23.8
	B2PLYP	^{1}H	12.0	12.0	47.3	23.8	−11.8	−11.8	23.5
	CCSD(T)[b]	^{1}H	5.3	5.3	40.7	17.1	−11.8	−11.8	23.6
		Expt [191]				21	−8	−8	16
^{6}MnO	OO-RI-MP2	^{55}Mn	439.3	535.9	535.9	503.7	−64.4	32.2	32.2
	OO-SCS-RI-MP2	^{55}Mn	430.3	511.6	511.6	484.5	−54.2	27.1	27.1
	B2PLYP	^{55}Mn	487.9	556.2	556.2	533.4	−45.5	22.7	22.7
	CCSD(T)[c]	^{55}Mn	425.0	478.4	478.4	460.6	−35.6	17.8	17.8
		Expt [192]	448	496	496	480	−32	16	16
	OO-RI-MP2	^{17}O	−9.2	−9.2	5.3	−4.4	−4.8	−4.8	9.6
	OO-SCS-RI-MP2	^{17}O	−11.3	−11.3	5.0	−5.8	−5.4	−5.4	10.9
	B2PLYP	^{17}O	−14.0	−14.0	3.4	−8.2	−5.8	−5.8	11.7
	CCSD(T)[c]	^{17}O	−16.6	−16.6	9.5	−7.9	−8.7	−8.7	17.4

Naphthalene Anion

In order to demonstrate the applicability of the OO-MP2 methods to larger molecules, we have calculated the naphthalene anion and collected the results in Table 5.20. For these calculations an augmented EPR-III [165] basis set was employed, which contains additional core polarization functions (2s2p1d) for all carbon atoms. The hydrogen and carbon atoms are numbered according to Fig. 5.7. The RI-MP2 method can neither reproduce the carbon nor the hydrogen hfccs correctly. Both OO-MP2 methods

[b] CCSD(T) results employing a (21s15p10d3f+2s)/[15s10p6d2f] basis set are taken from Ref. [164]
[c] CCSD(T) results employing a (15s11p6d)/[9s7p4d] basis set are taken from Ref. [164]

underestimate the isotropic hfccs for C_2 and C_5 by about 5 MHz, and overestimate the hfccs for C_3 and C_4 by ∼2.5 MHz in magnitude. However, the hydrogen hfccs are in excellent agreement with experiment, considering that no vibrational corrections are taken into account.

The carbon hfccs are best described by the B2PLYP functional and the error in the hydrogen hfccs is also small.

Table 5.20.: Isotropic Hyperfine Coupling Constants of the Naphthalene anion in [MHz]. $\langle S^2 \rangle$ values for the different methods are (0.785493).(0.865290).(0.750170).(0.750087).

atom	$A^{(A;c)}$				
	RI-MP2	OO-RI-MP2	OO-SCS-RI-MP2	RI-B2PLYP	Expt.
C_2	−5.33	13.68	13.87	18.21	(−)19.9 [193]
C_5	−9.62	13.76	13.96	18.26	
C_3	−5.06	−5.69	−5.71	−3.55	−3.4 [193]
C_4	2.41	−5.94	−6.01	−3.79	
H_7	−5.43	−14.76	−12.91	−15.27	−13.9 [194]
H_{10}	−3.29	−14.77	−12.94	−15.28	
H_8	−7.61	−6.93	−5.91	−6.01	−5.1 [194]
H_9	−11.55	−6.75	−5.72	−5.85	

In Table 5.21 the calculated Mulliken spin populations are shown. The spin populations for the carbon atoms differ by ∼2−4% for the OO-MP2 methods compared to the B2PLYP functional. This difference is reflected in the corresponding isotropic hfccs. The deviations for the H_7 and H_{10} atoms are considerably smaller, but for H_8 and H_9 the spin populations vary by 4−5%. Interestingly, contrary to many qualitative discussions, the hydrogen spin populations do not correlate well with the corresponding isotropic hfccs.

Table 5.21.: Mulliken spin populations in (%).

atom	$\rho^{(A)}$		
	OO-RI-MP2	OO-SCS-RI-MP2	RI-B2PLYP
C_2	21.1	21.3	21.8
C_5	21.2	21.4	21.8
C_3	9.0	8.6	8.0
C_4	8.7	8.3	7.8
H_7	−1.8	−1.7	−1.6
H_{10}	−1.8	−1.7	−1.6
H_8	−0.9	−0.9	−0.7
H_9	−0.9	−0.8	−0.6

In conclusion, the B2PLYP functional performs best for the hfccs of the naphthalene anion radical, followed by the OO-SCS-RI-MP2 method. The RI-MP2 method fails completely for the prediction of naphthalene anion hfccs.

Quinone Radical Anion

An even larger example, solvated quinones, is studied in this subsection. These systems were studied experimentally and theoretically (with the B3LYP functional) in Ref. [69]. Specifically, we recalculated the hfccs of the *p*-benzosemiquinone radical anion ($BQ^{\bullet-}$) coordinated with one, two, four and 20 deuterated water molecules employing the double-hybrid functional B2PLYP as well as the OO-RI-MP2 method and its SCS-variant. The structures of $BQ^{\bullet-}$ coordinated with one and two water molecules were optimized with the TPSS meta-GGA functional [67] and a basis set of triple-ζ quality (TZVP [64, 68]). The reference structures of Ref. [69] were used for the four and 20 water coordinated $BQ^{\bullet-}$.

For the calculation of the hfccs Barone's EPR-III basis set [165] in combination with the def2-TZVPP/JK [92] auxiliary basis set was employed. Furthermore, core polarization functions (2s2p1d) for first row elements were added to the one-electron basis and the auxiliary basis set was decontracted. For the $BQ^{\bullet-}$ coordinated with 20 water molecules, the EPR-III basis set was only employed for all carbon atoms and for the bridging hydrogens. A split-valence basis plus polarization functions (SVP [64, 85]) was used otherwise. The RIJCOSX [39] approximation was applied in both OO-MP2 methods, whereas the RI approximation was employed for the B2PLYP calculations.

The single point calculation of the $BQ^{\bullet-}$ solvated with 20 D_2O molecules and an orbital basis of 1890 basis functions as well as an auxiliary basis of dimension 3596 was computed on 16 processors and took roughly 4 days to complete.

In Table 5.22 the calculated hfccs for the bridging ^2H atoms are listed. The dipolar hfccs are generally slightly underestimated in magnitude by the OO-MP2 methods and decrease with increasing number of D_2O molecules. The B2PLYP functional slightly overestimates the magnitude of the anisotropic hfccs, but the trend with increasing solvent molecules is the same as for the OO-MP2 methods. The isotropic hfccs are excellently predicted by the OO-RI-MP2 method as well as by the B2PLYP functional. The SCS-variant of the OO-RI-MP2 method slightly overestimates the isotropic contribution but still yields predictions of excellent quality. The $BQ^{\bullet-}$ solvated with 20 D_2O molecules represents the most realistic model, and the calculated hfccs are in good agreement with experiment. All tested methods perform very well in this respect with B2PLYP being perhaps the most successful method tested here.

Table 5.22.: Calculated ^2H hfccs in [MHz] of $BQ^{\bullet-}$ in coordination with one, two, four and 20 water (D_2O) molecules (P_D=81.8989 MHz/au^3). Comparison with experimental results.

method		number of water molecules				
		one	two	four	20	Expt.
OO-RI-MP2	$A_{11}^{(A;d)}$	−0.46	−0.46	−0.44	−0.47	−0.49
	$A_{22}^{(A;d)}$	−0.43	−0.43	−0.40	−0.41	−0.47
	$A_{33}^{(A;d)}$	0.89	0.87	0.84	0.88	0.95
	$A^{(A;c)}$	0.02	0.03	0.04	0.01	0.03
OO-SCS-RI-MP2	$A_{11}^{(A;d)}$	−0.44	−0.44	−0.42	−0.46	−0.49
	$A_{22}^{(A;d)}$	−0.42	−0.41	−0.39	−0.40	−0.47
	$A_{33}^{(A;d)}$	0.86	0.85	0.82	0.86	0.95
	$A^{(A;c)}$	0.08	0.08	0.08	0.07	0.03
RI-B2PLYP	$A_{11}^{(A;d)}$	−0.50	−0.50	−0.48	−0.51	−0.49
	$A_{22}^{(A;d)}$	−0.48	−0.46	−0.44	−0.44	−0.47
	$A_{33}^{(A;d)}$	0.98	0.96	0.92	0.95	0.95
	$A^{(A;c)}$	0.01	0.02	0.03	0.00	0.03

5.3.5. Discussion

In this section, the orbital-optimized MP2 method was evaluated for the calculation of hyperfine coupling constants. The method was benchmarked for a series of small radicals and transition metal compounds and compared to CCSD(T) reference results. The resulting isotropic hfccs are almost of CCSD quality but are obtained with only iterative $\mathcal{O}(N^5)$ effort. The dipolar contribution to the hfccs are, however, less well predicted by the OO-MP2 methods. On average, spin-component scaling improves the description of the hfccs for small radicals, whereas the description of the spin density on transition metal nuclei could not be enhanced. Overall, it seems to be the best choice among the wave function based methods.

Of the tested methods OO-MP2 is perhaps slightly inferior to the double-hybrid functional B2PLYP that is also computationally more attractive. We do however, believe that it is highly useful to have a pure wave function based methodology available that is not plagued by self-interaction problems that occasionally can complicate calculations on radicals with extended π-systems. It is of course possible to also optimize the orbitals in the double-hybrid DFT approach. It remains an open question whether this would improve the results in a similar way as OO-MP2 improves upon MP2. Work in this direction is in progress.

The spin contamination in the OO-MP2 wave function is drastically reduced compared to the standard UHF wave function. In combination with the RIJCOSX approximation the OO-RI-MP2 method becomes applicable to fairly large systems, as demonstrated for the solvated *p*-benzosemiquinone radical anion where calculations with almost 2000 basis functions have been performed.

From the extensive set of hyperfine coupling constant calculations on small radicals and transition metal complexes it emerges that the OO-MP2 method represents a viable alternative to double-hybrid functionals, although the computational effort for OO-MP2 is considerably higher. Nevertheless, using various approximations discussed in this thesis, the method is still applicable to fairly large molecules.

5.4. The Orbital-Optimized RI-MP2 Gradient

5.4.1. Motivation

In the previous Section 5.3.5 the orbital optimized MP2 approach has shown to provide a reliable description of the electronic structure for a series of open-shell compounds. In the present section the OO-MP2 gradient as example for a basis function dependent first-order property is benchmarked against the more rigorous Coupled Cluster Singles Doubles approach. The influence of the improved description of the electronic structure on the resulting geometrical parameters is investigated. The goal is to obtain structures of CCSD quality at the cost of iterative MP2 theory. The working equations for the OO-MP2 gradient have been derived in Section 2.9.1.

5.4.2. Benchmark of the OO-RI-MP2 Gradient

In this section the performance of the OO-(SCS-)RI-MP2 method is benchmarked for the prediction of geometrical parameters. Therefore, a series of small radicals shown in Fig. 5.8 with complicated electronic structures has been optimized at the CCSD(T) [162] level and the geometrical parameters have been compared to the OO-(SCS-)RI-MP2 methods as well as to routinely applied methods, namely DFT (BP86 [71, 72], B3LYP [71, 195, 196]) and MBPT2. The structures have been optimized employing the TZVPP [66, 68] basis set under tight optimization criteria with the ORCA program package [25]. The

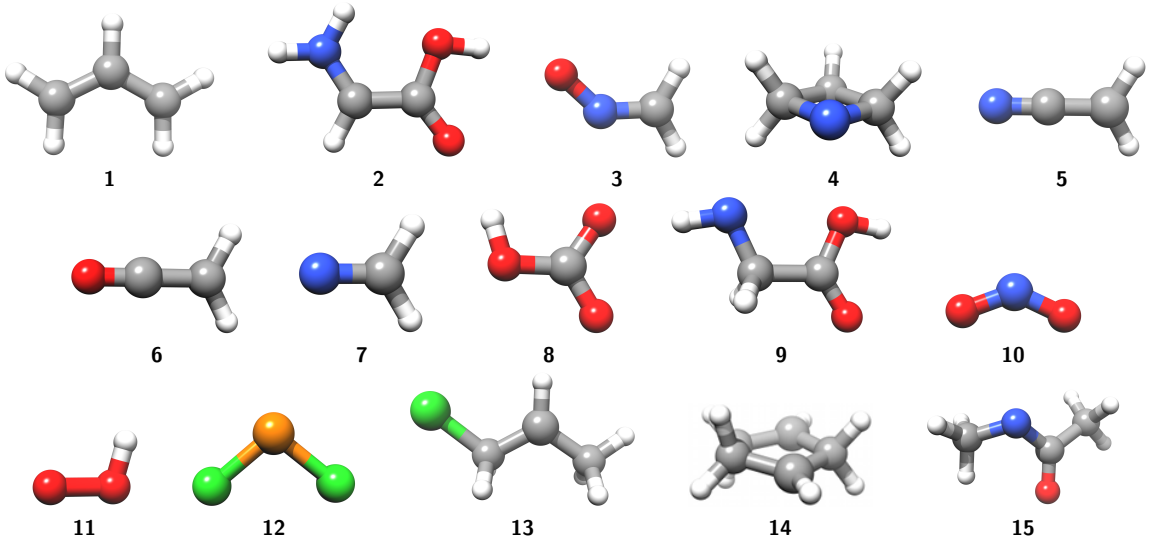

Figure 5.8.: Benchmark set for OO-RI-MP2 gradient calculations (**1**=C_3H_5•, **2**=c-$C_2H_4NO_2$•, **3**=H_2CNO•, **4**=*cyclo*-C_3H_6N•, **5**=H_2C_2N•, **6**=$H_2C_2O^+$•, **7**=H_2CN•, **8**=HCO_3•, **9**=n-$C_2H_4NO_2$•, **10**=NO_2•, **11**=O_2H•, **12**=PCl_2•, **13**=C_3H_6Cl•, **14**=*cyclo*-C_5H_8•, **15**=n-C_3H_7NO•).

energy convergence was chosen to be $10^{-8}E_h$ and 10^{-3} for the orbital gradient. The 'Resolution of the Identity' [22, 37, 38] approximation was employed for the gradient corrected density functional BP86 as well as for all MP2 variants. Since, analytic gradients for the CCSD(T) method are not yet available in the ORCA program package, numerical gradients have been calculated.

The errors in the structural parameters compared to the CCSD(T) reference geometries are listed in Table 5.23. The mean absolute errors in bond lengths for the gradient corrected density functional BP86, which is known to provide reliable structures for systems with negligible dispersion interactions, is about $\sim$1$-$1.5 pm. The only exception represents the phosphorus dichloride radical (**12**) whose structure was described worse. The B3LYP hybrid density functional performs considerably better than the BP86 functional. The mean errors in bond lengths are in few cases close to zero, whereas the corresponding mean absolute error is comparable to the OO-MP2 methods. Nevertheless, B3LYP demonstrates once again that it benefits from an enormous error compensation, but has, just like BP86, three outliers with mean absolute errors $>$1.5 pm. The maximum error in bond lengths, which is at the same time the overall maximum error of $\sim$7 pm for all methods, is obtained for the formaldiminoxy radical (**3**). Analogous conclusions can be drawn for the deviations in the bond angles.

The averaged mean absolute error for the RI-MP2 method is $\sim$1 pm, and the corresponding error range is 0.5$-$2.6 pm. The bond lengths are overall too short and the largest errors occur for the 1-chloro-2-propyl radical (**13**). The mean absolute errors for OO-RI-MP2 are $\sim$1 pm as well, whereas spin-component scaling reduces the error to $\sim$0.75 pm. The bond lengths of the nitrogen dioxide radical (**10**) are considerably too long, but there is no consistent trend observable. The mean absolute error in the bond angles is for all methods about 1 degree, which represents a satisfactory result. A graphical representation of the mean absolute errors in the structural parameters is shown is Fig. 5.9. In general, it turns out that orbital optimization has only a minor influence on the geometrical structures.

Table 5.23.: Statistical analysis of errors in the optimized geometries of molecules **1**-**15** from the BP86, RI-MP2 and OO-(SCS-)RI-MP2 methods compared to the reference CCSD(T) method. Errors are given relative to the parent MP2 method. All calculations were done with the TZVPP basis set (distances in pm, angles in degrees).[a]

		$\Delta^{\text{mean}}_{\text{distances}}$	$\lvert\Delta\rvert^{\text{mean absolute}}_{\text{distances}}$	$\lvert\Delta\rvert^{\text{max}}_{\text{distances}}$	$\Delta^{\text{mean}}_{\text{angles}}$	$\lvert\Delta\rvert^{\text{mean absolute}}_{\text{angles}}$	$\lvert\Delta\rvert^{\text{max}}_{\text{angles}}$
1	BP86	0.673	0.673	1.010	0.001	0.452	1.010
	B3LYP	−0.084	0.221	0.540	0.002	0.447	0.950
	RI-MP2	−0.863	0.863	1.610	−0.000	0.047	0.070
	OO-RI-MP2	−0.456	0.456	0.530	−0.000	0.100	0.200
	OO-SCS-RI-MP2	−0.359	0.359	0.370	−0.001	0.050	0.100
2	BP86	0.885	1.012	2.250	0.531	0.695	2.120
	B3LYP	−0.006	0.411	0.910	0.770	0.966	2.300
	RI-MP2	−0.504	0.531	1.520	0.433	0.729	1.650
	OO-RI-MP2	0.011	0.464	0.780	0.037	0.319	0.850
	OO-SCS-RI-MP2	0.029	0.284	0.560	−0.001	0.143	0.330
3	BP86	0.820	0.820	1.080	0.512	0.772	2.040
	B3LYP	3.108	3.108	6.990	−5.553	5.932	22.200
	RI-MP2	−1.838	1.838	4.340	1.672	1.962	6.690
	OO-RI-MP2	0.277	0.683	1.400	0.390	0.830	1.560
	OO-SCS-RI-MP2	0.207	0.572	1.360	0.262	0.602	1.050
4	BP86	0.659	0.677	1.150	0.027	0.375	1.170
	B3LYP	−0.019	0.251	0.540	0.031	0.232	0.680
	RI-MP2	−0.709	0.709	1.120	−0.004	0.066	0.250
	OO-RI-MP2	−0.617	0.617	1.030	−0.003	0.094	0.290
	OO-SCS-RI-MP2	−0.373	0.373	0.450	−0.005	0.041	0.110
5	BP86	0.387	1.148	1.520	0.000	0.687	1.030
	B3LYP	−0.413	0.612	1.760	0.000	0.580	0.870
	RI-MP2	−0.817	1.438	3.170	0.000	0.360	0.540
	OO-RI-MP2	0.027	0.633	1.320	−0.003	0.137	0.210
	OO-SCS-RI-MP2	0.058	0.448	0.830	0.003	0.077	0.110
6	BP86	0.450	1.320	1.740	−0.003	1.377	2.070
	B3LYP	−0.367	0.717	1.980	0.000	1.180	1.770
	RI-MP2	−0.425	0.525	0.820	0.000	0.040	0.060
	OO-RI-MP2	−0.065	0.760	1.390	0.000	0.253	0.380
	OO-SCS-RI-MP2	−0.075	0.500	0.850	0.000	0.133	0.200
7	BP86	0.860	1.033	1.420	0.003	0.943	1.410
	B3LYP	−0.050	0.610	0.990	0.000	0.560	0.840
	RI-MP2	−1.563	1.563	3.790	−0.003	0.010	0.010
	OO-RI-MP2	−0.213	0.213	0.270	−0.003	0.203	0.310
	OO-SCS-RI-MP2	−0.197	0.257	0.340	0.003	0.010	0.010
8	BP86	1.185	1.185	2.150	0.137	1.372	2.470
	B3LYP	0.098	0.893	1.600	0.320	1.630	2.620
	RI-MP2	−0.257	0.257	0.500	−0.040	0.155	0.210
	OO-RI-MP2	0.802	0.802	2.030	−0.155	1.350	2.390
	OO-SCS-RI-MP2	0.537	0.747	1.880	−0.122	1.283	2.310

[a] N(distances) for molecules **1**-**15**=7.8.4.10.4.4.3.4.8.2.2.2.9.13.10, N(angles) for molecules **1**-**15**=9.10.4.19.3.3.3.4.11.1.1.1.15.24.16.

Continued.

		$\lvert\Delta^{\text{mean}}_{\text{distances}}\rvert$	$\lvert\Delta^{\text{mean absolute}}_{\text{distances}}\rvert$	$\lvert\Delta^{\text{max}}_{\text{distances}}\rvert$	$\lvert\Delta^{\text{mean}}_{\text{angles}}\rvert$	$\lvert\Delta^{\text{mean absolute}}_{\text{angles}}\rvert$	$\lvert\Delta^{\text{max}}_{\text{angles}}\rvert$
9	BP86	0.925	1.077	1.380	−0.018	0.482	1.750
	B3LYP	0.063	0.330	0.780	0.154	0.452	1.310
	RI-MP2	−0.464	0.476	0.930	0.025	0.125	0.440
	OO-RI-MP2	−0.170	0.562	1.090	−0.055	0.263	0.860
	OO-SCS-RI-MP2	−0.067	0.348	0.500	−0.017	0.128	0.360
10	BP86	1.005	1.005	1.010	−0.410	0.410	0.410
	B3LYP	−0.465	0.465	0.470	0.060	0.060	0.060
	RI-MP2	0.050	0.050	0.060	−0.040	0.040	0.040
	OO-RI-MP2	3.495	3.495	3.500	−0.720	0.720	0.720
	OO-SCS-RI-MP2	2.225	2.225	2.230	−0.420	0.420	0.420
11	BP86	1.495	1.495	1.910	1.160	1.160	1.160
	B3LYP	0.235	0.455	0.690	1.500	1.500	1.500
	RI-MP2	−1.270	1.270	2.480	0.590	0.590	0.590
	OO-RI-MP2	1.150	1.150	1.950	−1.420	1.420	1.420
	OO-SCS-RI-MP2	0.895	0.895	1.590	−1.050	1.050	1.050
12	BP86	3.645	3.645	3.670	1.320	1.320	1.320
	B3LYP	3.085	3.085	3.110	0.960	0.960	0.960
	RI-MP2	−1.550	1.550	1.550	−0.230	0.230	0.230
	OO-RI-MP2	−1.100	1.100	1.100	0.030	0.030	0.030
	OO-SCS-RI-MP2	−0.430	0.430	0.430	−0.020	0.020	0.020
13	BP86	−0.997	1.650	5.250	−0.014	1.206	2.710
	B3LYP	−1.634	1.841	5.450	−0.009	1.167	2.630
	RI-MP2	−2.630	2.630	5.910	0.006	0.849	1.900
	OO-RI-MP2	−2.532	2.532	5.940	0.004	0.867	1.890
	OO-SCS-RI-MP2	−2.278	2.278	5.370	0.005	0.919	2.060
14	BP86	0.622	0.800	1.290	0.055	0.398	1.470
	B3LYP	0.012	0.298	0.480	0.046	0.325	1.040
	RI-MP2	−0.695	0.695	0.950	−0.020	0.063	0.170
	OO-RI-MP2	−0.609	0.609	0.990	−0.011	0.102	0.280
	OO-SCS-RI-MP2	−0.380	0.380	0.430	−0.016	0.033	0.070
15	BP86	0.349	1.311	3.920	0.358	1.889	6.320
	B3LYP	0.020	0.240	0.940	0.036	0.966	2.630
	RI-MP2	−0.561	0.561	0.810	−0.055	0.504	1.700
	OO-RI-MP2	−0.602	1.116	3.740	0.203	1.520	3.670
	OO-SCS-RI-MP2	−0.260	0.416	0.780	0.046	0.131	0.780

Timings

The timings for an illustrative gradient calculation with the OO-RI-MP2 method on the example of the adenine-thymine base pair, shown in Fig. 5.10, are listed in Table 5.24. Ahlrichs' TZV [63] basis set augmented by Pople's 2p and 2d polarization functions [10, 197, 198] for first and second row elements, respectively, has been chosen. The energy convergence criteria was chosen to be 10^{-7} E_h and the threshold for the orbital gradient was 10^{-3}.

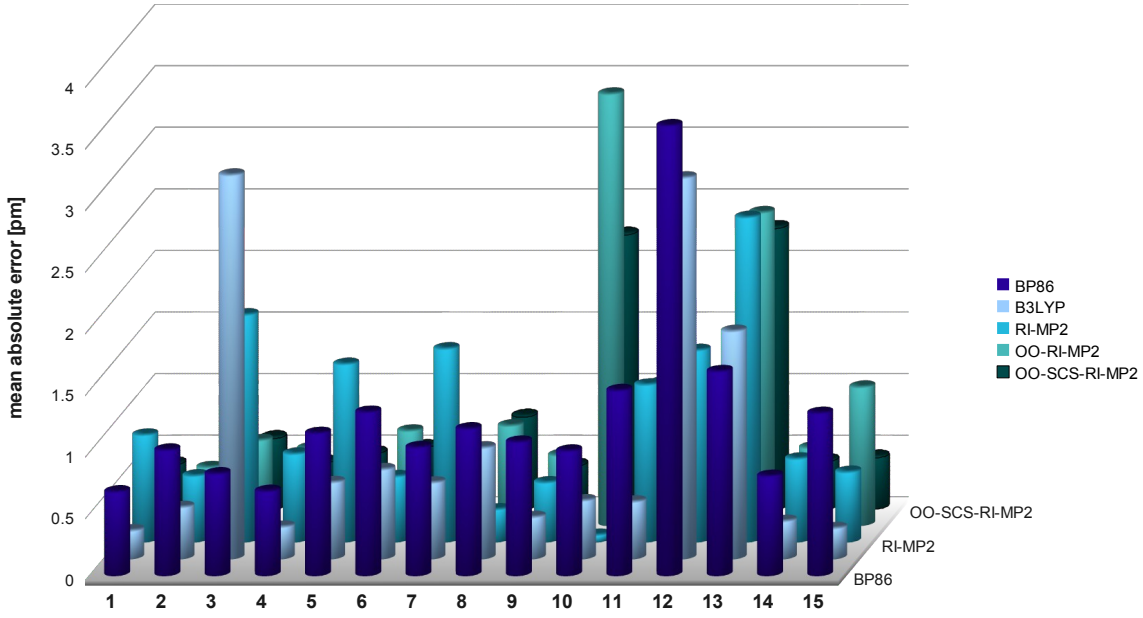

(a) Mean absolute errors in bond lengths for molecules **1**-**15**.

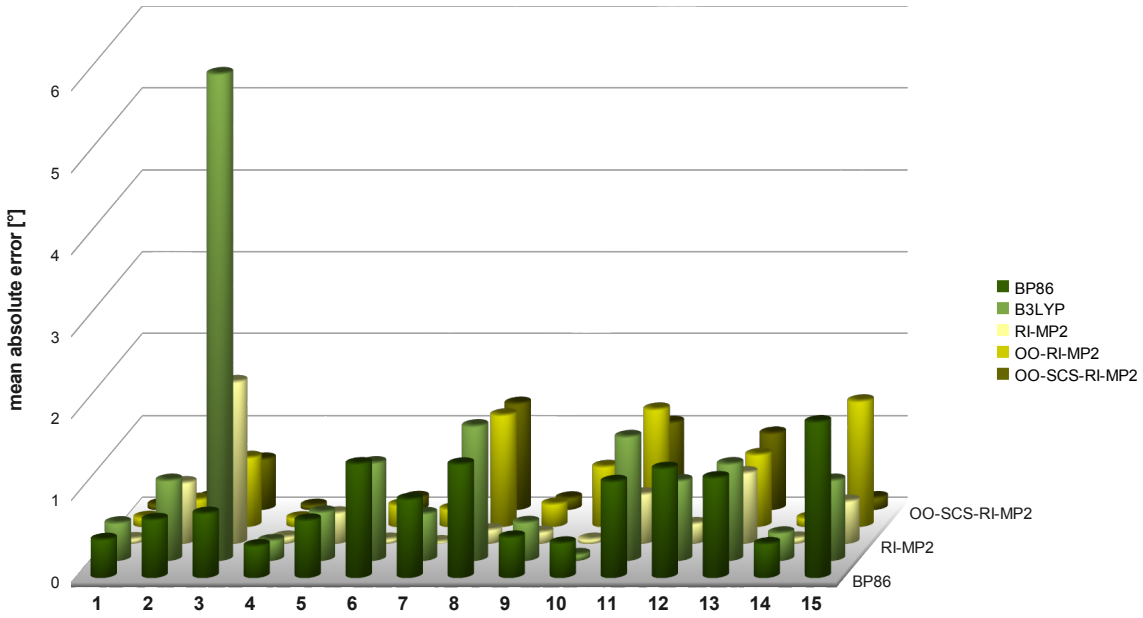

(b) Mean absolute error in bond angles for molecules **1**-**15**.

Figure 5.9.: Graphical representation of the mean absolute errors in the structural parameters.

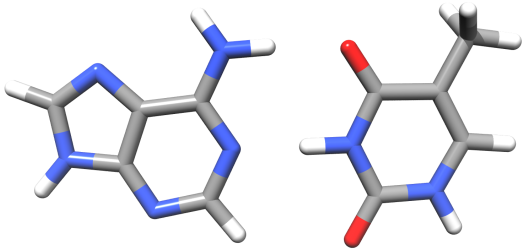

Figure 5.10.: Adenine-Thymine (AT) base pair (30 atoms).

The timings presented in Table 5.24 nicley reflect the iterative nature of the OO-RI-MP2 method. The time required for the solution of the SCF equations is saved, and is replaced by the cost of an iterative solution of the OO-MP2 equations. The calculation of the OO-RI-MP2 gradient takes ∼3.5 times as long as the evaluation of the RI-MP2 gradient. The time-consuming solution of the z-vector equations, required for the calculation of the RI-MP2 relaxed density, is replaced by the much cheaper DIIS step. The evaluation of the gradient is identical for both methods. The RIJCOSX approximation applied to the OO-RI-MP2 method (OO-RIJCOSX-MP2) accelerates the formation of the Fock matrix and the response-type matrix significantly. The calculation of the separable gradient also profits from the semi-numeric exchange gradient treatment, eq. 2.227. Overall, the RIJCOSX approximation yields a speedup of ∼1.2 compared to the parent OO-RI-MP2 method. Further speedup in the solution of the OO-MP2 equations can be obtained by an incremental Fock matrix formation, which is not implemented at the moment.

Table 5.24.: Timings in [s] for one gradient calculation of the AT base pair in a TZV(2d,2p) basis set (555 basis functions).

Gradient Components	RI-MP2	OO-RI-MP2	OO-RIJCOSX-MP2
Solution of SCF eqs.	4464.2	—	—
	(12 cycles)		
Fock matrix construction	—	4015.4	3396.8
Integral Transformation	84.9	1297.3	1204.5
K^{ij}(a,b)	485.8	6876.5	6849.8
T^{ij}(a,b)	21.1	339.0	333.9
D(virtual)	206.6	2931.0	2896.7
D(internal)	116.7	2089.9	2060.2
W(virtual)	412.8	5863.6	5782.4
W(internal)	313.9	4784.6	4718.4
Γ'^{P}_{ai}	478.4	6762.3	6715.7
L(3-ext)	97.2	1511.0	1408.3
L(3-int)	3.0	57.8	49.1
R(D)	330.5	4848.4	708.5
R(z)	330.3	—	—
z-vector solution	2184.6	—	—
DIIS step	—	15.4	11.3
Solution of OO-MP2 eqs.	—	42148.2	36873.4
		(13 cycles)	(13 cycles)
Separable Gradient (S)	2791.5	2791.1	540.1
Non-separable Gradient (NS)	243.3	707.1	759.7

Continued.

Gradient Components	RI-MP2	OO-RI-MP2	OO-RIJCOSX-MP2
Gradient (S + NS)	3034.8	3498.2	1299.8
Total Time	12622.3	45657.3	38190.7

5.4.3. Conclusions

In the present section the performance of the OO-(SCS-)RI-MP2 method is benchmarked for gradient calculations. The relaxed density required for the calculation of the conventional MP2 gradient is obtained by minimizing an extended Hylleraas functional in the OO-MP2 approach. At convergence, the relaxed density matrix and the one obtained as an expectation value over the first-order wave function become identical. The calculation of the OO-MP2 gradient is of the same computational effort as the conventional MP2 gradient, once the OO-MP2 calculation has converged. In general, the OO-RI-MP2 gradient calculation takes about 3−5 times longer than the conventional RI-MP2 calculation, strongly depending on the convergence of the OO-MP2 equations. The mean absolute error in the geometrical parameters amounts to ∼1 pm and ∼1 degree for bond lengths and angles, respectively, compared to CCSD(T) results. Spin-component scaling reduces the error in the bond lengths to ∼0.75 pm. Therefore, the OO-SCS-RI-MP2 structures are superior to the geometries obtained with conventional DFT methods. Nevertheless, the high computational effort of the OO-MP2 methods make them only routinely applicable for medium sized molecules with basis sets of at most triple-ζ quality.

5.5. Calculation of RI-MP2 Second-Order Molecular Properties

5.5.1. Polarizabilities

In Table 5.25 calculated and experimental static isotropic polarizabilities for a series of small organic compounds are listed. The theory for the calculation of static polarizabilities has been already discussed in Section 4.1.1. The polarizabilities have been calculated with two *ab initio* methods, i.e. Hartree-Fock and MP2, as well as with density functional theory employing a hybrid functional (B3LYP [71, 195, 196]) and a double-hybrid functional (B2PLYP [1]). The 'Resolution of the Identity' approximation was employed throughout the calculation of the MP2 correction. [21] The structures have been optimized at the RI-MP2/TZVP [64, 68] level. A polarized triple-ζ (TZVPP [66, 70]) and a quadruple-ζ (QZVP [66, 135]) basis set have been used for the property calculations. The energy convergence criterion was set to 10^{-10} E_h.

Table 5.25.: Calculated and experimental isotropic polarizabilities for a series of small organic compounds in [au]. Structures have been optimized at the RI-MP2/TZVP level.

Molecule	TZVPP				QZVP				Expt.[a]
	HF	B3LYP	RI-B2PLYP	RI-MP2	HF	B3LYP	RI-B2PLYP	RI-MP2	
CH_4	14.87	15.55	15.34	15.11	15.34	16.16	15.93	15.69	16.52
C_2H_2	20.31	20.43	20.04	19.44	21.79	22.02	21.57	20.89	23.53
C_2H_4	25.42	25.41	25.08	24.46	26.49	26.55	26.21	25.60	28.26
C_2H_6	26.31	27.58	27.25	26.92	26.82	28.32	27.95	27.58	28.52

Continued.

Molecule	TZVPP				QZVP				Expt.[a]
	HF	B3LYP	RI-B2PLYP	RI-MP2	HF	B3LYP	RI-B2PLYP	RI-MP2	
C_3H_4	32.77	34.00	33.29	32.38	34.29	35.73	34.93	33.94	41.76
cyclo-C_3H_6	33.92	35.30	35.01	34.75	34.46	36.15	35.83	35.55	38.06
C_3H_8	37.63	39.74	39.24	38.75	38.28	40.72	40.16	39.63	39.96
1-Butyne	44.63	46.72	45.81	44.71	46.25	48.60	47.61	46.44	50.07
1-Butene	48.90	50.47	49.76	48.74	50.15	52.02	51.27	50.21	53.85
trans-2-Butene	49.06	50.95	50.13	48.96	50.20	52.39	51.54	50.35	57.36
C_6H_6	64.12	65.71	65.22	64.55	66.25	67.90	67.44	66.80	67.57
cyclo-C_6H_{12}	66.11	70.00	69.25	68.57	66.85	71.22	70.39	69.65	74.32
CH_3OH	18.13	19.32	19.08	18.83	18.92	20.35	20.10	19.84	20.79
CH_3CHO	26.34	28.33	27.98	27.53	27.28	29.61	29.21	28.71	28.87
C_2H_5OH	29.57	31.64	31.22	30.78	30.45	32.86	32.41	31.95	34.50
MD	−4.39	−2.85	−3.35	−3.96	−3.34	−1.56	−2.09	−2.74	
MAD	4.39	2.85	3.35	3.96	3.34	1.80	2.16	2.74	
RMSE	4.96	3.50	4.00	4.64	4.01	2.44	2.91	3.55	

All of the employed methods tend to underestimate the static polarizabilities, which is reflected in the negative mean deviation (Table 5.25) and a mean absolute deviation, that is almost of the same magnitude. Hartree-Fock performs worst for the prediction of isotropic polarizabilities and the inclusion of dynamic correlation effects can not significantly improve the results. This is the case for both tested basis sets and has also been reported in Ref. [199]. Both density functionals outperform the *ab initio* methods, whereas the famous B3LYP demonstrates again its success when applied to simple organic compounds. Although, the B2PLYP results deviate by ∼0.5 au compared to the B3LYP hybrid functional, the values are still reasonable.

5.5.2. Calculation of g-tensors

In electron paramagnetic resonance spectroscopy it is common to interpret the experimental results in terms of a spin Hamiltonian. The ESR spin Hamiltonian $\mathcal{H}_S^{ESR}$ describes a model spin system which magnetic sublevels of the ground-state configuration $\mathcal{E}_n$ can be determined by solving eq. 5.20 in the basis of electron spin functions Θ_n. [200, 201]

$$\mathcal{H}_S^{ESR}\Theta_n = \mathcal{E}_n\Theta_n \tag{5.20}$$

The basic spin Hamiltonian used in ESR spectroscopy is most commonly written as,

$$\mathcal{H}_S^{ESR} = \vec{\mathcal{S}}\mathbf{D}\vec{\mathcal{S}} + \beta_e\vec{\mathcal{B}}\mathbf{g}\vec{\mathcal{S}} + \sum_A \vec{\mathcal{S}}\mathbf{A}^A\vec{\mathcal{I}}^A \tag{5.21}$$

where $\vec{\mathcal{S}}$ is the total electron spin, $\vec{\mathcal{I}}^A$ is the nuclear spin of atom A and $\vec{\mathcal{B}}$ represents the magnetic field. β_e is Bohr's magneton. The first term in eq. 5.21 refers to the electron spin-spin dipolar interaction in systems with more than one unpaired electron. The term is known as the zero-field splitting involving the

[a] Experimental results were taken from Ref. [199]

correspondent tensor. The last term in eq. 5.21 describes the interaction between electron and nuclear spin (hyperfine interaction), which is parameterized by the hyperfine coupling tensor $\mathbf{A}^A$. The quantity of interest in the actual section is the electronic g-tensor, which characterizes the electron Zeeman interaction between the total electron spin and the magnetic field. The expansion of the total energy in terms of the magnetic field, the total electron spin and the nuclear spins, yields,

$$E(\vec{\mathcal{B}},\vec{\mathcal{S}},\{\vec{\mathcal{I}}^A\}) = E_0 + \frac{1}{2}\sum_{\kappa\tau}\mathcal{S}_\kappa^T \left.\frac{\partial^2 E}{\partial\mathcal{S}_\kappa\partial\mathcal{S}_\tau}\right|_{|\mathcal{S}|=0}\mathcal{S}_\tau + \sum_{\kappa\tau}\mathcal{B}_\kappa^T \left.\frac{1}{\beta_e}\frac{\partial^2 E}{\partial\mathcal{B}_\kappa\partial\mathcal{S}_\tau}\right|_{|\mathcal{B}|=0,|\mathcal{S}|=0}\mathcal{S}_\tau + \sum_A\sum_{\kappa\tau}\vec{\mathcal{S}}_\kappa^T \left.\frac{\partial^2 E}{\partial\mathcal{S}_\kappa\partial\mathcal{I}_\tau^A}\right|_{|\mathcal{S}|=0,|\mathcal{I}|=0}\mathcal{I}_\tau^A. \tag{5.22}$$

By comparing eq. 5.22 with the spin Hamiltonian in eq. 5.21, the g-tensor can be identified as second energy derivative w.r.t. the total electron spin and the magnetic field (eq. 5.23).

$$g_{\kappa\tau} = \left.\frac{1}{\beta_e}\frac{\partial^2 E}{\partial\mathcal{B}_\kappa\partial\mathcal{S}_\tau}\right|_{|\mathcal{B}|=0,|\mathcal{S}|=0} \tag{5.23}$$

The following one-electron expressions for the g-tensor can be derived by connecting the terms present in the Breit-Pauli Hamiltonian to the parameters of the spin Hamiltonian. [201]

$$g_{\kappa\tau} = g_e\delta_{\kappa\tau} + \Delta g^{RMC}\delta_{\kappa\tau} + \Delta g^{GC}_{\kappa\tau} + \Delta g^{OZ/SOC}_{\kappa\tau} \tag{5.24}$$

$$\Delta g^{RMC} = -\frac{\alpha^2}{S}\sum_{\mu\nu}P^{\alpha-\beta}_{\mu\nu}\left\langle\varphi_\mu\left|\vec{\nabla}^2\right|\varphi_\nu\right\rangle \tag{5.25}$$

$$\Delta g^{GC}_{\kappa\tau} = \frac{1}{2S}\sum_{\mu\nu}P^{\alpha-\beta}_{\mu\nu}\left\langle\varphi_\mu\left|\sum_A\frac{Z_A}{r_A^{-3}}\left\{\mathbf{r}_A\mathbf{r}_O - r_{A,\kappa}r_{O,\tau}\right\}\right|\varphi_\nu\right\rangle \tag{5.26}$$

$$\Delta g^{OZ/SOC}_{\kappa\tau} = -\frac{1}{2S}\sum_{\mu\nu}\frac{\partial P^{\alpha-\beta}_{\mu\nu}}{\partial B_\kappa}\left\langle\varphi_\mu\left|\hat{h}^{SOC}_\tau\right|\varphi_\nu\right\rangle \tag{5.27}$$

The g-value of the free electron is,

$$g_e = 2.002319304386(20) \tag{5.28}$$

the second and third terms in eq. 5.24 are both first-order quantities, namely, the reduced mass correction and the gauge correction. The cross term between the spin-orbit coupling and orbital Zeeman interactions is a true response property. Note, that the perturbed operators are given in the form of the corresponding one-electron operators. The SOC operator, however, is a two-electron quantity, which is approximated here by an effective one-electron operator.

5.5.3. Numerical results for g-tensors

Table 5.26 lists the electronic g-shifts for a series of small radicals. Structures and CCSD reference data have been taken from Ref. [202]. Calculations have been performed at Hartree-Fock, MP2 and DFT levels of theory. In the MP2 framework g-tensors for both introduced derivative approaches analyzed in Section 2.6 are shown ('$\mathfrak{Re}/\mathfrak{Im}$' and '$\mathfrak{Im}/\mathfrak{Im}$'). For the DFT calculations the hybrid functional B3LYP [71, 195, 196] and the two double-hybrids B2PLYP [1] and B2K-PLYP [203] have been employed. The B2K-PLYP functional differs from the B2PLYP functional in incorporating a higher amount of exact exchange and MP2 correlation, respectively. Furthermore, Grimme's dispersion correction [204] is by

default added to the B2K-PLYP single point energy. The 'Resolution of the Identity' approximation was employed throughout the calculation of the MP2 correction. [21] All calculations were carried out using Dunning's aug-cc-pVTZ [65] with the corresponding auxiliary basis functions. The energy convergence criterion was set to 10^{-10} E_h and a large Lebedev-770 angular grid in combination with a radial integration accuracy of 5.650 (Grid7) has been employed in the DFT calculations. An effective one-electron spin-orbit operator has been used in all calculations. [205, 206]

As has been pointed out in Ref. [202] the g-tensor is in contrast to the chemical shielding tensor a global property and therefore, suffers less from the gauge-origin problem. In the following calculations the center of electronic charge was chosen as the common gauge origin.

Table 5.26.: Comparison of HF, DFT, MP2 and CCSD results for the electronic g-shift (relative to the g-value of the free electron) in [ppm] for various radicals.

		CCSD	RI-MP2		HF	DFT		
molecule	component	$\mathfrak{Re}/\mathfrak{Im}$	$\mathfrak{Im}/\mathfrak{Im}$	$\mathfrak{Re}/\mathfrak{Im}$		B3LYP	B2PLYP	B2K-PLYP
CN ($^2\sum^+$)	Δg_{xx}	−2151	−2160	−2249	−2237	−2193	−2113	−2243
	Δg_{zz}	−126	−83	−157	−81	−134	−124	−117
CO^+ ($^2\sum^+$)	Δg_{xx}	−2576	−1628	−1794	−3225	−2656	−2503	−2431
	Δg_{zz}	−125	−67	−216	−63	−133	−120	−113
BO ($^2\sum^+$)	Δg_{xx}	−1833	−1323	−1402	−2113	−1857	−1787	−1755
	Δg_{zz}	−61	−29	−103	−27	−68	−60	−56
NH ($^3\sum^-$)	Δg_{xx}	1451	1401	1407	1133	1363	1399	1408
	Δg_{zz}	−105	−110	−105	−109	−106	−107	−108
OH^+ ($^3\sum^-$)	Δg_{xx}	4101	4006	4013	3405	3704	3879	3948
	Δg_{zz}	−173	−179	−173	−178	−174	−175	−176
H_2O^+ ($^2B_1$)	Δg_{xx}	−188	−233	−212	−155	−188	−196	−198
	Δg_{yy}	16550	15997	16018	13123	13574	14647	15161
	Δg_{zz}	4905	4836	4856	4052	4681	4764	4783
CH_3 ($^2A''$)	Δg_{xx}	−85	−92	−83	−84	−89	−89	−89
	Δg_{zz}	636	621	628	506	649	640	633
O_2 ($^3\sum_g^-$)	Δg_{xx}	2853	2002	2048	3497	2677	2490	2493
	Δg_{zz}	−201	−229	−187	−232	−199	−211	−215
O_3^- ($^2B_1$)	Δg_{xx}	−662	453	566	−1502	−555	−551	−520
	Δg_{yy}	20276	29475	29541	23770	18429	16343	17272
	Δg_{zz}	12376	16643	16754	16102	11032	8985	9413
CO_2^- ($^2A_1$)	Δg_{xx}	914	550	571	1048	932	770	777
	Δg_{yy}	−5176	−5327	−5305	−5709	−5122	−5033	−5157
	Δg_{zz}	−758	−760	−730	−927	−716	−748	−762
H_2CO^+ ($^2B_2$)	Δg_{xx}	6270	6730	6763	5806	5910	6085	6249
	Δg_{yy}	145	−184	−150	662	91	41	48
	Δg_{zz}	945	1805	1834	3093	24	476	904
NO_2 ($^2A_1$)	Δg_{xx}	3677	2906	2932	4278	3628	3297	3307
	Δg_{yy}	−11952	−11313	−11288	−12588	−11837	−11280	−11389
	Δg_{zz}	−730	−315	−278	−1195	−695	−725	−721
NF_2 ($^2B_1$)	Δg_{xx}	−694	−529	−531	−1035	−667	−666	−670
	Δg_{yy}	6832	6880	6869	5768	6988	6774	6782
	Δg_{zz}	3858	3825	3821	2885	4126	3932	3864

Continued.

		CCSD	RI-MP2		HF	DFT		
molecule	component	$\mathfrak{Re}/\mathfrak{Im}$	$\mathfrak{Im}/\mathfrak{Im}$	$\mathfrak{Re}/\mathfrak{Im}$		B3LYP	B2PLYP	B2K-PLYP
NF_3^+ ($^2A_2''$)	Δg_{xx}	−1990	−1469	−1452	−3667	−1806	−2501	−1944
	Δg_{zz}	5440	6123	6117	4020	5914	5573	5630
MD			488	491	−107	−209	−310	−225
MAD			687	688	779	297	389	298
MAD (%)			31.1	31.0	42.5	9.0	9.6	7.8
Max. Error			9199	9265	3726	2976	3933	3004
RMSE			1794	1811	1263	680	970	776

Indeed, the MP2 results reported in Table 5.26 represent a general improvement over the Hartree-Fock results when compared to the CCSD reference. However, they are greatly inferior to the results provided by all density functionals. The large positive mean deviation is somewhat misleading, because it is mostly affected by the large overestimation of the g-shift in the O_3^- radical. In fact, there is no general trend observable for the RI-MP2 method. The differences in the calculated g-shifts arising from the two distinct approaches to MP2 second derivatives are typically in the range of $\leq$100 ppm. This might be due to the minor effect of orbital relaxation on the resulting g-shifts. [202]

The DFT results presented in Table 5.26 are outstanding. The astonishing good performance of the B3LYP hybrid functional has been already analyzed in Ref. [202] and it was argued that the Hartree-Fock exchange seems to damp the overestimation of the correlation effects. This appears also to be the case for the double-hybrid functionals, for which the increased amount of exact exchange and MP2 correlation in the B2K-PLYP functional yields the best g-shifts for the actual test set. Although, the root mean square error is somewhat larger compared to B3LYP the percentage mean absolute deviation is the smallest. Comparing B2PLYP with B2K-PLYP the latter performs only slightly better.

Table 5.27.: Comparison of HF, DFT, MP2 and experimental results for the components of the electronic g-tensor (relative to the g-value of the free electron) in [ppt] for various transition metal radicals.

		RI-MP2		HF	DFT			
molecule	component	$\mathfrak{Im}/\mathfrak{Im}$	$\mathfrak{Re}/\mathfrak{Im}$		B3LYP	B2PLYP	B2K-PLYP	Expt.
^{2}ScO	$\Delta g_\perp$	1.5	1.5	−2.9	−0.8	−0.1	0.0	−0.5
	$\Delta g_\parallel$	0.0	0.0	0.0	0.0	0.0	0.0	−0.5
^{7}MnH	$\Delta g_\perp$	−1.9	−1.9	−1.8	−1.4	−1.7	−1.8	−1.3
	$\Delta g_\parallel$	−0.3	−0.3	−0.3	−0.1	−0.3	−0.4	0.0
^{6}MnO	$\Delta g_\perp$	−0.2	−0.2	−1.3	2.1	2.4	2.9	−7.3
	$\Delta g_\parallel$	−0.4	−0.4	−0.4	−0.3	−0.4	−0.4	0.0
^{7}MnF	$\Delta g_\perp$	−1.0	−1.0	−1.0	−0.3	−0.7	−0.8	−3.3
	$\Delta g_\parallel$	−0.4	−0.3	−0.3	−0.3	−0.4	−0.4	−0.3
$^2TiF_3$	$\Delta g_\perp$	−357.8	−357.8	−107.4	−45.7	−88.7	−121.6	−111.9,−123.7
	$\Delta g_\parallel$	−1.3	−1.3	−1.3	−1.3	−1.3	−1.3	−11.1,−3.7
$^2[Cu(NH_3)_4]^{2+}$	$\Delta g_\perp$	142.0	142.0	94.9	42.2	65.4	83.6	47
	$\Delta g_\parallel$	844.2	844.2	469.7	156.1	271.9	365.5	245
$^2[Fe(CO)_5]^+$	$\Delta g_\perp$	217.6	217.8	103.8	56.4	87.3	109.9	80.8
	$\Delta g_\parallel$	−88.9	−88.7	−20.3	−2.6	−7.8	−15.2	5.7

In Table 5.27 few calculated g-shifts of small transition metal compounds are presented. The g-shifts have been calculated employing the RIJCOSX approximation and using an accurate triply polarized basis set, CP(PPP), for the metal nuclei. Unfortunately, for transition metal compounds there is no good test set available. Thus, the results can be only compared to the available experimental data and Table 5.27 can only serve as a rough estimate for the performance of RI-MP2 and DFT methods. Expectedly, the RI-MP2 g-shifts are disastrous. However, it is well-known that MP2 often fails in the description of transition metal compounds. Both MP2 derivative approaches yield similar results, since the introduced effects are one order of magnitude smaller than the scale in Table 5.27. The B2PLYP functional yields fairly good results, whereas the B2K-PLYP overshoots the magnitude of the electronic g-shifts. In summary, the double-hybrid functionals seem to be the preferred choice for the calculation of electronic g-tensors.

6. Application

6.1. 2,3,5,6-Tetrafluorophenylnitren-4-yl and 3,4,5,6-Tetrafluorophenylnitren-2-yl: Two Ground-State Quartet Triradicals

In this section the application of high-level quantum-mechanical methods for the characterization of the electronic structure of two complex organic radicals is reported. The section basically consists of a summary of two articles [207, 208] published in cooperation with the experimental group of Wolfram Sander at the Ruhr University in Bochum. Therefore, we will focus on the computational calculations, which have been performed.

6.1.1. Introduction

Arylnitrenes (**1**; see Scheme 6.2) are important reactive intermediates with triplet ground states and large singlet triplet splittings. Convenient precursors for spectroscopic studies are the corresponding aryl azides **2**, which photochemically or thermally split off N_2 to produce the nitrenes **1**. The kinetics, spectroscopy, and computational chemistry of these intermediates has recently been reviewed. [209] Under the conditions of matrix isolation a major photochemical process that diminishes the yield of nitrenes **1** is the ring expansion to 1,2-didehydroazepines **4**, via benzazirines **3** as intermediates. After many years of intense experimental and theoretical work in this field, the mechanistic details are now well established (see Scheme 6.2).

The introduction of a radical center into phenyl nitrenes **1** can lead to three isomeric nitreno radicals with the radical centers in *ortho, meta*, and *para* position, respectively, cf. Fig. 6.1. The electronic structure of these nitreno radicals is best described as a σ, σ, π-triradical with one unpaired electron located at the nitrogen atom in the σ-plane, one at the radical center of the phenyl ring (also in the σ-plane), and the third unpaired electron delocalized over the π-system and interacting with both unpaired σ-electrons. Density functional calculations predict for *ortho* (*o*) and *para* (*p*) compounds high-spin quartet (Q) ground states, while for the *meta*-nitrene a low-spin doublet (D) ground state is calculated. [210] For *o*- and *p*-nitreno radicals quinoid resonance structures can be formulated, which suggest that these triradicals also have some carbene (cyclohexadienylidene) character (see Scheme 6.1). In contrast, for the *meta*-isomer no such resonance structure is possible. Since both phenyl nitrenes and cyclohexadienylidenes have robust triplet ground states, a quartet state for *o*- and *p*-compounds is energetically favorable, since in this case local high-spin triplet configurations at the formal nitrene and carbene centers are maintained.

A synthetic route to nitreno radicals starts from iodophenyl azides, which on photolysis in low-temperature matrices split off N_2 to give the corresponding phenyl nitrene [211] and subsequently iodine atoms to give the nitreno radical. [212–215] However, phenyl nitrenes are photolabile [216] and easily rearrange to azirines [211] and ketenimines, [217] and cleavage of the C-I bond to form an additional radical

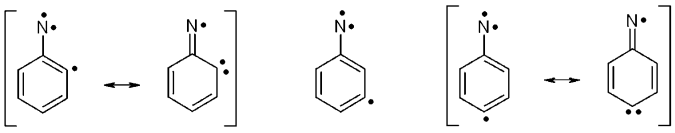

Figure 6.1.: Lewis structures of isomeric nitreno radicals with radical centers in *ortho, meta* and *para* position.

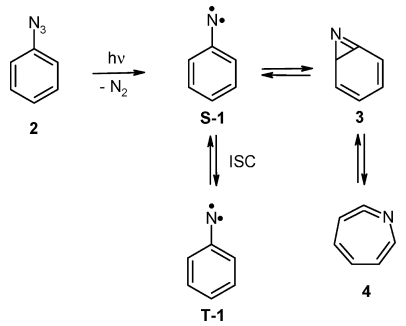

Figure 6.2.: Mechanism of the Rearrangement of Phenylnitrene **1**.

center competes with these rearrangements. Thus, photolysis of matrix-isolated (argon, 10 K) phenyl azide **2** produces mixtures of phenyl nitrene **1**, azirine **3**, and ketenimine **4** in photostationary equilibria, and the yield of nitrene **1** is low (Scheme 6.2). [209] Fluorine substituents in the *ortho* positions of **1** decrease the tendency of these rearrangements, [218–220] and therefore *ortho*-fluorinated phenyl nitrenes are obtained in higher yields under the same conditions. [209, 217, 221] The only nitreno radicals **5** that could be matrix-isolated and spectroscopically characterized are therefore those bearing *ortho*-fluoro substituents. [212, 213, 215] UV photolysis of azide **6a** produces nitrene **7a** together with ketenimine **9a** and nitreno radical **5a** (Scheme 6.3).

Although the yield of **5a** is low, it could be characterized by IR and EPR spectroscopy, which also confirmed its high-spin quartet ground state. In the photolysis mixture of azide **6b**, nitrene **7b**, and its rearranged products, the isomeric azirines **8b** and **8b′** and ketenimines **9b** and **9b′**, were identified (Scheme 6.4). [214] The *meta*-nitreno radical **5b** was not found, but a product of its ring opening and re-addition of iodine, namely, allene **10**, was observed. The radical center in *meta* position of the phenyl nitrene results in a 1,4-diradicaloid structure that has a tendency for β-cleavage. The cleavage is even more pronounced when two radical centers are formed in the two *meta* positions.

In Scheme 6.5 the photochemistry of 2-iodo-3,4,5,6-tetrafluorophenylnitren-2-yl is shown. Analog to **6a** not only the nitreno radical **5c** is built upon irradiation of **6c**, but a mixture of **5c** together with azirine **8c**, ketemine **9c** and the azirinyl radical **11**. **11** can be either formed by rearrangement of **5c** or by loss of an iodine atom from **8c**. The nitreno radical **5c** is only observed in low concentrations.

6.1.2. Electronic Structure Calculations

Theoretical background The EPR properties were calculated according to previously published methods that are implemented in the ORCA package. [25, 153, 222–231] Geometries were optimized using the BP86 functional, [71, 72] the TZVP basis set [70] (featuring a single set of polarization functions on each atom), and the 'Resolution of the Identity' approximation with matching auxiliary basis sets. [22, 30, 96, 232] Structures were verified to represent local minima through numeric frequency cal-

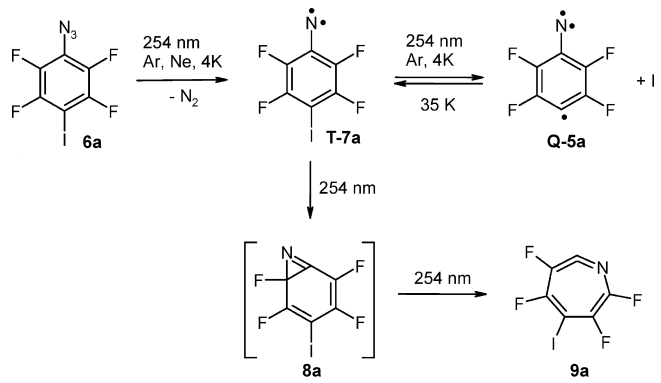

Figure 6.3.: Photochemistry of aryl azide **6a**.

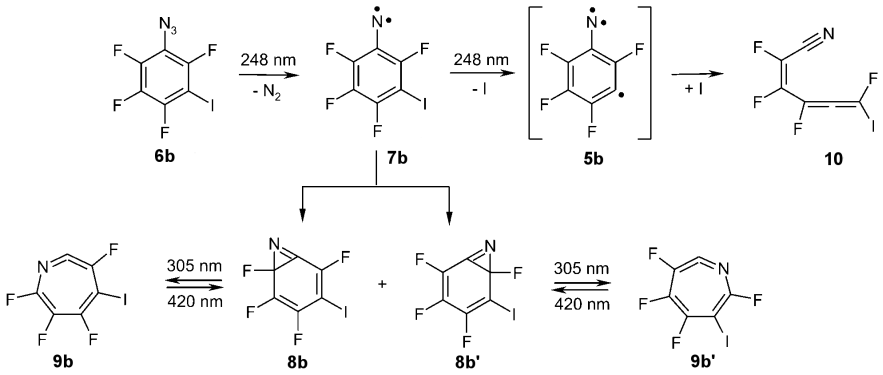

Figure 6.4.: Photochemistry of aryl azide **6b**.

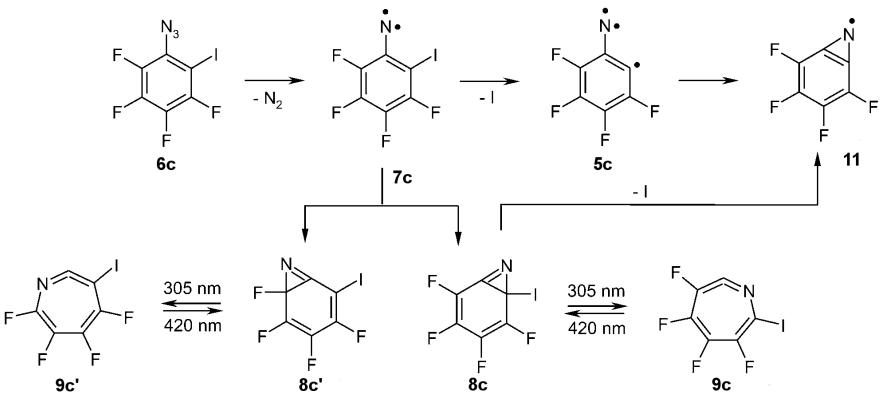

Figure 6.5.: Photochemistry of aryl azide **6c**.

culations. Property calculations were done with the B3LYP hybrid functional [71, 196, 233], because, on average, it has been proven to be superior to non-hybrid functionals in EPR property calculations. In these calculations, a more extensively polarized triple-ζ basis set (TZVPP, amounting to 2d1f polarization shells on all atoms) was used. [70] The spin-spin (SS) contribution to the zero-field splitting (ZFS) tensor was treated in the mean-field approximation based on the Kohn-Sham determinant. The SS contribution is given by [223, 234, 235]

$$D_{kl}^{(SS)} = -\frac{g_e^2}{16}\frac{\alpha^2}{S(2S-1)}\sum_{\mu\nu}\sum_{\kappa\tau}\left\{P_{\mu\nu}^{\alpha-\beta}P_{\kappa\tau}^{\alpha-\beta} - P_{\mu\kappa}^{\alpha-\beta}P_{\nu\tau}^{\alpha-\beta}\right\}\left\langle\mu\nu\left|r_{12}^{-5}\left\{3r_{12,k}r_{12,l}-\delta_{kl}r_{12}^2\right\}\right|\kappa\tau\right\rangle. \quad (6.1)$$

Here, α is the fine structure constant (1/137 in atomic units), g_e is the free-electron g-value (2.002319...), the indices μ, ν, κ, τ refer to atomic basis functions, and $P_{\mu\kappa}^{\alpha-\beta}$ is an element of the spin-density matrix. No approximations have been made to the two-electron spin-spin dipole integrals in eq. 6.1. As discussed previously, [223] it is advantageous to apply an open-shell spin-restricted formalism for this quantity, in conjunction with present-day DFT methods. We have used the spin densities from the spin-unrestricted natural orbital determinant for this purpose, as discussed in detail in the work of Sinnecker and Neese. [223] Second-order SOC contributions also have been treated throughout the study. Following the general formulation, in terms of infinite sums over states, [226] a linear response treatment was recently proposed in which the SOC contribution can be written as [224]

$$D_{kl}^{SOC;M} = f_M(S)\langle\langle h_k^{SOC}; h_l^{SOC}\rangle\rangle. \quad (6.2)$$

In eq. 6.2, M denotes the contributions to the SOC term ($M = 0, \pm1$) from excited states with $S' = S \pm 1$ (where S is the total spin quantum number of the electronic state for which the ZFS tensor is computed ($S > 1/2$)), $f_M(S)$ is a spin-dependent prefactor ($f_0 = -\frac{1}{(4S^2)}$, $f_{-1} = \frac{1}{[2S(2S-1)]}$, $f_{+1} = \frac{1}{[2(S+1)(2S+1)]}$), and $\langle\langle h_k^{SOC}; h_l^{SOC}\rangle\rangle$ is a shortcut notation for a spin-orbit linear response function. In a DFT framework, it is related to the derivatives of generalized spin densities, as explained in detail in Ref. [224]. This treatment supersedes the earlier proposals for the SOC contribution to the ZFS tensor in the reports of Neese and co-workers [236] and, in our opinion, also the work of Pederson and Khanna. [237] For alternative approaches, see the work of Reviakine and co-workers [238]. The spin-orbit operator used in eq. 6.2 was assumed to be of the spin-orbit mean-field (SOMF) type [239] in the multicenter implementation of Neese [230] that is equivalent to Berning *et al.* [240] It is believed to provide an accurate representation of the full Breit-Pauli two-electron SOC operator. The g-tensor has been calculated according to established procedures. [228, 230]

Electronic Structure Calculations of Q-5a The quartet ground state of **Q-5a**, calculated with DFT, shows a fairly complex spin-density distribution, which involves π- as well as σ-components (Fig. 6.6). More insight is obtained by identifying the singly occupied molecular orbitals (SOMOs) of the system. This is most conveniently done by examining the exactly singly occupied spin unrestricted natural orbitals transformed to a localized representation (Fig. 6.7). The analysis suggests the following interpretation: The electronic structure of **Q-5a** is best described as having two parallel-spin unpaired electrons localized on the nitrogen and one on the unsaturated carbon atom. The unpaired electron sitting in the in-plane nitrogen 'lone pair' is fairly well-localized and only slightly polarizes the σ-system of the ring. However, the unpaired electron sitting in the nitrogen out-of-plane lone pair is heavily delocalized into the π-system of the ring. Similarly, the carbon σ-lone pair is fairly delocalized into the σ-system of the ring. Schematically, the electronic structure may therefore be best-represented by the following leading resonance structure:

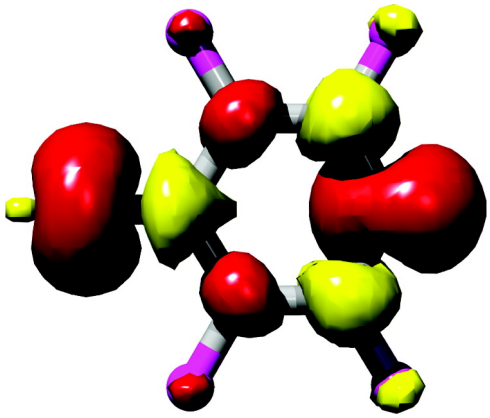

Figure 6.6.: Spin-density distribution in **Q-5a**. Positive values are contoured in red at the level of 0.003 $e^-/(Bohr^3)$; negative values are contoured in yellow at a level of 0.002 $e^-/(Bohr^3)$.

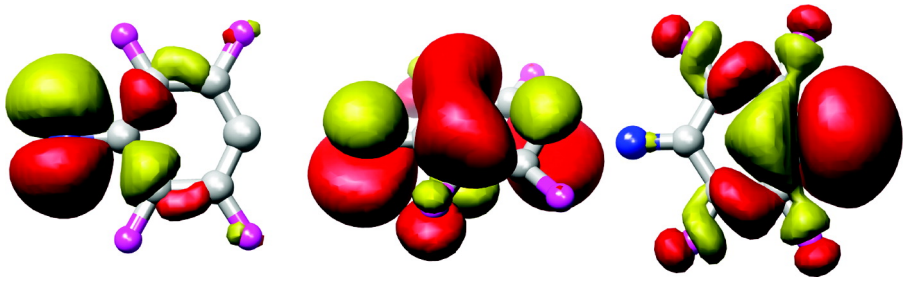

Figure 6.7.: Three singly occupied molecular orbitals of **Q-5a**: spin-unrestricted natural orbitals in a localized representation; Pipek-Mezey [241] localization and B3LYP/TZVPP.

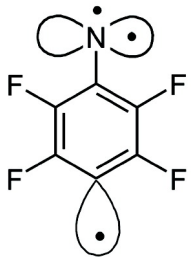

This is consistent with the notion that **Q-5a** is best-described as a σ, σ, π-triradical.

Ab initio calculations were performed to evaluate the extent to which **Q-5a** indeed has an isolated quartet ground state. Because not all of the doublet states are properly represented by a single determinant, we resorted to correlated multireference *ab initio* methods in form of the spectroscopy-oriented configuration interaction (SORCI) approach, [242] as implemented in the ORCA package. [25, 222] Calculations were performed on top of a state-averaged complete active space self-consistent field (SA-CASSCF) wave function for one quartet and two doublet states with three electrons in three orbitals. This constitutes the proper model space for answering the question raised previously. Starting orbitals were taken from the quasi-restricted orbitals (QROs) [225] of a calculation with the BP86 function and the TZVPP basis set (BP86/TZVPP). The active orbitals transform in the C_{2v} point group under the b_2 (in-plane nitrogen lone-pair), b_1 (out-of-plane nitrogen lone pair), and a_1 (carbon σ-lone pair) irreducible representations;

hence, the lowest quartet state of the system is designated as 1-$^4A_2$. The SORCI calculation was then performed on top of the SA-CASSCF(3,3) solution with $T_{sel} = 10^{-6}E_h$, $T_{pre} = 10^{-4}$, and $T_{nat} = 10^{-4}$ which provides essentially converged results for state energy differences. [243] The calculations indeed predict 1-$^4A_2$ to be the lowest state, followed by the first doublet (1-$^2A_2$) at 0.26 eV (6 kcal/mol) and the second doublet (2-$^2A_2$) at 0.95 eV (22 kcal/mol). Both low-lying doublet states are dominated by the same $(b_1)^1(b_2)^1(a_1)^1$ configuration that also applies to the 1-$^4A_2$ ground state and correspond to the two linearly independent spin-doublet couplings that can be formed for three unpaired electrons in three orbitals. This result has two implications. First, it calls the spin-unrestricted Kohn-Sham solutions for the lowest doublet state (but not for the quartet state) into question, because it is not described well by a single determinant. Indeed, if no special care is taken, B3LYP DFT calculations predict the first doublet state to be 0.7 eV above the ground state, which corresponds to an error of 0.5 eV (11 kcal/mol), relative to the more-reliable multireference *ab initio* calculation. Second, the quartet nature of the ground state becomes intelligible: The three SOMOs form an (accidentally) quasi-degenerate set (upon taking the ROHF solution of the 1-$^4A_2$ state as a reference, the orbital energies are within $<$2 eV of each other). Because the SOMOs are not well-separated spatially, the exchange interactions between the unpaired electrons must be large. Hence, the quartet state, which features the largest exchange stabilization, must be the ground state. These results show that, in agreement with the available experimental data, **Q-5a** has a clear spin-quartet ground state and a strong preference for three unpaired electrons, even in the low-lying doublet states.

Calculations of the EPR Parameters for Q-5a The EPR properties of **Q-5a** (1-$^4A_2$) were calculated with the B3LYP hybrid functional and a reasonably large TZVPP basis set, as described in the Experimental Section. The agreement between theory and experiment is very good for D, with respect to sign and magnitude, and is still reasonable for E (see Table 6.1). The near-perfect agreement observed for the value of D is, to some extent, certainly fortuitous; however, good agreement with the experiment is indeed anticipated from the results of Sinnecker and Neese. [223] The decomposition of D into individual contributions in Table 6.1 is interesting. Approximately 87% of D results from the direct spin-spin coupling (DSS), and still 13% comes from the SOC contribution. Interestingly, the calculated SS contribution is essentially local, with the largest contributions resulting from one-center integrals. Of the remaining contributions, the two-center terms reduce the local contributions by 18%, which emphasizes the importance of multicenter two-electron spin-spin integrals if quantitative agreement with the experiment is desired. The alternative breakdown of the SS term into Coulomb and exchange contributions shows that the latter are not negligible and possess the same sign as the Coulomb terms that are usually solely held responsible for the SS term within a point dipole model. Indeed, the exchange terms, which, to the best of our knowledge, have rarely been discussed in the experimental EPR literature, account for 20% of the SS term. This means that point dipole models are not realistic in the present systems; this is, of course, also consistent with the fact that the SS terms result from local one-center contributions, rather than from two-center Coulomb contributions as anticipated for a point dipole model.

Table 6.1.: Analysis of the calculated D-tensor (B3LYP/TZVPP) of **Q-5a**. All numbers are given in units of [cm^{-1}].

	D	E
total (calc)	0.261	0.017
experiment	0.285	0.043
spin–spin	0.226	0.024
spin–orbit	0.035	−0.007
spin–spin		
1-center	0.273	0.034
2-center	−0.049	−0.010
3-center	0.002	0.000
4-center	0.000	0.000
Coulomb	0.182	−0.018
exchange	0.044	0.042
spin–orbit		
$M = 0$ ($\alpha \rightarrow \alpha$)	−0.002	0.006
$M = 0$ ($\beta \rightarrow \beta$)	−0.001	0.006
$M = +1$ ($\beta \rightarrow \alpha$)	−0.001	−0.003
$M = -1$ ($\alpha \rightarrow \beta$)	0.040	−0.003

The limited SOC contributions to D are dominated by the spin-lowering spin-flip contributions, which result from the low-lying spin doublet states. This is consistent with previous results for other systems [224, 225, 244–248] for which the SOC term represents the largest contribution to D. The SS contributions are calculated without any spin polarization. Unfortunately, it has been found previously that inclusion of spin polarization into the calculation of the SS term (which is technically feasible, of course) significantly degrades the agreement with the experimental values. [223] Thus, currently, there does not seem to be a satisfactory solution to this problem in a DFT framework.

Interestingly, the easy axis of the D-tensor does not point out of the plane but rather along the C-N bond (Fig. 6.8). The calculated g-shifts are −86.5, 588, and 1012 ppm. The small shifts are typical of radicals that are composed of light atoms. The orientation of the g-tensor is displayed graphically in Fig. 6.8. Interestingly, the largest g-value — which also corresponds to the largest g-shift — is oriented perpendicular to the molecular plane and, therefore, also occurs perpendicular to the easy axis of the D-tensor. Nevertheless, the anisotropy in the g-tensor is sufficiently small, such that it is hardly possible to observe it under the present experimental conditions.

Electronic Structure Calculations for Q-5c The quartet ground state of **5c**, calculated with the B3LYP functional and the TZVPP basis set, shows a fairly complex spin-density distribution (Fig. 6.9) involving σ and π components. The spin-density distribution is very similar to that observed in 2,3,5,6-tetrafluorophenylnitren-4-yl (**Q-5a**), cf. Fig. 6.6.

The three singly occupied molecular orbitals (SOMOs) of **Q-5c** were identified by examining the exactly singly occupied spin-unrestricted natural orbitals transformed into a localized presentation (Fig. 6.10). The conclusions that can be drawn from inspection of the SOMOs confirm the description of **Q-5c** as

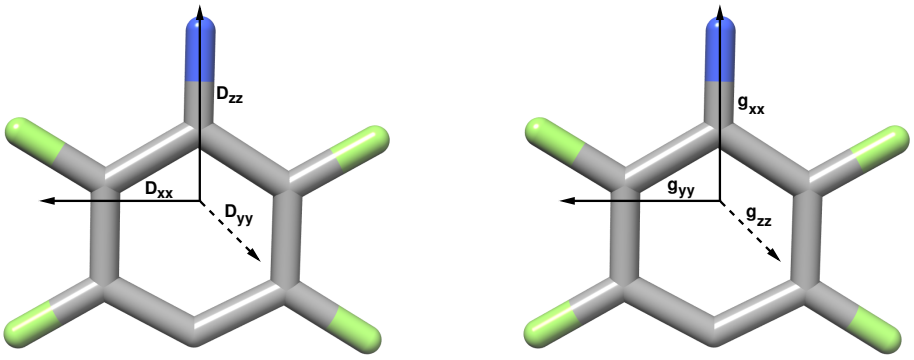

(a) *D*-tensor (b) g-tensor

Figure 6.8.: Orientation of the *D*- and g-tensor of **Q-5a**, based on the calculations (B3LYP/TZVPP).

a σ,σ,π-triradical. The unpaired electron in the in-plane nitrogen MO is well localized and only slightly polarizes the σ-system of the ring, whereas the unpaired electron located in the out-of-plane nitrogen MO is heavily delocalized into the π-system of the ring. Similarly, the carbon σ-lone pair is fairly delocalized into the σ-system of the ring.

To determine the extent to which **5c** has an isolated quartet ground state, SORCI calculations were performed on top of a state-averaged complete active space self-consistent field (SA-CASSCF) wave function with three electrons in three orbitals. This procedure has already proven to provide essentially converged results for state-energy differences and has also been applied in studying **5a**. Quasi-restricted orbitals from a BP86/TZVPP calculation served as starting orbitals.

The active orbitals of the **Q-5c** molecule transform into the C_s point group under a′ (in-plane nitrogen MO and carbon lone pair), and a″ (out-of-plane nitrogen MO) irreducible representations. Thus, the lowest quartet state of the system is designated as 1-^{4}A″. In fact, the SORCI calculation predicts 1-^{4}A″ to be the lowest state, followed by the first doublet (1-^{2}A″) at about 0.31 eV (7 kcal/mol) and the second doublet (2-^{2}A″) at about 0.81 eV (19 kcal/mol). The dominating electron configuration for both low-lying doublet states is in agreement with **5a** the $(a')^1(a')^1(a'')^1$ configuration, which corresponds to the two linearly independent spin-doublet couplings.

The three SOMOs form a quasidegenerate set of MOs, with differences in orbital energies of less than 2.3 eV. Furthermore, since the SOMOs are spatially not well separated, the exchange interactions between the unpaired electrons must be large. Thus, from both the theoretical and experimental results, it can be concluded that **5c** has a well-isolated spin-quartet ground state.

Calculations of the EPR Parameters for Q-5c Experimental and calculated EPR properties of **Q-5c** are compared in Table 6.2. The agreement between experiment and theory is reasonable. As expected, the dominant contribution to the ZFS tensor is the spin-spin (SS) interaction, which amounts to about 92% of the total *D*-value. The calculated SS contribution is essentially local, with the largest contributions resulting from one-center integrals. This was also found in the analysis of the ZFS contributions of the 2,3,5,6-tetrafluorophenylnitren-4-yl radical **Q-5a**.

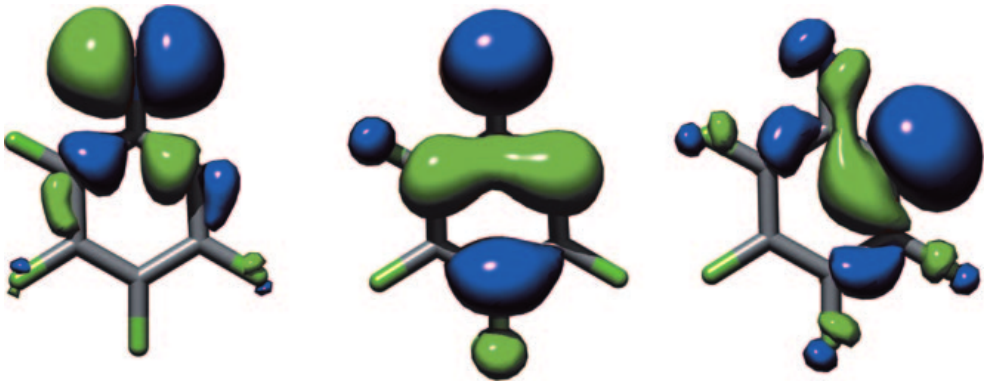

Figure 6.10.: Three singly occupied molecular orbitals of **Q-5c**: spin-unrestricted natural orbitals in a localized representation; Pipek-Mezey [241] localization and B3LYP/TZVPP.

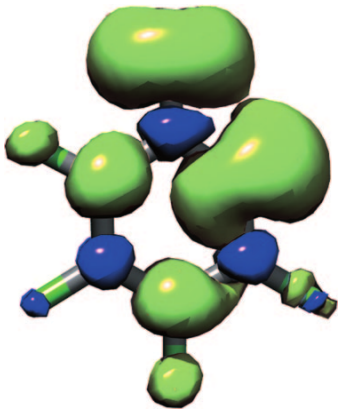

Figure 6.9.: Spin-density distribution in **Q-5c**. Positive values are contoured in green, negative values are contoured in blue, both at the level of 0.003 $e^-/(Bohr^3)$.

Table 6.2.: Analysis of the calculated *D*-tensor (B3LYP/TZVPP) of **Q-5c**. All numbers are given in units of $[cm^{-1}]$.

	D	*E*
total (calc)	0.284	0.023
experiment	0.357	0.014
spin–spin	0.262	0.022
spin–orbit	0.022	0.001
spin–spin		
1-center	0.315	−0.006
2-center	−0.047	0.034
3-center	−0.006	−0.005
4-center	0.000	0.000
Coulomb	0.172	0.025
exchange	0.091	−0.003

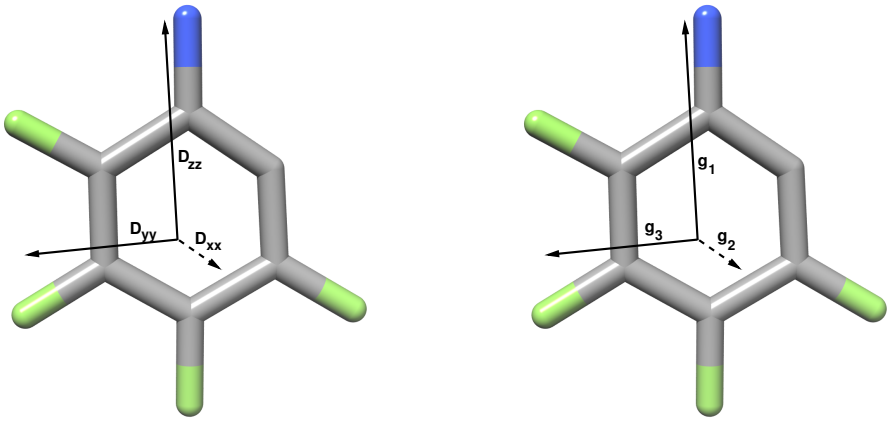

(a) *D*-tensor (b) g-tensor

Figure 6.11.: Orientation of the *D*- and g-tensor of **Q-5c**, based on the calculations (B3LYP/TZVPP).

Continued.

	D	*E*
spin–orbit		
$M = 0$ ($\alpha \rightarrow \alpha$)	0.006	−0.003
$M = 0$ ($\beta \rightarrow \beta$)	0.010	−0.003
$M = +1$ ($\beta \rightarrow \alpha$)	0.021	0.004
$M = -1$ ($\alpha \rightarrow \beta$)	−0.014	0.002

The spin-orbit coupling (SOC) contribution to *D* is about 8%, which is slightly smaller than the corresponding value in **Q-5a**. The SOC contribution to the *D*-tensor is dominated by spin-flip contributions. Unlike in **Q-5a**, the two spin-lowering and spin-raising spin-flip contributions are of opposite sign and play an important role.

The magnetic zy-plane of the *D*-tensor is located in the molecular plane of **Q-5c**, while the x-axis points out of the plane. An analogous result was found for **Q-5a**. However, while in **5a** the easy axis is oriented along the C-N bond, it is rotated about 1° away from the axis in **Q-5c**, and the origin of the *D*-tensor is shifted from the molecular axis defined by the C-N bond (Fig. 6.11). Because the nitreno radical simultaneously exhibits nitrene and carbene character, the large *E*-value of **5a** was interpreted by geometric considerations. The dipolar field of the nitrene contribution in **Q-5a** points along the C-N bond, while the carbene contribution points parallel to a hypothetical bond angle of 180° of the carbene moiety, and thus its dipolar field is oriented along the y-direction of the nitrene contribution. Thus, the nitrene and carbene contributions are perpendicular to each other, and since the nitrene character prevails over the carbene character, the easy axis of the quartet *D*-tensor is still oriented parallel to the C-N bond, and the carbene contribution to the dipolar field points along the y-direction, which results in significantly magnetically inequivalent y- and x-directions. The large *E*-value can therefore be interpreted as resulting from the carbene character of the 1-$^4A_2$ ground state.

The lower *E*-value of **Q-5c** can then be explained from analogous geometric considerations. Since the carbene center in the aromatic ring is located in *ortho* position to the nitrene center, the dipolar field of the carbene contribution is not located perpendicular to the magnetic z-axis of the nitrene center,

and this results in a considerable contribution parallel to the z-direction of the nitrene dipolar field and therefore to a smaller E-value of the quartet spin system compared to **Q-5a**. Like for **Q-5a**, the nitrene character in **Q-5c** still prevails over the carbene character, but unlike in **Q-5a** there is no symmetry axis along the C-N bond in **Q-5c**, and thus the easy axis of the spin system can be shifted by the influence of the dipolar field of the carbene. Since the D-value is heavily influenced by the spin density at the spin carrying centers, the higher D-value of **Q-5c** can be explained by larger spin density on its nitrene center compared to **Q-5a**. The nitrene centers in **Q-5c** and **Q-5a** bear spin populations of 1.598 and 1.577, respectively, calculated at the UB3LYP/6-311G(d,p) level of theory. The calculated g-shifts are -150, 778, and 1035 ppm. In contrast to **Q-5a**, the largest g value is oriented in the yz-plane of the D-tensor (Fig. 6.11).

6.1.3. Conclusions

The EPR measurements confirm the previous assignments of the products of the matrix photolysis of **6a**, based on IR spectroscopy. [212, 213] As expected, the primary photoproduct is nitrene **T-7a** formed in very high yield. The splitting of the C-I bond in **7** is much less efficient and competes with the rearrangement to **9**. Nevertheless, under conditions that allow the nitreno radical **5a** to be detected via IR spectroscopy, a clear EPR signal of the quartet **Q-5a** can be observed. It is pleasing that the previous assignment of the quartet state, based solely on IR spectroscopy, is now unequivocally confirmed by EPR spectroscopy. As observed in the IR experiments, [212, 213] the yield of **5a** is strongly dependent on the matrix temperature. At 10-15 K, only traces of **5a** are formed, whereas the highest yield is found if **6a** is irradiated at 4 K. Annealing at temperatures of $>$10 K results in the recombination of **5a** with the I atom, therefore, it was not possible to measure the Curie-Weiss behavior of **5a**.

The electronic structure of **Q-5a** can be best-described as a σ, σ, π-triradical with one unpaired electron located in an in-plane orbital at the N atom (σ) and one at the *para*-C atom of the phenyl ring (σ), while the third unpaired electron is in an out-of-plane orbital of the N atom and is heavily delocalized into the π-system. Because of the significant delocalization of the out-of-plane SOMO, **Q-5a** is expected to show both properties of a nitrene that is linked to a phenyl radical and of a carbene (cyclohexadienylidene) that is linked to a nitrogen-centered radical (iminyl radical), as shown in the resonance structures below.

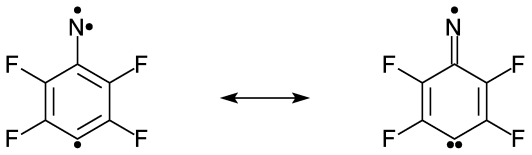

In accordance with this qualitative picture, the natural spin population [249] is calculated to 1.55 unpaired electrons at the N atom and to 1.21 at the *para*-C atom (UB3LYP/TZVPP). The value of D in nitreno radical **Q-5a** ($|D/hc| = 0.285$) is typical for quartet-ground state nitreno radicals. [250–252] However, the large E-value in **Q-5a** deserves a closer interpretation. In agreement with our calculations, Wasserman assumed that the direction of the principal magnetic axis z of phenyl nitrenes lies parallel to the N-C bond. [210, 253, 254] It is readily verified (e.g., by a calculation on linear $^3CH_2$) that the dipolar field created by two unpaired electrons in p_x and p_y orbitals indeed points along the z-direction and that the axial symmetry of the spin distribution in such an arrangement remains untouched and leads to $|E/hc| = 0$. Indeed, for carbenes, it has been reported that the z-axis lies parallel to a hypothetical 180°

bond angle, [255] and that the E-value consequently increases with decreasing bond angle at the carbene center. The addition of a symmetrical π-radical in the *para* position, as in Ref. [252] does not change the pseudo-cylindrical symmetry of these triradicals; the z-axis remains in the same position, and, hence, the E-value of these quartet systems should remain zero. However, this latter assumption cannot be verified. Our calculations demonstrate that the bulk of the E-value results from one-center contributions of the direct spin-spin coupling interaction. This information, together with the fact that **Q-5a** simultaneously exhibits nitrene and carbene character, then leads to a simple and appealing geometric interpretation of the large value of E, in contrast to the compounds reported in Refs. [250–252], which have E-values of zero. We assume, for **Q-5a**, a coordinate system where the z-axis points along the C-N bond, the x-axis is perpendicular to the molecular plane, and the y-axis, consequently, lies in the molecular plane. In the nitrene part of the electronic structure, the two SOMOs are comprised of p_x and p_y orbitals and their dipolar field is consequently directed along the z-direction. For the carbene part of the 1-$^4A_2$ ground state, the SOMOs are comprised of p_z and p_x contributions and, consequently, the resulting dipolar field points along the y-direction. Because the nitrene character prevails over the carbene character of **Q-5a**, the main magnetic axis is still pointing along the C-N bond in the z-direction. However, the carbene character is reflected by an enhanced dipolar field in the y-direction, which is strong enough to give significantly magnetically inequivalent y- and x-directions. We, therefore, come to the conclusion that the nonzero E-value in **Q-5a** mainly reflects the carbene character of the 1-$^4A_2$ ground state. This carbene character, in turn, is controlled by the properties of the π-system, because the out-of-plane spin-density arises from the conjugation of the nitrene out-of-plane SOMO and the π-system of the ring.

Finally, the fact that the D-value for **Q-5a** is a factor of 3 smaller than those of typical phenylnitrenes [256] is readily explained by the prefactor $1/[S(2S-1)]$ of the DSS term (vide infra), which amounts to 1 for a ground state spin of 1 and 1/3 for a ground-state spin of 3/2. Assuming an axial D-tensor, the level splitting of $2D$ (in $S = 3/2$) versus D (in $S = 1$) is more similar for both multiplicities but is still slightly smaller for the quartet system. This is explained by the partial cancellation of the carbene and nitrene contributions to the D-value, which oppose each other along the magnetic z-direction, as explained previously in some detail.

The photochemistry of phenyl azide **6c** is quite similar to that of the previously described **6a** and the corresponding triplet phenyl nitrenes **1** are produced as primary photoproducts.

Photolysis of the product mixtures **7c**, **8c** and **9c** yields two unusual products: nitreno radical **5c** with a high-spin quartet ground state and azirinyl radical **11**. The yield of **5c** is quite low, and it could only be detected by the sensitive and selective EPR spectroscopy. The EPR spectrum of **5c** could be simulated with the ZFS parameters $|D/hc|$=0.357 cm^{-1} and $|E/hc|$=0.0136 cm^{-1}. The D-value of **5c** is slightly larger than that of *para*-nitreno radicals such as **5a**, which are in the range between 0.278 and 0.291 cm^{-1}, while the E-value is considerably smaller than that of the *para*-nitreno radicals, which lie between 0.040 and 0.043 cm^{-1}.

The classical interpretation of the ZFS parameters in terms of spin-spin interactions is that D correlates with the distance between the unpaired electrons and E describes deviations from cylindrical symmetry. This simplified interpretation does not take into account spin-orbit contributions, which indeed contribute less than 10% to the ZFS parameters. The higher D-value of **5c** compared to **5a** correlates with a higher spin density at the nitrogen atom in **5c**. The higher E-value in the more symmetrical *para*-nitreno radical **5a** compared to **5c** is counterintuitive, but is in accordance with our model of describing nitreno radicals as unifying properties of both nitrenes and carbenes. In **5a** the dipolar field contribution of the carbene is perpendicular to that of the nitrene moiety, whereas in **5c** there is a much smaller angle between the

dipolar field vectors of the carbene and nitrene units. Since the spin-spin interactions in nitrenes are larger than in carbenes (the D-values of nitrenes are much larger than those of carbenes), the nitrene structure in **5a** determines the magnetic z-axis, but the carbene structure results in a large contribution in the y-direction and thus a large E-value. In **5c** the symmetry is lower and the magnetic axes are not restricted to the Cartesian axes as in C_{2v}-symmetrical **5a**. Thus, the less symmetrical **5c** has a significantly smaller E-value than **5a**. This description is in accordance with the electronic structure of a σ, σ, π-triradical.

7. Conclusions

The accurate calculation of molecular properties for medium-sized to large chemical systems still represents a challenge for computational chemistry. Although the formalism for the quantum chemical calculation of second-order properties by linear response theory has been known for a long time, an efficient implementation has not been available for a long time. The goal of this thesis was to fill this gap by implementing an efficient algorithm for the calculation of second-order properties.

The theory of second derivatives for non-variational methods, in particular second-order Møller-Plesset (MP2) perturbation theory, has been rederived and in the case of imaginary perturbations an alternative Ansatz has been found, that differs significantly in its working equations from the formulas proposed in the literature. The formalism for MP2 second derivatives has been extended for the use of the popular 'Resolution of the Identity' approximation. The recently developed RIJCOSX approximation, which has been implemented for the calculation of RIJCOSX-MP2 geometries, has also been successfully applied to the calculation of second-order RI-MP2 properties. The speedups observed for the RIJCOSX-MP2 second derivatives combined with a semi-numerical treatment of the most expensive 4-external contribution to the $\boldsymbol{\sigma}$-vector compared to the conventional RI-MP2 method turned out to be very large for medium-sized compounds with extended basis sets. A benchmark study has been performed on a static polarizability calculation of a 16-annulene system in a quadruple-ζ basis set (N_{Bas}=1360, N_{BasJ}=960, N_{BasC}=2992). The calculation could be completed in $\sim$17 days and represents, to our knowledge, the largest reported RI-MP2 polarizability computation.

The efficiency of the RIJCOSX approximation has been compared to another current approach developed by Weigend and co-workers (RI-JK). The error of the RI-JK algorithm for calculated SCF energies is seen to be more smooth for the tested systems and for small compounds RI-JK is preferable over RIJCOSX. However, the RIJCOSX approximation turned out to be more efficient for large systems with accurate basis sets. In addition, energy derivatives can be more efficiently formulated in the RIJCOSX framework, which is entirely derived in the AO basis.

Furthermore, the theory of second derivatives for the new class of double-hybrid density functionals has been derived. The implementation has been validated and the numerical results showed a great performance of double-hybrid functionals, in particular, for the prediction of magnetic molecular properties. A benchmark study demonstrated that fairly large systems with a reasonable large basis set could be handled with our present implementation.

MP2 often provides erratic results when applied to open-shell systems, transition metal complexes or compounds with a complicated electronic structure, due to a reference wave function of poor quality. Therefore, an alternative approach has been derived, which improves MP2 results through incorporation of orbital relaxation effects. For this purpose the molecular orbitals are optimized alongside with the double excitation amplitudes, based on the well-known Hylleraas functional. The orbital-optimized MP2 method has shown to improve the energetics of open-shell species and transition states. The calculated hyperfine coupling constants are almost of CCSD quality with only iterative $\mathcal{O}(N^5)$ effort. The formalism has been extended to first and second derivatives.

A related Ansatz has been propsed by Lochan and Head-Gordon [58] with their 'orbital-optimized opposite-spin scaled second-order correlation' (O2) method. In their energy functional the alpha-beta correlation in the MP2 expression is empirically enlarged, while the same-spin contribution is completely neglected. This reduces the computational cost to iterative $\mathcal{O}(N^4)$ effort. However, the Ansatz presented in this thesis is more general, and by applying 'spin-component scaling' [102] the O2-approach can also be maintained.

Finally, the characterization of 2,3,5,6-Tetrafluorophenylnitren-4-yl and 3,4,5,6-Tetrafluorophenylnitren-2-yl was an example of a successful combination of theory and application. The analysis of the singly occupied spin-unrestricted natural orbitals could confirm the notion, that both nitreno radicals are best described as σ, σ, π-triradicals. Multireference *ab initio* calculations predict well isolated $^4A_2$ and $^4A''$ ground states for the radical compounds. The calculation of the zero-field splitting tensor could provide a detailed insight into the orientation and the individual contributions of the D-tensor It could be shown how high-level quantum-chemical methods can help to understand and confirm experimental spectra.

Future Prospects The implemented algorithm for RI-MP2 second derivatives is for basis functions, which do not depend on the respective perturbation. Since, computed magnetic properties strongly depend on the chosen gauge-origin, several attempts have been made to overcome this problem. All proposed approaches use local or distributed gauge origins. The most popular Ansatz is formulated in the AO basis and uses local gauge origins for atomic orbitals (GIAO). In this case, the basis functions will depend on the magnetic field. Therefore, the implemented algorithm will have to be adjusted for the use of GIAOs and for the calculation of geometric second derivatives.

Furthermore, the actual implementation stores the $\boldsymbol{\sigma}$-vector and several integral types on disc. It would be desirable to avoid this storage for large systems and, thus, to develop an integral direct algorithm.
An efficient parallelization is scheduled for the near future as well.

The formalism for second OO-MP2 derivatives has been derived and a preliminary algorithm for the solution of the coupled-perturbed OO-MP2 (CP-OO-MP2) equations has been presented. However, the implementation has to be done in the near future. Although it has been pointed out in Section 3.3 that the solution of the CP-OO-MP2 equations is of high computational effort, it would be very interesting to investigate the effect of orbital relaxation on the calculated response properties. From our knowledge, it would be the first implementation for second derivatives amongst such orbital-optimized methods methods.
An alternative Ansatz is to relax the orbitals in a double-hybrid DFT approach. This has never investigated before and it remains an open question whether this would improve the results in a similar way as OO-MP2 improves upon MP2. If this would be the case, the orbital-optimized double-hybrid DFT approach might become the 'new' standard for molecular property calculations.

A. Double Hybrid Density Functionals: A Detailed Derivation of the Third Functional Derivatives

Formulate the derivative of the XC part of the response operator,

$$\begin{aligned}
\frac{\partial}{\partial\kappa}\left(\overline{R}^{XC}(\mathbf{D}')_{ai\alpha}\right) = \frac{\partial}{\partial\kappa}\Bigg(\int\Bigg\{ & \underbrace{\left[\frac{\partial^2 f}{\partial\rho_\alpha\partial\rho_\alpha}\rho_\alpha^{\mathbf{D}'}(\mathbf{r})\frac{\partial^2 f}{\partial\rho_\alpha\partial\rho_\beta}\rho_\beta^{\mathbf{D}'}(\mathbf{r}) + \frac{\partial^2 f}{\partial\gamma_{\alpha\alpha}\partial\rho_\alpha}\gamma_{\alpha\alpha}^{\mathbf{D}'}(\mathbf{r}) + \frac{\partial^2 f}{\partial\gamma_{\alpha\beta}\partial\rho_\alpha}\gamma_{\alpha\beta}^{\mathbf{D}'}(\mathbf{r}) + \frac{\partial^2 f}{\partial\gamma_{\beta\beta}\partial\rho_\beta}\gamma_{\beta\beta}^{\mathbf{D}'}(\mathbf{r})\right]}_{A.1-A.5} \times \\
& (\psi_a^\alpha(\mathbf{r})\psi_i^\alpha(\mathbf{r})) \\
& + \underbrace{2\left[\frac{\partial^2 f}{\partial\rho_\alpha\partial\gamma_{\alpha\alpha}}\rho_\alpha^{\mathbf{D}'}(\mathbf{r}) + \frac{\partial^2 f}{\partial\rho_\beta\partial\gamma_{\alpha\alpha}}\rho_\beta^{\mathbf{D}'}(\mathbf{r}) + \frac{\partial^2 f}{\partial\gamma_{\alpha\alpha}\partial\gamma_{\alpha\alpha}}\gamma_{\alpha\alpha}^{\mathbf{D}'}(\mathbf{r}) + \frac{\partial^2 f}{\partial\gamma_{\alpha\beta}\partial\gamma_{\alpha\alpha}}\gamma_{\alpha\beta}^{\mathbf{D}'}(\mathbf{r}) + \frac{\partial^2 f}{\partial\gamma_{\beta\beta}\partial\gamma_{\alpha\alpha}}\gamma_{\beta\beta}^{\mathbf{D}'}(\mathbf{r})\right]}_{B.1-B.5} \times \\
& \vec{\nabla}\rho_\alpha(\mathbf{r})\vec{\nabla}(\psi_a^\alpha(\mathbf{r})\psi_i^\alpha(\mathbf{r})) \\
& + \underbrace{\left[\frac{\partial^2 f}{\partial\rho_\alpha\partial\gamma_{\alpha\beta}}\rho_\alpha^{\mathbf{D}'}(\mathbf{r}) + \frac{\partial^2 f}{\partial\rho_\beta\partial\gamma_{\alpha\beta}}\rho_\beta^{\mathbf{D}'}(\mathbf{r}) + \frac{\partial^2 f}{\partial\gamma_{\alpha\alpha}\partial\gamma_{\alpha\beta}}\gamma_{\alpha\alpha}^{\mathbf{D}'}(\mathbf{r}) + \frac{\partial^2 f}{\partial\gamma_{\alpha\beta}\partial\gamma_{\alpha\beta}}\gamma_{\alpha\beta}^{\mathbf{D}'}(\mathbf{r}) + \frac{\partial^2 f}{\partial\gamma_{\beta\beta}\partial\gamma_{\alpha\beta}}\gamma_{\beta\beta}^{\mathbf{D}'}(\mathbf{r})\right]}_{C.1-C.5} \times \\
& \vec{\nabla}\rho_\beta(\mathbf{r})\vec{\nabla}(\psi_a^\alpha(\mathbf{r})\psi_i^\alpha(\mathbf{r})) \\
& + \underbrace{\left[2\frac{\partial f}{\partial\gamma_{\alpha\alpha}}\vec{\nabla}\rho_\alpha^{\mathbf{D}'}(\mathbf{r}) + \frac{\partial f}{\partial\gamma_{\alpha\beta}}\vec{\nabla}\rho_\beta^{\mathbf{D}'}(\mathbf{r})\right]}_{D.1-D.2}\vec{\nabla}(\psi_a^\alpha(\mathbf{r})\psi_i^\alpha(\mathbf{r}))\Bigg\}d\mathbf{r}\Bigg)
\end{aligned} \tag{A.1}$$

A-terms,

$$\begin{aligned}
\mathbf{A.1} &= \frac{\partial}{\partial\kappa}\left(\frac{\partial^2 f}{\partial\rho_\alpha\partial\rho_\alpha}\rho_\alpha^{\mathbf{D}'}(\psi_a^\alpha\psi_i^\alpha)\right) \\
&= \Bigg[\frac{\partial^3 f}{\partial\rho_\alpha\partial\rho_\alpha\partial\rho_\alpha}\left(2\sum_{jb\alpha}U_{bj}^\kappa\psi_b\psi_j\right) + \frac{\partial^3 f}{\partial\rho_\alpha\partial\rho_\alpha\partial\rho_\beta}\left(2\sum_{jb\beta}U_{bj}^\kappa\psi_b\psi_j\right) + 2\frac{\partial^3 f}{\partial\rho_\alpha\partial\rho_\alpha\partial\gamma_{\alpha\alpha}}\vec{\nabla}\left(2\sum_{jb\alpha}U_{bj}^\kappa\psi_b\psi_j\right)\vec{\nabla}\rho_\alpha \\
&\quad + \frac{\partial^3 f}{\partial\rho_\alpha\partial\rho_\alpha\partial\gamma_{\alpha\beta}}\left\{\vec{\nabla}\left(2\sum_{jb\alpha}U_{bj}^\kappa\psi_b\psi_j\right)\vec{\nabla}\rho_\beta + \vec{\nabla}\left(2\sum_{jb\beta}U_{bj}^\kappa\psi_b\psi_j\right)\vec{\nabla}\rho_\alpha\right\} \\
&\quad + 2\frac{\partial^3 f}{\partial\rho_\alpha\partial\rho_\alpha\partial\gamma_{\beta\beta}}\vec{\nabla}\left(2\sum_{jb\beta}U_{bj}^\kappa\psi_b\psi_j\right)\vec{\nabla}\rho_\beta\Bigg]\rho_\alpha^{\mathbf{D}'}(\psi_a^\alpha\psi_i^\alpha)
\end{aligned} \tag{A.2}$$

$$\begin{aligned}
\mathbf{A.2} &= \frac{\partial}{\partial\kappa}\left(\frac{\partial^2 f}{\partial\rho_\alpha\partial\rho_\beta}\rho_\beta^{\mathbf{D}'}(\psi_a^\alpha\psi_i^\alpha)\right) \\
&= \Bigg[\frac{\partial^3 f}{\partial\rho_\alpha\partial\rho_\beta\partial\rho_\alpha}\left(2\sum_{jb\alpha}U_{bj}^\kappa\psi_b\psi_j\right) + \frac{\partial^3 f}{\partial\rho_\alpha\partial\rho_\beta\partial\rho_\beta}\left(2\sum_{jb\beta}U_{bj}^\kappa\psi_b\psi_j\right) + 2\frac{\partial^3 f}{\partial\rho_\alpha\partial\rho_\beta\partial\gamma_{\alpha\alpha}}\vec{\nabla}\left(2\sum_{jb\alpha}U_{bj}^\kappa\psi_b\psi_j\right)\vec{\nabla}\rho_\alpha \\
&\quad + \frac{\partial^3 f}{\partial\rho_\alpha\partial\rho_\beta\partial\gamma_{\alpha\beta}}\left\{\vec{\nabla}\left(2\sum_{jb\alpha}U_{bj}^\kappa\psi_b\psi_j\right)\vec{\nabla}\rho_\beta + \vec{\nabla}\left(2\sum_{jb\beta}U_{bj}^\kappa\psi_b\psi_j\right)\vec{\nabla}\rho_\alpha\right\} \\
&\quad + 2\frac{\partial^3 f}{\partial\rho_\alpha\partial\rho_\beta\partial\gamma_{\beta\beta}}\vec{\nabla}\left(2\sum_{jb\beta}U_{bj}^\kappa\psi_b\psi_j\right)\vec{\nabla}\rho_\beta\Bigg]\rho_\beta^{\mathbf{D}'}(\psi_a^\alpha\psi_i^\alpha)
\end{aligned} \tag{A.3}$$

$$
\begin{aligned}
\mathbf{A.3} &= \frac{\partial}{\partial\kappa}\left(\frac{\partial^2 f}{\partial\rho_\alpha\partial\gamma_{\alpha\alpha}}\gamma^{\mathbf{D}'}_{\alpha\alpha}(\psi_a^\alpha\psi_i^\alpha)\right)\\
&= \left[\frac{\partial^3 f}{\partial\rho_\alpha\partial\gamma_{\alpha\alpha}\partial\rho_\alpha}\left(2\sum_{jb\alpha}U^\kappa_{bj}\psi_b\psi_j\right)+\frac{\partial^3 f}{\partial\rho_\alpha\partial\gamma_{\alpha\alpha}\partial\rho_\beta}\left(2\sum_{jb\beta}U^\kappa_{bj}\psi_b\psi_j\right)+2\frac{\partial^3 f}{\partial\rho_\alpha\partial\gamma_{\alpha\alpha}\partial\gamma_{\alpha\alpha}}\vec{\nabla}\left(2\sum_{jb\alpha}U^\kappa_{bj}\psi_b\psi_j\right)\vec{\nabla}\rho_\alpha\right.\\
&\quad+\frac{\partial^3 f}{\partial\rho_\alpha\partial\gamma_{\alpha\alpha}\partial\gamma_{\alpha\beta}}\left\{\vec{\nabla}\left(2\sum_{jb\alpha}U^\kappa_{bj}\psi_b\psi_j\right)\vec{\nabla}\rho_\beta+\vec{\nabla}\left(2\sum_{jb\beta}U^\kappa_{bj}\psi_b\psi_j\right)\vec{\nabla}\rho_\alpha\right\}\\
&\quad\left.+2\frac{\partial^3 f}{\partial\rho_\alpha\partial\gamma_{\alpha\alpha}\partial\gamma_{\beta\beta}}\vec{\nabla}\left(2\sum_{jb\beta}U^\kappa_{bj}\psi_b\psi_j\right)\vec{\nabla}\rho_\beta\right]\gamma^{\mathbf{D}'}_{\alpha\alpha}(\psi_a^\alpha\psi_i^\alpha)\\
&\quad+2\frac{\partial^2 f}{\partial\rho_\alpha\partial\gamma_{\alpha\alpha}}\vec{\nabla}\rho^{\mathbf{D}'}_\alpha\vec{\nabla}\left(2\sum_{jb\alpha}U^\kappa_{bj}\psi_b\psi_j\right)(\psi_a^\alpha\psi_i^\alpha)
\end{aligned}
\tag{A.4}
$$

$$
\begin{aligned}
\mathbf{A.4} &= \frac{\partial}{\partial\kappa}\left(\frac{\partial^2 f}{\partial\rho_\alpha\partial\gamma_{\alpha\beta}}\gamma^{\mathbf{D}'}_{\alpha\beta}(\psi_a^\alpha\psi_i^\alpha)\right)\\
&= \left[\frac{\partial^3 f}{\partial\rho_\alpha\partial\gamma_{\alpha\beta}\partial\rho_\alpha}\left(2\sum_{jb\alpha}U^\kappa_{bj}\psi_b\psi_j\right)+\frac{\partial^3 f}{\partial\rho_\alpha\partial\gamma_{\alpha\beta}\partial\rho_\beta}\left(2\sum_{jb\beta}U^\kappa_{bj}\psi_b\psi_j\right)+2\frac{\partial^3 f}{\partial\rho_\alpha\partial\gamma_{\alpha\beta}\partial\gamma_{\alpha\alpha}}\vec{\nabla}\left(2\sum_{jb\alpha}U^\kappa_{bj}\psi_b\psi_j\right)\vec{\nabla}\rho_\alpha\right.\\
&\quad+\frac{\partial^3 f}{\partial\rho_\alpha\partial\gamma_{\alpha\beta}\partial\gamma_{\alpha\beta}}\left\{\vec{\nabla}\left(2\sum_{jb\alpha}U^\kappa_{bj}\psi_b\psi_j\right)\vec{\nabla}\rho_\beta+\vec{\nabla}\left(2\sum_{jb\beta}U^\kappa_{bj}\psi_b\psi_j\right)\vec{\nabla}\rho_\alpha\right\}\\
&\quad\left.+2\frac{\partial^3 f}{\partial\rho_\alpha\partial\gamma_{\alpha\beta}\partial\gamma_{\beta\beta}}\vec{\nabla}\left(2\sum_{jb\beta}U^\kappa_{bj}\psi_b\psi_j\right)\vec{\nabla}\rho_\beta\right]\gamma^{\mathbf{D}'}_{\alpha\beta}(\psi_a^\alpha\psi_i^\alpha)\\
&\quad+\frac{\partial^2 f}{\partial\rho_\alpha\partial\gamma_{\alpha\beta}}\left\{\vec{\nabla}\rho^{\mathbf{D}'}_\alpha\vec{\nabla}\left(2\sum_{jb\beta}U^\kappa_{bj}\psi_b\psi_j\right)+\vec{\nabla}\rho^{\mathbf{D}'}_\beta\vec{\nabla}\left(2\sum_{jb\alpha}U^\kappa_{bj}\psi_b\psi_j\right)\right\}(\psi_a^\alpha\psi_i^\alpha)
\end{aligned}
\tag{A.5}
$$

$$
\begin{aligned}
\mathbf{A.5} &= \frac{\partial}{\partial\kappa}\left(\frac{\partial^2 f}{\partial\rho_\alpha\partial\gamma_{\beta\beta}}\gamma^{\mathbf{D}'}_{\beta\beta}(\psi_a^\alpha\psi_i^\alpha)\right)\\
&= \left[\frac{\partial^3 f}{\partial\rho_\alpha\partial\gamma_{\beta\beta}\partial\rho_\alpha}\left(2\sum_{jb\alpha}U^\kappa_{bj}\psi_b\psi_j\right)+\frac{\partial^3 f}{\partial\rho_\alpha\partial\gamma_{\beta\beta}\partial\rho_\beta}\left(2\sum_{jb\beta}U^\kappa_{bj}\psi_b\psi_j\right)+2\frac{\partial^3 f}{\partial\rho_\alpha\partial\gamma_{\beta\beta}\partial\gamma_{\alpha\alpha}}\vec{\nabla}\left(2\sum_{jb\alpha}U^\kappa_{bj}\psi_b\psi_j\right)\vec{\nabla}\rho_\alpha\right.\\
&\quad+\frac{\partial^3 f}{\partial\rho_\alpha\partial\gamma_{\beta\beta}\partial\gamma_{\alpha\beta}}\left\{\vec{\nabla}\left(2\sum_{jb\alpha}U^\kappa_{bj}\psi_b\psi_j\right)\vec{\nabla}\rho_\beta+\vec{\nabla}\left(2\sum_{jb\beta}U^\kappa_{bj}\psi_b\psi_j\right)\vec{\nabla}\rho_\alpha\right\}\\
&\quad\left.+2\frac{\partial^3 f}{\partial\rho_\alpha\partial\gamma_{\beta\beta}\partial\gamma_{\beta\beta}}\vec{\nabla}\left(2\sum_{jb\beta}U^\kappa_{bj}\psi_b\psi_j\right)\vec{\nabla}\rho_\beta\right]\gamma^{\mathbf{D}'}_{\beta\beta}(\psi_a^\alpha\psi_i^\alpha)\\
&\quad+2\frac{\partial^2 f}{\partial\rho_\alpha\partial\gamma_{\beta\beta}}\vec{\nabla}\rho^{\mathbf{D}'}_\beta\vec{\nabla}\left(2\sum_{jb\beta}U^\kappa_{bj}\psi_b\psi_j\right)(\psi_a^\alpha\psi_i^\alpha)
\end{aligned}
\tag{A.6}
$$

B-terms,

$$
\begin{aligned}
\mathbf{B.1} &= 2\frac{\partial}{\partial\kappa}\left(\frac{\partial^2 f}{\partial\gamma_{\alpha\alpha}\partial\rho_\alpha}\rho^{\mathbf{D}'}_\alpha\vec{\nabla}\rho_\alpha\vec{\nabla}(\psi_a^\alpha\psi_i^\alpha)\right)\\
&= 2\left[\frac{\partial^3 f}{\partial\gamma_{\alpha\alpha}\partial\rho_\alpha\partial\rho_\alpha}\left(2\sum_{jb\alpha}U^\kappa_{bj}\psi_b\psi_j\right)+\frac{\partial^3 f}{\partial\gamma_{\alpha\alpha}\partial\rho_\alpha\partial\rho_\beta}\left(2\sum_{jb\beta}U^\kappa_{bj}\psi_b\psi_j\right)+2\frac{\partial^3 f}{\partial\gamma_{\alpha\alpha}\partial\rho_\alpha\partial\gamma_{\alpha\alpha}}\vec{\nabla}\left(2\sum_{jb\alpha}U^\kappa_{bj}\psi_b\psi_j\right)\vec{\nabla}\rho_\alpha\right.\\
&\quad+\frac{\partial^3 f}{\partial\gamma_{\alpha\alpha}\partial\rho_\alpha\partial\gamma_{\alpha\beta}}\left\{\vec{\nabla}\left(2\sum_{jb\alpha}U^\kappa_{bj}\psi_b\psi_j\right)\vec{\nabla}\rho_\beta+\vec{\nabla}\rho_\alpha\vec{\nabla}\left(2\sum_{jb\beta}U^\kappa_{bj}\psi_b\psi_j\right)\right\}\\
&\quad\left.+2\frac{\partial^3 f}{\partial\gamma_{\alpha\alpha}\partial\rho_\alpha\partial\gamma_{\beta\beta}}\vec{\nabla}\left(2\sum_{jb\beta}U^\kappa_{bj}\psi_b\psi_j\right)\vec{\nabla}\rho_\beta\right]\rho^{\mathbf{D}'}_\alpha\vec{\nabla}\rho_\alpha\vec{\nabla}(\psi_a^\alpha\psi_i^\alpha)\\
&\quad+2\frac{\partial^2 f}{\partial\gamma_{\alpha\alpha}\partial\rho_\alpha}\rho^{\mathbf{D}'}_\alpha\vec{\nabla}\left(2\sum_{jb\alpha}U^\kappa_{bj}\psi_b\psi_j\right)\vec{\nabla}(\psi_a^\alpha\psi_i^\alpha)
\end{aligned}
\tag{A.7}
$$

$$\begin{aligned}
\mathbf{B}.\mathbf{2} &= 2\frac{\partial}{\partial\kappa}\left(\frac{\partial^2 f}{\partial\gamma_{\alpha\alpha}\partial\rho_\beta}\rho_\beta^{\mathbf{D}'}\vec{\nabla}\rho_\alpha\vec{\nabla}(\psi_a^\alpha\psi_i^\alpha)\right)\\
&= 2\left[\frac{\partial^3 f}{\partial\gamma_{\alpha\alpha}\partial\rho_\beta\partial\rho_\alpha}\left(2\sum_{jb\alpha}U_{bj}^\kappa\psi_b\psi_j\right)+\frac{\partial^3 f}{\partial\gamma_{\alpha\alpha}\partial\rho_\beta\partial\rho_\beta}\left(2\sum_{jb\beta}U_{bj}^\kappa\psi_b\psi_j\right)+2\frac{\partial^3 f}{\partial\gamma_{\alpha\alpha}\partial\rho_\beta\partial\gamma_{\alpha\alpha}}\vec{\nabla}\left(2\sum_{jb\alpha}U_{bj}^\kappa\psi_b\psi_j\right)\vec{\nabla}\rho_\alpha\right.\\
&\quad+\frac{\partial^3 f}{\partial\gamma_{\alpha\alpha}\partial\rho_\beta\partial\gamma_{\alpha\beta}}\left\{\vec{\nabla}\left(2\sum_{jb\alpha}U_{bj}^\kappa\psi_b\psi_j\right)\vec{\nabla}\rho_\beta+\vec{\nabla}\rho_\alpha\vec{\nabla}\left(2\sum_{jb\beta}U_{bj}^\kappa\psi_b\psi_j\right)\right\}\\
&\quad\left.+2\frac{\partial^3 f}{\partial\gamma_{\alpha\alpha}\partial\rho_\beta\partial\gamma_{\beta\beta}}\vec{\nabla}\left(2\sum_{jb\beta}U_{bj}^\kappa\psi_b\psi_j\right)\vec{\nabla}\rho_\beta\right]\rho_\beta^{\mathbf{D}'}\vec{\nabla}\rho_\alpha\vec{\nabla}(\psi_a^\alpha\psi_i^\alpha)\\
&\quad+2\frac{\partial^2 f}{\partial\gamma_{\alpha\alpha}\partial\rho_\beta}\rho_\beta^{\mathbf{D}'}\vec{\nabla}\left(2\sum_{jb\alpha}U_{bj}^\kappa\psi_b\psi_j\right)\vec{\nabla}(\psi_a^\alpha\psi_i^\alpha)
\end{aligned}\tag{A.8}$$

$$\begin{aligned}
\mathbf{B}.\mathbf{3} &= 2\frac{\partial}{\partial\kappa}\left(\frac{\partial^2 f}{\partial\gamma_{\alpha\alpha}\partial\gamma_{\alpha\alpha}}\gamma_{\alpha\alpha}^{\mathbf{D}'}\vec{\nabla}\rho_\alpha\vec{\nabla}(\psi_a^\alpha\psi_i^\alpha)\right)\\
&= 2\left[\frac{\partial^3 f}{\partial\gamma_{\alpha\alpha}\partial\gamma_{\alpha\alpha}\partial\rho_\alpha}\left(2\sum_{jb\alpha}U_{bj}^\kappa\psi_b\psi_j\right)+\frac{\partial^3 f}{\partial\gamma_{\alpha\alpha}\partial\gamma_{\alpha\alpha}\partial\rho_\beta}\left(2\sum_{jb\beta}U_{bj}^\kappa\psi_b\psi_j\right)+2\frac{\partial^3 f}{\partial\gamma_{\alpha\alpha}\partial\gamma_{\alpha\alpha}\partial\gamma_{\alpha\alpha}}\vec{\nabla}\left(2\sum_{jb\alpha}U_{bj}^\kappa\psi_b\psi_j\right)\vec{\nabla}\rho_\alpha\right.\\
&\quad+\frac{\partial^3 f}{\partial\gamma_{\alpha\alpha}\partial\gamma_{\alpha\alpha}\partial\gamma_{\alpha\beta}}\left\{\vec{\nabla}\left(2\sum_{jb\alpha}U_{bj}^\kappa\psi_b\psi_j\right)\vec{\nabla}\rho_\beta+\vec{\nabla}\rho_\alpha\vec{\nabla}\left(2\sum_{jb\beta}U_{bj}^\kappa\psi_b\psi_j\right)\right\}\\
&\quad\left.+2\frac{\partial^3 f}{\partial\gamma_{\alpha\alpha}\partial\gamma_{\alpha\alpha}\partial\gamma_{\beta\beta}}\vec{\nabla}\left(2\sum_{jb\beta}U_{bj}^\kappa\psi_b\psi_j\right)\vec{\nabla}\rho_\beta\right]\gamma_{\alpha\alpha}^{\mathbf{D}'}\vec{\nabla}\rho_\alpha\vec{\nabla}(\psi_a^\alpha\psi_i^\alpha)\\
&\quad+2\frac{\partial^2 f}{\partial\gamma_{\alpha\alpha}\partial\gamma_{\alpha\alpha}}\left[\gamma_{\alpha\alpha}^{\mathbf{D}'}\vec{\nabla}\left(2\sum_{jb\alpha}U_{bj}^\kappa\psi_b\psi_j\right)+2\vec{\nabla}\rho_\alpha^{\mathbf{D}'}\vec{\nabla}\left(2\sum_{jb\alpha}U_{bj}^\kappa\psi_b\psi_j\right)\vec{\nabla}\rho_\alpha\right]\vec{\nabla}(\psi_a^\alpha\psi_i^\alpha)
\end{aligned}\tag{A.9}$$

$$\begin{aligned}
\mathbf{B}.\mathbf{4} &= 2\frac{\partial}{\partial\kappa}\left(\frac{\partial^2 f}{\partial\gamma_{\alpha\alpha}\partial\gamma_{\alpha\beta}}\gamma_{\alpha\beta}^{\mathbf{D}'}\vec{\nabla}\rho_\alpha\vec{\nabla}(\psi_a^\alpha\psi_i^\alpha)\right)\\
&= 2\left[\frac{\partial^3 f}{\partial\gamma_{\alpha\alpha}\partial\gamma_{\alpha\beta}\partial\rho_\alpha}\left(2\sum_{jb\alpha}U_{bj}^\kappa\psi_b\psi_j\right)+\frac{\partial^3 f}{\partial\gamma_{\alpha\alpha}\partial\gamma_{\alpha\beta}\partial\rho_\beta}\left(2\sum_{jb\beta}U_{bj}^\kappa\psi_b\psi_j\right)+2\frac{\partial^3 f}{\partial\gamma_{\alpha\alpha}\partial\gamma_{\alpha\beta}\partial\gamma_{\alpha\alpha}}\vec{\nabla}\left(2\sum_{jb\alpha}U_{bj}^\kappa\psi_b\psi_j\right)\vec{\nabla}\rho_\alpha\right.\\
&\quad+\frac{\partial^3 f}{\partial\gamma_{\alpha\alpha}\partial\gamma_{\alpha\beta}\partial\gamma_{\alpha\beta}}\left\{\vec{\nabla}\left(2\sum_{jb\alpha}U_{bj}^\kappa\psi_b\psi_j\right)\vec{\nabla}\rho_\beta+\vec{\nabla}\rho_\alpha\vec{\nabla}\left(2\sum_{jb\beta}U_{bj}^\kappa\psi_b\psi_j\right)\right\}\\
&\quad\left.+2\frac{\partial^3 f}{\partial\gamma_{\alpha\alpha}\partial\gamma_{\alpha\beta}\partial\gamma_{\beta\beta}}\vec{\nabla}\left(2\sum_{jb\beta}U_{bj}^\kappa\psi_b\psi_j\right)\vec{\nabla}\rho_\beta\right]\gamma_{\alpha\beta}^{\mathbf{D}'}\vec{\nabla}\rho_\alpha\vec{\nabla}(\psi_a^\alpha\psi_i^\alpha)\\
&\quad+2\frac{\partial^2 f}{\partial\gamma_{\alpha\alpha}\partial\gamma_{\alpha\beta}}\left[\gamma_{\alpha\beta}^{\mathbf{D}'}\vec{\nabla}\left(2\sum_{jb\alpha}U_{bj}^\kappa\psi_b\psi_j\right)+\left\{\vec{\nabla}\rho_\alpha^{\mathbf{D}'}\vec{\nabla}\left(2\sum_{jb\beta}U_{bj}^\kappa\psi_b\psi_j\right)+\vec{\nabla}\rho_\beta^{\mathbf{D}'}\vec{\nabla}\left(2\sum_{jb\alpha}U_{bj}^\kappa\psi_b\psi_j\right)\right\}\vec{\nabla}\rho_\alpha\right]\vec{\nabla}(\psi_a^\alpha\psi_i^\alpha)
\end{aligned}\tag{A.10}$$

$$\begin{aligned}
\mathbf{B}.\mathbf{5} &= 2\frac{\partial}{\partial\kappa}\left(\frac{\partial^2 f}{\partial\gamma_{\alpha\alpha}\partial\gamma_{\beta\beta}}\gamma_{\beta\beta}^{\mathbf{D}'}\vec{\nabla}\rho_\alpha\vec{\nabla}(\psi_a^\alpha\psi_i^\alpha)\right)\\
&= 2\left[\frac{\partial^3 f}{\partial\gamma_{\alpha\alpha}\partial\gamma_{\beta\beta}\partial\rho_\alpha}\left(2\sum_{jb\alpha}U_{bj}^\kappa\psi_b\psi_j\right)+\frac{\partial^3 f}{\partial\gamma_{\alpha\alpha}\partial\gamma_{\beta\beta}\partial\rho_\beta}\left(2\sum_{jb\beta}U_{bj}^\kappa\psi_b\psi_j\right)+2\frac{\partial^3 f}{\partial\gamma_{\alpha\alpha}\partial\gamma_{\beta\beta}\partial\gamma_{\alpha\alpha}}\vec{\nabla}\left(2\sum_{jb\alpha}U_{bj}^\kappa\psi_b\psi_j\right)\vec{\nabla}\rho_\alpha\right.\\
&\quad+\frac{\partial^3 f}{\partial\gamma_{\alpha\alpha}\partial\gamma_{\beta\beta}\partial\gamma_{\alpha\beta}}\left\{\vec{\nabla}\left(2\sum_{jb\alpha}U_{bj}^\kappa\psi_b\psi_j\right)\vec{\nabla}\rho_\beta+\vec{\nabla}\rho_\alpha\vec{\nabla}\left(2\sum_{jb\beta}U_{bj}^\kappa\psi_b\psi_j\right)\right\}\\
&\quad\left.+2\frac{\partial^3 f}{\partial\gamma_{\alpha\alpha}\partial\gamma_{\beta\beta}\partial\gamma_{\beta\beta}}\vec{\nabla}\left(2\sum_{jb\beta}U_{bj}^\kappa\psi_b\psi_j\right)\vec{\nabla}\rho_\beta\right]\gamma_{\beta\beta}^{\mathbf{D}'}\vec{\nabla}\rho_\alpha\vec{\nabla}(\psi_a^\alpha\psi_i^\alpha)\\
&\quad+2\frac{\partial^2 f}{\partial\gamma_{\alpha\alpha}\partial\gamma_{\beta\beta}}\left[\gamma_{\beta\beta}^{\mathbf{D}'}\vec{\nabla}\left(2\sum_{jb\alpha}U_{bj}^\kappa\psi_b\psi_j\right)+\vec{\nabla}\rho_\beta^{\mathbf{D}'}\vec{\nabla}\left(2\sum_{jb\beta}U_{bj}^\kappa\psi_b\psi_j\right)\vec{\nabla}\rho_\alpha\right]\vec{\nabla}(\psi_a^\alpha\psi_i^\alpha)
\end{aligned}\tag{A.11}$$

C-terms,

$$
\begin{aligned}
\mathbf{C.1} &= \frac{\partial}{\partial\kappa}\left(\frac{\partial^2 f}{\partial\gamma_{\alpha\beta}\partial\rho_\alpha}\rho_\alpha^{\mathbf{D}'}\vec{\nabla}\rho_\beta\vec{\nabla}(\psi_a^\alpha\psi_i^\alpha)\right)\\
&= \left[\frac{\partial^3 f}{\partial\gamma_{\alpha\beta}\partial\rho_\alpha\partial\rho_\alpha}\left(2\sum_{jb\alpha}U_{bj}^\kappa\psi_b\psi_j\right)+\frac{\partial^3 f}{\partial\gamma_{\alpha\beta}\partial\rho_\alpha\partial\rho_\beta}\left(2\sum_{jb\beta}U_{bj}^\kappa\psi_b\psi_j\right)+2\frac{\partial^3 f}{\partial\gamma_{\alpha\beta}\partial\rho_\alpha\partial\gamma_{\alpha\alpha}}\vec{\nabla}\left(2\sum_{jb\alpha}U_{bj}^\kappa\psi_b\psi_j\right)\vec{\nabla}\rho_\alpha\right.\\
&\quad+\frac{\partial^3 f}{\partial\gamma_{\alpha\beta}\partial\rho_\alpha\partial\gamma_{\alpha\beta}}\left\{\vec{\nabla}\left(2\sum_{jb\alpha}U_{bj}^\kappa\psi_b\psi_j\right)\vec{\nabla}\rho_\beta+\vec{\nabla}\rho_\alpha\vec{\nabla}\left(2\sum_{jb\beta}U_{bj}^\kappa\psi_b\psi_j\right)\right\}\\
&\quad\left.+2\frac{\partial^3 f}{\partial\gamma_{\alpha\beta}\partial\rho_\alpha\partial\gamma_{\beta\beta}}\vec{\nabla}\left(2\sum_{jb\beta}U_{bj}^\kappa\psi_b\psi_j\right)\vec{\nabla}\rho_\beta\right]\rho_\alpha^{\mathbf{D}'}\vec{\nabla}\rho_\beta\vec{\nabla}(\psi_a^\alpha\psi_i^\alpha)\\
&\quad+\frac{\partial^2 f}{\partial\gamma_{\alpha\beta}\partial\rho_\alpha}\rho_\alpha^{\mathbf{D}'}\vec{\nabla}\left(2\sum_{jb\beta}U_{bj}^\kappa\psi_b\psi_j\right)\vec{\nabla}(\psi_a^\alpha\psi_i^\alpha) \qquad \text{(A.12)}\\
\mathbf{C.2} &= \frac{\partial}{\partial\kappa}\left(\frac{\partial^2 f}{\partial\gamma_{\alpha\beta}\partial\rho_\beta}\rho_\beta^{\mathbf{D}'}\vec{\nabla}\rho_\beta\vec{\nabla}(\psi_a^\alpha\psi_i^\alpha)\right)\\
&= \left[\frac{\partial^3 f}{\partial\gamma_{\alpha\beta}\partial\rho_\beta\partial\rho_\alpha}\left(2\sum_{jb\alpha}U_{bj}^\kappa\psi_b\psi_j\right)+\frac{\partial^3 f}{\partial\gamma_{\alpha\beta}\partial\rho_\beta\partial\rho_\beta}\left(2\sum_{jb\beta}U_{bj}^\kappa\psi_b\psi_j\right)+2\frac{\partial^3 f}{\partial\gamma_{\alpha\beta}\partial\rho_\beta\partial\gamma_{\alpha\alpha}}\vec{\nabla}\left(2\sum_{jb\alpha}U_{bj}^\kappa\psi_b\psi_j\right)\vec{\nabla}\rho_\alpha\right.\\
&\quad+\frac{\partial^3 f}{\partial\gamma_{\alpha\beta}\partial\rho_\beta\partial\gamma_{\alpha\beta}}\left\{\vec{\nabla}\left(2\sum_{jb\alpha}U_{bj}^\kappa\psi_b\psi_j\right)\vec{\nabla}\rho_\beta+\vec{\nabla}\rho_\alpha\vec{\nabla}\left(2\sum_{jb\beta}U_{bj}^\kappa\psi_b\psi_j\right)\right\}\\
&\quad\left.+2\frac{\partial^3 f}{\partial\gamma_{\alpha\beta}\partial\rho_\beta\partial\gamma_{\beta\beta}}\vec{\nabla}\left(2\sum_{jb\beta}U_{bj}^\kappa\psi_b\psi_j\right)\vec{\nabla}\rho_\beta\right]\rho_\alpha^{\mathbf{D}'}\vec{\nabla}\rho_\beta\vec{\nabla}(\psi_a^\alpha\psi_i^\alpha)\\
&\quad+\frac{\partial^2 f}{\partial\gamma_{\alpha\beta}\partial\rho_\beta}\rho_\beta^{\mathbf{D}'}\vec{\nabla}\left(2\sum_{jb\beta}U_{bj}^\kappa\psi_b\psi_j\right)\vec{\nabla}(\psi_a^\alpha\psi_i^\alpha) \qquad \text{(A.13)}\\
\mathbf{C.3} &= \frac{\partial}{\partial\kappa}\left(\frac{\partial^2 f}{\partial\gamma_{\alpha\beta}\partial\gamma_{\alpha\alpha}}\gamma_{\alpha\alpha}^{\mathbf{D}'}\vec{\nabla}\rho_\beta\vec{\nabla}(\psi_a^\alpha\psi_i^\alpha)\right)\\
&= \left[\frac{\partial^3 f}{\partial\gamma_{\alpha\beta}\partial\gamma_{\alpha\alpha}\partial\rho_\alpha}\left(2\sum_{jb\alpha}U_{bj}^\kappa\psi_b\psi_j\right)+\frac{\partial^3 f}{\partial\gamma_{\alpha\beta}\partial\gamma_{\alpha\alpha}\partial\rho_\beta}\left(2\sum_{jb\beta}U_{bj}^\kappa\psi_b\psi_j\right)+2\frac{\partial^3 f}{\partial\gamma_{\alpha\beta}\partial\gamma_{\alpha\alpha}\partial\gamma_{\alpha\alpha}}\vec{\nabla}\left(2\sum_{jb\alpha}U_{bj}^\kappa\psi_b\psi_j\right)\vec{\nabla}\rho_\alpha\right.\\
&\quad+\frac{\partial^3 f}{\partial\gamma_{\alpha\beta}\partial\gamma_{\alpha\alpha}\partial\gamma_{\alpha\beta}}\left\{\vec{\nabla}\left(2\sum_{jb\alpha}U_{bj}^\kappa\psi_b\psi_j\right)\vec{\nabla}\rho_\beta+\vec{\nabla}\rho_\alpha\vec{\nabla}\left(2\sum_{jb\beta}U_{bj}^\kappa\psi_b\psi_j\right)\right\}\\
&\quad\left.+2\frac{\partial^3 f}{\partial\gamma_{\alpha\beta}\partial\gamma_{\alpha\alpha}\partial\gamma_{\beta\beta}}\vec{\nabla}\left(2\sum_{jb\beta}U_{bj}^\kappa\psi_b\psi_j\right)\vec{\nabla}\rho_\beta\right]\gamma_{\alpha\alpha}^{\mathbf{D}'}\vec{\nabla}\rho_\beta\vec{\nabla}(\psi_a^\alpha\psi_i^\alpha)\\
&\quad+\frac{\partial^2 f}{\partial\gamma_{\alpha\beta}\partial\gamma_{\alpha\alpha}}\left[\gamma_{\alpha\alpha}^{\mathbf{D}'}\vec{\nabla}\left(2\sum_{jb\beta}U_{bj}^\kappa\psi_b\psi_j\right)+2\vec{\nabla}\rho_\alpha^{\mathbf{D}'}\vec{\nabla}\left(2\sum_{jb\alpha}U_{bj}^\kappa\psi_b\psi_j\right)\vec{\nabla}\rho_\beta\right]\vec{\nabla}(\psi_a^\alpha\psi_i^\alpha) \qquad \text{(A.14)}\\
\mathbf{C.4} &= \frac{\partial}{\partial\kappa}\left(\frac{\partial^2 f}{\partial\gamma_{\alpha\beta}\partial\gamma_{\alpha\beta}}\gamma_{\alpha\beta}^{\mathbf{D}'}\vec{\nabla}\rho_\beta\vec{\nabla}(\psi_a^\alpha\psi_i^\alpha)\right)\\
&= \left[\frac{\partial^3 f}{\partial\gamma_{\alpha\beta}\partial\gamma_{\alpha\beta}\partial\rho_\alpha}\left(2\sum_{jb\alpha}U_{bj}^\kappa\psi_b\psi_j\right)+\frac{\partial^3 f}{\partial\gamma_{\alpha\beta}\partial\gamma_{\alpha\beta}\partial\rho_\beta}\left(2\sum_{jb\beta}U_{bj}^\kappa\psi_b\psi_j\right)+2\frac{\partial^3 f}{\partial\gamma_{\alpha\beta}\partial\gamma_{\alpha\beta}\partial\gamma_{\alpha\alpha}}\vec{\nabla}\left(2\sum_{jb\alpha}U_{bj}^\kappa\psi_b\psi_j\right)\vec{\nabla}\rho_\alpha\right.\\
&\quad+\frac{\partial^3 f}{\partial\gamma_{\alpha\beta}\partial\gamma_{\alpha\beta}\partial\gamma_{\alpha\beta}}\left\{\vec{\nabla}\left(2\sum_{jb\alpha}U_{bj}^\kappa\psi_b\psi_j\right)\vec{\nabla}\rho_\beta+\vec{\nabla}\rho_\alpha\vec{\nabla}\left(2\sum_{jb\beta}U_{bj}^\kappa\psi_b\psi_j\right)\right\}\\
&\quad\left.+2\frac{\partial^3 f}{\partial\gamma_{\alpha\beta}\partial\gamma_{\alpha\beta}\partial\gamma_{\beta\beta}}\vec{\nabla}\left(2\sum_{jb\beta}U_{bj}^\kappa\psi_b\psi_j\right)\vec{\nabla}\rho_\beta\right]\gamma_{\alpha\beta}^{\mathbf{D}'}\vec{\nabla}\rho_\beta\vec{\nabla}(\psi_a^\alpha\psi_i^\alpha)\\
&\quad+\frac{\partial^2 f}{\partial\gamma_{\alpha\beta}\partial\gamma_{\alpha\beta}}\left[\gamma_{\alpha\beta}^{\mathbf{D}'}\vec{\nabla}\left(2\sum_{jb\beta}U_{bj}^\kappa\psi_b\psi_j\right)+\left\{\vec{\nabla}\rho_\alpha^{\mathbf{D}'}\vec{\nabla}\left(2\sum_{jb\beta}U_{bj}^\kappa\psi_b\psi_j\right)+\vec{\nabla}\rho_\beta^{\mathbf{D}'}\vec{\nabla}\left(2\sum_{jb\alpha}U_{bj}^\kappa\psi_b\psi_j\right)\right\}\vec{\nabla}\rho_\beta\right]\vec{\nabla}(\psi_a^\alpha\psi_i^\alpha)
\end{aligned}
$$

(A.15)

$$
\begin{aligned}
\mathbf{C.5} &= \frac{\partial}{\partial\kappa}\left(\frac{\partial^2 f}{\partial\gamma_{\alpha\beta}\partial\gamma_{\beta\beta}}\gamma^{\mathbf{D}'}_{\beta\beta}\vec{\nabla}\rho_\beta\vec{\nabla}(\psi^\alpha_a\psi^\alpha_i)\right)\\
&= \left[\frac{\partial^3 f}{\partial\gamma_{\alpha\beta}\partial\gamma_{\beta\beta}\partial\rho_\alpha}\left(2\sum_{jb\alpha}U^\kappa_{bj}\psi_b\psi_j\right)+\frac{\partial^3 f}{\partial\gamma_{\alpha\beta}\partial\gamma_{\beta\beta}\partial\rho_\beta}\left(2\sum_{jb\beta}U^\kappa_{bj}\psi_b\psi_j\right)+2\frac{\partial^3 f}{\partial\gamma_{\alpha\beta}\partial\gamma_{\beta\beta}\partial\gamma_{\alpha\alpha}}\vec{\nabla}\left(2\sum_{jb\alpha}U^\kappa_{bj}\psi_b\psi_j\right)\vec{\nabla}\rho_\alpha\right.\\
&\quad+\frac{\partial^3 f}{\partial\gamma_{\alpha\beta}\partial\gamma_{\beta\beta}\partial\gamma_{\alpha\beta}}\left\{\vec{\nabla}\left(2\sum_{jb\alpha}U^\kappa_{bj}\psi_b\psi_j\right)\vec{\nabla}\rho_\beta+\vec{\nabla}\rho_\alpha\vec{\nabla}\left(2\sum_{jb\beta}U^\kappa_{bj}\psi_b\psi_j\right)\right\}\\
&\quad\left.+2\frac{\partial^3 f}{\partial\gamma_{\alpha\beta}\partial\gamma_{\beta\beta}\partial\gamma_{\beta\beta}}\vec{\nabla}\left(2\sum_{jb\beta}U^\kappa_{bj}\psi_b\psi_j\right)\vec{\nabla}\rho_\beta\right]\gamma^{\mathbf{D}'}_{\beta\beta}\vec{\nabla}\rho_\beta\vec{\nabla}(\psi^\alpha_a\psi^\alpha_i)\\
&\quad+\frac{\partial^2 f}{\partial\gamma_{\alpha\beta}\partial\gamma_{\beta\beta}}\left[\gamma^{\mathbf{D}'}_{\beta\beta}\vec{\nabla}\left(2\sum_{jb\beta}U^\kappa_{bj}\psi_b\psi_j\right)+2\vec{\nabla}\rho^{\mathbf{D}'}_\beta\vec{\nabla}\left(2\sum_{jb\beta}U^\kappa_{bj}\psi_b\psi_j\right)\vec{\nabla}\rho_\beta\right]\vec{\nabla}(\psi^\alpha_a\psi^\alpha_i)
\end{aligned}
\tag{A.16}
$$

D-terms,

$$
\begin{aligned}
\mathbf{D.1} &= 2\frac{\partial}{\partial\kappa}\left(\frac{\partial f}{\partial\gamma_{\alpha\alpha}}\vec{\nabla}\rho^{\mathbf{D}'}_\alpha\vec{\nabla}\left(\psi^\alpha_a\psi^\alpha_i\right)\right)\\
&= 2\left[\frac{\partial^2 f}{\partial\gamma_{\alpha\alpha}\partial\rho_\alpha}\left(2\sum_{jb\alpha}U^\kappa_{bj}\psi_b\psi_j\right)+\frac{\partial^2 f}{\partial\gamma_{\alpha\alpha}\partial\rho_\beta}\left(2\sum_{jb\beta}U^\kappa_{bj}\psi_b\psi_j\right)+2\frac{\partial^2 f}{\partial\gamma_{\alpha\alpha}\partial\gamma_{\alpha\alpha}}\vec{\nabla}\left(2\sum_{jb\alpha}U^\kappa_{bj}\psi_b\psi_j\right)\vec{\nabla}\rho_\alpha\right.\\
&\quad+\frac{\partial^2 f}{\partial\gamma_{\alpha\alpha}\partial\gamma_{\alpha\beta}}\left\{\vec{\nabla}\left(2\sum_{jb\alpha}U^\kappa_{bj}\psi_b\psi_j\right)\vec{\nabla}\rho_\beta+\vec{\nabla}\rho_\alpha\vec{\nabla}\left(2\sum_{jb\beta}U^\kappa_{bj}\psi_b\psi_j\right)\right\}\\
&\quad\left.+2\frac{\partial^2 f}{\partial\gamma_{\alpha\alpha}\partial\gamma_{\beta\beta}}\vec{\nabla}\left(2\sum_{jb\beta}U^\kappa_{bj}\psi_b\psi_j\right)\vec{\nabla}\rho_\beta\right]\vec{\nabla}\rho^{\mathbf{D}'}_\alpha\vec{\nabla}(\psi^\alpha_a\psi^\alpha_i)
\end{aligned}
\tag{A.17}
$$

$$
\begin{aligned}
\mathbf{D.2} &= \frac{\partial}{\partial\kappa}\left(\frac{\partial f}{\partial\gamma_{\alpha\beta}}\vec{\nabla}\rho^{\mathbf{D}'}_\beta\vec{\nabla}\left(\psi^\alpha_a\psi^\alpha_i\right)\right)\\
&= \left[\frac{\partial^2 f}{\partial\gamma_{\alpha\beta}\partial\rho_\alpha}\left(2\sum_{jb\alpha}U^\kappa_{bj}\psi_b\psi_j\right)+\frac{\partial^2 f}{\partial\gamma_{\alpha\beta}\partial\rho_\beta}\left(2\sum_{jb\beta}U^\kappa_{bj}\psi_b\psi_j\right)+2\frac{\partial^2 f}{\partial\gamma_{\alpha\beta}\partial\gamma_{\alpha\alpha}}\vec{\nabla}\left(2\sum_{jb\alpha}U^\kappa_{bj}\psi_b\psi_j\right)\vec{\nabla}\rho_\alpha\right.\\
&\quad+\frac{\partial^2 f}{\partial\gamma_{\alpha\beta}\partial\gamma_{\alpha\beta}}\left\{\vec{\nabla}\left(2\sum_{jb\alpha}U^\kappa_{bj}\psi_b\psi_j\right)\vec{\nabla}\rho_\beta+\vec{\nabla}\rho_\alpha\vec{\nabla}\left(2\sum_{jb\beta}U^\kappa_{bj}\psi_b\psi_j\right)\right\}\\
&\quad\left.+2\frac{\partial^2 f}{\partial\gamma_{\alpha\beta}\partial\gamma_{\beta\beta}}\vec{\nabla}\left(2\sum_{jb\beta}U^\kappa_{bj}\psi_b\psi_j\right)\vec{\nabla}\rho_\beta\right]\vec{\nabla}\rho^{\mathbf{D}'}_\beta\vec{\nabla}(\psi^\alpha_a\psi^\alpha_i)
\end{aligned}
\tag{A.18}
$$

Collecting terms and summarizing yields,

$$
\mathbf{A} = \sum_\zeta\sum_\xi\frac{\partial^3 f}{\partial\rho_\alpha\partial\zeta\partial\xi}\xi^{\mathbf{U}^\kappa}\zeta^{\mathbf{D}'}\left(\psi^\alpha_a\psi^\alpha_i\right)+\left[\frac{\partial^2 f}{\partial\rho_\alpha\partial\gamma_{\alpha\alpha}}\gamma^{\mathbf{U}^\kappa\mathbf{D}'}_{\alpha\alpha}+\frac{\partial^2 f}{\partial\rho_\alpha\partial\gamma_{\alpha\beta}}\gamma^{\mathbf{U}^\kappa\mathbf{D}'}_{\alpha\beta}+\frac{\partial^2 f}{\partial\rho_\alpha\partial\gamma_{\beta\beta}}\gamma^{\mathbf{U}^\kappa\mathbf{D}'}_{\beta\beta}\right]\left(\psi^\alpha_a\psi^\alpha_i\right)
\tag{A.19}
$$

$$
\begin{aligned}
\mathbf{B} &= 2\sum_\zeta\sum_\xi\frac{\partial^3 f}{\partial\gamma_{\alpha\alpha}\partial\zeta\partial\xi}\xi^{\mathbf{U}^\kappa}\zeta^{\mathbf{D}'}\vec{\nabla}\rho_\alpha\vec{\nabla}\left(\psi^\alpha_a\psi^\alpha_i\right)\\
&\quad+2\left[\frac{\partial^2 f}{\partial\gamma_{\alpha\alpha}\partial\rho_\alpha}\rho^{\mathbf{D}'}_\alpha\vec{\nabla}\rho^{\mathbf{U}^\kappa}_\alpha+\frac{\partial^2 f}{\partial\gamma_{\alpha\alpha}\partial\rho_\beta}\rho^{\mathbf{D}'}_\beta\vec{\nabla}\rho^{\mathbf{U}^\kappa}_\alpha+\frac{\partial^2 f}{\partial\gamma_{\alpha\alpha}\partial\gamma_{\alpha\alpha}}\left(\gamma^{\mathbf{D}'}_{\alpha\alpha}\vec{\nabla}\rho^{\mathbf{U}^\kappa}_\alpha+\gamma^{\mathbf{U}^\kappa\mathbf{D}'}_{\alpha\alpha}\vec{\nabla}\rho_\alpha\right)\right.\\
&\quad\left.+\frac{\partial^2 f}{\partial\gamma_{\alpha\alpha}\partial\gamma_{\alpha\beta}}\left(\gamma^{\mathbf{D}'}_{\alpha\beta}\vec{\nabla}\rho^{\mathbf{U}^\kappa}_\alpha+\gamma^{\mathbf{U}^\kappa\mathbf{D}'}_{\alpha\beta}\vec{\nabla}\rho_\alpha\right)+\frac{\partial^2 f}{\partial\gamma_{\alpha\alpha}\partial\gamma_{\beta\beta}}\left(\gamma^{\mathbf{D}'}_{\beta\beta}\vec{\nabla}\rho^{\mathbf{U}^\kappa}_\alpha+\gamma^{\mathbf{U}^\kappa\mathbf{D}'}_{\beta\beta}\vec{\nabla}\rho_\alpha\right)\right]\vec{\nabla}\left(\psi^\alpha_a\psi^\alpha_i\right)
\end{aligned}
\tag{A.20}
$$

$$
\begin{aligned}
\mathbf{C} &= \sum_\zeta\sum_\xi\frac{\partial^3 f}{\partial\gamma_{\alpha\beta}\partial\zeta\partial\xi}\xi^{\mathbf{U}^\kappa}\zeta^{\mathbf{D}'}\vec{\nabla}\rho_\beta\vec{\nabla}\left(\psi^\alpha_a\psi^\alpha_i\right)\\
&\quad+\left[\frac{\partial^2 f}{\partial\gamma_{\alpha\beta}\partial\rho_\alpha}\rho^{\mathbf{D}'}_\alpha\vec{\nabla}\rho^{\mathbf{U}^\kappa}_\beta+\frac{\partial^2 f}{\partial\gamma_{\alpha\beta}\partial\rho_\beta}\rho^{\mathbf{D}'}_\beta\vec{\nabla}\rho^{\mathbf{U}^\kappa}_\beta+\frac{\partial^2 f}{\partial\gamma_{\alpha\beta}\partial\gamma_{\alpha\alpha}}\left(\gamma^{\mathbf{D}'}_{\alpha\alpha}\vec{\nabla}\rho^{\mathbf{U}^\kappa}_\beta+\gamma^{\mathbf{U}^\kappa\mathbf{D}'}_{\alpha\alpha}\vec{\nabla}\rho_\beta\right)\right.\\
&\quad\left.+\frac{\partial^2 f}{\partial\gamma_{\alpha\beta}\partial\gamma_{\alpha\beta}}\left(\gamma^{\mathbf{D}'}_{\alpha\beta}\vec{\nabla}\rho^{\mathbf{U}^\kappa}_\beta+\gamma^{\mathbf{U}^\kappa\mathbf{D}'}_{\alpha\beta}\vec{\nabla}\rho_\beta\right)+\frac{\partial^2 f}{\partial\gamma_{\alpha\beta}\partial\gamma_{\beta\beta}}\left(\gamma^{\mathbf{D}'}_{\beta\beta}\vec{\nabla}\rho^{\mathbf{U}^\kappa}_\beta+\gamma^{\mathbf{U}^\kappa\mathbf{D}'}_{\beta\beta}\vec{\nabla}\rho_\beta\right)\right]\vec{\nabla}\left(\psi^\alpha_a\psi^\alpha_i\right)
\end{aligned}
\tag{A.21}
$$

$$
\mathbf{D} = \sum_\zeta 2\frac{\partial^2 f}{\partial\gamma_{\alpha\alpha}\partial\zeta}\zeta^{\mathbf{U}^\kappa}\vec{\nabla}\rho^{\mathbf{D}'}_\alpha\vec{\nabla}\left(\psi^\alpha_a\psi^\alpha_i\right)+\frac{\partial^2 f}{\partial\gamma_{\alpha\beta}\partial\zeta}\zeta^{\mathbf{U}^\kappa}\vec{\nabla}\rho^{\mathbf{D}'}_\beta\vec{\nabla}\left(\psi^\alpha_a\psi^\alpha_i\right).
\tag{A.22}
$$

Bibliography

[1] Grimme, S. *J. Chem. Phys.* **2006,** *124,* 034108.

[2] Møller, C.; Plesset, M. S. *Phys. Rev.* **1934,** *46,* 618.

[3] Cremer, D. In *Encyclopedia of Computational Chemistry*, Vol. 3; von Ragué Schleyer, P., Ed.; John Wiley & Sons Ltd: Chichester, 1998.

[4] Bartlett, R. J.; Silver, D. M. *Int. J. Quant. Chem.* **1974,** *S8,* 271.

[5] Binkley, J. S.; Pople, J. A. *Int. J. Quant. Chem.* **1975,** *9,* 229.

[6] Pople, J. A.; Binkley, J. S.; Seeger, R. *Int. J. Quant. Chem.* **1976,** *10,* 1.

[7] Bartlett, R. J.; Shavitt, I. *Chem. Phys. Lett.* **1977,** *50,* 190.

[8] Bartlett, R. J.; Purvis, G. D. *J. Chem. Phys.* **1978,** *68,* 2114.

[9] Krishnan, R.; Pople, J. A. *Int. J. Quant. Chem.* **1978,** *14,* 91.

[10] Krishnan, R.; Binkley, J. S.; Seeger, R.; Pople, J. A. *J. Chem. Phys.* **1980,** *72,* 650.

[11] Pople, J. A.; Krishnan, R.; Schlegel, H. B.; Binkley, J. S. *Int. J. Quant. Chem.* **1979,** *16,* 225.

[12] Salter, E. A.; Trucks, G. W.; Fitzgerald, G.; Bartlett, R. J. *Chem. Phys. Lett.* **1987,** *141,* 61.

[13] Salter, E. A.; Trucks, G. W.; Bartlett, R. J. *J. Chem. Phys.* **1989,** *90,* 1752.

[14] Handy, N. C.; Schaefer III, H. F. *J. Chem. Phys.* **1984,** *81,* 5031.

[15] Adamowicz, L.; Laidig, W. D.; Bartlett, R. J. *Int. J. Quant. Chem. Symp.* **1984,** *18,* 245.

[16] Harrison, R. J.; Fitzgerald, G. B.; Laidig, W. D.; Bartlett, R. J. *Chem. Phys. Lett.* **1986,** *124,* 291.

[17] Gauss, J. *Chem. Phys. Lett.* **1992,** *191,* 614.

[18] Goldstone, J. *Proc. R. Soc. London, Ser. A* **1957,** *A239,* 267.

[19] Brillouin, L. In *Acta Sci. Ind. No. 159*; Hermann et Cie.: Paris, 1934.

[20] Kendall, R. A.; Früchtl, H. A. *Theor. Chim. Acta* **1997,** *97,* 158.

[21] Feyereisen, M.; Fitzgerald, G.; Komornicki, A. *Chem. Phys. Lett.* **1993,** *208,* 359.

[22] Vahtras, O.; Almlöf, J.; Feyereisen, M. W. *Chem. Phys. Lett.* **1993,** *213,* 514.

[23] Biczysko, M.; Panek, P.; Scalmani, G.; Bloino, J.; Barone, V. *J. Chem. Theory Comput.* **2010,** *6,* 2115.

[24] Hylleraas, E. A. *Z. Physik* **1930,** *65,* 209.

[25] Neese, F.; Becker, U.; Ganyushin, D.; Koßmann, S.; Hansen, A.; Liakos, D.; Petrenko, T.; Riplinger, C.; Wennmohs, F. *ORCA - an ab initio, density functional and semiempirical program package, Version 2.7.0;* University of Bonn: Bonn, Germany, 2009.

[26] Pulay, P.; Saebø, S. *Theor. Chim. Acta* **1986,** *69,* 357.

[27] Løwdin, P. O. *Phys. Rev.* **1955,** *97,* 1474.

[28] Eichkorn, K.; Treutler, O.; Öhm, H.; Häser, M.; Ahlrichs, R. *Chem. Phys. Lett.* **1995,** *242,* 652.

[29] Eichkorn, K.; Weigend, F.; Treutler, O.; Ahlrichs, R. *Theor. Chem. Acc.* **1997,** *97,* 119.

[30] Neese, F. *J. Comput. Chem.* **2003,** *24,* 1740.

[31] Koßmann, S.; Neese, F. *J. Chem. Theory Comput.* **2010,** *6,* 2325.

[32] Weigend, F.; Häser, M.; Patzelt, H.; Ahlrichs, R. *Chem. Phys. Lett.* **1998,** *294,* 143.

[33] Weigend, F.; Koehn, A.; Hättig, C. *J. Chem. Phys.* **2002,** *116,* 3175.

[34] Hättig, C. *Phys. Chem. Chem. Phys.* **2005,** *7,* 59.

[35] Panas, I.; Almlöf, J. *Int. J. Quant. Chem.* **1992,** *42,* 1073.

[36] Ahmadi, G. R.; Almlöf, J. *Chem. Phys. Lett.* **1995,** *246,* 364.

[37] Baerends, E. J.; Ellis, D. E.; Ros, P. *Chem. Phys.* **1973,** *2,* 41.

[38] Whitten, J. L. *J. Chem. Phys.* **1973,** *58,* 4496.

[39] Neese, F.; Wennmohs, F.; Hansen, A.; Becker, U. *Chem. Phys.* **2008,** *356,* 98.

[40] Friesner, R. A. *Chem. Phys. Lett.* **1985,** *116,* 39.

[41] Friesner, R. A. *J. Chem. Phys.* **1986,** *85,* 1462.

[42] Friesner, R. A. *J. Chem. Phys.* **1987,** *86,* 3522.

[43] Won, Y.; Lee, J.-G.; Ringnalda, M. N.; Friesner, R. A. *J. Chem. Phys.* **1991,** *94,* 8152.

[44] Becke, A. D. *J. Chem. Phys.* **1988,** *88,* 2547.

[45] Ko, C.; Malick, D. K.; Braden, D. A.; Friesner, R. A.; Martinez, T. J. *J. Chem. Phys.* **2008,** *128,* 104103.

[46] Hohenberg, P.; Kohn, W. *Phys. Rev.* **1964,** *136,* B864.

[47] Kohn, W.; Sham, L. J. *Phys. Rev.* **1965,** *140,* A1133.

[48] Perdew, J. P.; Schmidt, K. In *Density Functional Theory and Its Application to Materials*; Doren, V. V.; Alsenoy, C. V.; Geerlings, P., Eds.; AIP: Melville, NY, 2001.

[49] Neese, F.; Schwabe, T.; Grimme, S. *J. Chem. Phys.* **2007,** *126,* 124115.

[50] Scuseria, G. E.; Schaefer III., H. F. *Chem. Phys. Lett.* **1987,** *142,* 354.

[51] Brillouin, L. **1932,** *3,* 373.

[52] Weigend, F.; Häser, M. *Theor. Chem. Acc.* **1997,** *97,* 331.

[53] Pulay, P. *J. Comput. Chem.* **1982,** *3,* 556.

[54] Hellmann, H. *Einführung in die Quantenchemie;* Franz Deuticke: Leipzig, 1937.

[55] Feynman, R. P. *Phys. Rev.* **1939,** *56,* 340.

[56] Schlegel, H. B. *J. Chem. Phys.* **1986,** *84,* 4530.

[57] Chen, W.; Schlegel, H. B. *J. Chem. Phys.* **1994,** *101,* 5957.

[58] Lochan, R. C.; Head-Gordon, M. *J. Chem. Phys.* **2007,** *126,* 164101.

[59] Koßmann, S.; Neese, F. *J. Phys. Chem. A* **2010,** *114,* 11768.

[60] Krack, M.; Köster, A. M. *J. Chem. Phys.* **1998,** *108,* 3226.

[61] Gill, P. M.-W.; Johnson, B. G.; Pople, J. A. *Chem. Phys. Lett.* **1993,** *209,* 506.

[62] Stanton, J. F.; Gauss, J.; Harding, M. E.; Szalay, P. G. "CFOUR, Coupled-Cluster techniques for Computational Chemistry", 2010 Version 1.0, with contributions from A. A. Auer, R. J. Bartlett, U. Benedikt, C. Berger, D. E. Bernholdt, Y. J. Bomble, L. Cheng, O. Christiansen, M. Heckert, O. Heun, C. Huber, T.-C. Jagau, D. Jonsson, J. Jusélius, K. Klein, W.J. Lauderdale, D. A. Matthews, T. Metzroth, D. P. O'Neill, D. R. Price, E. Prochnow, K. Ruud, F. Schiffmann, W. Schwalbach, S. Stopkowicz, A. Tajti, J. Vázquez, F. Wang, J. D. Watts and the integral packages MOLECULE (J. Almlöf and P. R. Taylor), PROPS (P. R. Taylor), ABACUS (T. Helgaker, H. J. Aa. Jensen, P. Jørgensen, and J. Olsen), and ECP routines by A. V. Mitin and C. van Wüllen. For the current version, see http://www.cfour.de.

[63] Schäfer, A.; Horn, H.; Ahlrichs, R. *J. Chem. Phys.* **1992,** *97,* 2571.

[64] R. Ahlrichs and co-workers: Polarization functions were obtained from the TurboMole basis set library under ftp.chemie.uni-karlsruhe.de/pub/basen.

[65] Dunning, Jr., T. H. *J. Chem. Phys.* **1989,** *90,* 1007.

[66] Ahlrichs, R.; Furche, F.; Hättig, C.; Klopper, W. M.; Sierka, M.; Weigend, F. *TurboMole basis*

set library; TURBOMOLE GmbH: Karlsruhe, Germany, ftp.chemie.uni-karlsruhe.de/pub/BASES (accessed June 24, 2010).

[67] Tao, J.; Perdew, J. P.; Staroverov, V. N.; Scuseria, G. E. *Phys. Rev. Lett.* **2003,** *91,* 146401.

[68] Schäfer, A.; Huber, C.; Ahlrichs, R. *J. Chem. Phys.* **1994,** *100,* 5829.

[69] Sinnecker, S.; Reijerse, E.; Neese, F.; Lubitz, W. *J. Am. Chem. Soc.* **2004,** *126,* 3280.

[70] Schäfer, A.; Huber, C.; Ahlrichs, R. *J. Chem. Phys.* **1994,** *100,* 5829.

[71] Becke, A. D. *Phys. Rev. A* **1988,** *38,* 3098.

[72] Perdew, J. P. *Phys. Rev. B* **1986,** *33,* 8822.

[73] Lushington, G. H. In *Calculation of NMR and EPR Parameters. Theory and Applications*; Kaupp, M.; Bühl, M.; Malkin, V. G., Eds.; Wiley-VCH Verlag: Weinheim, 2004.

[74] Helgaker, T.; Jaszuński, M.; Ruud, K. *Chem. Rev.* **1999,** *99,* 293.

[75] Sauer, S. P. A. "Quantum Chemical Methods for the Calculation of Electromagnetic Molecular Properties", 2006 Lecture Notes for the SFB 663 Lecture Course in Mülheim a. d. Ruhr und in Düsseldorf.

[76] Gauss, J. In *Modern Methods and Algorithms in Quantum Chemistry*, Vol. 3; John von Neumann Institute for Computing: Jülich, NIC Series, 2000.

[77] Kutzelnigg, W. In *Calculation of NMR and EPR Parameters. Theory and Applications.*; Wiley-VCH Verlag: Weinheim, 2004.

[78] Kutzelnigg, W. *Isr. J. Chem.* **1980,** *19,* 193.

[79] Schindler, M.; Kutzelnigg, W. *J. Chem. Phys.* **1982,** *76,* 1919.

[80] London, F. *J. Phys. Radium* **1937,** *8,* 397.

[81] Hameka, H. F. *Mol. Phys.* **1958,** *1,* 203.

[82] Hameka, H. F. *Mol. Phys.* **1959,** *2,* 64.

[83] Ditchfield, R. *Mol. Phys.* **1974,** *26,* 789.

[84] Wolinski, K.; Hinton, J. F.; Pulay, P. *J. Am. Chem. Soc.* **1990,** *112,* 8251.

[85] Schäfer, A.; Horn, H.; Ahlrichs, R. *J. Chem. Phys.* **1992,** *97,* 2571.

[86] Purvis, G. D.; Bartlett, R. J. *J. Chem. Phys.* **1982,** *76,* 1910.

[87] Füsti-Molnar, L.; Pulay, P. *J. Chem. Phys.* **2002,** *117,* 7827.

[88] Treutler, O.; Ahlrichs, R. *J. Chem. Phys.* **1995,** *102,* 346.

[89] Burant, J. C.; Scuseria, G. E.; Frisch, M. J. *J. Chem. Phys.* **1996,** *105,* 8969.

[90] Ochsenfeld, C.; White, C. A.; Head-Gordon, M. *J. Chem. Phys.* **1998,** *109,* 1663.

[91] Weigend, F.; Kattanneck, M.; Ahlrichs, R. *J. Chem. Phys.* **2009,** *130,* 164106.

[92] Weigend, F. *Phys. Chem. Chem. Phys.* **2002,** *4,* 4285.

[93] Bebe, N. H. F.; Linderberg, J. *Int. J. Quant. Chem.* **1977,** *12,* 683.

[94] Koch, H.; de Meras, A. S.; Pedersen, T. B. *J. Chem. Phys.* **2003,** *118,* 9481.

[95] Neese, F. *Electronic Structure in Bioinorganic Chemistry: Combined Spectroscopic/Theoretical studies on Mononuclear Non-Heme Iron Centers and Development of a Large Scale Ab Initio and Density Functional Electronic Structure Package,* Thesis, Universität Konstanz, 2001.

[96] Eichkorn, K.; Weigend, F.; Treutler, O.; Ahlrichs, R. *Theor. Chim. Acta* **1997,** *97,* 119.

[97] Weigend, F. *Phys. Chem. Chem. Phys.* **2006,** *8,* 1057.

[98] Weigend, F. *J. Comput. Chem.* **2008,** *29,* 167.

[99] Weigend, F.; Ahlrichs, R. *Phys. Chem. Chem. Phys.* **2005,** *7,* 3297.

[100] McMurchie, L. E.; Davidson, E. R.

[101] Polly, R.; Werner, H. J.; Manby, F. R.; Knowles, P. J. *Mol. Phys.* **2004,** *102,* 2311.

[102] Grimme, S. *J. Chem. Phys.* **2003,** *118,* 9095.

[103] Gerenkamp, M.; Grimme, S. *Chem. Phys. Lett.* **2004,** *392,* 229.

[104] Jung, Y. S.; Lochan, R. C.; Dutoi, A. D.; Head-Gordon, M. *J. Chem. Phys.* **2004,** *121,* 9793.

[105] Jung, Y. S.; Shao, Y.; Head-Gordon, M. *J. Comput. Chem.* **2007,** *28,* 1953.

[106] Saebø, S.; Almlöf, J. *Chem. Phys. Lett.* **1989,** *154,* 83.

[107] Head-Gordon, M.; Pople, J. A.; Frisch, M. J. *Chem. Phys. Lett.* **1988,** *153,* 503.

[108] Haase, F.; Ahlrichs, R. *J. Comput. Chem.* **1993,** *14,* 907.

[109] Saebø, S.; Pulay, P. *J. Chem. Phys.* **2001,** *115,* 3975.

[110] Baker, J.; Pulay, P. *J. Comput. Chem.* **2002,** *23,* 1150.

[111] Saebø, S.; Baker, J.; Wolinski, K.; Pulay, P. *J. Chem. Phys.* **2004,** *120,* 11423.

[112] Ishimura, K.; Pulay, P.; Nagase, S. *J. Comput. Chem.* **2006,** *27,* 407.

[113] Baker, J.; Wolinski, K.; Malagoli, M.; Kinghorn, D.; Wolinski, P.; Magyarfalvi, G.; Saebø, S.; Janowski, T.; Pulay, P. *J. Comput. Chem.* **2009,** *30,* 317.

[114] Almlöf, J. *Chem. Phys. Lett.* **1991,** *181,* 319.

[115] Häser, M.; Almlöf, J. *J. Chem. Phys.* **1992,** *96,* 489.

[116] Häser, M. *Theor. Chim. Acta* **1993,** *87,* 147.

[117] Ayala, P. Y.; Kudin, K. N.; Scuseria, G. E. *J. Chem. Phys.* **2001,** *115,* 9698.

[118] Lambrecht, D. S.; Doser, B.; Ochsenfeld, C. *J. Chem. Phys.* **2005,** *123,* 184102.

[119] Doser, B.; Lambrecht, D. S.; Ochsenfeld, C. *Phys. Chem. Chem. Phys.* **2008,** *10,* 3335.

[120] Schweizer, S.; Doser, B.; Ochsenfeld, C. *J. Chem. Phys.* **2008,** *128,* 154101.

[121] Doser, B.; Lambrecht, D. S.; Kussmann, J.; Ochsenfeld, C. *J. Chem. Phys.* **2009,** *130,* 064107.

[122] Rauhut, G.; Pulay, P.; Werner, H. J. *J. Comput. Chem.* **1998,** *19,* 1241.

[123] El Azhary, A.; Rauhut, G.; Pulay, P.; Werner, H. J. *J. Chem. Phys.* **1998,** *108,* 5185.

[124] Hetzer, G.; Schütz, M.; Stoll, H.; Werner, H. J. *J. Chem. Phys.* **2000,** *113,* 9443.

[125] Werner, H. J.; Manby, F. R.; Knowles, P. J. *J. Chem. Phys.* **2003,** *118,* 8149.

[126] Schütz, M.; Werner, H. J.; Lindh, R.; Manby, F. R. *J. Chem. Phys.* **2004,** *121,* 737.

[127] Saebø, S.; Pulay, P. *Chem. Phys. Lett.* **1985,** *113,* 13.

[128] Saebø, S.; Pulay, P. *Annu. Rev. Phys. Chem.* **1993,** *44,* 213.

[129] Pulay, P. *Chem. Phys. Lett.* **1983,** *100,* 151.

[130] Frisch, M. J.; Head-Gordon, M.; Pople, J. A. *Chem. Phys. Lett.* **1990,** *166,* 275.

[131] Frisch, M. J.; Head-Gordon, M.; Pople, J. A. *Chem. Phys. Lett.* **1990,** *166,* 281.

[132] Rhee, Y. M.; DiStasio, R. A.; Lochan, R. C.; Head-Gordon, M. *Chem. Phys. Lett.* **2006,** *426,* 197.

[133] DiStasio, R. A.; Steele, R. P.; Rhee, Y. M.; Shao, Y.; Head-Gordon, M. *J. Comput. Chem.* **2007,** *28,* 839.

[134] Simandiras, E. D.; Handy, N. C.; Amos, R. D. *Chem. Phys. Lett.* **1987,** *133,* 324.

[135] Weigend, F.; Furche, F.; Ahlrichs, R. *J. Chem. Phys.* **2003,** *119,* 12753.

[136] Hellweg, A.; Hättig, C.; Hoefener, S.; Klopper, W. *Theor. Chim. Acta* **2007,** *117,* 587.

[137] Dunlap, B. I.; Connolly, J. W. D.; Sabin, J. R. *J. Chem. Phys.* **1979,** *71,* 3396.

[138] Aikens, C. M.; Webb, S. P.; Bell, R. L.; Fletcher, G. D.; Schmidt, M. W.; Gordon, M. S. *Theor. Chim. Acta* **2003,** *110,* 233.

[139] E. Valeev and J. T. Fermann: LIBINT integral library obtained from http://www.files.chem.vt.edu/chem-dept/valeev/software/libint/download.html (accessed June

24, 2010).

[140] McConnell, H. M. *J. Chem. Phys.* **1961,** *35,* 1520.

[141] Hameka, H. F.; Turner, A. G. *J. Magn. Reson.* **1985,** *64,* 66.

[142] Chipman, D. M. *Theor. Chim. Acta* **1992,** *82,* 93.

[143] Gauld, J. W.; Eriksson, L. A.; Radom, L. *J. Phys. Chem. A* **1997,** *101,* 1352.

[144] Perera, S. A.; Watts, J. D.; Bartlett, R. J. *J. Chem. Phys.* **1994,** *100,* 1425.

[145] Al Derzi, A. R.; Fau, S.; Bartlett, R. J. *J. Phys. Chem. A* **2003,** *107,* 6656.

[146] Wetmore, S. D.; Eriksson, L. A.; Boyd, R. J. *J. Chem. Phys.* **1998,** *109,* 9451.

[147] Improta, R.; Barone, V. *Chem. Rev.* **2004,** *104,* 1231.

[148] Carmichael, I. *J. Phys. Chem.* **1991,** *95,* 108.

[149] Carmichael, I. *J. Phys. Chem. A* **1997,** *101,* 4633.

[150] Suter, H. U.; Engels, B. *J. Chem. Phys.* **1994,** *100,* 2936.

[151] Barone, V. *J. Chem. Phys.* **1994,** *101,* 6834.

[152] Munzarová, M.; Kubáček, P.; Kaupp, M. *J. Am. Chem. Soc.* **2000,** *122,* 11900.

[153] Neese, F. *J. Chem. Phys.* **2003,** *118,* 3939.

[154] Staroverov, V. N.; Scuseria, G. E.; Tao, J.; Perdew, J. P. *J. Chem. Phys.* **2003,** *119,* 12129.

[155] Koßmann, S.; Kirchner, B.; Neese, F. *Mol. Phys.* **2007,** *105,* 2049.

[156] Chai, J.-D.; Head-Gordon, M. *J. Chem. Phys.* **2008,** *128,* 084106.

[157] Chai, J.-D.; Head-Gordon, M. *Phys. Chem. Chem. Phys.* **2008,** *10,* 6615.

[158] Trucks, G. W.; Salter, E. A.; Sosa, C.; Bartlett, R. J. *Chem. Phys. Lett.* **1988,** *147,* 359.

[159] Trucks, G. W.; Salter, E. A.; Noga, J.; Bartlett, R. J. *Chem. Phys. Lett.* **1988,** *150,* 37.

[160] Kurlancheek, W.; Head-Gordon, M. *Mol. Phys.* **2009,** *107,* 1223.

[161] Neese, F.; Schwabe, T.; Koßmann, S.; Schirmer, B.; Grimme, S. *J. Chem. Theory Comput.* **2009,** *5,* 3060.

[162] Raghavachari, K.; Trucks, G. W.; Pople, J. A.; Head-Gordon, M. *Chem. Phys. Lett.* **1989,** *157,* 479.

[163] J. F. Stanton, J. Gauss, J. D. Watts, P. G. Szalay, R. J. Bartlett, with contributions from A. A. Auer, D. E. Bernholdt, O. Christiansen, M. E. Harding, M. Heckert, O. Heun, C. Huber, D. Jonsson, J. Jusélius, W. J. Lauderdale, T. Metzroth, C. Michauk, D. P. O'Neill, D. R. Prince, K. Ruud, F. Schiffmann, M. E. Varner, J. Vázquez and the integral packages MOLECULE (J. Almlöf and P. R. Taylor), PROPS (P. R. Taylor), and ABACUS (T. Helgaker, H. J. Aa. Jensen, P. Jørgensen, and J. Olsen), "ACES II Mainz-Austin-Budapest-Version", 2005.

[164] Munzarová, M.; Kaupp, M. *J. Phys. Chem. A* **1999,** *103,* 9966.

[165] Barone, V. In *Recent Advances in Density Functional Theory, Part I*; Chong, D. P., Ed.; World Scientific Publishing Co.: Singapore, 1995.

[166] Kutzelnigg, W.; Fleischer, U.; Schindler, M. In *NMR-Basic Principles and Progress*, Vol. 213; Springer Verlag: Heidelberg, 1991.

[167] Neese, F. *Inorg. Chim. Acta* **2002,** *337C,* 181.

[168] Weltner, Jr., W. *Magnetic Atoms and Molecules;* Dover: New York, 1983.

[169] Harvey, J. S. M.; Evans, L.; Lew, H. *Can. J. Phys.* **1972,** *50,* 1719.

[170] Graham, W. R. M.; Weltner, Jr., W. *J. Chem. Phys.* **1976,** *65,* 1516.

[171] Macdonald, J. R.; Golding, R. M. *Theor. Chim. Acta* **1978,** *47,* 1.

[172] Holloway, Jr., W. W.; Lüscher, E.; Novick, R. *Phys. Rev.* **1962,** *126,* 2109.

[173] Harvey, S. M. *Proc. R. Soc. London, Ser. A* **1965,** *285,* 581.

[174] Knight, Jr., L. B.; Wise, M. B.; Davidson, E. R.; McMurchie, L. E. *J. Chem. Phys.* **1982,** *76,* 126.

[175] Brom, Jr., J. M.; Weltner, Jr., W. *J. Chem. Phys.* **1972,** *57,* 3379.

[176] Easley, W. C.; Weltner, Jr., W. *J. Chem. Phys.* **1970,** *52,* 197.

[177] Knight, Jr., L. B.; Steadman, J.; Miller, P. K.; Bowman, D. E.; Davidson, E. R.; Feller, D. *J. Chem. Phys.* **1984,** *80,* 4593.

[178] Engels, B.; Eriksson, L. A.; Lunell, S. In *Advances in Quantum Chemistry*, Vol. 27; Academic Press Inc.: 1996.

[179] Feller, D.; Davidson, E. R. In *Modern Density Functional Theory: A Tool for Chemistry*; Maksić, Z. B., Ed.; Springer Verlag: 1991.

[180] Knight, Jr., L. B.; Wise, M. B.; Childers, A. G.; Davidson, E. R.; Daasch, W. R. *J. Chem. Phys.* **1980,** *73,* 4198.

[181] Knight, Jr., L. B.; Weltner, Jr., W. *J. Chem. Phys.* **1971,** *55,* 5066.

[182] van Lenthe, E.; van der Avoird, A.; Wormer, P. E. S. *J. Chem. Phys.* **1998,** *108,* 4783.

[183] Ishii, N.; Shimizu, T. *Phys. Rev. A* **1993,** *48,* 1691.

[184] Eriksson, L. A. In *Encyclopedia of Computational Chemistry*; v. R. Schleyer, P., Ed.; Wiley VCH: Chichester, 1997.

[185] Chipman, D. M. *J. Chem. Phys.* **1983,** *78,* 3112.

[186] Malkin, V. G.; Malkina, O. L.; Eriksson, L. A.; Salahub, D. R. In *Modern Density Functional Theory: A Tool for Chemistry*; Seminario, J. M.; Politzer, P., Eds.; Elsevier Science: 1995.

[187] Foner, S. N.; Cochran, E. L.; Bowers, V. A.; Jen, C. K. *Phys. Rev. Lett.* **1958,** *1,* 91.

[188] Gazzoli, G.; Espositi, C. D.; Favero, P. G.; Severi, G. *Nuovo Cimento* **1981,** *B 61,* 243.

[189] Childs, J.; Steimle, T. C. *J. Phys. Chem.* **1988,** *88,* 6168.

[190] DeVore, C.; Weltner, Jr., W. *J. Am. Chem. Soc.* **1977,** *99,* 4700.

[191] Varberg, D.; Field, R. W.; Merer, A. J. *J. Chem. Phys.* **1991,** *95,* 1563.

[192] Namiki, K.; Saito, S. *J. Chem. Phys.* **1997,** *107,* 8848.

[193] Tuttle, Jr., T. R.; Weissman, S. I. *J. Chem. Phys.* **1956,** *25,* 189.

[194] Carrington, A.; Dravnieks, F.; Symons, M. C. R. *J. Chem. Soc.* **1959,** 947.

[195] Becke, A. D. *J. Chem. Phys.* **1993,** *98,* 5648.

[196] Lee, C.; Yang, W.; Parr, R. G. *Phys. Rev. B* **1988,** *37,* 785.

[197] Clark, T.; Chandrasekhar, J.; Schleyer, P. V. R. *J. Comput. Chem. 84,*.

[198] Frisch, M. J.; Pople, J. A.; Binkley, J. S. *J. Chem. Phys.* **1984,** *80,* 365.

[199] Bolshakov, V.; Rossikhin, V.; Voronkov, E.; Okovytyy, S.; Leszczynski, J. *Chem. Phys.* **2010,** *372,* 67.

[200] Neese, F. *Magn. Reson. Chem.* **2004,** *42,* 187.

[201] Munzarová, M. *Quantum Chemical Calculations of EPR Parameters for Transition Metal Complexes,* Thesis, Max-Planck-Institut für Festkörperforschung Stuttgart, 2001.

[202] Gauss, J.; Kállay, M.; Neese, F. *J. Phys. Chem. A* **2010,** *113,* 11541.

[203] Tarnopolsky, A.; Karton, A.; Sertchook, R.; Vuzman, D.; Martin, J. M. L. *J. Phys. Chem. A* **2008,** *112,* 3.

[204] Grimme, S.; Anthony, J.; Ehrlich, S.; Krieg, H. *J. Chem. Phys.* **2010,** *132,* 154104.

[205] Koseki, S.; Gordon, M. S.; Schmidt, M. W.; Matsunaga, N. *J. Phys. Chem.* **1995,** *99,* 12764.

[206] Koseki, S.; Schmidt, M. W.; Gordon, M. S. *J. Phys. Chem. A* **1998,** *102,* 10430.

[207] Sander, W.; Grote, D.; Koßmann, S.; Neese, F. *J. Am. Chem. Soc.* **2008,** *130,* 4396.

[208] Grote, D.; Finke, C.; Koßmann, S.; Neese, F.; Sander, W. *Chem. Eur. J.* **2010,** *16,* 4496.

[209] Gritsan, N.; Platz, M. *Chem. Rev.* **2006,** *106,* 3844.

[210] Bettinger, H.; Sander, W. *J. Am. Chem. Soc.* **2003,** *125,* 9726.

[211] Morawietz, J.; Sander, W. *J. Org. Chem.* **1996,** *61,* 4351.

[212] Wenk, H.; Sander, W. *Angew. Chem.* **2002,** *114,* 2873.

[213] Wenk, H.; Sander, W. *Angew. Chem. Int. Ed. Engl.* **2002,** *41,* 2742.

[214] Sander, W.; Winkler, M.; Cakir, B.; Grote, D.; Bettinger, H. *J. Org. Chem.* **2007,** *72,* 715.

[215] Sander, W.; Grote, D.; Kossmann, S.; Neese, F. *J. Am. Chem. Soc.* **2008,** *130,* 4396.

[216] Leyva, E.; Platz, M.; Persy, G.; Wirz, J. *J. Am. Chem. Soc.* **1986,** *108,* 3783.

[217] Carra, C.; Nussbaum, R.; Bally, T. *ChemPhysChem* **2006,** *7,* 1268.

[218] Poe, R.; Schnapp, K.; Young, M.; Grayzar, J.; Platz, M. *J. Am. Chem. Soc.* **1992,** *114,* 5054.

[219] Schnapp, K.; Platz, M. *Bioconjugate Chem.* **1993,** *4,* 178.

[220] Karney, W.; Borden, W. *J. Am. Chem. Soc.* **1997,** *119,* 3347.

[221] Gritsan, N.; Gudmundsdóttir, A.; Tigelaar, D.; Zhu, Z.; Karney, W.; Hadad, C.; Platz, M. *J. Am. Chem. Soc.* **2001,** *123,* 1951.

[222] Neese, F. *ORCA - an ab initio, density functional and semiempirical program package, Version 2.6-71;* Institute for physical and theoretical chemistry: Bonn, Germany, 2008.

[223] Sinnecker, S.; Neese, F. *J. Phys. Chem. A* **2006,** *110,* 12267.

[224] Neese, F. *J. Chem. Phys.* **2007,** *127,* 164112.

[225] Neese, F. *J. Am. Chem. Soc.* **2006,** *128,* 10213.

[226] Neese, F.; Solomon, E. I. **1998,** *37,* 6568.

[227] Neese, F. *J. Phys. Chem. A* **2001,** *105,* 4290.

[228] Neese, F. *J. Chem. Phys.* **2001,** *115,* 11080.

[229] Neese, F. *Curr. Opin. Chem. Biol.* **2003,** *7,* 125.

[230] Neese, F. *J. Chem. Phys.* **2005,** *122,* 034107.

[231] Neese, F. *J. Biol. Inorg. Chem.* **2006,** *11,* 702.

[232] Eichkorn, K.; Öhm, O. T. H.; Häser, M.; Ahlrichs, R. *Chem. Phys. Lett.* **1995,** *240,* 283.

[233] Becke, A. D. *J. Chem. Phys.* **1993,** *98,* 1372.

[234] McWeeny, R.; Mizuno, Y. *Proc. R. Soc. London, Ser. A* **1961,** *A259,* 554.

[235] Petrenko, T. T.; Petrenko, T. L.; Bratus, V. Y. *J. Phys.: Condens. Matter* **2002,** *14,* 12433.

[236] Ray, K.; Weyhermüller, T.; Neese, F.; Wieghardt, K. **2005,** *44,* 5345.

[237] Pederson, M. R.; Khanna, S. N. *Phys. Rev. B* **1999,** *60,* 9566.

[238] Reviakine, R.; Arbuznikov, A.; Tremblay, J.-C.; Remenyi, C.; Malkina, O. L.; Malkin, V. G.; Kaupp, M. *J. Chem. Phys.* **2006,** *125,* 054110.

[239] Hess, B. A.; Marian, C. M.; Wahlgren, U.; Gropen, O. **1996,** *251,* 365.

[240] Berning, A.; Schweizer, M.; Werner, H. J.; Knowles, P. J.; Palmieri, P. *Mol. Phys.* **2000,** *98,* 1823.

[241] Pipek, J.; Mezey, P. G. *J. Chem. Phys.* **1989,** *90,* 4916.

[242] Neese, F. *J. Chem. Phys.* **2003,** *119,* 9428.

[243] Wanko, M.; Hoffmann, M.; Strodel, P.; Thiel, W.; Neese, F.; Frauenheim, T.; Elstner, M. *J. Phys. Chem. B* **2005,** *109,* 3606.

[244] Zein, S.; Duboc, C.; Lubitz, W.; Neese, F. **2008,** *47,* 134.

[245] Duboc, C.; Phoeung, T.; Zein, S.; Pecaut, J.; Collomb, M. N.; Neese, F. **2007,** *46,* 4905.

[246] Carmieli, R.; Larsen, T. M.; Reed, G. H.; Zein, S.; Neese, F.; Goldfarb, D. *J. Am. Chem. Soc.* **2007,** *129,* 4240.

[247] Neese, F. *J. Inorg. Biochem.* **2006,** *100,* 716.

[248] Schöneboom, J. C.; Neese, F.; Thiel, W. *J. Am. Chem. Soc.* **2005,** *127,* 5840.

[249] Reed, A. E.; Weinstock, R. B.; Weinhold, F. *J. Chem. Phys.* **1985,** *83,* 1736.

[250] Serwinski, P.; Esat, B.; Lahti, P.; Liao, Y.; Walton, R.; Lan, J. *J. Org. Chem.* **2004,** *69,* 5247.

[251] Taylor, P.; Serwinski, P.; Lahti, P. *Org. Lett.* **2005,** *7,* 3693.

[252] Lahti, P.; Esat, B.; Liao, Y.; Serwinski, P.; Lan, J.; Walton, R. *Polyhedron* **2001,** *20,* 1647.

[253] Smolinsky, G.; Wasserman, E.; Yager, W. *J. Am. Chem. Soc.* **1962,** *84,* 3220.

[254] Smolinsky, G.; Snyder, L.; Wasserman, E. *Rev. Mod. Phys.* **1963,** *35,* 576.

[255] Smolinsky, G.; Snyder, L.; Wasserman, E. *Acc. Chem. Res.* **1977,** *10,* 27.

[256] Wasserman, E. *Prog. Phys. Org. Chem.* **1971,** *8,* 319.